

Remediation of Crude Oil Spill on Water by Waste Poly(ethylene)- derived Sorbent

OLEDIBE, Mary-Joan Chikaodili

Available from the Sheffield Hallam University Research Archive (SHURA) at:

https://shura.shu.ac.uk/36307/

A Sheffield Hallam University thesis

This thesis is protected by copyright which belongs to the author.

The content must not be changed in any way or sold commercially in any format or medium without the formal permission of the author.

When referring to this work, full bibliographic details including the author, title, awarding institution and date of the thesis must be given.

Please visit https://shura.shu.ac.uk/36307/ and http://shura.shu.ac.uk/information.html for further details about copyright and re-use permissions.

Remediation of Crude Oil Spill on Water by Waste Poly(ethylene)-derived Sorbent

OLEDIBE, MARY-JOAN CHIKAODILI

A thesis submitted in partial fulfilment of the requirements of Sheffield Hallam University for the degree of Doctor of Philosophy

Declaration

I hereby declare that:

- 1. I have not been enrolled for another award of the University, or other academic or professional organisation, whilst undertaking my research degree.
- 2. None of the material contained in the thesis has been used in any other submission for an academic award.
- 3. I certify that this thesis is my own work. The use of all published or other sources of material consulted have been properly and fully acknowledged.
- 4. The work undertaken towards the thesis has been conducted in accordance with the SHU Principles of Integrity in Research and the SHU Research Ethics Policy and ethics approval has been granted for all research studies in the thesis.
- 5. The word count of the thesis is 60,000

Name	Mary-Joan Chikaodili Oledibe
Award	PhD
Date	February 2025
Research Institute	Materials and Engineering Research Institute (MERI)
Director of Studies	Dr. Francis Clegg

"The greatest threat to our planet is the belief that someone else will save it."

- Robert Swan

Eneasato, my de	ed memory of my ear parents-in-law, ove and encourage	Mr. & Mrs Sylves	ster Lebeke Oledil	

Acknowledgement

I present this dissertation with immense relief and deep gratitude after a long and eventful journey. This achievement would not have been possible without the unwavering support, guidance, and encouragement of many individuals.

First and foremost, I wish to thank God Almighty, who has been my source of sustenance in this country since I arrived in the United Kingdom in February 2021.

I extend my heartfelt appreciation to my Director of Studies (DOS), Dr. Francis Clegg. Thank you for your patience, wisdom, and steadfast support throughout the years. Your expertise, guidance, and encouragement have been invaluable to both my research and personal challenges. More than anything, I am grateful for the kindness and integrity you have consistently shown. Without your mentorship, this work would have remained just a dream. Thank you. I also appreciate my second Supervisor, Prof. Chris Sammon, for his contribution, which added flavour to this work.

This journey would not have been possible without the financial support provided by my Sponsors, the Petroleum Technology Development Fund (PTDF) Nigeria and my office, the Ministry of Petroleum Resources, Abuja, Nigeria. I am truly appreciative of the opportunity and for funding my PhD research work in the United Kingdom.

My deepest gratitude also to Dr. Hassan, whose support and friendship were instrumental in helping me push through the practical stages of my research work. You taught me most of the things I know about modelling, you are highly appreciated.

I am deeply grateful for the friendships and support I have received throughout this journey. A heartfelt thank you goes to Dr. Ronak, Dr. Olalekan, Captain Rebecca (my neighbour), Mrs. Ladi Okoko, Dr. Mukesh, Dr. Popoola, as well as my many friends and fellow church members from both Emmanuel church and Baptist Church, for their unwavering encouragement and companionship. I also extend my sincere appreciation to the technical staff of MERI and all members of the Harmer Lab team, whose contributions have been instrumental to the success of my work.

To all my dear colleagues in the lab and PhD office, your friendship has meant the world to me throughout these years. Thank you for making my time at SHU such a rewarding experience.

Above all, I owe everything to my loving family. To my husband, Chidiebere, and children (Amarachi, Blessed and Godswill), my mother (Mediatrix), brothers (Iyke, Emeka and Ugo), Mrs. Chichi Onuorah and family, Mrs. Joy Udeh and family. I am immensely grateful. Your unwavering support, patience, sacrifices and belief in me have been the foundation of my success.

Abbreviations

ANOVA Analysis of variance

ASTM American Society of Testing and Materials

DTGS Deuterated triglycine sulphate

DSC Differential Scanning Calorimetry

FTIR Fourier-transform infrared spectroscopy

GC-MS Gas Chromatography-Mass Spectrometry

HDPE High-density polyethylene

IRR Irradiance

ITOPF International Tanker Owners Pollution Federation Limited

LDPE Low-density polyethylene

LLDPE Linear low-density polyethylene

NOSDRA National Oil Spill Detection and Response Agency

NWF Natural wool fibres

PE Polyethylene

PS-PMMA/DVB Polystyrene-polymethyl methacrylate/divinylbenzene

rPET Recycled polyethylene terephthalate

RSM Response surface methodology

RWNM Recycled wool-based nonwoven material

SEM Scanning electron microscope

TGA Thermogravimetric analysis

UV Ultraviolet

WWSP Waste Water Sachet Polyethylene

Abstract

This research addresses two major environmental concerns: the growing accumulation of waste water sachet polyethylene (WWSP), which poses a significant environmental nuisance, and the need for effective sorbents for crude oil spill remediation on water surfaces. This study explores the transformation of WWSP into high-performance oil sorbents through mechanical and weathering (artificial and accelerated to simulate natural environmental ageing) modifications.

Comprehensive characterisation of both PE and crude oil (natural and synthetic) was conducted to understand their chemical composition and interfacial properties. Contact angle measurements were performed to evaluate the hydrophobicity and oleophilicity of different forms of PE. DSC, TGA and FTIR were performed on the PE to investigate their chemical composition and thermal behaviour. SEM was carried out on the various types of PE (before and after modifications) to assess their surface morphology. GC-MS, TGA, and Rheology were used to determine the oil's chemical composition, volatility, thermal stability, and viscosity under shear stress. I-optimal design of experiments was employed to systematically assess the impact of adsorbent quantity, particle size, adsorbent type, and UV-weathering duration on adsorption capacity and efficiency. The results highlighted strong interactions between these factors, significantly influencing sorbent performance.

Results reveal that waste PE-based sorbents are made up of LLDPE and LDPE at almost equal proportions. These sorbents exhibit significant oil adsorption capacities when modified mechanically or physically (UV-weathered). Shredded PE reaches up to 7.1 g/g with reusability of 18 cycles, then when roughened (Shredded-roughened PE) achieves an increased adsorption capacity of 8.6 g/g, UV-weathered PE, exposed to high values of irradiance (1.55 W/m²) and temperature of 70° C, shows an adsorption capacity of 6.5 g/g after 75 hours and declines to ≤ 3.5 g/g after 150 hours. The findings highlight the critical role of surface area and roughness in enhancing oil retention by improving sorbent-oil interactions. Additionally, moderate weathering enhances adsorption capacity, though prolonged exposure leads to a decline. Oil type affected adsorption, with lighter oils being adsorbed faster due to lower viscosity. Smaller particle sizes (2.8 mm $\leq x \geq 2.0$ mm) increased surface area giving higher adsorption capacity, and efficiency up to 100% but became less effective beyond the optimal loading capacity. These insights reinforce the potential of waste PE as a low-cost, sustainable solution for oil spill cleanup.

Overall, this research has demonstrated that waste polyethylene that littered the environment can be used in a simplified manner to clean up crude oil spilt on the water even after lying in the environment for some period and contributing to sustainable environmental management and efficient oil spill remediation technologies.

Table of Contents

Declaration	i
Acknowledgement	iv
Abbreviations	V
Abstract	vi
Table of Contents	vii
Table of Figures	xii
List of Tables	xix
APPENDICES	xxi
Chapter 1	1
1.0 Introduction	1
1.1 Causes of oil spillage	4
1.1.1 Natural Causes	4
1.1.2 Human-Induced Causes	4
1.1.3 Mysterious Causes	4
1.2 Problem statement and motivation	8
1.3 Combining the Problem of Plastic Pollution to Remediate Oil Spillages	10
1.4 Aim and Objectives	11
Chapter 2	
2.0 Literature Review	12
2.1 Methods used in the management and remediation of crude oil-polluted water	12
2.1.1 Physical Remediation Methods	12
2.1.1.1 Booms	12
2.1.1.2. Skimmers	15
2.1.1.3. Sorbent materials	16
2.1.2 Chemical remediation methods	22
2.1.3: Bioremediation method	23
2.1.4: Thermal remediation method	24
2.2 Global oil spill disasters and remediation methods deployed	26
2.2.1 The proposed sorbent for oil spill clean-up - used-water sachet polyethylene	31
2.3 Adsorption technology	32
2.3.1 Factors affecting adsorption and the efficiency of oil recovery	32
2.4 Overview of polyethylene	35
2.4.1 Types of polyethylene	36
2.4.2 Key properties of plastic-based oil sorbents	37

2.4.3. The sachet water waste problem in Nigeria	38
2.4.4. Hydrophobicity of Polyethylene and adsorption mechanism	39
CHAPTER 3	42
3.0 METHODOLOGY	42
3.1 Materials	42
3.1.1 Preparation of Polyethylene sorbents	42
3.1.1.1 Shredded Polyethylene	43
3.1.1.2: Shredded-roughened Polyethylene	44
3.1.1.3 UV weathered PE	46
3.2. Characterisation tests	48
3.2.1 Instruments used for the characterisation of Oils (Natural Crude, Phillip, Camlab)	48
3.2.1.1 Gas chromatography and Mass Spectrometer (GC-MS)	49
3.2.1.2 Thermogravimetric analysis (TGA)	52
3.2.1.3 Contact angle	53
3.2.1.4 Rheometry	57
3.2.2 Instruments used for the characterisation of the Polyethylene water sachets	59
3.2.2.1 Differential Scanning Calorimetry (DSC)	59
3.2.2.2 Fourier Transform Infrared Spectroscopy (FTIR)	61
3.2.2.3 Scanning Electron Microscopy (SEM)	63
3.3 Adsorption methodologies for the oil spill clean-up and reuse of PE sorbents	66
3.3.1 Adsorption and sorbent reuse procedure (1): Batch adsorption protocol	66
3.3.2 Adsorption, sorbent recovery, and recycling procedure (2): Column adsorption	69
3.4 Adsorption factors and statistical design of experiments	70
Chapter 4	73
4.0 Characterisation of polyethylene sachets and crude oils	73
4.1. Characterisation of pristine polyethylene water sachets	74
4.1.1. Characterisation of pristine PE using Fourier transform infrared spectroscopy (FTI	•
4.1.2. Characterisation of pristine PE using Differential Scanning Calorimetry (DSC)	
4.1.3. Characterisation of pristine PE by thermogravimetric analysis (TGA)	
4.2 Characterisation of ultraviolet-weathered PE water sachets	83
4.2.1. Characterisation of ultraviolet-weathered PE water sachets by FTIR	
4.2.2 Natural weathered PE samples	
4.2.3 Characterisation of Polyethylene sachet with SEM	
4.2.3.1 Characterisation of Ultraviolet/Natural weathered sachet PE	98
4.3. Effect of different instruments used for the shredding	105

4.3.	1 The FTIR analysis showing the effects of shredding and roughening on PE	107
4.4. Cl	haracterisation of the Crude oil	109
4.4.	1 Oil Characterisation by GC-MS	109
4.	.4.1.1. GC-MS – pristine (natural and synthetic oils)	110
4.4.	2. GC-MS – Weathered oils	116
4.4.	3 Characterisation of oils with TGA	118
4.	.4.3.1. TGA – Oils	118
4.5 Rh	eology of Natural crude oil	128
4.6. Co	ontact angle measurement and Surface energy	129
Chapter	5	134
5.0 Prelir	minary batch experiments	134
5.1 Int	roduction	134
5.1.	1 Assessment of contact time for adsorption of crude oil	135
5.	.1.1.1 Experimental procedures for determining the contact time	135
5.1.	2 Adsorption experiments with PE square sheets	138
5.1.	3 Determination of the quantity of adsorbent to be used for adsorption experiment	ts 140
5.1.	4 Shredding of PE and particle size distributions of sorbents	144
5.1.	5 Determination of sorbent oven drying time after adsorption	146
	6 To determine the extent of evaporation of crude oil in the oven at a constant perature of 60 degrees.	147
5.2 AS	TM procedure for the sorbent tests	148
5.2.	1 Dynamic degradation test from ASTM F726-17	148
5.3 Fin	nal adsorption experiment	152
5.3.	1 Adsorption Protocol with Shredded PE	152
5.3.	2 Assessment of oil contamination in water after clean-up	152
5.3.	3. Desorption procedure and reusability of sorbent	154
	.3.3.1 Method 1 for Desorption procedure and reusability of sorbent (oven-dried- orbent)	154
	.3.3.2 Method 2 for Desorption procedure and reusability of sorbent (non-oven dri	•
	6	
	misation of conditions for oil adsorption by the developed sorbents	
6.1	Introduction	
6.2	Optimisation of Philips and Natural crude oils removal from water: I-optimal des	
6.3 Re	sults	164
6.3.	1 I-optimal experimental designs	164

(6.3.1.1 Experiments with Phillip Synthetic Oil	165
(6.3.1.2 Optimisation of parameters for Phillip oil adsorption by the polyethylene s	orbent
		190
6.4:	I-optimal experiments with the Natural crude oil	
6.5	Experiments with the UV-weathered PE	196
6.5	5.1 Effects of UV weathered PE on adsorption of Philip oil and crude oil	196
-	r7	
7.0 Col	umn Adsorption	203
7.1 lr	ntroduction	205
7.2	Materials	206
7.3	Methodology	206
7.3	Preparation of the PE sorbent (Particle Sizing and Surface treatment)	206
7.3	3.2 Packing Method	206
7.3	Preparation of the Oil-Water Mixture	206
7.3	Column Loading and Flow Initiation	207
7.3	Sorbent removal after oil adsorption measurement	207
7.3	Result of column experiment	209
7.3	3.7 Observations in the column experiment	209
7.3	3.8 Formular used for the calculations for the values on the Table 7.1	215
Chapte	r 8	216
8.0 Disc	cussion of Results, Conclusion, Limitations, Challenges and Further Work	216
8.1 lr	ntroduction	216
8.2	Characterisation of Polyethylene	216
8.3.	Effect of shredding and roughening of PE	218
8.4.	Effects of Weathering on Surface Morphology	220
8.5	Particle Size Distribution and effects on adsorption	220
8.6	PE chemical composition, hydrophobicity and oil selectivity	222
8.8 C	characterisation of Crude Oils	224
8.9 O	ptimisation of Adsorption Parameters	225
8.9	9.1 Effect of Using Non-Weathered PE	225
8.9	2.2 Effect of Using UV-Weathered PE	226
8.10	Preliminary column adsorption with optimised conditions scaled up from batch	
•	riment	
	Comparing this work with other previous work carried out on polyethylene-based	` ,
	ents	232
01/	A A DECLEMENT	7.57

8.	.13 Limitations/observations/challenges	233
	8.13.1 Limitations	233
	8.13.2 Challenges faced	
	8.13.3. Recommendation for Further work	235
Refe	erences	238
APP	ENDICES	254

Table of Figures

Figure 1. 1:Map of Nigeria showing the Oil Producing States in the Niger Delta Region2
Figure 1. 2: Oil spill data summary recorded by NOSDRA in Nigeria for 20233
Figure 1. 3: Oil spill data summary recorded by NOSDRA in Nigeria for 20233
Figure 1. 4: On October 12, 2004, oil from a leaking pipeline caught fire in Goi-Bodo, a
swampy region of the Niger Delta, Nigeria5
Figure 1. 5: Leakage from a suspected sabotaged underground pipeline6
Figure 1. 6: Oil spill spreading in a flowing stream6
Figure 1. 7: Suspected illegal oil siphoning activities from a pipe transporting crude oil7
Figure 1. 8:Weathering process of oil on the sea surface9
Figure 2. 1: How oil spill containment boom contains spilt oil on water13
Figure 2. 2: Improvised adsorbent boom constructed from netting and straw14
Figure 2. 3: How skimmers work in recovering spilled oil on the surface of water16
Figure 2. 4: Deepwater Horizon oil spill: beach cleanup (Workers contracted by BP cleaning
up oil on a beach in Port Fourchon, Louisiana, May 23, 2010)27
Figure 2. 5: A Coast Guardsman checks oil recovery mesh from the Exxon March 28, 1989.28
Figure 2. 6: Pom poms fibres attract and hold heavy oils used in the Exxon Valdez oil spill28
Figure 2. 7: Ixtoc I oil spill; the oil well blow out29
Figure 2. 8: Clean up in Barangay La Paz with locally made sorbents30
Figure 2. 9: Schematic representation of adsorption phenomena
Figure 2. 10: Schematic of water droplet's contact angle describing different surface
wettability35
Figure 2. 11: Illustration of Polyethylene Structures (a) HDPE, (b) LLDPE, and (c) LDPE37
Figure 3. 1: Different water sachets with ink-printed markings for marketing information42
Figure 3. 2: (a) washed PE (b) PE cut into small pieces prior to shredding (c) 3devo polymer
grinding machine used to shred PE (d) Nutribullet blender (e) shredded PE (f) grinding set of
plates used to improvise the roughening of shredded PE (g) electronic sieve shaker44

Figure 3. 3: RETSCH's Vibratory Disc Mill RS 200, used as an improvise for PE surface
roughening (b) Open RETSCH's Vibratory Disc Mill RS 200, showing the embedded grinding
set held in position by the quick action lever45
Figure 3. 4: UVA-340 Lamps Compared to Sunlight47
Figure 3. 5: (a): Q-lab UV Accelerated weathering tester (b): Accelerated weathering tester
showing the fluorescent UV lamps48
Figure 3. 6: Schematic diagram of the GCMS basic principle of operation50
Figure 3. 7:GCMS (ThermoScientific Trace 1310 Gas chromatograph: ISQ 7000 Single
Quadrupole Mass Spectrometer)51
Figure 3. 8: Laboratory set-up of Mettler-Toledo TGA/DSC-1 instrument (Stare System) for
Thermal analysis53
Figure 3. 9: Telescope goniometer for contact angle measurements DataPhysics OCA 15EC56
Figure 3. 10:Anton Paar Physica MCR 301 rheometer for rheology measurements58
Figure 3. 11: Schematic illustration of the bob and cup setting for viscosity measurements 59
Figure 3. 12: Simple schematic diagram of Differential Scanning Calorimetry (DSC) for
Thermal analysis60
Figure 3. 13: Differential Scanning Calorimetry (DSC) for Thermal analysis61
Figure 3. 14: Fourier Transform Infrared Spectroscopy (FTIR) infrared spectral analysis63
Figure 3. 15: Scanning Electron Microscopy (SEM) Quanta 65065
Figure 3. 16: Batch adsorption process used for the laboratory demonstration of oil spill
cleaning exercise using PE sorbent
Figure 3. 17: Column adsorption process for oil spill cleaning exercise using PE sorbent70
Figure 4. 1: spectra of Greenmark sachet polyethylene samples, top spectrum is back side,
bottom spectrum is front side74
Figure 4. 2: FTIR spectra of ink (on polyethylene)75
Figure 4. 3: DSC first heating curves for all the PE samples to check for uniformity/similarity
and repeatability77
Figure 4. 4: DSC first cooling curves for all the PE samples to check for uniformity/similarity
and repeatability78
Figure 4. 5: DSC second heating curves for all the PE samples to check for
uniformity/similarity and repeatability78

Figure 4. 6: DSC curve of the second cycle of melting of a Munirah Gold PE sample80
Figure 4. 7: Thermogravimetric (top) and derivative thermogravimetric (bottom) curves for
Greenmark PE at a heating rate of 20°C/min under nitrogen or air82
Figure 4. 8: FTIR spectra of the five PE Pristine samples84
Figure 4. 9: FTIR spectrum representing all Pristine PE samples84
Figure 4. 10: FTIR spectra of the various inks on all the PE samples before weathering85
Figure 4. 11: FTIR spectra of the various inks on all the PE samples before weathering86
Figure 4. 12: Comparison of various areas of the oxidised sites of the UV weathered PE87
Figure 4. 13: Area ratio vs duration for all PE samples (NIS)89
Figure 4. 14: FTIR spectra of the ink on Golden age PE before and after weathering90
Figure 4. 15: FTIR spectra of the ink on Munirah gold PE before and after weathering90
Figure 4. 16: FTIR spectra of ROYALLINK PE after UV exposure at different time intervals
highlighting differences in the oxidised regions for the back and front (side facing UV bulb
directly) sides of the PE91
Figure 4. 17: FTIR spectra of Munirah Gold PE sample after UV exposure at different time
intervals, highlighting differences in the oxidised regions for the back and front (side facing
UV bulb directly) sides of the PE92
Figure 4. 18: FTIR spectra of Golden Age PE sample after UV exposure at different time
intervals, highlighting differences in the oxidised regions for the back and front (side facing
UV bulb directly) sides of the PE92
Figure 4. 19: FTIR spectra of all the PE samples after UV exposure at same time intervals
(240 hours) comparing differences in the oxidised regions for the back and front (side facing
UV bulb directly) sides of the PE93
Figure 4. 20: A selection of the PE water sachets spread on the aluminium zinc, directly
exposed to the sunlight, and supported with plastic pipes and stones to avoid being blown
away by the wind94
away by the wind94 Figure 4. 21: Spectra of naturally weathered PE samples (multiple colours) compared to UV-
Figure 4. 21: Spectra of naturally weathered PE samples (multiple colours) compared to UV-
Figure 4. 21: Spectra of naturally weathered PE samples (multiple colours) compared to UV-weathered PE samples (red spectrum)95
Figure 4. 21: Spectra of naturally weathered PE samples (multiple colours) compared to UV-weathered PE samples (red spectrum)

Figure 4. 24: Spectrum of naturally weathered PE samples (1200 hours) compared to UV-
weathered PE samples of 168 hours at the 1700 cm ⁻¹ and 1350 cm ⁻¹ region97
Figure 4. 25: Spectrum of natural weathered PE samples (1200 hours) compared to UV-
weathered PE samples of 168 hours at the 1700 cm ⁻¹ and 1350 cm ⁻¹ region (zoomed image)
98
Figure 4. 26: (a) Pristine PE (b) Naturally weathered PE for 50 days (1200 hrs) (c) UV-
weathered PE for 75 hours (d) UV-weathered PE for 150 hours99
Figure 4. 27: SEM images of virgin, natural sunlight, UV- weathered (75 hrs), UV Weathered
(150 hrs) PE samples
Figure 4. 28: (a) Shredded PE consisting of large flakes body with elongated strands (b)
Shredded-roughened PE
Figure 4. 29: SEM images of Shredded, and shredded-roughened PE samples103
Figure 4. 30: (a) Blades from the Nutribullet 900 series blender used for the shredding
procedure (b) sample of shredded pristine PE (c) sample of UV weathered PE105
Figure 4. 31:3devo Shredder view showing many blades
Figure 4. 32: showing the finely shredded pristine PE from the 3Devo shredder107
Figure 4. 33: FTIR spectrum of plain, shredded, and shredded-roughened PE samples108
Figure 4. 34: FTIR spectrum of shredded, shredded-roughened and plain PE samples stacked
to reveal the changes
Figure 4. 35: GCMS chromatographs of the fresh natural crude oil 1 (top chromatogram) and
Synthetic crude oil (Camlab (bottom chromatogram) and Phillip (middle chromatogram))
samples
Figure 4. 36: Chromatograph showing a complex composition of 3 natural crude oils (Bonny
light) from the same source but at different times
Figure 4. 37: Venn diagram showing various numbers of compositional similarities and
differences in the oils Error! Bookmark not defined.
Figure 4. 38: Chromatograph showing intensity changes of weathered crude oil 2 on various
days
Figure 4. 39: Chromatograph showing intensity changes of weathered Phillip synthetic oil on
various days117
Figure 4. 40: Chromatograph showing intensity changes of weathered Camlab synthetic oil
on various days117

Figure 4. 41: TGA graph of Crude oil 1 weathered for various days119
Figure 4. 42: TGA graph of Crude oil 2 weathered for various days119
Figure 4. 43: TGA graph of Crude oil 3 weathered for various days120
Figure 4. 44: TGA graph of Phillip oil weathered for various days120
Figure 4. 45: TGA graph of Camlab oil weathered for various days121
Figure 4. 46: TGA graph of Camlab, Phillip synthetic oils, and Crude oils 2 and 3 weathered
for one day
Figure 4. 47: TGA graph of 3 crude oils showing the weight loss changes within the 2 major
temperature regions (above) and 3 temperature regions (below) as weathering days
increase
Figure 4. 48: TGA graph of Camlab and Phillip synthetic oils showing the weight loss changes
within the 3 major different temperature ranges as weathering days increase125
Figure 4. 49: Rheology graph of pristine and weathered natural crude oil at a constant
temperature of 20 degrees centigrade
Figure 4. 50: A screenshot of contact angle measurement for a water droplet on a
polyethylene surface using the SCA20 software
Figure 4. 51: Graph displaying the contact angle analysis of various fluids on PE samples and
their error bars
Figure 4. 52: Graph displaying the surface energies of various PE types on various fluids and
their error bars
Figure 5. 1: Graph of contact time versus adsorbed oil (Phillip oil)137
Figure 5. 2: Adsorption experiment with square PE to check the effect of contact time and
film integrity
Figure 5. 3: Graph displaying the adsorption capacity of the different oils as the sorbent
weight increases
Figure 5. 4: Graph of weight of sorbent vs quantity of oil adsorbed142
Figure 5. 5: Efficiency of the oils as the sorbent increased from 0.5g – 5g143
Figure 5. 6: Particle size distribution of the shredded PE of 3Devo and Nutribullet shredders
Figure 5. 7: Graph showing how the constant weight time (drying time) was determined .146

Figure 5. 8: Evaporation curve of the oil after 240 minutes at a temperature of 60 degrees
centigrade147
Figure 5. 9: (a) Sorbent in the Gyratory Water Bath shaker (Model G76D) during test (b) and
(c) sorbent left to settle after the test149
Figure 5. 11: Adsorption experiment with crude oil and Shredded PE sorbent and extraction
of residual oil from remediated water with DCM153
Figure 5. 12: GCMS chromatograph showing the results of DCM extract composition of two
remediated water samples after adsorption experiments153
Figure 5. 13: Recycling process (a – f)155
Figure 5. 14: Adsorption capacity (oil and water) of recycled PE after repeated adsorption
and mechanical pressing156
Figure 5. 15: Desorption procedure and reusability of sorbent (using a non-oven-dry
adsorbent method)159
Figure 6. 1: : Normal probability plot of studentised residuals(a) and correlation between
actual and predicted values (b) of adsorption capacity for Phillip oil173
Figure 6. 2: (a) Adsorption capacity of Phillip oil with shredded-roughened PE Particle size
2.8 mm \leq x \geq 2.0 mm (b) Adsorption capacity of Phillip oil with shredded PE Particle size 2.8
mm ≤ x ≥ 2.0 mm
Figure 6. 3: (a) Adsorption capacity of Phillip oil with shredded-roughened PE Particle size
6.3 mm \leq x \geq 2.8 mm (b) Adsorption capacity of Phillip oil with shredded PE Particle size 6.3
mm ≤ x ≥ 2.8 mm175
Figure 6. 4: (a) Adsorption capacity of Phillip oil with shredded-roughened PE Particle size
8.0 mm \leq x \geq 6.3 mm (b) Adsorption capacity of Phillip oil with shredded PE Particle size 8.0
mm ≤ x ≥ 6.3 mm176
Figure 6. 5: Normal probability plot of studentised residuals(a) and correlation between
actual and predicted values (b) of adsorption efficiency for Phillip oil186
Figure 6. 6: (a) Adsorption efficiency of Phillip oil with shredded-roughened PE (X) Particle
size 2.8 mm \leq x \geq 2.0 mm (b) Adsorption efficiency of Phillip oil with shredded-roughened PE
(X) Particle size 6.3 mm \leq x \geq 2.8 mm (c) Adsorption efficiency of Phillip oil with shredded-
roughened PE (X) Particle size 8.0 mm \leq x \geq 6.3 mm

Figure 6. 7: (a) Adsorption efficiency of Phillip oil with shredded PE (W) Particle size 2.8 mm
\leq x \geq 2.0 mm (b) Adsorption efficiency of Phillip oil with shredded PE (W) Particle size 6.3
mm \leq x \geq 2.8 mm (c) Adsorption efficiency of Phillip oil with shredded PE (W)) Particle size
8.0 mm ≤ x ≥ 6.3 mm
Figure 7. 1: (a) Column filled with PE sorbent and secured with a flexible sieve net at base (b)
base of column (c) Oil-water mixture pouring into the column (d)- (g) gradual
movement/shift of the adsorption zone downwards and the shrinking of the non-work zone
(h) water exits first from the column (i) adsorbent removed from the column and spread in a
glassware hefore nut in oven (i) adsorbent after oven-drying 208

List of Tables

Table 2. 1: Properties of some sorbent materials
Table 2. 2 : Functions and categories of chemical dispersants
Table 2. 3: Features of different oil spill clean-up techniques25
Table 3. 1: Set parameters for the weathering of PE sachets equivalent to normal noon
sunlight46
Table 3. 2: Set parameters for the weathering of PE sachets for the double irradiation47
Table 4. 1: Area ratio of the carbonyl bands with alkane bands of PE
Table 4. 2: Select components identified by GCMS from the Crude oil and their associated
intensities, retention time, peak area and molecular structure113
Table 4. 3: Contact angle measurements of various forms of PE samples130
Table 5. 1: Weights of crude oil adsorbed on and amounts drained off square-shaped PE at
various time intervals
Table 5. 2: Water adsorbency calculations150
Table 6. 1: The ANOVA table for the two-factor interaction model for Response 1;
Adsorption capacity for Phillip oil on shredded (W), and shredded-roughened PE (X)167
Table 6. 2: The ANOVA table for the reduced quadratic model for Response 2; Adsorption
Efficiency for Phillip oil on shredded (W), and shredded-roughened PE (X)180
Table 6. 3: Results of confirmatory experiments for analysed Optimal-I design model for
adsorption of Philip synthetic oil199
Table 6. 4: Results of confirmatory experiments for analysed Optimal-I design model for
adsorption of Natural crude oil200
Table 7. 1: Optimised conditions for the adsorption of Phillip and Natural crude oils204
Table 7. 2: Comparing the predicted values of the model for the oils in a batch experiment
with the scaled-up values in the column adsorption experiment212

Table	8. 1: Comparing this work with other previous v	work carried o	out on polyethylen	e-based
(LDPE) sorbents			229

APPENDICES

Appendix A (Chapter 4)

Appendix A 1: GCMS account of Fresh Crude oil composition254
Appendix A 2: GC-MS account of Phillip synthetic oil compositionError! Bookmark not
defined.
Appendix A 3: GC-MS account of Camlab synthetic oil compositionError! Bookmark not
defined.
Appendix A 4: Pie chart showing the distribution of hydrocarbon types in crude oil, Phillip
and Camlab Synthetic oils based on GC-MS peak area ≥1500 counts/min266
Appendix A 5: GC-MS chromatogram for fresh and weathered crude oil 3268
Appendix A 6: Physical weight loss experiment of 20g sample for the different oils in the
fume cupboard for 65 days270
Appendix A 7: TGA results of weathered Oils for various days272
Appendix B (Chapter 6)
Appendix B 1: A 27-run Optimal Custom design for adsorption factors (generated with
Design-Expert® 13 software) for optimal experimental design (I-optimal) of Phillip oil
adsorption onto Shredded (W), and shredded-roughened PE (X) with their corresponding
responses
Appendix B 2: A 27-run Optimal Custom design for adsorption factors (generated with
Design-Expert® 13 software) for optimal experimental design (I-optimal) of Natural crude
oil adsorption onto Shredded (W), and shredded-roughened (X) PE with their
corresponding responses276
Appendix B 3: A 32-Run I-optimal design for evaluating adsorption factors and responses
for Phillip oil adsorption on UV-weathered polyethylene using design-expert® 13 software
Appendix B 4: A 32-Run I-optimal design for evaluating adsorption factors and responses
for Natural crude oil adsorption on UV-weathered polyethylene using design-expert® 13
software

Appendix B 5: Analysis of Variance (ANOVA) of reduced 2FI model for the response 1			
(adsorption capacity for Natural crude oil on Shredded, and Shredded-roughened PE) 28	3		
Appendix B 6: Analysis of Variance (ANOVA) of reduced quadratic model for the response			
2 (adsorption efficiency) for Natural crude oil on Shredded, and Shredded-roughened PE)			
28	4		
Appendix B 7: Analysis of Variance (ANOVA) of 2FI model for the response 2 (adsorption			
capacity for Natural crude oil on UV-weathered PE)28	5		
Appendix B 8: Analysis of Variance (ANOVA) of 2FI model for the response 2 (adsorption			
efficiency for Natural crude oil on UV-weathered PE)28	7		
Appendix B 9: Final Equation in Terms of Actual Factors for adsorption capacity and			
efficiency of Natural crude oil on shredded, and shredded-roughened PE28	9		
Appendix B 10:Final Equation in Terms of Actual Factors for adsorption capacity and			
efficiency of Phillip oil on UV-weathered PE29	0		
Appendix B 11: Final Equation in Terms of Actual Factors for adsorption capacity and			
efficiency of Natural crude oil on UV-weathered PE29	2		
Appendix B 12: Optimised conditions for adsorption capacity for Phillip oil by the non-			
weathered PE29	4		
Appendix B 13: Optimised conditions for adsorption efficiency for Phillip oil using the non	-		
weathered PE29	5		
Appendix B 14: : Optimised conditions for adsorption capacity for Phillip oil using the			
weathered PE29	6		
Appendix B 15: Optimised conditions for adsorption efficiency for Phillip oil using the			
weathered PE29	7		
Appendix B 16: Optimised conditions for adsorption capacity for Natural crude oil using			
the non-weathered PE29	8		
Appendix B 17: Optimised conditions for adsorption efficiency for Natural crude oil using			
the non-weathered PE29	9		
Appendix B 18: Optimised conditions for adsorption capacity for Natural crude oil using			
the UV-weathered PE30	0		
Appendix B 19: Optimised conditions for adsorption efficiency for Natural crude oil using			
the LIV weethered DF	1		

Appendix B 20: Adsorption capacity of natural crude oil with shredded PE (W) Particle size
2.8 mm ≤ $x \ge 2.0$ mm, shredded PE (W) Particle size 6.3 mm ≤ $x \ge 2.8$ mm and shredded PE
(W) Particle size 8.0 mm $\le x \ge 6.3$ mm
Appendix B 21: Adsorption efficiency of natural crude oil with shredded PE (W) Particle size
2.8 mm $\leq x \geq$ 2.0 mm, shredded PE (W) Particle size 6.3 mm $\leq x \geq$ 2.8 mm and shredded PE
(W) Particle size 8.0 mm $\le x \ge 6.3$ mm
Appendix B 22: Adsorption capacity of natural crude oil with shredded-roughened PE (X)
Particle size 2.8 mm $\le x \ge 2.0$ mm, shredded-roughened PE (X) Particle size 6.3 mm $\le x \ge 2.8$
mm and shredded-roughened PE (X) Particle size 8.0 mm \leq x \geq 6.3 mm304
Appendix B 23:Adsorption efficiency of natural crude oil with shredded-roughened PE (X)
Particle size 2.8 mm \leq x \geq 2.0 mm, shredded-roughened PE (X) Particle size 6.3 mm \leq x \geq
2.8 mm and shredded-roughened PE (X) Particle size 8.0 mm ≤ x ≥ 6.3 mm305
Appendix B 24: Adsorption capacity of natural crude oil with 0 hr UV weathered PE Particle
size 2.8 mm $\leq x \geq$ 2.0 mm, 75 hr UV weathered PE Particle size 2.8 mm $\leq x \geq$ 2.0 mm and
150 hr UV weathered PE Particle size 2.8 mm ≤ x ≥ 2.0 mm
Appendix B 25: Adsorption efficiency of natural crude oil with 0 hr UV weathered PE
Particle size 2.8 mm $\le x \ge 2.0$ mm, 75 hr UV weathered PE Particle size 2.8 mm $\le x \ge 2.0$
mm and 150 hr UV weathered PE Particle size 2.8 mm $\leq x \geq$ 2.0 mm307
Appendix B 26: Adsorption capacity of natural crude oil with 0 hr UV weathered PE
Particle size 6.3 mm \le x \ge 2.8 mm, 75 hr UV weathered PE Particle size 6.3 mm \le x \ge 2.8
mm and 150 hr UV weathered PE Particle size 6.3 mm ≤ x ≥ 2.8 mm
Appendix B 27: Adsorption efficiency of natural crude oil with 0 hr UV weathered PE
Particle size 6.3 mm \le x \ge 2.8 mm, 75 hr UV weathered PE Particle size 6.3 mm \le x \ge 2.8
mm and 150 hr UV weathered PE Particle size 6.3 mm ≤ x ≥ 2.8 mm
Appendix B 28: Adsorption capacity of natural crude oil with 0 hr UV weathered PE Particle
size 8.0 mm $\leq x \geq$ 6.3 mm, 75 hr UV weathered PE Particle size 8.0 mm $\leq x \geq$ 6.3 mm and
150 hr UV weathered PE Particle size 8.0 mm ≤ x ≥ 6.3 mm
Appendix B 29: Adsorption efficiency of natural crude oil with 0 hr UV weathered PE
Particle size 8.0 mm \le x \ge 6.3 mm, 75 hr UV weathered PE Particle size 8.0 mm \le x \ge 6.3
mm and 150 hr UV weathered PE Particle size 8.0 mm ≤ x ≥ 6.3 mm
Appendix B 30: : Adsorption capacity of Phillip oil with shredded PE (W) Particle size 2,8
$mm \le x \ge 2.0 \text{ mm}$. 6.3 $mm \le x \ge 2.8 \text{ mm}$ and 8.0 $mm \le x \ge 6.3 \text{ mm}$

Appendix C (Chapter 7)

Appendix C 1: Calculations for column Packing density	313
Appendix C 2: Results of the column adsorption experiment with tl	he optimised conditions
by the model (scaled up 5X) for shredded PE (W) and shredded-rou	ighened PE (X)
adsorption for Phillip and Natural crude oils	314
Appendix D Ethics approval	
Appendix D: Converis ethics declaration	315

Chapter 1

1.0 Introduction

Nigeria, is rich in oil, known for its significant economic dependence on the petroleum sector, encounters numerous oil spillage incidents, especially in the South area (Niger Delta) comprising of the states of Abia, Akwa Ibom, Bayelsa, Cross River, Delta, Edo, Imo, Ondo, and Rivers as shown in Figure 1.1 (1). This region also houses the majority of international oil companies. Nigeria extracts approximately 2.5 million barrels of crude oil daily, making it the top oil producer in Africa and the sixth-largest oil-producing nation globally. The country primarily produces light crude oils with low sulphur content, for example, Bonny Light, Antan Blend, Escravos Light, Qua-Iboe Light, Forcados Blend, Pennington Light, and Ukpokiti (2). The harmful effects of crude oil on the environment during extraction, production, illegal bunkering, and transportation, along with frequent natural seepage, rapidly lead to severe devastation in the affected areas. These activities take place frequently, with official records indicating over 900 oil spills in 2023 (Figure 1.2). Such incidents have a profound impact on the relationship between local communities and their natural environment, particularly affecting their primary means of sustenance, which is mostly farming and fishing. The contamination of farmlands due to oil pollution severely diminishes agricultural productivity, while water pollution disrupts fishing activities, leading to a significant loss of livelihood for many individuals in the region. The persistent degradation of land and water resources continues to threaten the long-term sustainability of these traditional occupations.

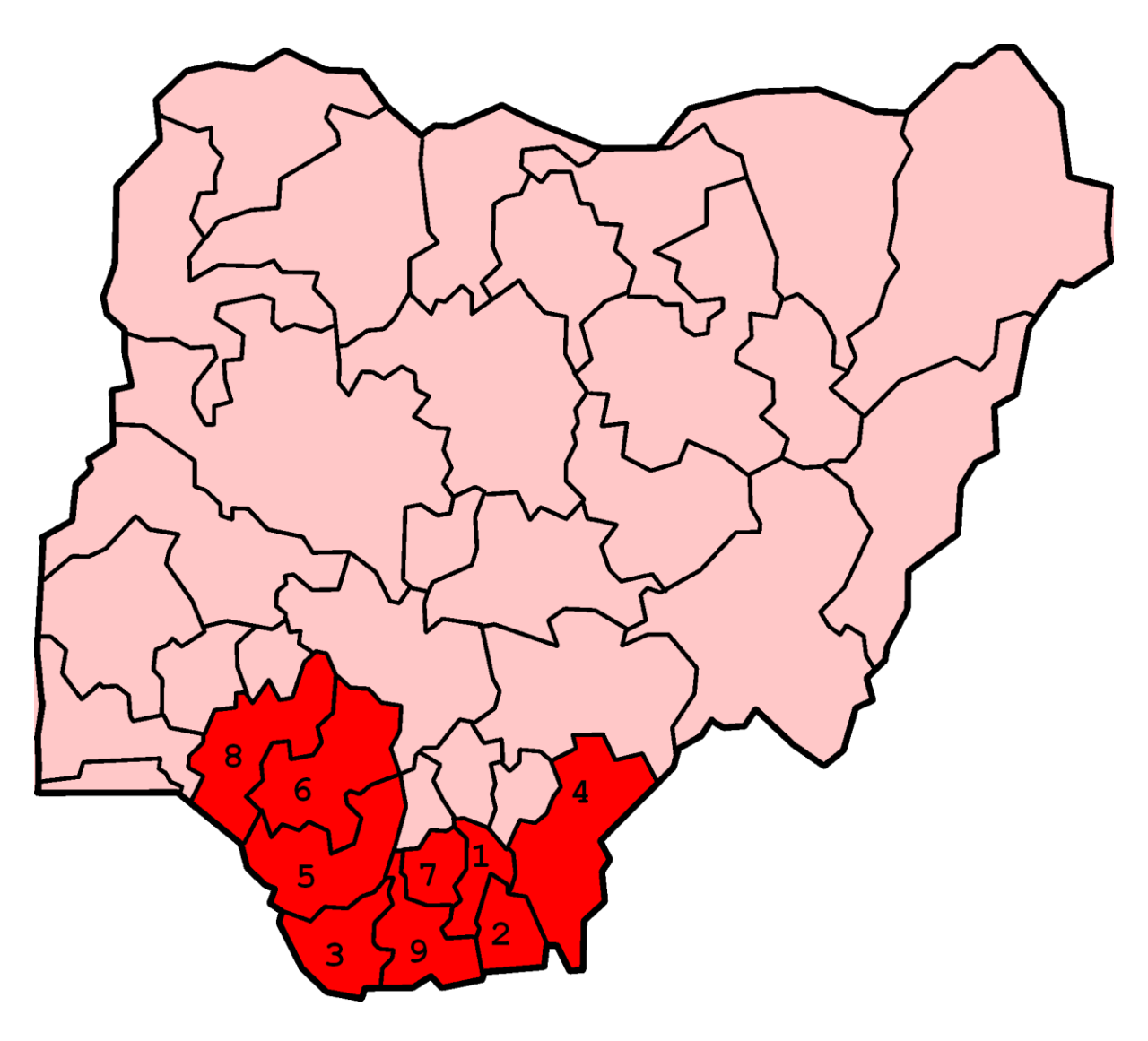


Figure 1. 1:Map of Nigeria showing the Oil Producing States in the Niger Delta Region 1. Abia, 2. Akwa Ibom, 3. Bayelsa, 4. Cross River, 5. Delta, 6. Edo, 7.Imo, 8. Ondo, and 9. Rivers

Source (55)

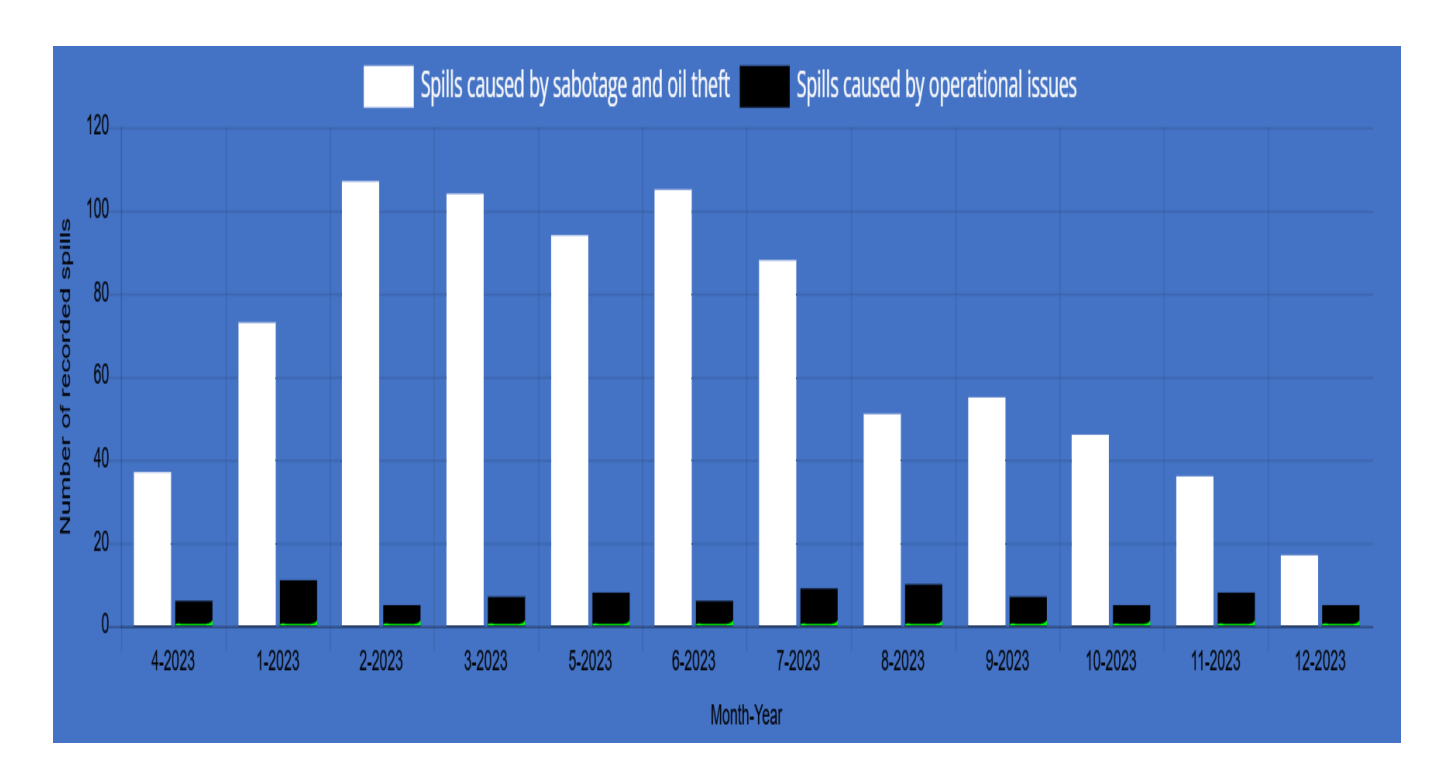


Figure 1. 2: Oil spill data summary recorded by NOSDRA in Nigeria for 2023

Source (56)

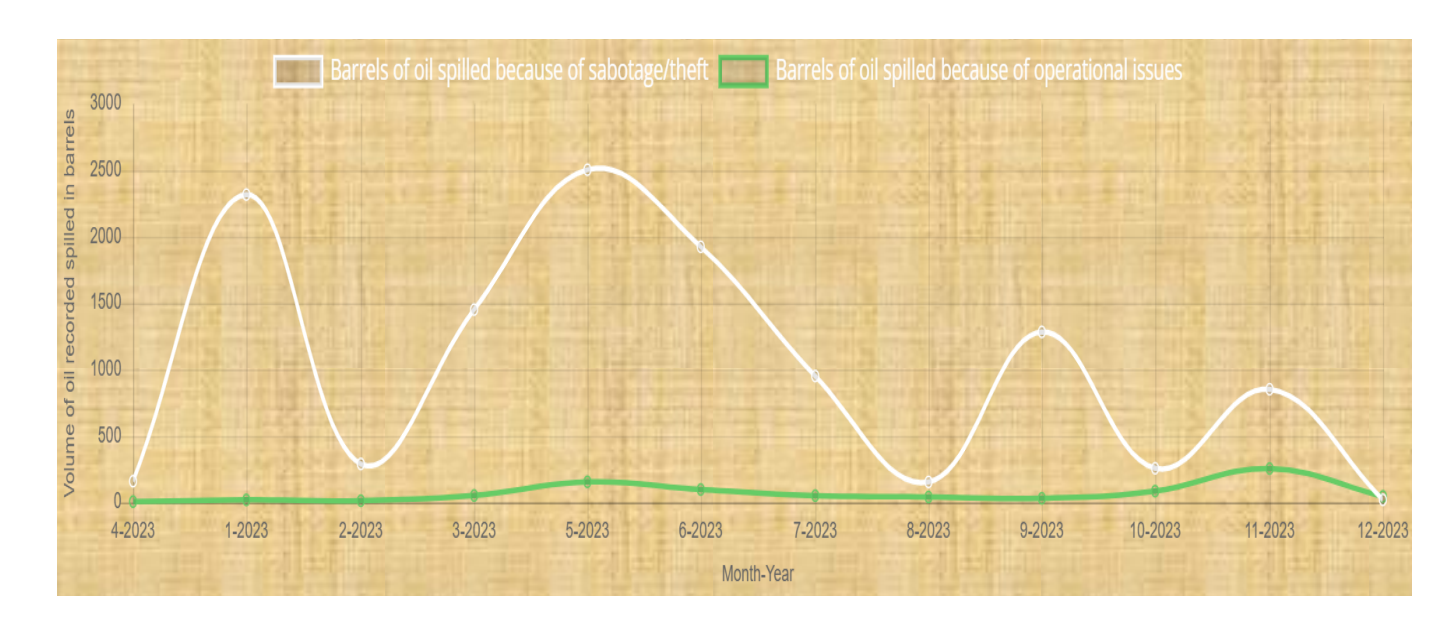


Figure 1. 3: Oil spill data summary recorded by NOSDRA in Nigeria for 2023

Source (56)

1.1 Causes of oil spillage

Oil spillage in Nigeria can be broadly classified into three primary categories based on its causes: natural, human-induced, and mysterious.

1.1.1 Natural Causes

Oil spills resulting from natural causes occur due to environmental and geological phenomena. One significant natural factor is the movement of tectonic plates beneath the ocean floor. When these plates shift, cracks and fissures may form, allowing crude oil to seep to the surface. Additionally, natural disasters can disrupt oil reservoirs or pipelines, leading to unintended oil releases. This form of spillage is an inherent geological process and has been observed in various oil-rich regions worldwide.

1.1.2 Human-Induced Causes

Most oil spills in Nigeria stem from human activities. These spills occur due to several manmade factors, including acts of vandalism, oil bunkering, and sabotage. In some cases, individuals deliberately puncture oil pipelines to illegally siphon crude oil, an activity that often leads to environmental devastation. Furthermore, operational negligence whether by oil industry workers, tanker drivers, or maintenance personnel contributes to oil spillage. Accidental spills can also take place during transportation, drilling, or refining operations. Equipment failure, corrosion of pipelines, and inadequate safety measures further exacerbate the frequency and severity of these spills (Figures 1.4, 1.5, 1.6, and 1.7).

1.1.3 Mysterious Causes

The term "mysterious cause" is used to describe oil spillages whose origins are unclear or difficult to determine. Unlike spills that can be directly attributed to natural geological events or human activities, these occurrences remain ambiguous, often leaving investigators without concrete explanations. Such incidents may result from a combination of undetected leaks, underground seepage, or other unidentified mechanisms. Due to the uncertainty surrounding

their causes, mysterious spills present a unique challenge in terms of attribution and mitigation efforts (34).



Figure 1. 4: On October 12, 2004, oil from a leaking pipeline caught fire in Goi-Bodo, a swampy region of the Niger Delta, Nigeria

Source (154)



Figure 1. 5: Leakage from a suspected sabotaged underground pipeline (56)



Figure 1. 6: Oil spill spreading in a flowing stream Source: Pinterest images



Figure 1. 7: Suspected illegal oil siphoning activities from a pipe transporting crude oil (56)

1.2 Problem statement and motivation

When crude oil enters the marine environment, it undergoes a series of intricate weathering processes that drastically change its composition and behaviour. These processes include dispersion, where the oil spreads into smaller droplets, breaks up and spreads across the water surface due to wave action and currents; evaporation, which causes lighter components to vaporise reducing the volume of the spill but often leaving behind a denser, more viscous residue; and photochemical oxidation, where sunlight triggers chemical reactions that further break down the oil, leading to the formation of new compounds which alter the oil's properties. Additionally, agglomeration leads to the clustering of oil particles, while dissolution allows some components to mix with seawater. Microbial degradation occurs as bacteria break down hydrocarbons, and adsorption causes oil to attach to suspended particles in the water. Over time, these interactions can result in the formation of tar balls, which are dense, sticky residues that persist in the marine ecosystem (10) (Figure 1.8). Each of these processes contributes to the transformation of the spilt crude oil in different ways.

These physicochemical transformations increase the solubility of certain oil components in water, thereby complicating clean-up efforts. Of particular concern is the release of toxic water-soluble aromatic hydrocarbons found in freshly spilt crude oil, which pose significant risks to marine organisms and ecosystems (11). The level of environmental degradation and the success of oil spill remediation largely depend on how quickly and effectively response measures are implemented. Given the severe toxic effects associated with oil spills, it is crucial to have well-established containment and remediation strategies in place to mitigate the impact of such incidents whenever they occur promptly.

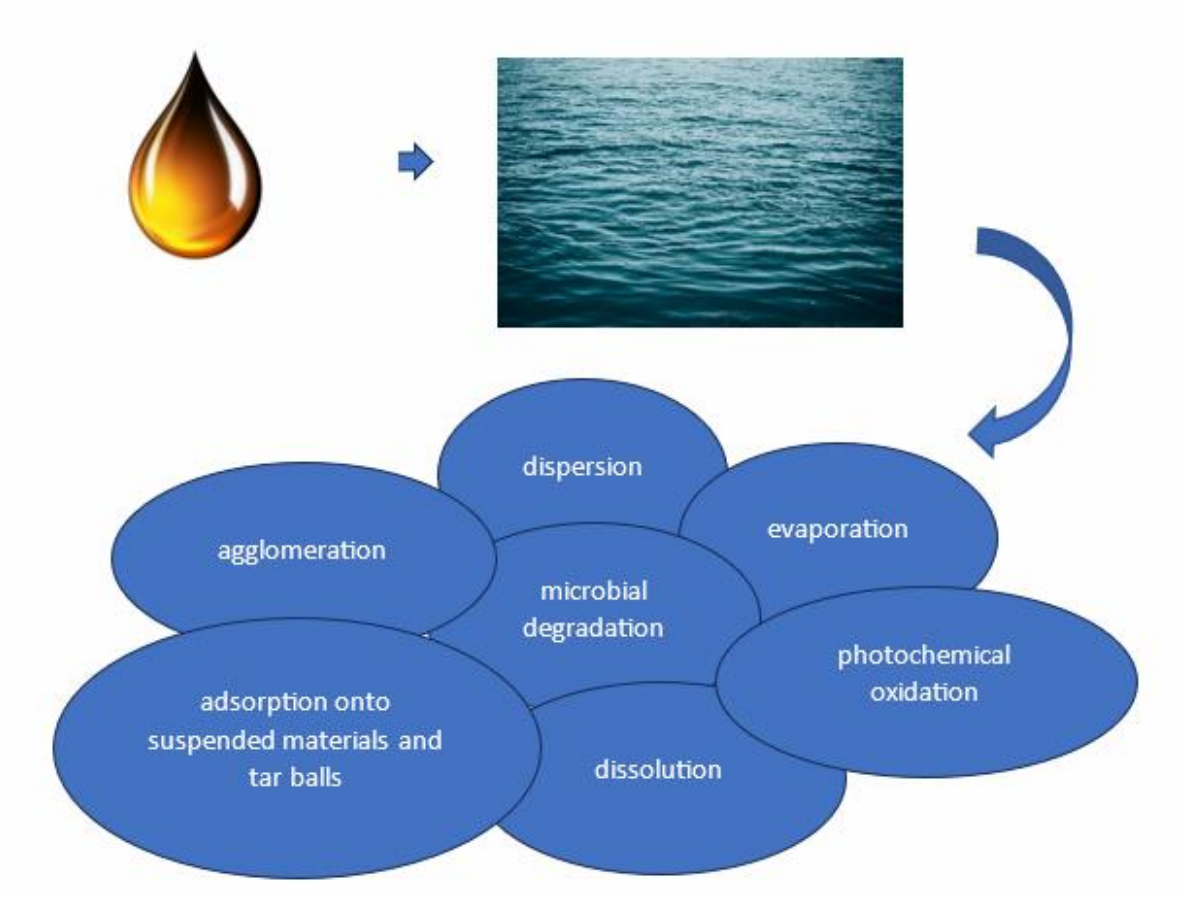


Figure 1. 8: Weathering process of oil on the sea surface

Building on the above considerations and aiming to prevent the further dissolution of oxygenated byproducts resulting from the photo-oxidation of spilled oil on water surfaces, this study focuses on the bulk removal of crude oil from contaminated marine, estuary, and river environments.

Numerous researchers have explored the use of polymeric waste materials, such as high-density polyethylene (HDPE) bottles and recycled polyethylene terephthalate (rPET), as sorbents for oil spill remediation (8). However, there is a notable gap in detailed scientific investigations specifically examining the effectiveness of low-density polyethylene (LDPE) for crude oil sorption. This study seeks to address that research gap.

For this research, polyethylene (PE) water sachets commonly referred to as "pure water sachet polyethylene" were repurposed to develop an oil sorbent. The ideal characteristics of an effective oil spill sorbent include rapid oil absorption, high sorption capacity, superior

selectivity for oil over water, minimal water uptake, low density for enhanced buoyancy, and cost-effectiveness (5).

1.3 Combining the Problem of Plastic Pollution to Remediate Oil Spillages.

Various remediation techniques have been employed to restore water bodies contaminated by oil spills. These methods include the use of oil booms and skimmers to contain and collect oil, bioremediation to enhance microbial degradation, in-situ burning to rapidly eliminate surface oil, and the application of sorbents to absorb spilled oil. Other approaches involve hot water and high-pressure washing to remove oil residues, chemical dispersants to break down the oil into smaller droplets, and manual labour for physical clean-up efforts.

Among these existing oil spill response methods, sorbents are considered one of the most efficient and cost-effective technologies for oil removal. Sorbents are materials that absorb or adsorb oil from the water surface, preventing further spread and environmental damage. They are generally categorised into three main types: natural organic sorbents (such as peat moss, sawdust, and straw) (5), inorganic sorbents (including materials like vermiculite, clay, and perlite) (6), and synthetic sorbents (such as polyurethane foam, polypropylene, and polyethylene-based materials) (7). Each type varies in sorption capacity, biodegradability, and suitability for different spill conditions.

An ideal oil sorbent should possess several key characteristics to ensure optimal performance in spill remediation. Given the desirable attributes for optimal performance, researchers continue to explore innovative sorbent materials that can enhance the efficiency of oil spill cleanup while simultaneously addressing other environmental challenges.

This study focuses on developing sorbents derived from waste water polyethylene sachets (WWPS), a material classified under synthetic sorbents. Waste water polyethylene sachets, commonly used for packaging drinking water, contribute significantly to plastic pollution due to their widespread disposal and persistence in the environment. By repurposing these sachets as oil sorbents, this research aims to provide a dual-benefit solution—reducing plastic waste while effectively mitigating the environmental damage caused by oil spills. Polyethene's inherent hydrophobic properties and adaptable structural form holds great potential as a cost-effective and efficient material for oil removal from water surfaces.

1.4 Aim and Objectives

The primary aim of this research is to investigate the potential of polyethylene waste disposed of in the environment (and from proposed collection schemes) as an effective and fast-acting sorbent for the clean-up of crude oil-polluted water, while also exploring mechanisms of oil recovery and reuse after remediation.

The main objectives of this study include;

- (i) To characterise different types of waste polyethylene sachets using techniques such as FTIR, DSC, SEM, TGA, and contact angle measurements, and to evaluate the adsorption performance of modified PE (mechanically treated and UV-weathered) for crude oil removal.
- (ii) To characterise crude oil samples (artificial crude oil and Bonny light crude oil) to determine their composition and properties that may influence adsorption behaviour.
- (iii) To develop and apply a process model using Response Surface Methodology (RSM) to identify and optimise key process variables affecting the oil adsorption performance of the PE-based sorbent.
- (iv) To explore recovery and reuse strategies for the oil-loaded sorbent, including sorbent regeneration, oil recovery potential, and assessment of the practical viability of the remediation process.

Chapter 2

2.0 Literature Review

This chapter describes research work previously carried out to develop various types of materials for oil spill clean-up. Some of these materials are reviewed according to their various classifications within the industry. Other instances include where they have been applied in global oil spillage incidents; their benefits, significances, and weaknesses are discussed extensively alongside the proposed sorbent.

2.1 Methods used in the management and remediation of crude oil-polluted water.

There are many ways to clean up oil-polluted water. The current remediation techniques are classified into: (a) physical (b) chemical (c) biological and (d) thermal (57).

2.1.1 Physical Remediation Methods

Physical remediation techniques are commonly utilised to manage oil spills in aquatic environments. These methods function primarily as containment barriers, preventing the further spread of spilled oil while preserving its original physical and chemical properties. By acting as a first line of defence, they help to control the movement of oil on the water surface, making it easier to recover and remove. Several types of physical barriers are employed in oil spill management, including: booms, skimmers and sorbent materials. Physical remediation techniques are widely employed to manage oil spills in aquatic environments. These methods primarily serve as barriers to contain and control the spread of spilled oil without altering its physical or chemical properties. These physical methods play a crucial role in oil spill response efforts, effectively limiting environmental contamination and facilitating subsequent clean-up processes.

2.1.1.1 Booms

Booms are a common type of oil spill response equipment which contain and deflect the oil spill passage away from sensitive resources or to a collection/recovery point (Figure 2.1) (59). They are floating barriers designed to contain and prevent the further spread of oil on the water surface.

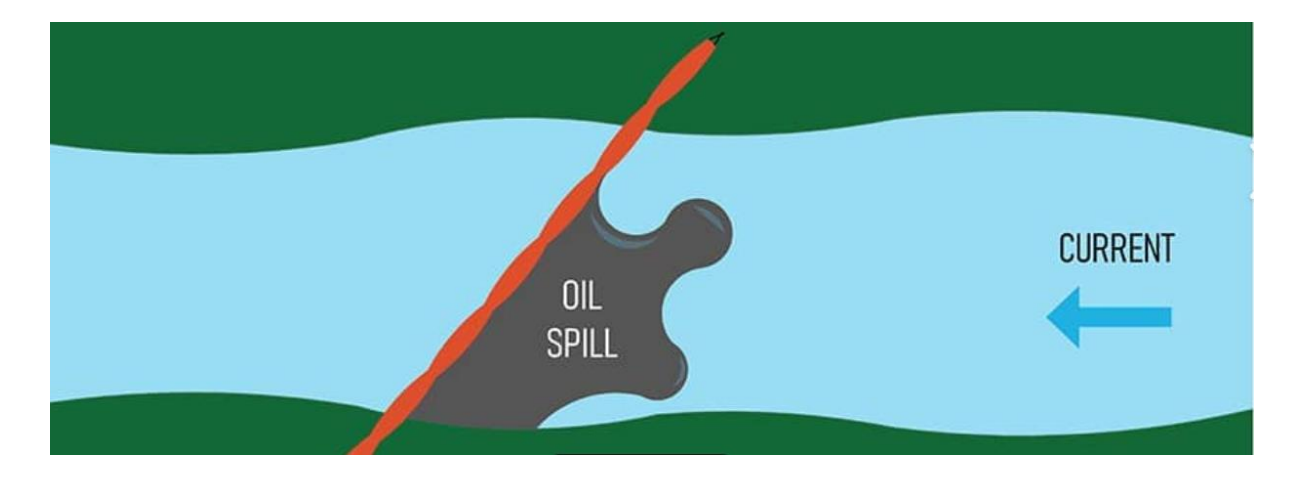


Figure 2. 1: How oil spill containment boom contains spilt oil on water Source: (143)

There are 2 types of booms

- (i) Containment Booms
- (ii) Absorbent/adsorbent Booms

(i) Containment Booms

Containment booms are designed to control the spread of oil, guide and channel oil slicks along specific pathways, and facilitate the removal of spills from the water's surface. These booms are also effective for containing spills on land. Containment booms are further classified into three main categories:

- (a) Fence Booms These are rigid or semi-rigid floating barriers that create a vertical screen to contain oil, with approximately 60% of their structure submerged and 40% above the water surface. Fence booms are light in weight, easy to manage, and simple to store, making them suitable for use in calm waters. They also come with certain limitations, such as limited stability in strong winds and fast currents, reduced manoeuvrability when being towed, and lower effectiveness in rough, high-wave environments.
- (b) Curtain Booms: These are flexible, non-absorbent floating structures featuring a foamfilled chamber above water and a submerged skirt for containment. Constructed from

materials such as polyurethane, polystyrene, bubble wrap, or cork, curtain booms offer superior performance compared to fence booms, particularly in offshore environments and towing operations. However, they can be challenging to clean and store after use.

(c) Fire-Resistant Booms: These booms are made from fireproof metals and are specifically designed to facilitate in-situ burning of oil spills at temperatures up to 1093°C. They are available in different types, including water-cooled, stainless steel, thermally resistant, and ceramic fire-resistant booms. While highly effective in preventing oil fires from reaching shorelines, they are typically heavy, costly, and difficult to tow (128).

(II) Absorbent/Adsorbent Booms

Absorbent/adsorbent booms (Figure 2.2) serve a dual function, they contain the spread of oil while simultaneously absorbing or adsorbing free-floating oil from the water's surface. These booms contribute to the rapid recovery of contained spills and can be deployed both on water and on land.

.



Figure 2. 2: Improvised adsorbent boom constructed from netting and straw Source: (59)

2.1.1.2. Skimmers

Skimmers (Figure are mechanical devices used to remove oil from the water's surface by skimming and collecting it. According to Dave et al. (112), they are often used alongside booms to extract oil without altering its properties, allowing for reprocessing and potential reuse. These devices can be self-propelled, shore-based, or vessel-operated, making them adaptable to various settings.

Skimmers are categorised into three main types: weir skimmers, oleophilic skimmers, and suction skimmers. Their efficiency depends on factors such as oil type, viscosity, thickness, debris presence, environmental conditions, and weather. While skimmers perform best in calm waters, their effectiveness can be reduced by floating debris.

Types of Skimmers:

(a) Weir Skimmers

Weir skimmers function similarly to small dams, collecting floating oil through gravity-assisted separation before transferring it to storage tanks. These skimmers are highly stable in wavy conditions and are particularly effective for removing low-viscosity, non-emulsified oils. However, they are less efficient when dealing with emulsified oil and are susceptible to clogging due to debris accumulation.

(b) Oleophilic Skimmers

Oleophilic skimmers are designed using oil-attracting materials such as disks, drums, belts, brushes, and ropes. These materials enable the recovery of up to 90% of spilt oil by allowing it to adhere to their surfaces before being scraped or squeezed off. Oleophilic skimmers are versatile and can function effectively in various environments, including debris-filled and icy waters. However, they are ineffective when dealing with oil that has been mixed with chemical dispersants and often requires manual removal of debris to maintain their efficiency.

(c) Suction Skimmers

These skimmers utilise vacuum pumps or air-venturi systems to draw oil into storage tanks. These skimmers are highly effective for oils of different viscosities, making them particularly useful for beach clean-ups, confined spaces, and offshore recovery when deployed alongside booms. Despite their effectiveness, suction skimmers have several drawbacks; they are prone to clogging, require skilled operators, and pose safety risks

when dealing with flammable oils, as the suction process can create conditions that increase the risk of explosions (112).

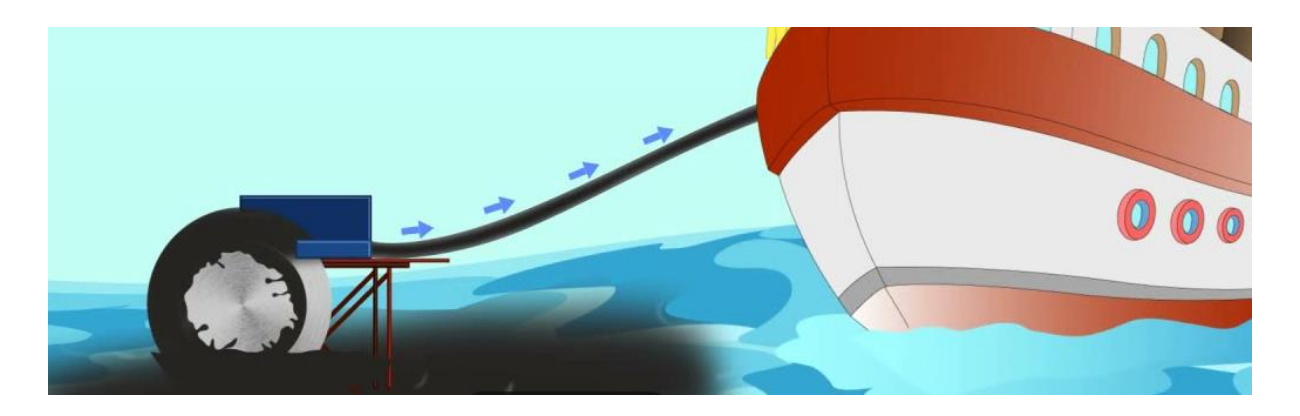


Figure 2. 3: How skimmers work in recovering spilled oil on the surface of water

Source: oil booms for oil spills - Search Images (bing.com)

2.1.1.3. Sorbent materials

Oil sorbents are specialised, water-insoluble materials or composite substances engineered to recover liquid contaminants using absorption, adsorption, or a combination of both processes. Absorption occurs when the sorbent takes in oil into its internal structure, while adsorption involves oil adhering to the material's surface.

These sorbents are widely regarded as one of the most efficient and cost-effective solutions for oil spill remediation, especially in shoreline clean-ups where other techniques may be less practical (20). Hydrophobic sorbents are highly valued for their effectiveness in oil spill response, as they selectively absorb oil while repelling water. They play a critical role in mitigating environmental damage by capturing and containing spilt oil, thereby preventing further spread. These components are commonly employed either as a primary method for recovering oil floating on water or as a final cleanup step after mechanical skimming operations.

The efficacy of sorbents in oil spill clean-up depends on several key properties, including their oil sorption capacity, buoyancy, and reusability. Sorbents are typically applied in different forms based on the nature and extent of contamination. They may be distributed as loose granules or powders, integrated into woven or felted fabrics, or deployed as booms, where

the sorbent composition is enclosed within long mesh tubes to contain and absorb the oil effectively (57, 111).

Researchers classify sorbents used for remediating of crude oil-contaminated water into three main categories (a) natural organic sorbents(b) natural inorganic sorbents and (c) synthetic sorbents (17, 18, 19).

Table 2.1 summarises some of the basic properties of these sorbents (50, 112). The table shows that each type of sorbent has trade-offs in terms of cost, efficiency, reusability, and environmental impact.

Table 2.1: Properties of some sorbent materials

Type of	Sorption	Reusability and	Advantages	Disadvantages	Reference
sorbents/structure	capacity	recovery method			
	g/g				
Natural organics			Applied to sorb	Labour intensive	
Cotton fibre	30 - 40	3 cycles	all types of oil	Applicable only in	
(fibre)		(centrifugation,	Inexpensive	certain weather	
		mechanical pressing		conditions	
		and squeezing)		Problem of disposal	
					50, 112, 129
Rice husk	4.6 - 6.7	5 cycles	Readily available	They adsorb water	
(shredded fibrous)		(centrifugation,	oil recovery is	along with oil and	
		mechanical pressing	possible to an	sink	
		and squeezing)	extent		
Natural inorganics				Application is labour	
Clay (granular)	2.1 – 7.2	Not reusable	Can be used to	intensive and only in	
			sorb all types of	certain weather	25, 26, 27,
			oil	conditions	50,112
	40 —				
	42.75		Inexpensive	Disposal problems	

Magnetic		3 cycles (vacuum	Readily available	Potential health risk	
exfoliated		and air pump			
graphite (granular)		filtration)			
Synthetic					
materials	10 – 16	30 cycles (vacuum	Can be used to	Expensive	
Polypropylene		squeezing followed	sorb all types of	Effective as final	
(porous discs)		by swelling)	oil	clean up step	
			Inexpensive	Labour intensive	
			High hydrophobic	Applicable only in	
			and oleophilic	certain weather	
			properties	conditions	50, 112
Macroporous			No maintenance	Disposal problems	
butyl rubber	15 - 23		required	Non-	
(porous discs)			Simple operation	biodegradability	
				Storage problems	
				because it occupies	
				space	

(a) Natural organic sorbents

These are plant-based materials such as peat moss, sawdust, and cotton. Their natural hydrophobicity and oleophilicity make them effective in absorbing oil while repelling water. However, their oil sorption capacity can vary based on their specific structure and composition. These can include peat moss, kapok, cotton, sawdust, vegetable fibres, milkweed, straw, fibre, corn cobs, peat moss, , sugarcane bagasse, root, coconut shells and rice husks (57).

Choi and Cloud (114) reported that milkweed sorbed about 40 g of crude oil/g from the surface of a simulated seawater polluted with crude oil. From their results, the oil adsorption of kapok fibre used in a mat, block, band, or screen sorbed 11.1 g/g of B-heavy oil (a blend of

crude oil from various sources) and 7.8 g/g of machine oil (lubricant) in water. This study also reported that oil sorption capacity of cotton fibre was lower than milkweed floss, but did not mention the specific amount for the adsorption capacity. The large amount of wax can explain the exceptionally high oil sorption by milkweed fibre on the fibre surface, and the larger and non-collapsing fibre lumen, which gives more void volume for absorbed oil. The efficiency of sorbent reusability was determined by the oil sorption capacity of each sorbent after repeated sorption and desorption cycles of only 3 cycles, so it was not mentioned approximately how many times/cycles the materials could be reused. All the above-mentioned are organic sorbents and they have a high rate of water sorption and sinking. Banerjee et al., (11) reported that sawdust achieved a maximum adsorption capacity of 3.6 g/g while oleic acid grafted sawdust achieved 6 g/g within 5 minutes. The reusability of the material was not reported. Ghaly et al. (67) in their work, using Peat moss to adsorb oil from water, reported a maximum adsorption of 6.7g/g for peat moss.

Tijani et al (151) in a study examined the oil sorption capacity of three different types of straw: oat, wheat, and barley. The findings indicated that barley straw, with an average particle size ranging from 150 to 1000 mm, exhibited the highest oil sorption capacity at approximately 6.07 g/g. Oat and wheat straw, both with an average particle size of 425 to 600 mm, demonstrated oil sorption capacities of around 5 g/g and 5.49 g/g, respectively. Furthermore, the results revealed that oat straw maintained its effectiveness over multiple cycles, showing only an 18.45% reduction in absorbency after six reuse cycles.

In the work by Nwadiogbu et al. (113) on using corn cobs, chemically modified with acetic anhydride to make them suitable sorbents by increasing their hydrophobicity. The acetylation successfully increased the hydrophobicity of the corn cobs, giving a higher oil sorption capacity (0.0768 mg/g) and faster sorption compared to the raw corn cobs with a sorption capacity of 0.0043 mg/g. With these reported values, their adsorbing capacities are typically very low compared to other sorbents. Jintao et al. (64) used kenaf balls containing coiled kenaf fibres to sorb oil in a different assembly. These kenaf balls, weighing between 0.2 g and 10 g, were reported to sorb up to 1000% of their weight, and in some cases, the value reached up to 1800%. Their major disadvantage was that they could not be reused for another cycle of sorption, all the kenaf balls had to be burnt or could be dumped into a landfill. The sorption ability of loose natural wool fibres (NWF) and recycled wool-based nonwoven material

(RWNM) was assessed by Rajakovic et al. (21). They demonstrated that a high sorption capacity was achieved with wool-based sorbent (5.48 g/g for RWNM and 5.56 g/g for NWF). They argued the reason for the good sorption capacity of NWF could be the presence of grease (lanolin) and waxes on the surface of raw wool fibres.

Natural sorbents are cheap, abundant, ecologically friendly and readily available, but all these organic sorbents become water-wet and sink [1]. Another major disadvantage for the natural organic adsorbents are that they are labour-intensive, difficult to collect after use in oil spills and are difficult to dispose of. Moreover, a rise in demand for these materials could threaten their availability, particularly due to their seasonal nature (129).

(b) Natural inorganic mineral sorbents

These are fine-grained minerals, either in their raw form or processed, that are used for oil spill remediation. Unlike organic sorbents, these materials generally function through adsorption (where oil adheres to the surface of the particles) rather than absorption (where oil is soaked into the material). Certain inorganic sorbents are specifically designed to sink floating oil, while others can be modified to improve their oil retention capacity. Examples of these materials include stearate-treated chalk, silicone-coated pulverized fly ash, zeolites, graphite, activated carbon, organoclay, silica (sand), silica gel, clay, glass, vermiculite, and volcanic ash (20; 24).

Research indicates that natural inorganic sorbents like clay, alumina-phosphates, zeolite, silica, and alumina have oil sorption capacities ranging from 4–20 g/g. However, their buoyancy properties are limited which can affect their performance in aquatic environments (150).

Rajakovic et al. (21) used sepiolite to adsorb oil from waste water and adsorption of 0.19 g/g was recorded. Natural inorganic sorbents are less commonly used due to several drawbacks, including seabed pollution, low retention capacity, high costs, and excessive density, making transportation challenging. Additionally, loose materials like clay and vermiculite are difficult to apply in windy conditions and pose potential health risks if inhaled (25; 26; 27; 112).

(c) Synthetic adsorbents

Synthetic adsorbents, made from high-molecular-weight polymers, are the most commonly used commercial sorbents due to their low cost, ease of use, durability, reusability, and non-

polar nature. Examples include polyethylene, polyurethane, polypropylene, polyester foam, and polystyrene, which exhibit excellent hydrophobic and oleophilic properties with high sorption capacity. These sorbents are available in various forms, such as sheets, rolls, booms, or powders for direct application on water surfaces (18).

Teas et al. (18) reported that polypropylene had an oil adsorption capacity of 4.5 g/g light cycle oil or light gasoline oil. Lee et al. (66) discuss the development of electrospun fibrous matrices made from polyolefin materials (LLDPE), to create fine fibres with a large surface area, and embedded with magnetic nanoparticles. Its equilibrium absorption capacity for crude oil was 34.12 ± 1.96 g/g, but it is a single-use sorbent and cannot be reused. Its production process and cost are also complex and expensive to produce.

Also, Lin et al. (29) investigated the oil sorption efficiency of tyre powders for oil spill remediation. Their findings confirmed that tyres are oleophilic, capable of absorbing up to 2.2 g/g of oil, and highly reusable, though no specific reuse figures were provided. However, tyres are non-biodegradable and may release harmful chemicals, including polycyclic aromatic hydrocarbons (PAHs) and phenolic compounds (e.g., bisphenols), raising environmental concerns regarding their use in oil spill remediation (114).

Hailan et al (132) in their work, used recycled LDPE processed into foam (foam 1) to adsorb crude oil, and an adsorption capacity of 4-5g/g was achieved. They also formulated foam 2 from recycled LDPE-based foams initially used for various packaging, and after going through some modifications, achieved an adsorption capacity of between 8-12g/g for crude oil with about 10 cycles of reuse.

Some researchers have carried out various works using LDPE powders and LDPE pellet wax after going through some plasma and physical modification, and were able to achieve less than 0.10g/g adsorption capacity for crude oil (131) with limited use.

Hailan et al (96) in another work, physically and chemically modified polyethylene wax and was used for crude oil adsorption and achieved an adsorption capacity of 3.4 \pm 0.2 g/g, with only a single use

2.1.2 Chemical remediation methods

Chemical methods are often combined with physical techniques in marine oil spill response to contain spills and protect shorelines and marine ecosystems. These chemicals alter the physical and chemical properties of oil, improving clean-up efficiency (14).

The primary chemicals used in oil spill control are summarised in Table 2.2. The chemical dispersants are formulated with surfactants for oil breakup, solvents for dilution and handling, and stabilizers for chemical and environmental stability.

Table 2. 2: Functions and categories of chemical dispersants

Component	Function	Categories	References
Surfactants	Facilitates oil dispersion,	Ionic: Function like soaps, acting	
	increasing surface area	as colloidal electrolytes.	
	for microbial breakdown	Non-ionic: Contain weak	112
		solubilizing groups like ether	
		linkages or hydroxyl groups.	
Solvents	Dilutes dispersants to	Petroleum hydrocarbons: These	
	lower viscosity, depress include mineral spirits, kerose		
	freezing points and	No.2 fuel oil, heavy aromatic	112
	optimise concentration.	naphthas b.p >150°C	
		Alcoholic/hydroxyl group	
		compounds: consists of	
		alcohols, glycols, glycol ethers	
		and water	
Stabilisers	Regulates pH and colour,	Polycarboxylates, Tritom [™] , LTSA-	
	prevents corrosion, and	35 MIL	112
	enhances hard water		
	stability.		

- (i) Dispersants Surfactant-based solutions that break oil slicks into smaller droplets, promoting dilution and biodegradation in the water column. They are typically sprayed and mixed by wind or boat propellers. Common dispersants include Slickgone NS, Neos AB3000, and Corexit products. They are effective in rough seas and areas where mechanical recovery is not possible, as they prevent oil from sticking to surfaces and accelerate biodegradation by increasing the oil's surface area. However, their flammability poses health and environmental risks, and they can contribute to shoreline fouling and drinking water contamination (28;12;51;112).
- (ii) Solidifiers: Solidifiers are hydrophobic polymers that transform liquid oil into a solid, rubber-like material, making it easier to remove. They can be applied as dry particulates or in forms like pucks and pads. Solidifiers work best in moderately rough seas, where wave action aids mixing. While they offer an alternative to dispersants, their lower efficiency and the large amount required for effective solidification (16-200% of the oil's mass) have limited their use in the past (28;109).

2.1.3: Bioremediation method

In bioremediation microorganisms are used to degrade hydrocarbons, restoring environmental quality by accelerating natural attenuation. In marine oil spills, microorganisms capable of degrading hydrocarbons are abundant. Alkanes (C10-C26) and lower-molecular-weight aromatics are the most easily degraded. Branched alkanes and higher-molecular-weight aromatics are more resistant. Bacteria, such as Pseudomonas and Vibrio, dominate the degradation process. Biodegradation is influenced by factors like nutrient availability, oil concentration, time, and natural degradation progress. Nutrients like nitrogen and phosphorus are often scarce, slowing biodegradation. Additionally, high oil concentrations can cause a lag phase in the process. Environmental factors, such as temperature and oxygen, also play significant roles.

To enhance bioremediation, bioaugmentation (introducing hydrocarbon-degrading microorganisms) and biostimulation (adding fertilizers or dispersants) are applied. While

bioaugmentation has shown limited success due to competition with indigenous species, biostimulation with nutrients has proven effective, although its efficacy decreases for extensively degraded oil. Surfactants and dispersants can increase the bioavailability of oil to microbes. Despite concerns about eutrophication, studies by Atlas and Bartha (137) and Atlas (136) found that oleophilic fertilizers do not trigger harmful algal blooms or cause acute toxicity. However, some complex components of crude oil are not biodegradable, and their accumulation can harm marine life.

Bioremediation offers an environmentally friendly and cost-effective approach to oil spill treatment, but it has limitations. It requires long treatment times, and microbial tolerance to high concentrations is low. The method depends on environmental conditions, available nutrients, and the type of hydrocarbons present, making it difficult to evaluate its efficiency for all spills. Furthermore, bioremediation does not recover oil and is more effective in the presence of indigenous microorganisms (136; 112).

2.1.4: Thermal remediation method

In Situ Burning is a rapid oil spill cleanup method requiring minimal equipment, effective since the 1960s, especially in ice-covered waters and spill-affected areas. It works best in calm winds for fresh oils and light refined products, minimizing harm to marine life.

However, residual ash may sink and contaminate groundwater but can be removed mechanically. Oil thickness and oxygen supply determine efficiency, with burning agents (gasoline, light crude) and wicking agents (straw, silica) enhancing the process.

Despite its effectiveness, in situ burning has limitations, including the risk of flashbacks, secondary fires, and the potential environmental and health hazards from the byproducts of burning. It can also impact nearby vegetation and aquatic life, causing long-term alterations. Additionally, no oil recovery occurs with this method, and it is best suited for open water (112).

In summary, each method varies in efficiency, cost and environmental impact as shown in Table 2.3. Physical and biological methods are more environmentally friendly, while chemical and thermal methods pose greater risks despite being effective in specific scenarios.

Table 2. 3: Features of different oil spill clean-up techniques
Source (57)

Classification	Advantages	Disadvantages	Cost	Environmental impacts	References
Physical methods or Mechanical	Effective oil spill removal Easy and straightforward operation Minimal secondary pollution	Time-consuming and labour intensive	Medium/low	Environmentally friendly, high biodegradability (organic sorbents) and non-biodegradability (inorganic and synthetic sorbents)	57
Chemical	Easy operation for oil spill removal Effective for large spill areas	Little influence on high- viscous oil Low effectiveness	High	Causes harm to aquatic organisms	57
Biological	Highly effective in oil spill removal	Not effective for large oil spill and no oil recovery	Low	Eco friendly	57, 112, 136
Thermal	Rapid oil spill removal	Safety level is of great concern	Low	They leave behind highly-viscous residues and harmful emissions after use, and no oil recovery	57, 112

2.2 Global oil spill disasters and remediation methods deployed.

Several major oil spills have highlighted the necessity of using multiple clean-up methods, as no single approach is sufficient for managing large-scale spills. Some examples are discussed below.

(i) The Deepwater Horizon (BP) oil spill in the Gulf of Mexico in 2010 which persisted for 87 days and resulted in the release of approximately 4.9 million barrels of crude oil. The spill affected a 100-mile stretch of coastline, causing severe environmental damage and leading to the loss of 11 workers and around 25,000 birds. Various clean-up techniques were employed to mitigate the impact. These included skimmers for oil removal, floating booms to contain the spread, and controlled burning to reduce surface oil. Additionally, 1.84 million US gallons (7,000 m³) of Corexit dispersant were applied, which led to the formation of persistent emulsions that were difficult to clean. BP also introduced a synthetic sorbent material, commonly referred to as "paper towels", designed in sheet form to absorb oil. Furthermore, organic sorbents were also utilised as part of the clean-up strategy, demonstrating the need for a multifaceted approach to oil spill response (Figure 2.4).



Figure 2. 4: Deepwater Horizon oil spill: beach cleanup (Workers contracted by BP cleaning up oil on a beach in Port Fourchon, Louisiana, May 23, 2010)

Source: (142)

(ii) The Exxon Valdez oil spill, which occurred in Prince William Sound, Alaska, in 1989, is regarded as one of the most severe environmental disasters in history. Approximately 11 million gallons of crude oil were released into the surrounding waters, causing widespread ecological damage. The spill led to the loss of numerous marine species and had long-lasting effects on the local ecosystem. A range of clean-up methods was implemented at various stages, including the use of booms to contain the oil, dispersants to break it down (Figure 2.5), and in-situ burning to reduce surface contamination. However, some techniques proved ineffective due to the formation of emulsions caused by the cold weather conditions (152). Additionally, pom-poms (hanks of polypropylene fibers) were utilised as a part of the clean-up efforts, as depicted in Figures 2.5 and 2.6.



Figure 2. 5: A Coast Guardsman checks oil recovery mesh from the Exxon March 28, 1989

Source (144)



Figure 2. 6: Pom poms fibres attract and hold heavy oils used in the Exxon Valdez oil spill Source:(144)

(iii) The Ixtoc I oil spill occurred in the Bay of Campeche, Gulf of Mexico, from June 3, 1979, to March 23, 1980, as a result of a wellhead blowout, releasing approximately 3 million barrels of crude oil (Figure 2.7). The clean-up efforts included the application of naturally derived, treated peat-based sorbents and Corexit 9527 chemical dispersants. However, dispersants were not utilised in the U.S. waters affected by the spill due to their ineffectiveness in treating weathered oil. Ultimately, the on-scene coordinator (OSC) requested that Mexico halt the use of dispersants north of 25°N to prevent further environmental complications.



Figure 2. 7: Ixtoc I oil spill; the oil well blow out Source: (145)

- (iv) In 1993, the Braer oil spill released approximately 85,000 tons of Gullfaks crude oil after the ship lost power due to a broken pipeline on deck. Strong hurricane winds drove the vessel aground on the southern tip of Shetland. The response strategy mainly involved chemical dispersants. It was estimated that 85% of the oil dispersed into the water column, 14% evaporated, and only about 1% reached the shore (138).
- (v) Similarly, the MT Solar 1 oil spill occurred on August 11, 2006, when the tanker, carrying over two million liters of bunker fuel, sank during a storm approximately 20.5 km off the southern coast of Guimaras, Philippines. The spill released 2,100 tons of intermediate fuel

oil, severely impacting 124 km of coastline, mangroves, and tropical habitats. Locals attempted cleanup efforts using improvised sorbent booms and pads made from organic origins, but these proved less effective than commercial sorbents. Cleanup activities in severely affected areas, such as Barangay La Paz, faced additional challenges, including the management and disposal of spent sorbents and oil-contaminated debris. The plastic bags used for storage deteriorated under sunlight, causing oil leakage. Ultimately, much of the oil-contaminated and spent sorbents were moved to cement plants for use as alternative fuel or raw material (50).



Figure 2. 8: Clean up in Barangay La Paz with locally made sorbents

Source: (146)

(vi) The 1996 Sea Empress oil spill released 72,000 tons of crude and heavy fuel oil near Milford Haven Bay. Cleanup efforts included suction equipment, excavators, absorbents, water flushing, and manual methods. These measures effectively reduced fish mortality and limited shoreline contamination. Local volunteers also contributed significantly to the response as the assemblies were sometimes created locally by these volunteers (138, 50).

2.2.1 The proposed sorbent for oil spill clean-up - used-water sachet polyethylene

The above major spills incidents highlight the need for effective and efficient methods for oil spill remediation to minimise the impacts on the environment. They are also highly important for local, smaller-scale oil spills. The proposed sorbent developed herein (used-water sachet polyethylene) is modified to be more effective by increasing the surface area and relying on its oleophilic nature to enhance the oil removal process. Shredding and roughening processes are employed to create fine flakes with a large surface and contact areas, thus optimising the oil adsorption capabilities and preventing of the adsorbed oil from being released or escaping. The van der Waals force and intermolecular interactions involved render the oil to the particle surface. Due to better chemical and physical compatibility between oil and polyethylene flakes surface, the oil will more easily overcome the energy barrier to adsorb onto the flakes (23). The proposed sorbent can be produced and utilised by locals, who are the most affected by these catastrophic events which occur too often. It is intended that its use should be part of a comprehensive oil spill response plan, including containment, and recovery in the oil-producing areas.

The use of the sorbent and the recycling or disposal of the collected oil-saturated materials will be carefully managed since the process relies on physical adsorption (physisorption). Physisorption occurs due to the accumulation of molecules at an interface driven by weak intermolecular forces, such as Van der Waals interactions. Consequently, the adsorption efficiency decreases with increasing temperature, as the weak forces are more easily disrupted.

This highlights the importance of tailoring the design and treatment of sachet water polyethylene materials to suit specific applications and environmental conditions. For instance, the sorbent could be deployed in loose form for direct oil collection, stacked in columns for adsorption systems, or encased in a structure for controlled applications. The versatility of this material design highlights its potential for various oil spill remediation scenarios.

2.3 Adsorption technology

Adsorption is a physical process where contaminants transition from an aqueous solution to a solid adsorbent surface, which can then be regenerated and reused. This technique is widely regarded as one of the most effective and cost-efficient methods for removing crude oil from water bodies. Adsorption as an oil spill clean-up method is a surface-based phenomenon (Figure 2.9), where pollutant molecules adhere to the outermost atomic layers of a solid material. The process occurs through two primary mechanisms:

- (i) Physisorption: A weaker interaction driven by van der Waals forces or hydrogen bonding.
- (ii) Chemisorption: A stronger process involving covalent or ionic bonding, leading to a more permanent attachment of pollutants to the adsorbent.

Before being captured by the adsorbent, the contaminant is referred to as the adsorptive substance. Once bound to the surface, it is called the adsorbate (15; 16).

Adsorption is favoured for oil spill remediation due to its simplicity, cost-effectiveness, and high efficiency, making it a key method in environmental cleanup efforts.

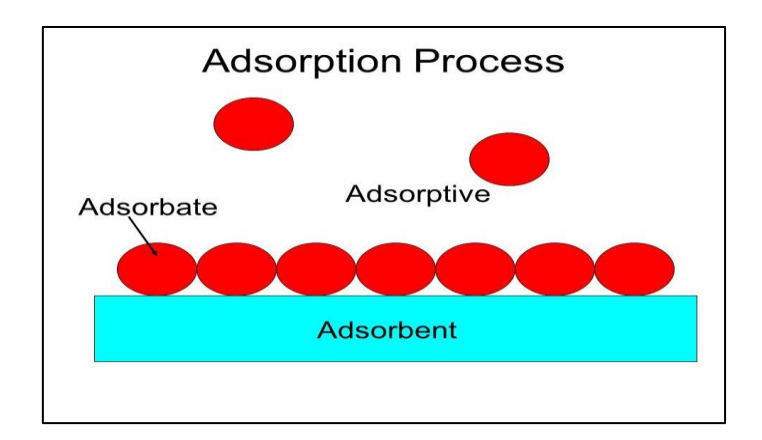


Figure 2. 9: Schematic representation of adsorption phenomena (M, Hassan 2020 RF2)

2.3.1 Factors affecting adsorption and the efficiency of oil recovery

(i) Oil viscosity

Viscosity, is defined as a fluid's resistance to flow due to intermolecular cohesion, significantly influences the effectiveness of sorbents in marine oil spill cleanup. Research indicates that

sorbents perform better on low-viscosity oils, while higher viscosity can hinder the release of absorbed oil during collection. Additionally, substrates with very large pore diameters exhibit greater absorption capacity for highly viscous oils (112; 134).

(ii) Sorbent surface roughness

Researchers suggest that increased surface roughness improves a substrate's oil absorption capacity. Substrates with thin structural layers and multiscale or hierarchical roughness tend to exhibit high hydrophobicity (high water contact angle) and strong oleophilicity (low oil contact angle). The coarse, fibrous nature of these surfaces positively influences porosity and pore size, enhancing absorption efficiency. Additionally, Broje and Keller (135) found that materials with greater surface roughness can boost oil recovery rates by up to 20%.

(iii) The critical surface tension of the sorbents

This refers to the maximum surface tension at which a liquid fully wets the solid surface. There is a strong correlation between critical surface tension and absorption properties, with lower critical surface tension values increasing the material's ability to repel water. Studies indicate that highly hydrophobic materials are ideal for oil spill clean-ups. However, if the critical surface tension falls below the threshold needed to repel water, oil absorption capacity diminishes. Overall, sorbents with low surface tension or energy are more effective at absorbing oil (112).

(iv) The thickness of a floating oil layer

In an oil spill, a slick forms as the oil spreads across the water surface, creating a thick layer. Research has explored how effective sorbents are in removing oil layers of different thicknesses. For instance, Husseien et al. (61) observed that oil adsorption capacity of barley straw sorbents more than doubled as the oil layer thickness increased from 1 to 5 mm. However, when the thickness exceeded the sorbent's capacity threshold, its effectiveness decreased.

(v) Oil retention

The ability of sorbents to retain absorbed oil is crucial for preventing leaks during transportation to post-cleanup processing sites. The pore structure of the sorbent affects its oil retention rate. Lin et al. (29) found that higher porosity reduces a sorbent's effectiveness in retaining oil. Therefore, when evaluating sorbent efficiency, both porosity and pore size distribution should be considered.

(vi) Contact angle

The wettability of a solid surface by liquid droplets is often described by the contact angle (θ), which indicates how well a surface controls droplet motion. It plays a significant role in the effectiveness of sorbent materials. Hydrophobicity and oleophilicity are crucial properties for oil sorbents, as they enhance oil/water separation efficiency. Materials are classified based on their contact angle: hydrophilic (θ < 90°), hydrophobic (90° < θ < 150°), or superhydrophobic (θ > 150°). A higher contact angle indicates stronger liquid-liquid interactions and greater hydrophobicity. Hydrophobic materials, typically nonpolar substances like hydrocarbons, tend to repel water due to differences in polarity. Wettability is influenced by the surface's free energy, as described by Young's equation (60). The contact angle range for each wetting and non-wetting scenario is shown in Figure 2.10.

The wettability of a liquid droplet on a static, smooth solid surface is influenced by the surface free energy of the solid. This relationship is mathematically described by Young's equation.

$$Y_{sv} = Y_{sl} + Y_{lv} \cos \theta \qquad 2.1$$

where θ is the contact angle and Y_{sv} , Y_{sl} , and Y_{lv} represent the interfacial surface tensions of the solid–vapor, solid–liquid, and liquid–vapor interfaces.

The above equation 2.1 shows that the contact angle is determined by the balance among the three interfacial energies (60).

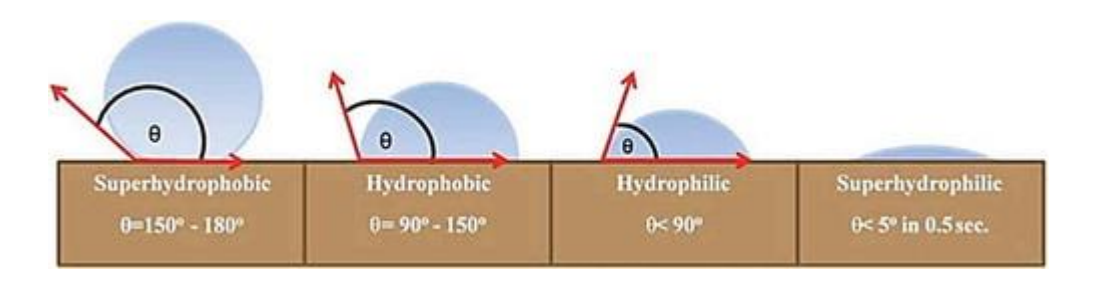


Figure 2. 10: Schematic of water droplet's contact angle describing different surface wettability

(139).

(vii) Temperature

Temperature is an important factor affecting the oil absorption capacity of sorbents. In many cases, higher temperatures enhance the oil uptake by various substrates, such as kapok fiber (64) and modified polymer-based sorbents like 3D cross-linked polystyrene-polymethyl methacrylate/divinylbenzene (PS-PMMA/DVB) (63), where a significant increase in oil absorption was noted. However, the opposite effect was observed with cotton grass, as shown in the study by Suni et al. (65), where the cotton grass-based substrate performed better in absorbing diesel oil at lower temperatures.

(viii) Buoyancy of sorbents

The buoyancy of sorbents is a key factor influencing their adsorption efficiency. For sorbents to be effective, they must retain their floating ability even when saturated with water or oil. Natural organic sorbents typically have high initial buoyancy but may eventually become waterlogged and sink. Some exceptionally light sorbents can float on spilt oils, but this can also hinder their oil absorption capacity. In the case of foam-based sorbents, buoyancy is primarily determined by the number of open cells; the more open cells there are, the better the buoyancy (60).

2.4 Overview of polyethylene

Polyethylene is a thermoplastic polymer synthesised from petroleum-derived ethylene monomers with the general chemical formula $(C_2H_4)_n$. It is composed of long chains of ethylene units, making it one of the most versatile and widely used plastics globally.

The polymerisation of ethylene occurs through a radical mechanism, which requires extremely high pressures and temperatures. This process is initiated by the addition of an organic peroxide radical initiator, which triggers the formation of long molecular chains, resulting in polyethylene's characteristic structure. It is classified as a semi-crystalline thermoplastic, meaning it possesses both amorphous (disordered) and crystalline (ordered) regions. This unique molecular arrangement contributes to its high durability, flexibility, and chemical resistance. Due to these properties, polyethylene is the most extensively used commodity plastic worldwide (155).

2.4.1 Types of polyethylene

There are several types of polyethylene, each with distinct properties and applications

- (i) High-density polyethylene (HDPE): Known for its high crystallinity and stability, HDPE has a high tensile strength due to fewer short branches in its structure, allowing the chains to pack into ordered crystals.
- (ii) Low-density polyethylene (LDPE): LDPE is ductile and elastic with a high degree of chain branching, leading to weaker intermolecular interactions, lower tensile strength, and increased flexibility.
- (iii) Linear low-density polyethylene (LLDPE): LLDPE has a linear structure with many short branches, offering high transparency, ductility, and toughness, making it ideal for film applications [2].
- (iv) Ultra-high-molecular-weight polyethylene (UHMWPE): UHMWPE consists of long, aligned chains that provide exceptional strength, abrasion, and impact resistance. It is used in medical devices, industrial machinery, and as lining material (153).

The various forms of these types of PEs are depicted in Figure 2.11

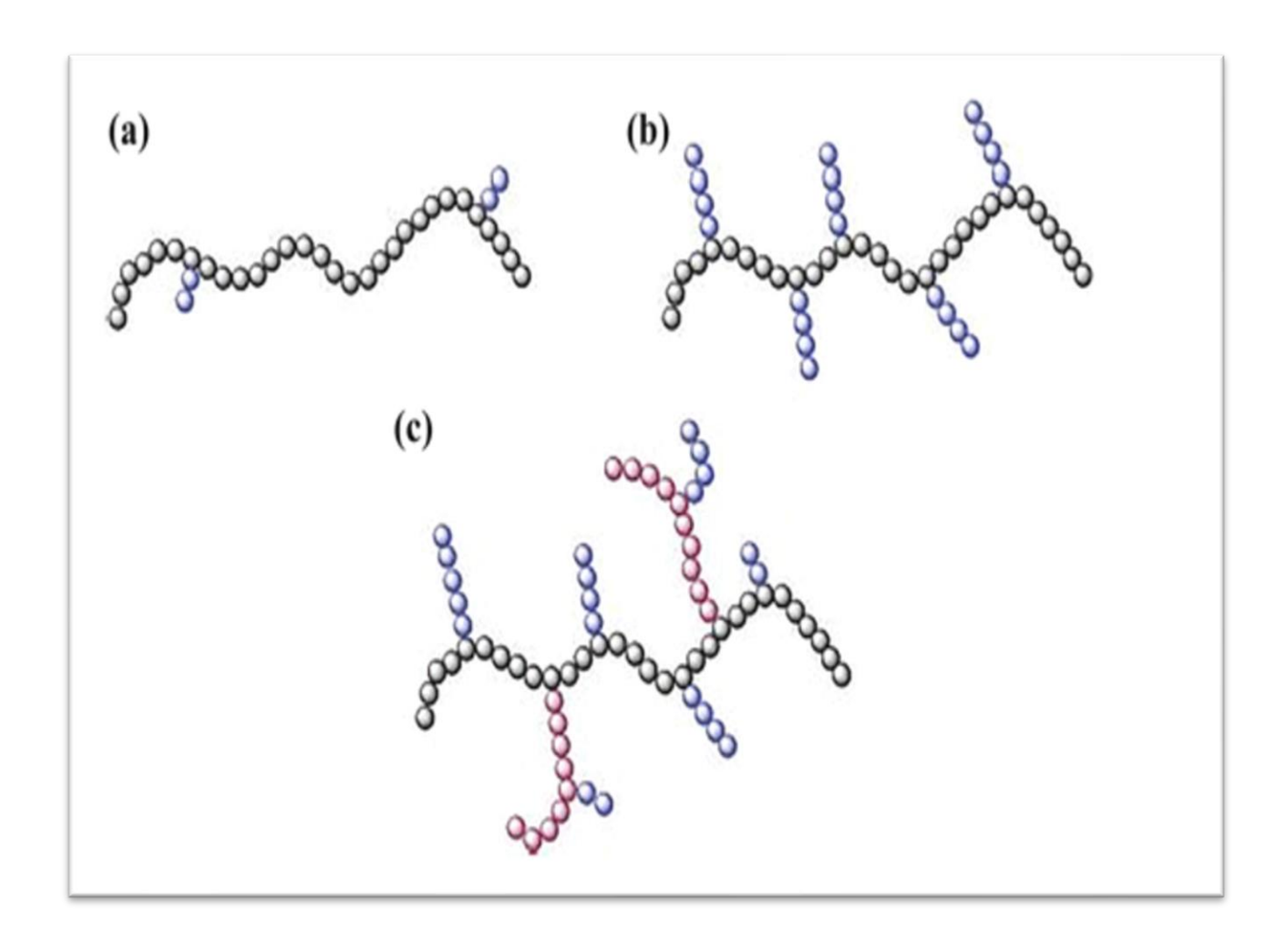


Figure 2. 11: Illustration of Polyethylene Structures (a) HDPE, (b) LLDPE, and (c) LDPE (32)

2.4.2 Key properties of plastic-based oil sorbents.

Oil Oil sorbents made from plastics must possess several essential characteristics to be effective in oil spill cleanup. These properties enhance their efficiency, durability, and reusability in environmental remediation. The most important features include:

(i) Oil Affinity and Compatibility:

Plastic-based sorbents should exhibit strong attraction and compatibility with oil to maximise absorption or adsorption. Their non-polar nature allows them to interact effectively with hydrocarbons, ensuring efficient oil uptake.

(ii) High Surface Area and Surface-to-Thickness Ratio:

A large surface area or high surface-to-thickness ratio is crucial for effective oil sorption. Greater exposure increases the contact between the sorbent and spilled oil, leading to higher absorption capacity and faster cleanup.

(iii) Porous/ Spongy Structure:

The presence of an extensive porous network enhances oil penetration into the material, allowing for greater oil retention. A well-structured porous system improves oil entrapment and prevents rapid desorption, ensuring efficient removal of oil contaminants.

(iv) Mechanical Strength and Recyclability:

Oil sorbents must have sufficient mechanical durability to withstand repeated use without degradation. The ability to retain structural integrity during handling, transport, and disposal is essential. Additionally, the potential for recyclability enhances sustainability by reducing plastic waste.

(v) Low Degree of Crosslinking:

A lower level of crosslinking enhances the sorbent's flexibility and oil absorption capacity, as highly crosslinked materials tend to be more rigid and less absorbent.

These properties are particularly important when plastic sorbents are fabricated in the form of films, sheets, and mats. Their performance can be further optimized through various fabrication and modification techniques, such as: Chemical conversion (surface modification to improve oil affinity), Grafting (adding functional groups for better absorption), Gamma radiation treatment (enhancing porosity and structural properties), Mechanical abrasion (increasing surface roughness for better oil retention), Porous film fabrication (creating high-capacity sorbent materials), Electrospinning (producing ultra-fine fibers for enhanced sorption efficiency)

By leveraging these techniques, plastic-based oil sorbents can be engineered to maximise oil removal efficiency, making them a valuable tool in oil spill remediation efforts (8,31).

2.4.3. The sachet water waste problem in Nigeria

Sachet water, popularly known as "pure water," is a primary drinking water source in Nigeria due to the unreliable and insufficient public water supply. It is packaged in small, heat-sealed

polyethylene bags and sold at an affordable price, making it accessible to a large portion of the population. In urban areas, over 80% of households depend on sachet or bottled water for drinking (157). The industry has grown significantly, with estimates indicating over 1,500 production plants operating in a large city (161). The low capital requirement and minimal regulatory enforcement have enabled widespread and often informal production practices.

The consumption results in enormous plastic waste, and it is estimated to generate about 50–60 million used sachets daily (162). In a recent study conducted in the town of Kafanchan, average individual consumption reached four sachets per day, leading to nearly 1 metric ton of sachet waste daily in that locality alone (159).

Despite the high volume of plastic waste, collection and recycling systems are underdeveloped. Less than 20% of plastic waste is recycled in Nigeria (158). Initiatives such as RecyclePoints and WeCyclers have introduced community-based recycling programs, offering incentives for household collection of plastic waste. However, these programs cover only a fraction of the population and are concentrated in a few urban areas (157). Most urban and rural areas lack organised waste management systems, resulting in open dumping or burning of sachets (160). The improper disposal of these sachets after usage leads to blocked drains and urban flooding, as well as increased breeding grounds for mosquitoes and other disease vectors (162). Public knowledge about the environmental effects of sachet waste remains low, contributing to careless disposal habits (160). So, while sachet water addresses the urgent need for clean drinking water in Nigeria, it creates a major environmental burden due to the improper disposal method and non-biodegradable plastic waste it generates.

2.4.4. Hydrophobicity of Polyethylene and adsorption mechanism

Hydrophilic surfaces exhibit high attraction to water molecules, while hydrophobic surfaces actively repel water. This means that it repels water and does not mix with it. Instead, it forms beads or droplets when it encounters water. This property is crucial for the cleanup process, as it allows polyethylene to interact with oil while excluding water.

To apply this concept practically, this research work has developed two methods that utilise polyethylene's hydrophobic properties. These methods can take the form of floating flakes in a batch process or stacked flakes in a column process. When crude oil is spilt on water, it

forms a thin layer that spreads over the surface. Polyethylene, being hydrophobic and oleophilic, is naturally attracted to the oil, and the oil adheres to its surface. As they move through the water, the hydrophobic polyethylene effectively gathers the oil while leaving the water behind. The oil molecules cling to the polyethylene thereby collects the oil, making it easier to remove the oil from the water.

Despite the increasing concern over plastic waste, limited research has been conducted on utilizing recycled plastic waste as oil sorbent films with high practical uptake capacity. Most studies on plastic waste have primarily focused on its economical and environmentally friendly disposal rather than exploring its potential for value-added reuse. Given this gap, the present study seeks to investigate the feasibility of converting waste-water sachet polyethylene (WWSP) into an effective oil sorbent material.

WWSP, a widely used synthetic polymer, has a density ranging from 0.88 to 0.96 kg/m³ and a melting point between 115°C and 135°C (140). It is highly hydrophobic and possesses a broad molecular weight range, making it suitable for various industrial applications. However, its non-biodegradability presents significant environmental challenges, particularly in terms of pollution and the increasing scarcity of landfill space for plastic waste disposal (43).

To address the environmental burden posed by WWSP, researchers have explored different waste recovery and repurposing methods. One such approach involves repurposing used sorbent materials for tertiary applications after their initial use. For instance, Dahunsi et al. (52) conducted a study on the incorporation of WWSP into bitumen modification to mitigate its environmental impact. Their findings revealed that the dynamic viscosity of modified bitumen increased with higher WWSP content, demonstrating the material's potential to enhance bitumen properties. Specifically, the study identified an optimal WWSP content range of 2.5% to 7.5%, within which the modified bitumen exhibited improved performance. Additionally, WWSP was recognised as a cost-effective and readily available material that, when properly utilised, could serve as a beneficial additive in construction applications.

By investigating the conversion of WWSP into an oil sorbent, this study aims to contribute to the development of sustainable and practical waste recovery mechanisms, reducing environmental pollution while creating value-added applications for recycled plastic materials.

Hailan et al (96), in an academic review, examine polymeric sorbents, particularly polyolefins like polyethylene and polypropylene, for removing spilt oil from water surfaces. They discovered that these materials are particularly suitable due to their natural hydrophobicity and oleophilic properties, and they can be processed into various forms such as powders, pellets, sheets, membranes, and foams. While the materials have limited longevity under harsh environmental conditions, their disposal through combustion and pyrolysis is relatively straightforward since they lack problematic elements like nitrogen and sulphur. The technology shows promise for both environmental cleanup and waste management by extending the lifespan of produced plastics through new functionality.

Another example, by Ademiluyi, and Akpan, (147) investigated the potential of WWSP for the production of fuel oil using pyrolysis. The WWSP was pyrolysed at different temperatures. The chromatographic analysis shows that the fuel oil produced (up to 450 °C) contained paraffins, isoparaffins, olefins, naphthalenes, aromatics and polyaromatics ranging from C3 – C38. It could be refined further to produce domestic kerosene and gasoline.

With the above evaluations and more, the sorbent developed herein could have a further tertiary life. It could still be converted into a useful raw material for the industries, to produce fuel oils through pyrolysis or used in road construction, however, there is a need to be evaluated further for a workable ratio as the spent sorbent will already have some fraction of bitumen contained in it.

CHAPTER 3

3.0 METHODOLOGY

This chapter describes the materials, material preparations, equipment and the procedures used in characterising the crude oil, the polyethylene water sachets, and the adsorption procedures. It also describes the methods used for the preparation of the different forms of PE sorbent (shredded, roughened, and UV-weathered).

3.1 Materials

The natural crude oil (Bonny light) used for experiments herein was sourced from Port Harcourt, South-South region of Nigeria and the artificial crude oils (Phillip and Camlab) were ordered from Philip Harris Education, Hyde, Cheshire and Camlab Chemicals, Camlab Ltd, Norman Way, Cambridge, respectively. The PE water sachets (pre-used and unused) were picked from the streets and different water packaging facilities in Minna, Niger state, the Northern part of Nigeria. The solvent, dichloromethane, was ordered from Merck, UK and of analytical grade purity, general grade salt (NaCl) from Fisher Scientific, UK, de-ionised water with a conductivity of 128.8 μ S/cm was obtained from a Milipak Express 20 water purifying system, (Model:MPGP02001) and used for all the experiments.

3.1.1 Preparation of Polyethylene sorbents

There are different types of PE water sachets used for this research work (Figure 3.1), from different water providers (e.g. Greenmark, Golden age, Royalunik, Zagbayi etc). There are different printed marketing information on the sachets.



Figure 3. 1: Different water sachets with ink-printed markings for marketing information

The polyethylene water sachets used to prepare sorbents were first washed with detergent to remove all dirt and dried at room temperature. The polyethylene sachets were then transformed into various forms:

(a) shredded (b) shredded -roughened and (c) UV-weathered polyethylene.

3.1.1.1 Shredded Polyethylene

Two (2) different types of shredding machines (3devo polymer grinding machine, and Nutribullet blender (Figure 3.2 (c,d,e)) were used in the course of this PE shredding before the final procedure was determined, but had issues of constant breaking down and overheating, thus only one (nutribullet blender) was used for the final procedure.

The water sachets were cut into small pieces (roughly ≥ 30 mm ≤ 50 mm) and fed into the polymer grinding machine to shred. The shredded PE was size graded using electronic sieve shakers (figure 3.2 (h)) into three different sizes, $\leq 2.36 \geq 1.80$ mm, $\leq 1.80 \geq 1.18$ mm, and ≤ 1.18 mm for the preliminary experiments, and 8.0mm $\leq x \geq 6.3$ mm, 6.3mm $\leq x \geq 2.8$ mm, 2.8mm $\leq x \geq 2.0$ mm for the final procedure.



Figure 3.:2 (a) washed PE (b) PE cut into small pieces prior to shredding (c) 3devo polymer grinding machine used to shred PE (d) Nutribullet blender (e) shredded PE (f) grinding set of plates used to improvise the roughening of shredded PE (g) electronic sieve shaker

3.1.1.2: Shredded-roughened Polyethylene

A Retsch vibratory disc mill RS 200 (Figure 3.3a), was used for the roughening process of the shredded PE. This equipment is made up of the mill and the grinding set of plates (Figure 3.2f), which operates through a combination of pressure and friction. A quick-action lever firmly secures the grinding set to the vibration plate (Figure 3.3b), which is then subjected to circular horizontal vibrations. These vibrations, generated by a frequency-controlled 1.5 kW 3-phase motor, facilitate the grinding process. The centrifugal force exerted on the grinding rings within the dish applies significant pressure and friction to the PE sample, achieving substantial and visible roughness within 2 minutes. To protect the grinding sets from damage, a sensor detects their presence and automatically adjusts the speed to a maximum of 700 rpm. Furthermore, the noise-insulated grinding chamber's cover features a safety interlock mechanism, ensuring it can only be opened when the mill is stationary.

For this research work, salt (NaCl) was used as an aid for the roughening process of the polyethylene samples. Sodium chloride (NaCl) was selected as a roughening agent for polyethylene due to its effective abrasive properties and practical advantages over traditional rougheners such as sand. Its crystalline and moderate-hard structure allows for controlled abrasion, creating a uniform surface texture without damaging the polymer matrix (163). Unlike sand, which has variable grain size and hardness, NaCl offers more consistency and is easily removed by water due to its high solubility (164), especially in water and also prevents contamination and simplifies post-treatment cleanup. NaCl is chemically inert, and non-toxic, reducing the risk of unwanted reactions or residues that could interfere with the process (165). NaCl is also safer to handle compared to silica-based sand, which may pose respiratory hazards during processing (166).

Salt was added to the grinding set alongside the PE samples at a ratio of 5:2 by weight. All the roughening process for this work was set at 700 rpm for 2 minutes.



Figure 3. 2: RETSCH's Vibratory Disc Mill RS 200, used as an improvised tool for PE surface roughening (b) Open RETSCH's Vibratory Disc Mill RS 200, showing the embedded grinding set held in position by the quick-action lever.

3.1.1.3 UV weathered PE

The ageing process is usually accelerated by simultaneously increasing the intensity of UV light and temperature of the exposed samples. Although, the representativeness of artificial ageing is still an ongoing issue, the Q-lab technical bulletin (81) has showed that a UVA-340 fluorescent lamp provides better correlation and representation of actual outdoor weathering, and that irradiance of 0.76 W/m² UV is equivalent to noon summer sunlight.

The Q-lab accelerated Weathering Tester (QUV) replicates the harmful effects of weathering by utilising innovative condensation and water spray systems to simulate rain and dew. The UVA-340 fluorescent lamp offers an optimal simulation of sunlight, particularly in the crucial short wavelength range from 365 nm down to the solar cutoff of 295 nm, with its peak emission occurring at 340 nm (Figure 3.4), while fluorescent UV lamps (Figure 3.5b) imitate sunlight. The exposure temperature and daily sequence of UV periods, condensation, and spray are automatically regulated. In days or weeks, the QUV can replicate the effects that might typically take months or years of outdoor exposure. According to Q-lab manual, it is stated that 0.83 W/m2 at 340nm is the irradiance specified in ISO 4892-3 Cycle 3 and 4 or use 0.73 W/m2 at 340nm to match the maximum irradiance of natural sunlight per ASTM G177 but it developed its custom test cycle which was programmed in their UV-tester as shown in Table 3.1 and 3.2, which was used for this experiment.

For experiments herein, the water sachets were weathered using a Q-lab UV weathering tester (figure 3.5) as programmed to replicate the PE's real-life situations after their use and discarded into the environment. Thus, the standard test cycle D: ASTM G154 CYCLE 4 and Cycle K: ISO 4892-3 cycle 1 were used as shown in Table 3.1 and 3.2 (81).

Table 3. 1: Set parameters for the weathering of PE sachets equivalent to normal noon sunlight

Cycle K: ISO 4892-3 Cycle 1					
Lamp Type: UVA-340					
Programmed in Models: QUV/basic, QUV/se, QUV/spray, QUV/spray/rp (No irradiance setting on QUV/basic)					
STEP	FUNCTION	Irradiance (W/m²)	Temperature (°C)	Time (hh:mm)	
1	UV	0.76	60	8:00	
2	Condensation	N/A	50	4:00	
3	Final Step - Go to Step 1				

Table 3. 2: Set parameters for the weathering of PE sachets for the double irradiation

Cycle D: ASTM G154 CYCLE 4							
Lamp Type: UVA-340							
Programmed in Models: QUV/se, QUV/spray, QUV/spray/rp							
STEP	FUNCTION	Irradiance (W/m²)	Temperature (°C)	Time (hh:mm)			
1	UV	1.55	70	8:00			
		ì					
2	Condensation	N/A	50	4:00			

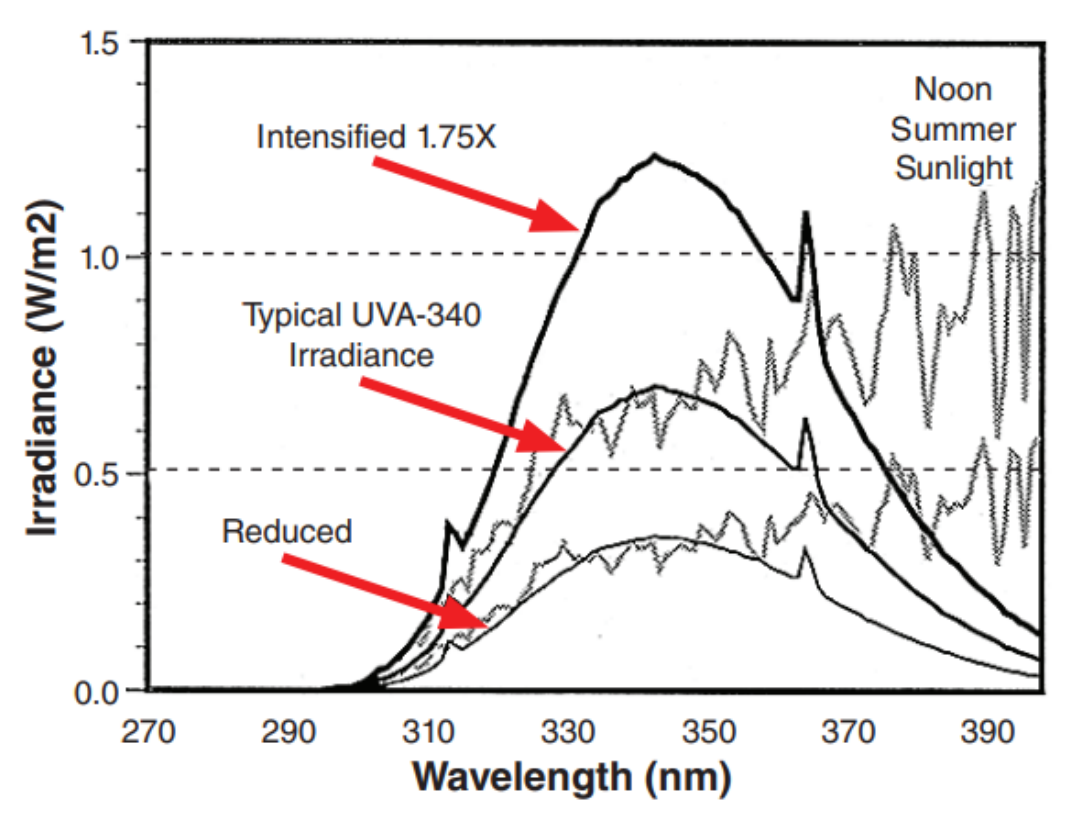


Figure 3. 3: UVA-340 Lamps Compared to Sunlight

Source: (73)

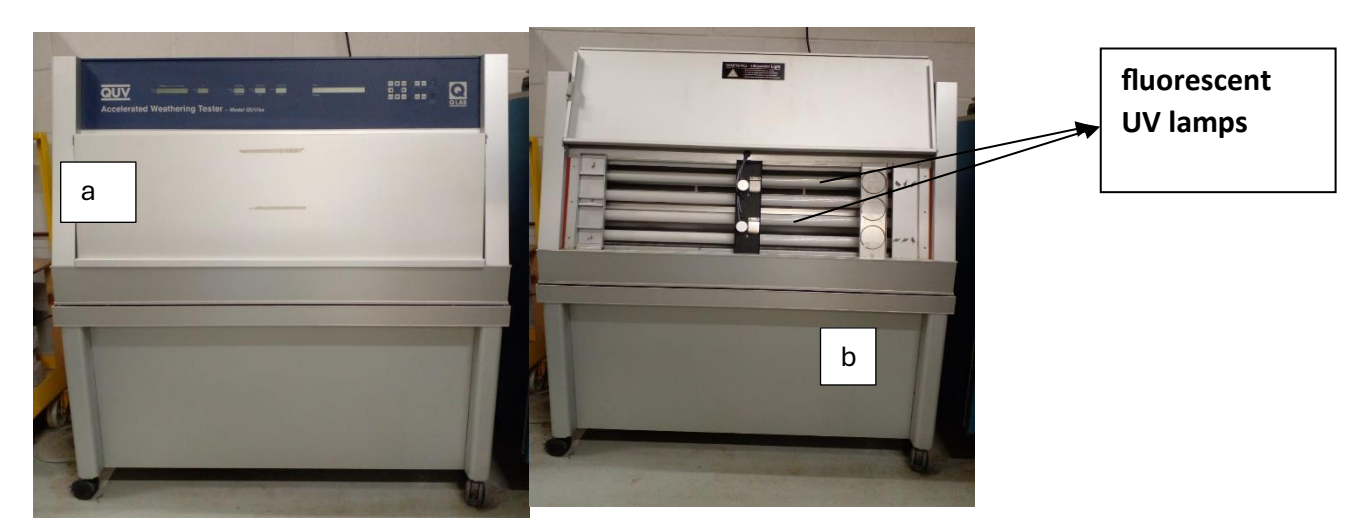


Figure 3. 4: (a): Q-lab UV Accelerated weathering tester (b): Accelerated weathering tester showing the fluorescent UV lamps

3.2. Characterisation tests

3.2.1 Instruments used for the characterisation of Oils (Natural Crude, Phillip, Camlab)

Samples obtained from crude oil and oil spills exhibit complex compositions, comprising a broad spectrum of components ranging from simple alkanes to complex asphaltic compounds, each possessing boiling points that vary greatly from a few degrees to several hundred degrees. Therefore, the chemical analysis methods employed need to deliver sufficient precision and detailed characterisation, especially regarding the essential toxic compounds. This focus is paramount as the environmental repercussions of oil spills are significantly impacted not only by the total volume of oil but also by the levels of these crucial toxic substances. Consequently, these analytical techniques must be adept at addressing the specific queries posed within an environmental assessment study (68).

The characterisation of crude oil is crucial in understanding its chemical and physical properties, which in turn guide the selection of appropriate sorbent materials and the design of effective sorption methods. The techniques used to characterise the oil include Gas chromatography and Mass Spectrometer (GC-MS), Thermogravimetric analysis (TGA), Contact angle, and Rheometry.

For the weathering of the oils, 20 mL of the oils were exposed in vials (50 mL) inside the fume cupboard in the laboratory for days. They were also manually weighed to check the physical weight loss.

3.2.1.1 Gas chromatography and Mass Spectrometer (GC-MS)

Gas chromatography (GC) is a technique used to separate and analyse volatile components in a mixture. It begins by vaporising a liquid sample, which is then introduced into a chromatographic column coated with a stationary phase. As the sample passes through the column, its different components interact with the stationary phase, causing them to separate based on their unique chemical properties, such as polarity or volatility. The separated components are then directed into a Mass Spectrometer (MS) for further analysis.

Within the mass spectrometer, the compounds are ionised in the ion source, transforming neutral molecules into positively charged ions. These ions are fragmented, creating a unique set of ionised fragments, or "fingerprints," which help identify the compounds. These charged particles are passed through a quadrupole mass analyser, which filters the ions based on their mass-to-charge (m/z) ratio, allowing only ions with specific m/z values to reach the detector. The mass spectrometer then cycles through various voltage settings to analyse a range of m/z ratios, generating a mass spectrum.

The resulting mass spectrum serves as a detailed profile of the sample, offering both qualitative and quantitative information. The spectrum can be calibrated, making it possible to identify the compounds in the sample and measure their relative concentrations. This combination of GC and MS allows for precise identification and quantification of complex mixtures (79). This process is described in the schematic diagram as shown in Figure 3.6.

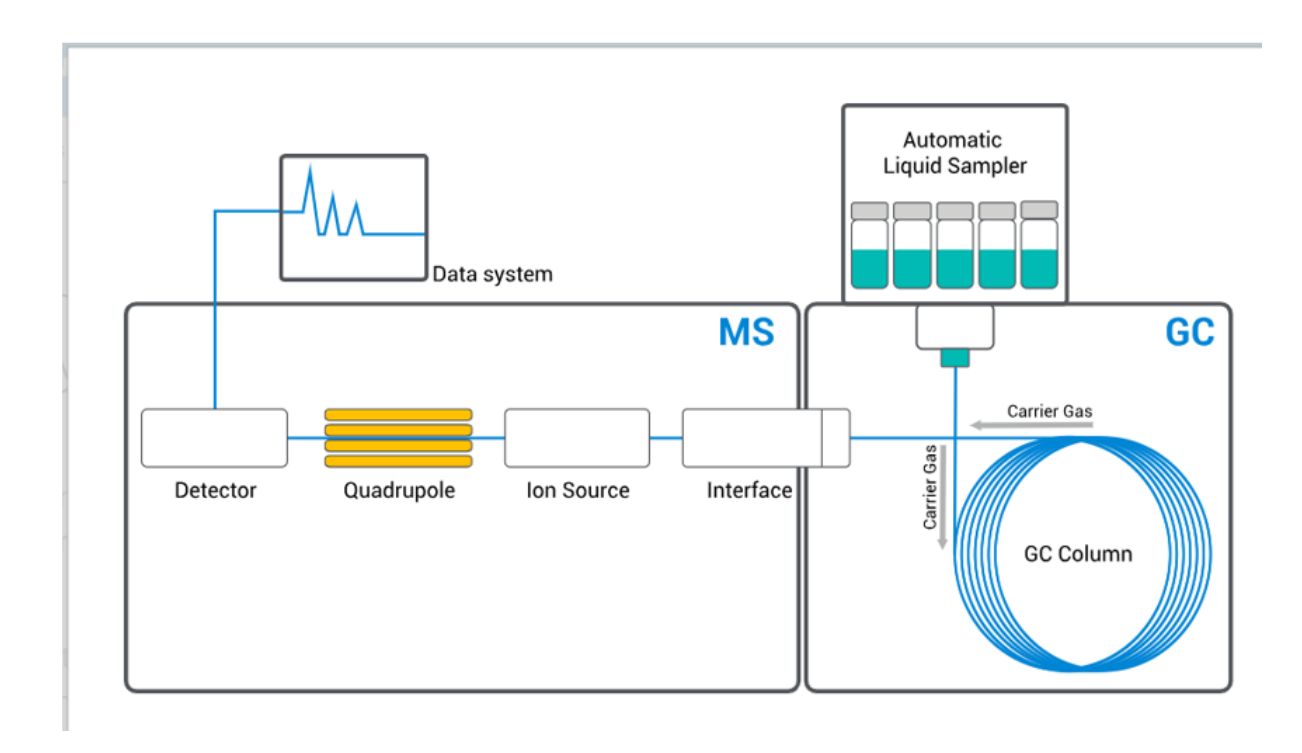


Figure 3. 5: Schematic diagram of the GCMS basic principle of operation Source (148)

For this research work, the pristine and weathered oils were analysed using ThermoScientific Trace 1310 chromatograph: ISQ 7000 Single Quadrupole Mass Spectrometer) (Figure 3.7). The GC-MS equipment was operated in split mode control with a split flow of 30 mL/minute and a split ratio of 20. The GC inlet temperature was set to 250°C. The oven temperature was initially held at 35°C for 4 minutes and then increased to 320°C at a rate of 4°C/minute. The volume injected was 0.2 microliters. The GC Column used is Thermoscientific TG-5MS (length 30 m, ID 0.25 mm, film 0.25 μ m), and the liner is ThermoScientific LinerGOLDTM Split straight liner with quartz wool.

The MS transfer line and ion source temperatures were maintained at 280°C. The scanned range was 40-300 amu with a scan time of 0.2 seconds. Data collection began at 2.5 minutes, and the MS operated in Electron Impact (EI) mode. Chromeleon Console software and a NIST library database were used for the analysis of the samples.

Due to the complex and variable composition of crude oil, specific compound calibration was not used. Instead, a relative quantification approach was applied, assuming proportional detector response. The GC/MS system was tuned using Perfluorotributylamine (PFTBA) to

ensure accurate mass calibration, peak resolution, and ion intensity. While no absolute calibration curves were developed, the system was optimized for reliable comparative profiling, and surrogate standards can be used if semi-quantitative data is needed.

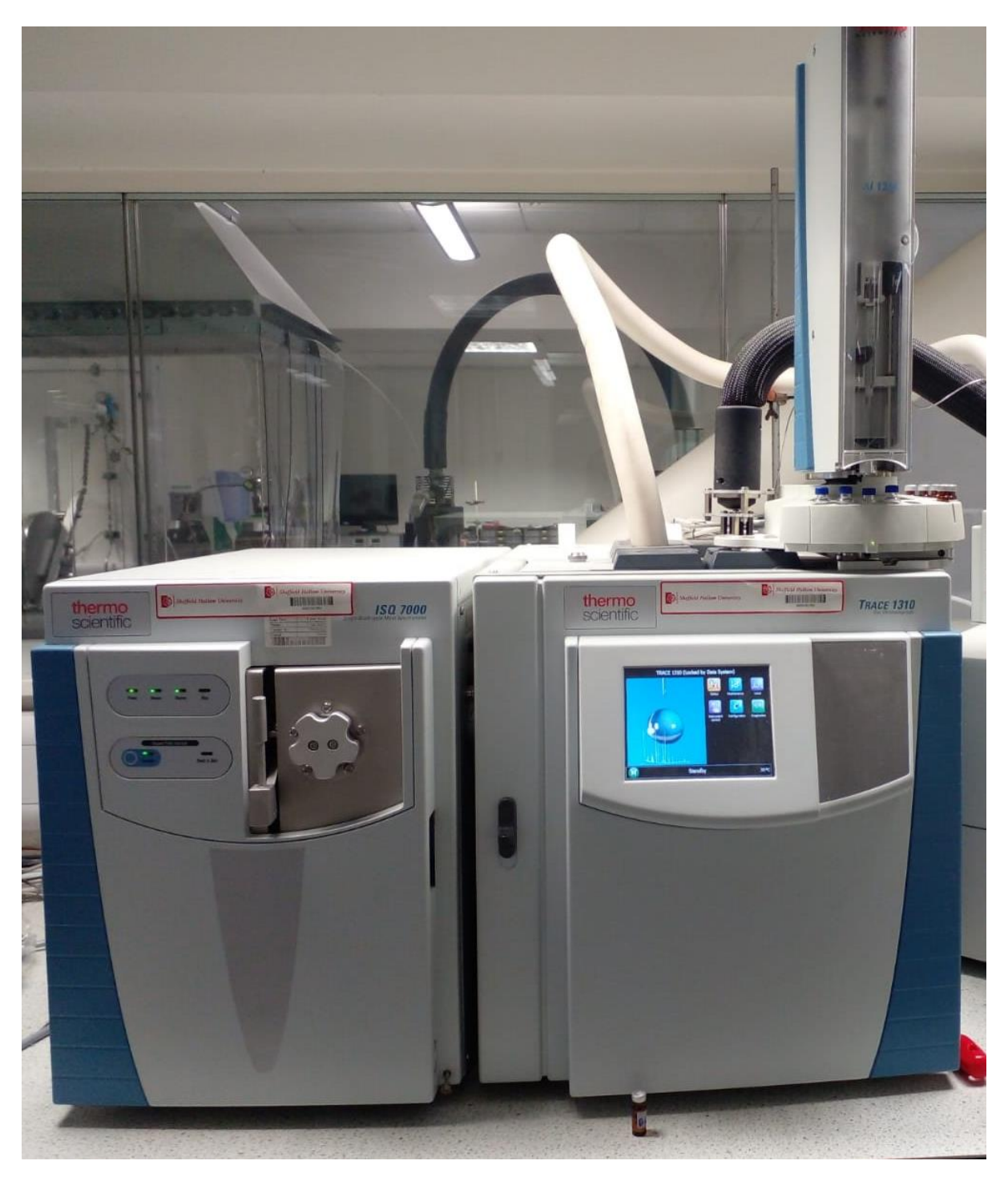


Figure 3. 6:GCMS (ThermoScientific Trace 1310 Gas chromatograph: ISQ 7000 Single Quadrupole Mass Spectrometer)

3.2.1.2 Thermogravimetric analysis (TGA)

TGA is a commonly utilised instrumental technique in thermal investigations, primarily employed to characterise materials by monitoring their mass changes in response to temperature variations. Key properties typically assessed through TGA include purity, composition, decomposition temperatures, decomposition reactions, and levels of adsorbed moisture. TGA is often combined with Differential Scanning Calorimetry (DSC) to provide complementary insights that aid in interpreting thermal experiments. Within a controlled atmosphere, TGA measures the sample's mass as it undergoes heating, cooling, or is held at a constant temperature. A typical mass-loss curve during thermal analysis, such as for polymers, may involve five distinct steps: the loss of volatile components (e.g., moisture), decomposition, pyrolysis, or oxidation of carbon (i.e. with the atmosphere switching from nitrogen to oxygen), and the residual inert inorganic ash fillers (80). In this thesis work, a computer-programmed TGA/DSC-1 instrument (Mettler-Toledo; Stare System) (Figure 3.8) was employed to determine the thermal stability of the crude oil.

To study the effects of atmospheric exposure on crude oil, 20 g of each of the five crude oil samples was placed separately in 250 mL beakers and left in a fume cupboard for several days. Samples were analysed at specific intervals (0, 1, 25, 35, and 44 days) to observe changes over time. For analysis, approximately 30 mg of each sample was taken and subjected to Thermogravimetric Analysis (TGA).

The TGA was performed using alumina pans under a controlled atmosphere (nitrogen or air) with a purge rate of 40 mL/min. The temperature was gradually increased from 35°C to 800°C at a consistent heating rate of 20°C/min. This setup allowed for the assessment of the thermal stability and compositional changes in the crude oil samples due to prolonged exposure to atmospheric conditions.

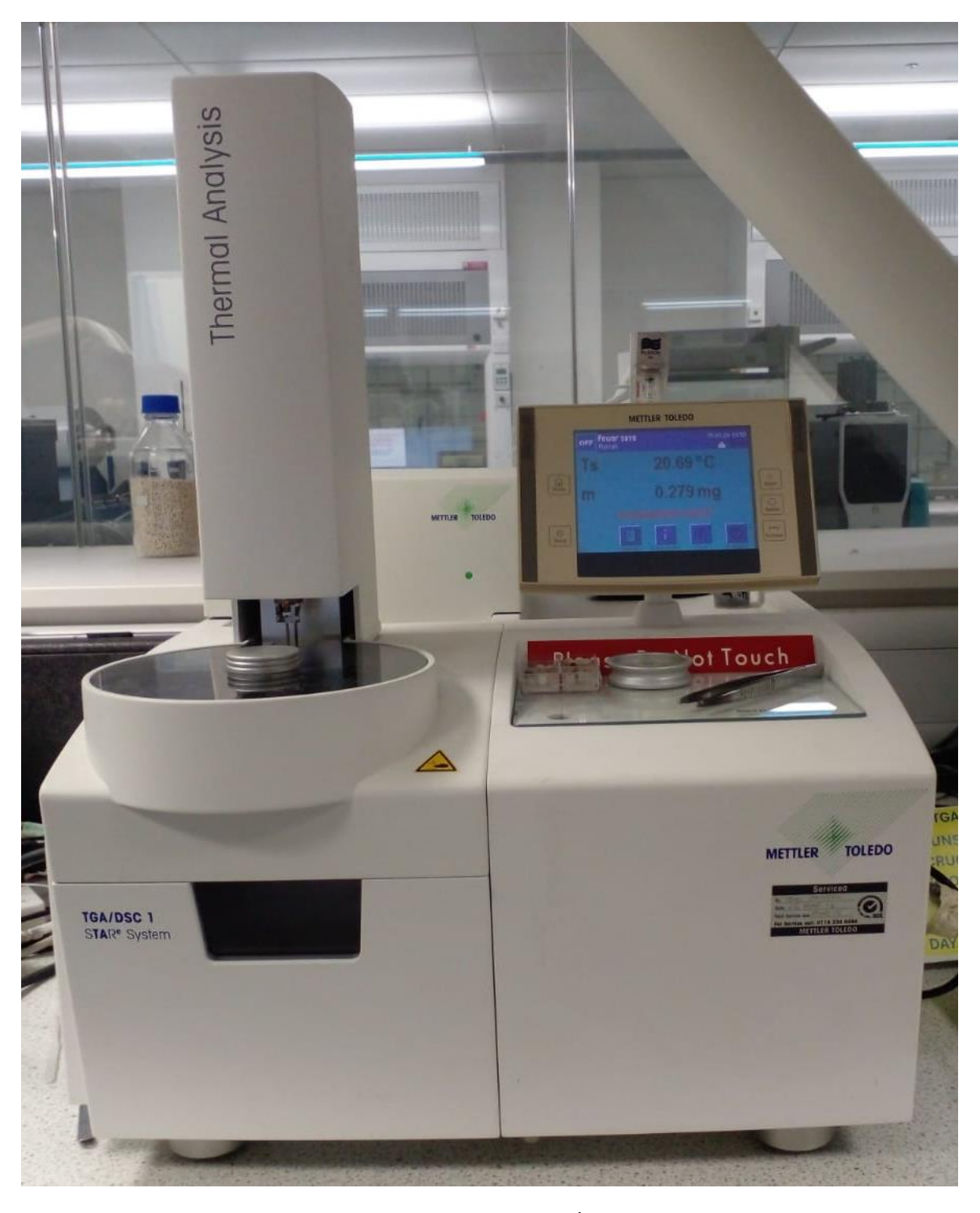


Figure 3. 7: Laboratory set-up of Mettler-Toledo TGA/DSC-1 instrument (Stare System) for Thermal analysis

3.2.1.3 Contact angle

The degree of wettability of liquid droplets on a solid surface is commonly described in terms of the contact angle (θ). The optical contact angle (OCA) measuring device used for this

research work is the DataPhysics OCA 15EC, made in Germany (Figure 3.9). In addition to featuring standard functionalities seen in OCA devices, it showcases unique attributes, such as a high-resolution CCD (charged-coupled device) video camera with 752 x 582 pixels and a frame rate of up to 50 images per second. While alternative measurement methods based on various sample configurations exist, the goniometer technique remains widely recognised as the most practical and versatile.

The contact angle is the angle formed at the junction where a liquid, air, and solid surface intersect. It serves as an indicator of a material's wettability, or how easily a liquid spreads across its surface. A low contact angle suggests that the liquid tends to spread and adhere to the surface, indicating higher wettability. Conversely, a high contact angle signifies a surface's tendency to repel the liquid, demonstrating lower wettability.

The sessile-drop goniometry method is the most commonly used technique for assessing surface wettability due to its simplicity and accuracy. This method involves analysing the shape of a droplet placed on the surface to determine the contact angle (74).

Additionally, surface energy refers to the intermolecular forces present at a material's surface, influencing its ability to attract or repel other substances. The magnitude of surface energy determines the degree of interaction between materials, affecting adhesion, coating, and wettability properties.

Low contact angle = high surface energy; High contact angle = low surface energy (75)

After determining the contact angle, another important parameter, surface tension, can be estimated. Surface tension arises from intermolecular forces at a material's surface and plays a key role in its wetting behavior. However, the liquid used for measuring the contact angle may not always represent all practical liquid samples.

In cases where the solid surface tension is already known, the wetting behavior and contact angle of a liquid with a known surface tension can be predicted. Typically, solid surface tension is evaluated by measuring the contact angle of standard liquids with well-defined surface tension properties on the solid surface (88).

To determine the surface tension and surface energy of the various forms of PE, the Owens, Wendt, Rabel and Kaelble (WORK) method was applied as a standard method, it uses the contact angle measurement with several liquids.

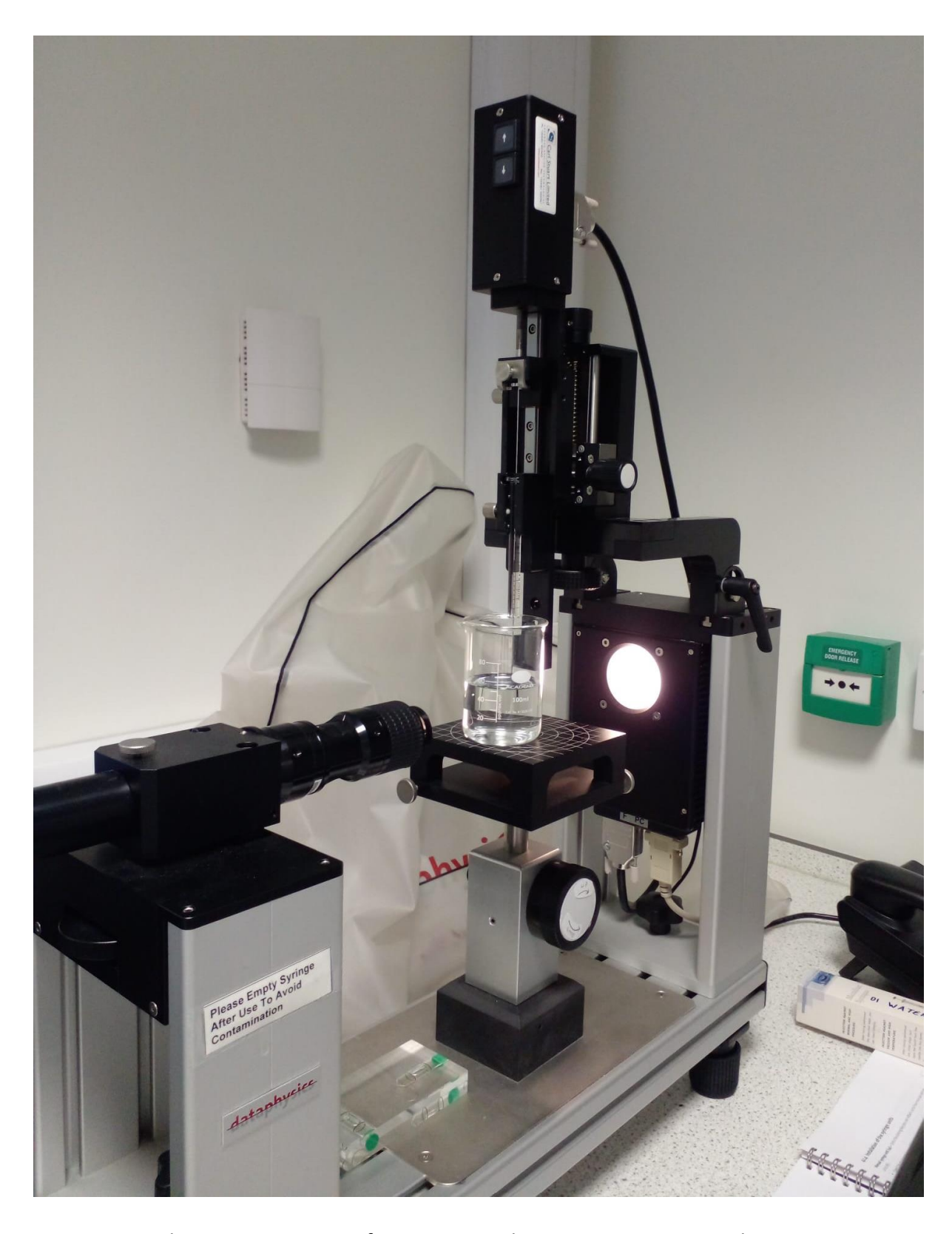


Figure 3. 8: Telescope goniometer for contact angle measurements DataPhysics OCA 15EC

3.2.1.4 Rheometry

Viscosity quantifies a fluid's resistance to flow, arising from the internal frictional forces between its molecules (86). In this work rheological measurements of the oils were carried out using an Anton Paar Physica MCR 301 rheometer (Figure 3.10). All measurements were carried out using a bob and cup accessory set up at 20 °C and 40 °C (Figure 3.11). In this setup, the bob rotates at a predetermined speed (shear rate) while the cup remains stationary. The electronic controller adjusts the motor's current based on the input shear rate to generate the required torque. As the fluid exerts a resistive torque on the motor, the rotational speed changes, detected by a position sensor which signals the controller. The controller then recalculates and adjusts the motor's current to maintain the preset speed. Shear stress and viscosity are calculated using Equation 3.1 (86). A water bath regulates the system temperature, and an air bearing centres the drive shaft for minimal friction. The sample's deformation is recorded using a digital encoder that processes 10⁶ impulses per revolution. This high-resolution capability allows for precise measurement of small yield stress values, strains, and shear rates (76).



Figure 3. 9:Anton Paar Physica MCR 301 rheometer for rheology measurements

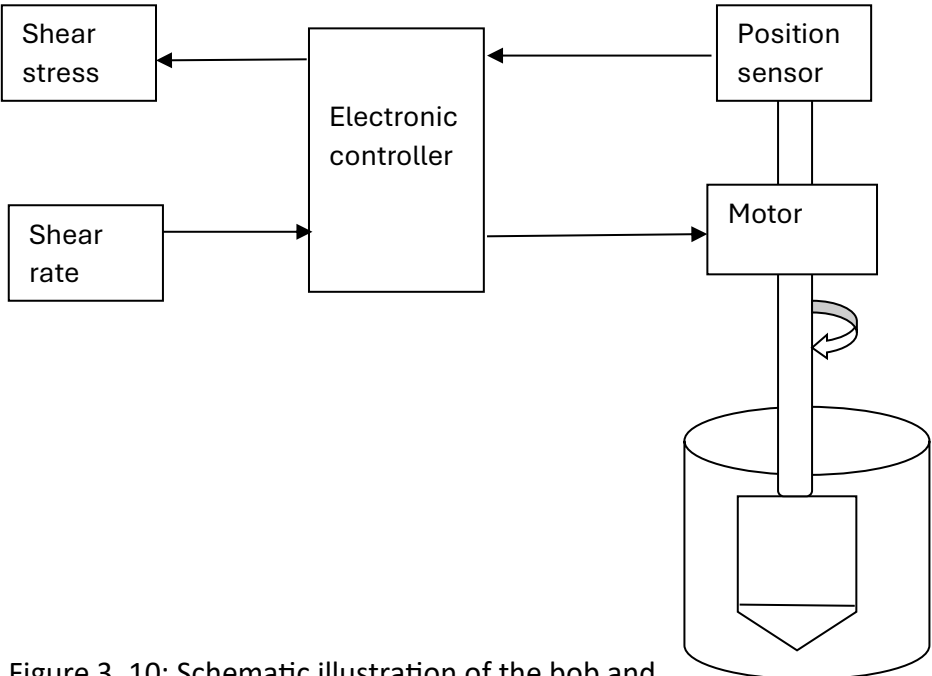


Figure 3. 10: Schematic illustration of the bob and cup setting for viscosity measurements (86)

Viscosity (η) =
$$\frac{shear\ stress}{shear\ rate} = \frac{M/A}{shear\ rate}$$
 3.1

Where M is the resultant torque and A is the contact area (area of the bob)

All tested samples were equilibrated at the desired measuring temperature for at least 2 minutes before the test started. At the start of each rheology test, three measurements were conducted to verify the reproducibility of the Anton Paar Physica MCR 301 rheometer system. The experimental measurements demonstrated satisfactory reproducibility.

3.2.2 Instruments used for the characterisation of the Polyethylene water sachets

3.2.2.1 Differential Scanning Calorimetry (DSC)

According to ASTM E473-16 (149), Differential Scanning Calorimetry (DSC) is a method where the disparity in heat flow rates between a substance and a reference material is gauged relative to temperature changes, while both the substance and reference undergo controlled temperature conditions (Figure 3.12). In the context of polyethylene, DSC measures the

melting temperature (Tm), crystallization temperature (Tc), and the associated enthalpy changes (ΔH) which are critical for understanding the thermal properties and crystallinity of the material.

For this research work, DSC analysis of the polyethylene water sachets was performed using a computer programmed Perkin Elmer DSC 8000 instrument (Figure 3.13), with approximately 5 mg PE and heated from 25°C to 150°C at 5°C/min under a nitrogen atmosphere purge of 40 ml/min. An empty aluminium pan was used as a reference.

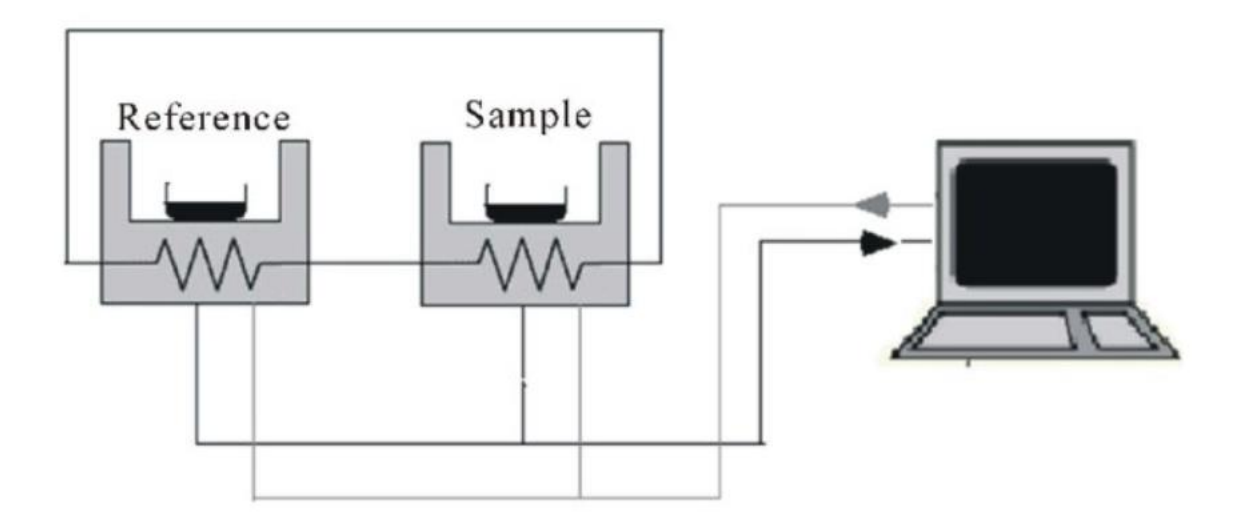


Figure 3. 11: Simple schematic diagram of Differential Scanning Calorimetry (DSC) for Thermal analysis

(87)



Figure 3. 12: Differential Scanning Calorimetry (DSC) for Thermal analysis

3.2.2.2 Fourier Transform Infrared Spectroscopy (FTIR)

FTIR is a widely used method for infrared spectral analysis, offering several benefits over traditional dispersive techniques. FTIR provides higher sensitivity, better resolution, and faster data collection, allowing entire spectra to be recorded in seconds. Unlike dispersive instruments, FTIR uses a Michelson interferometer to measure all wavelengths at once, avoiding the need for dispersing elements like prisms or gratings. This method captures an interferogram in the time domain, which is then converted using an apodization function to eliminate unnecessary data. FTIR systems typically consist of a radiation source, optics, wavelength discrimination, and a detector. The infrared beam passes through the interferometer, the sample, and the detector to record the interferogram. To reduce noise, multiple scans are often averaged. The FTIR spectrum is compared with a background spectrum collected under similar conditions. The Attenuated Total Reflectance (ATR) accessory in FTIR allows for fast, non-destructive, and efficient analysis with minimal sample preparation, providing accurate results with low noise (80).

For this research work, FTIR spectra were collected using a Nicolet 6700 FTIR spectrometer (Figure 3.14) operated by OMNIC software. Spectra were acquired within the wavenumber in the range of 500-4000 cm⁻¹ with a 4 cm⁻¹ resolution and 32 co-added scans. The instrument employed a deuterated triglycine sulphate (DTGS) detector, with cut samples of sachet polyethylene placed on the ATR crystal for spectrum recording. Both background and sample spectra were collected at room temperature. Analysis was conducted without further sample preparation.

- (i) Characterise the sachet polyethylene sample composition and;
- (ii) to evaluate the chemical changes in the UV-weathered PE film samples prepared under different weathering conditions (i.e., the influences of increasing irradiance, temperature, and time).

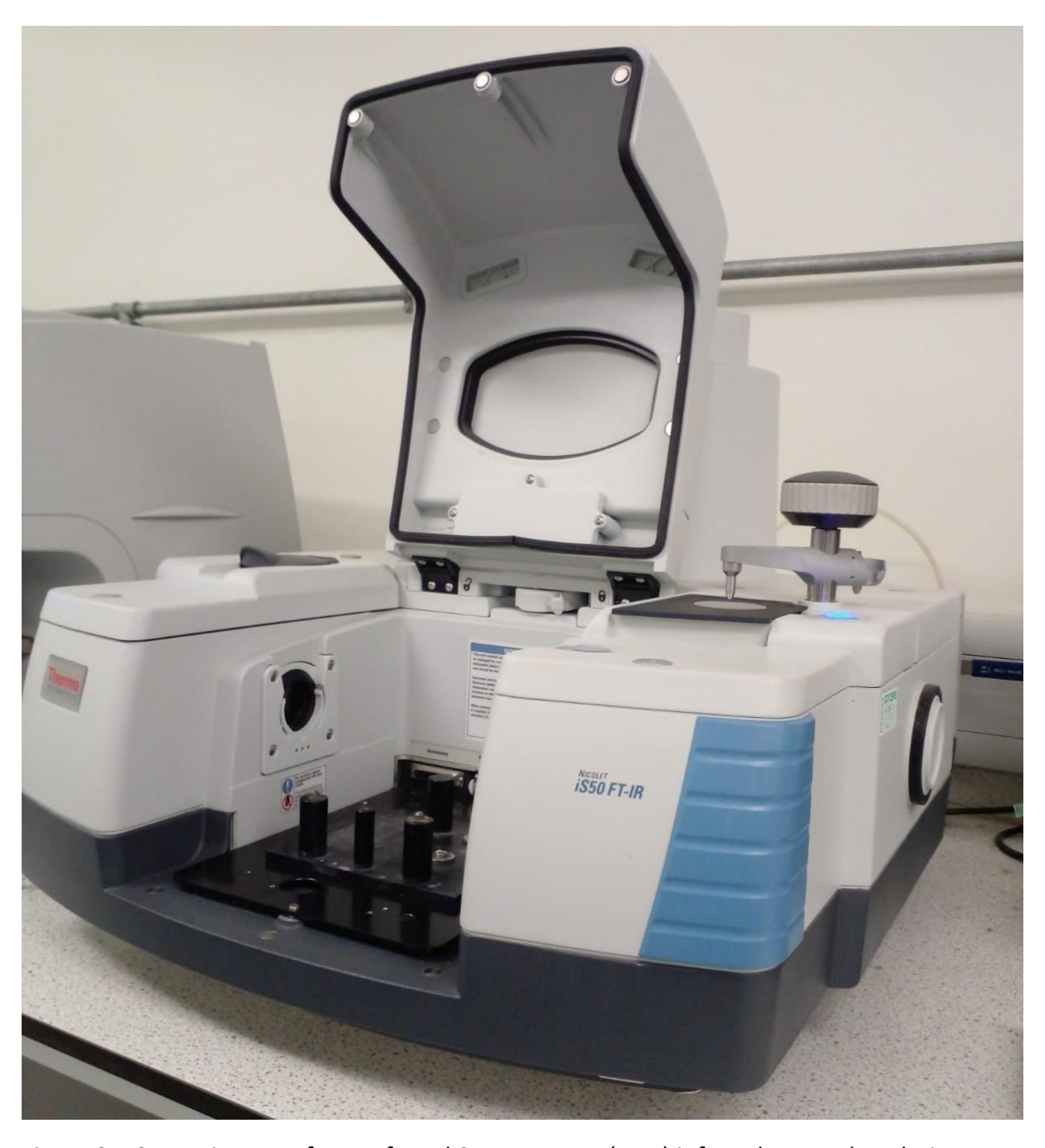


Figure 3. 13: Fourier Transform Infrared Spectroscopy (FTIR) infrared spectral analysis

3.2.2.3 Scanning Electron Microscopy (SEM)

Scanning Electron Microscopy can be used to detect changes in surface structure and roughness of materials. The SEM utilises electrons rather than light to generate highly magnified images. It employs an electron gun to emit a beam of electrons at the microscope's apex. This electron beam traverses a vertical trajectory in a vacuum-sealed environment through the microscope. En route, electromagnetic fields and lenses manipulate the beam, directing it towards the specimen. Upon interaction with the specimen, it generates various

signals due to interactions between the electrons and the specimen's atoms. These interactions produce secondary electrons (low-energy electrons emitted from the specimen's surface), backscattered electrons (high-energy electrons reflected from the sample), and characteristic X-rays. The detected signals are converted into electrical signals and processed to create a digital image (78).

Samples of various forms of polyethylene (PE) surfaces were analysed using the Quanta 650 scanning electron microscope (Figure 3.15) to observe potential changes in surface structure, particularly after UV weathering. To prevent sample charging during imaging, the samples were first coated with a thin layer of evaporated carbon using a carbon evaporator. Scanning electron microscopy (SEM) images were obtained by detecting secondary electrons, with the accelerating voltage set to 25 kV.

.



Figure 3. 14: Scanning Electron Microscopy (SEM) Quanta 650

3.3 Adsorption methodologies for the oil spill clean-up and reuse of PE sorbents

Adsorption experiments are commonly conducted by either batch or column procedures.

3.3.1 Adsorption and sorbent reuse procedure (1): Batch adsorption protocol

Within the literature, batch techniques are commonly described and employed to determine adsorption performance and kinetics. These approaches are cost-effective and straightforward, making them preferred options for small to medium-scale processes utilising basic batch equipment. The appeal of these methods lies in their simplicity, utilisation of well-established experimental procedures, and ease of interpreting results, which are frequently cited as significant factors driving their widespread adoption (82).

Generally, for the batch experiment herein (Figure 3.16), various quantities of crude oil (ranging from 5g – 10g) were mixed for 10 seconds with 250 ml deionised water in a 500 ml glass beaker. To simulate mild dispersion, each oil/water mixture was given a slight, short, single-rolling shake by hand for approximately 10 seconds. The use of deionised water and minimal mixing ensured that the system remained controlled and reproducible across different trials. Various weights of the PE sorbent, differing in type and particle size, were added into the mixture. A contact time of 5 minutes was maintained to allow interaction between the sorbent and the oil. After the sorbents were lifted from the water using sieves. The sorbents were then allowed to drain for 5 mins (tilting the sieves at an angle of about 45° to assist removal of any excess oil and help remove any trapped water droplets). The drainage time was selected as it suits the material, based on standard practices reported in literature, where drain times ranged from 30 seconds (29) to 5 minutes (167) and up to 10 minutes (133). The 5-minute duration adopted was to represent a balance between ensuring adequate removal of unadsorbed liquids and minimising evaporation and degradation effects.

It is then weighed and placed in a drying oven at 60 °C for 4 hours to enable any adsorbed/trapped water in the adsorbents to evaporate, and then the sorbents are reweighed. The weight of oil adsorbed is calculated by mass difference, subtracting the weight of the dry sorbent from the loaded sorbent after sorption. The adsorption capacity (g/g) and efficiency (%) were then calculated using standard gravimetric equations.

Preliminary investigations were carried out on the effects of salinity and pH and there were no significant impact on the adsorption performance under the tested conditions. Thus, the main experimental design focused on evaluating the influence of PE type, particle size and oil quantity.

While parameters such as temperature and mixing speed were not varied in this initial stage of the experiment to maintain a controlled, baseline setup as they are known to influence oil dispersion and adsorption dynamics in environmental settings. It was also excluded to isolate the effects of sorbent material characteristics (PE type, particle size, and oil quantity), on adsorption performance. This enabled to avoid confounding effects, which could have made it difficult to attribute changes in performance directly to the material properties. But again, these factors not included in this work could be considered in future work to simulate more realistic field conditions.

Adsorption capacity (Q) based on mass measurements is calculated according to equation 3.2 (119).

$$Q = \frac{\text{weight of adsorbed oil}}{\text{weight of dry sorbent}}$$
3.2

Adsorption efficiency (R) based on mass measurements is calculated as:

$$R = \left(\frac{\text{weight of adsorbed oil}}{\text{Initial weight of oil}}\right) \times 100\%$$
3.3

Adsorbed oil = the net mass of oil retained by the sorbent after draining and oven drying, determined by the mass difference between the oil-loaded sorbent and the dried sorbent. Oil losses during the draining stage were considered negligible based on preliminary observations. A minor loss of approximately 3% was observed during oven drying, attributed to the volatilisation of light hydrocarbons. This percentage may slightly underestimate adsorption efficiency, but the procedure was applied consistently across all samples to allow reliable comparative analysis.

The drying time of 4 hours at 60 °C was established by monitoring the weight of a PE sample after soaking with water, draining excess water, and exposure to an oven temperature of 60 °C for various time intervals until a constant weight was obtained (section 5.1.5).

For the sorbent reusability procedure, after the sorbent was lifted from the oil-water mixture, the loaded sorbent was physically squeezed using flexible sieves to separate the sorbent from the sorbent/oil mixture. After each cycle, the sorbent was inspected for appearance, and any signs of damage or degradation. The sorbent was no longer reused when the shredded PE could not redisperse on the water's surface.

To track Adsorption over multiple cycles, as the remaining capacity will typically decrease with each cycle as a result of saturation, incomplete regeneration or damage of the sorbent. After n number of cycles, the total adsorption capacity as at that cycle could be calculated as:

Total Remaining Capacity after n cycles =
$$\frac{Qn}{QQ} \times 100$$
 3.4

Where Q_n = adsorption capacity at the nth cycle

Qo = initial adsorption capacity of the sorbent (which is the maximum amount of oil that the sorbent can adsorb when it is fresh)

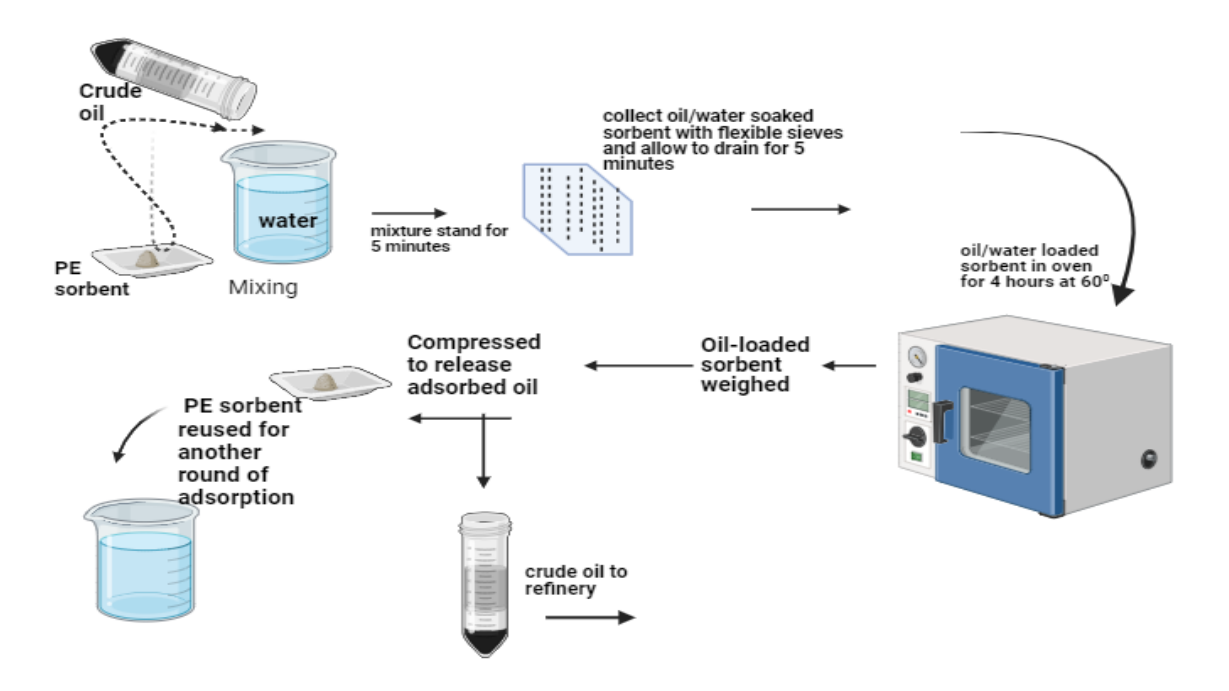


Figure 3. 15: Batch adsorption process used for the laboratory demonstration of oil spill cleaning exercise using PE sorbent

3.3.2 Adsorption, sorbent recovery, and recycling procedure (2): Column adsorption

Batch experiments are used to assess adsorption effectiveness and capacity, but continuous adsorption in fixed-bed columns is preferred in industrial settings due to its scalability and operational ease (85).

In the column experiment a glass column (1.0 -2.0 cm internal diameter (ID) and 30-50 cm length) was filled with one type of PE at a time (shredded, shredded-roughened, UV-weathered) of the same particle size range to create a high surface area available for adsorption, at the base a sieve/mesh support was used to contain the adsorbent. A mixture of water and crude oil (within a water: oil ratio of 1:25 - 1:50), after a single rolling shake by hand, was poured into the top of the column. The effluent was collected at the base of the column and analysed. Column studies are terminated when the column reaches exhaustion by a predefined means (83). For the sorbent recovery and reusability procedure:-

Once the sorbent was saturated with crude oil the water-oil mixture flow was stopped. Any remaining water from the column was drained. Oil was desorbed from the sorbent by a squeezing mechanism to desorb the crude oil from the sorbent. Dry the sorbent material completely. This can be done by air drying, vacuum drying, or using a drying oven. Inspect the sorbent for any physical damage or degradation. Check for changes in texture, colour, or structural integrity. Reactivate the sorbent, if necessary, by thermal treatment or chemical reactivation methods to restore the sorbent's adsorption capacity. Repack the cleaned and reactivated sorbent back into the adsorption column. Resume the crude oil adsorption process with the regenerated sorbent.

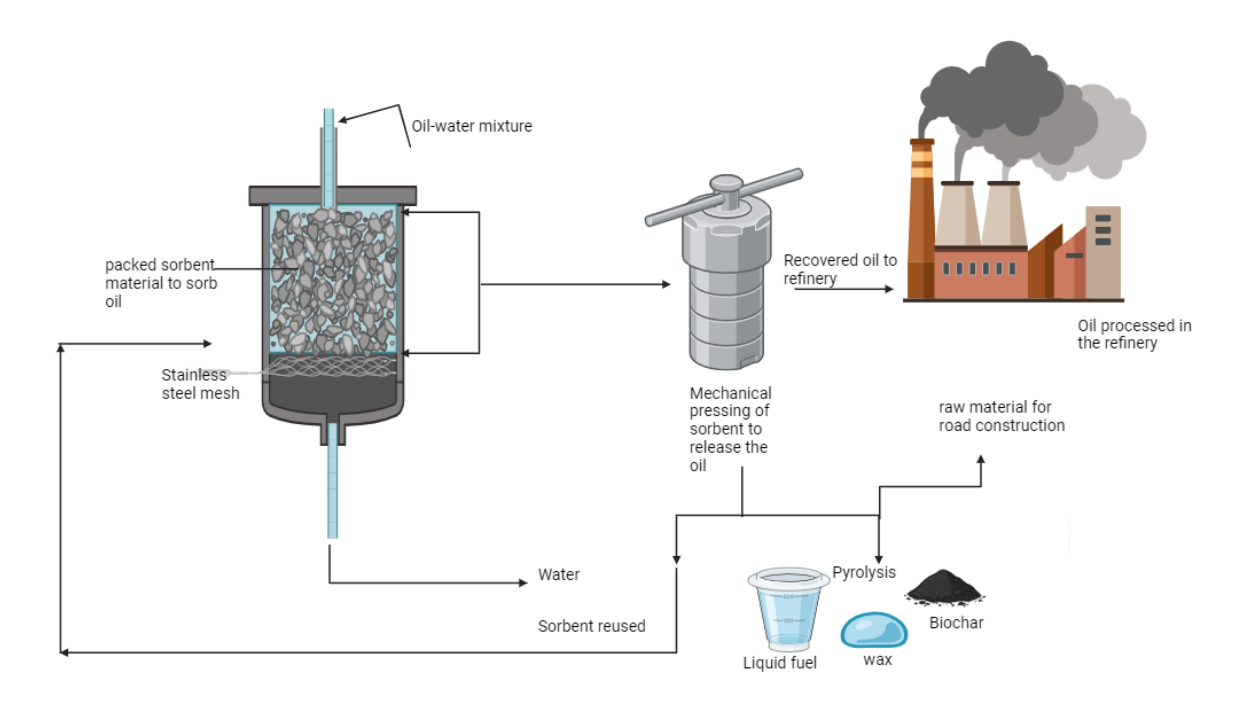


Figure 3. 16: Column adsorption process for oil spill cleaning exercise using PE sorbent

Figure 3.16 is the large-scale column adsorption process for oil spill cleaning exercise using the PE sorbent. In a large column filled with sorbents, the oil-water mixture is continuously poured in at a slow rate. The mixture is allowed to pass through the sorbent, while the sorbent selectively adsorbs the oil. The water passes through the column and exits at the bottom of the column where it is collected. The laded sorbent is taken out of the column and mechanically pressed to release the adsorbed oil. The recovered oil is taken to the refinery and reprocessed into various products, while the spent sorbent is reused another round of adsorption, or undergoes pyrolysis and produces liquid fuel, biochar, wax and raw materials for road construction.

3.4 Adsorption factors and statistical design of experiments

The various parameters, namely, mass of PE, type of PE, size of PE and mass of oil, were identified as potentially influential in the adsorption with PE material. These variables were selected based on preliminary findings. To understand their individual and interactive effects with one another is essential for optimisation performance. Table 3.3 lists the factors' descriptions and possible interactions with each other.

The vital features of an adsorption process are extremely complicated, and therefore finding the optimum values of operating parameters (conditions) becomes essential to maximise adsorption effectiveness.

Since adsorption processes often involve complex, non-linear interactions between variables, a factorial design of experiments (DoE) was adopted to explore both main effects and interactions systematically. This approach aids in identifying statistically significant factors and the combinations that result in maximum adsorption performance.

Traditional experimental methods, like altering one factor at a time, can be inefficient and resource-intensive, especially when dealing with multiple factors and potential interactions between them. To overcome these challenges, statistical design of experiments offers a systematic approach, allowing for the simultaneous variation of multiple factors while reducing the number of experiments needed. This approach involves fitting empirical models to experimental data, providing insights into the system being studied. A diverse range of experimental designs exists for studies, with the selection based on the study's objectives, whether focusing on screening or response surface analyses.

Process optimisation becomes a vital platform to determine the values of design parameters at which the response reaches its optimum levels. Thus, for this research work, the optimum conditions were determined using the Stat Ease design expert software (Version 12).

Screening designs, typically employed at the outset of a study, aim to pinpoint the primary factors influencing the response. They enable the assessment of numerous factors with relatively few experiments, potentially leading to adjustments in the range of factors studied based on screening results.

Response surface designs, used for more detailed evaluations, come into play once the primary factors affecting the response have been identified. These designs facilitate a clearer and more visually comprehensible understanding of the relationship between responses and factors through response surface plots. Additionally, they assist in pinpointing optimal conditions, which can involve maximising or minimising a response or approximating it to a targeted value (80).

Table 3. 3: Factors' descriptions and interactions

Factor	Description	Туре	Test levels	Possible interactions
Α	Mass of PE	Numeric	0.5g-1g	AB, AC, AD
В	Type of PE	Categorical	Shredded, shredded-roughened	AB, BC, BD
			and UV-weathered	
С	Particle size of	Categorical	2.8 mm ≤ x ≥ 2.0 mm	CD, AC, BC
	PE		6.3 mm ≤ x ≥ 2.8 mm	
			8.0 mm ≤ x ≥ 6.3 mm	
D	Mass of oil	Numeric	5g – 10g	AD, BD, CD

Chapter 4

4.0 Characterisation of polyethylene sachets and crude oils

This chapter focuses on the characterisation of PE water sachets and crude oils, and the effects of PE weathering (natural and artificial UV light), shredding, and roughening using different preparation and characterisation techniques. It details the procedures used to collect data and how the PE sachets and oils were analysed. This study included natural-weathered polyethylene to compare its compositional and structural transformations with accelerated UV-weathered PE. The objective was to evaluate how natural weathering impacts the structural and chemical properties of PE relative to controlled UV exposure. This comparison aimed to provide insights into the duration and extent of environmental exposure that PE can endure while remaining viable for oil spill cleanup applications.

However, the naturally weathered PE was not included in the oil adsorption experiments due to its limited availability and insufficient degree of weathering. The sample was weathered for only 50 days (1200 hours), whereas natural weathering typically requires significantly longer periods to induce substantial material degradation. This limited weathering period was insufficient for meaningful comparative adsorption analysis, as the structural and chemical changes observed were not as pronounced as those in the UV-weathered samples.

The characterisation of the PE water sachets was carried out to understand the polyethylene nature, its chemical composition, its various forms, and ultimately how these characteristics will affect the adsorption properties. The crude oils were characterised to understand the chemistry of the crude oil on the adsorption behaviour and also to understand how oil composition changes when exposed to the air. The purpose of data collection and analysis in this chapter is to systematically gather verifiable evidence and analyse it to assess the effectiveness and feasibility of PE as a sorbent material for oil spill remediation. This study aims to contribute to the scientific understanding and potentially inform practical applications of PE in environmental remediation efforts, its sorption capabilities, mechanisms, and its performance in real-world applications and environmental conditions.

The methods used for data collection and analysis in this chapter typically involve both experimental procedures and analytical techniques.

4.1. Characterisation of pristine polyethylene water sachets

The polyethylene water sachets as described in Section 3.1.1. are from different water providers (e.g. Greenmark, Golden age, Royalunik, Zagbayi, Yarima and Munirah gold). There is printed marketing information on the sachets, done with different coloured inks (royal blue, dark blue, etc.).

4.1.1. Characterisation of pristine PE using Fourier transform infrared spectroscopy (FTIR)

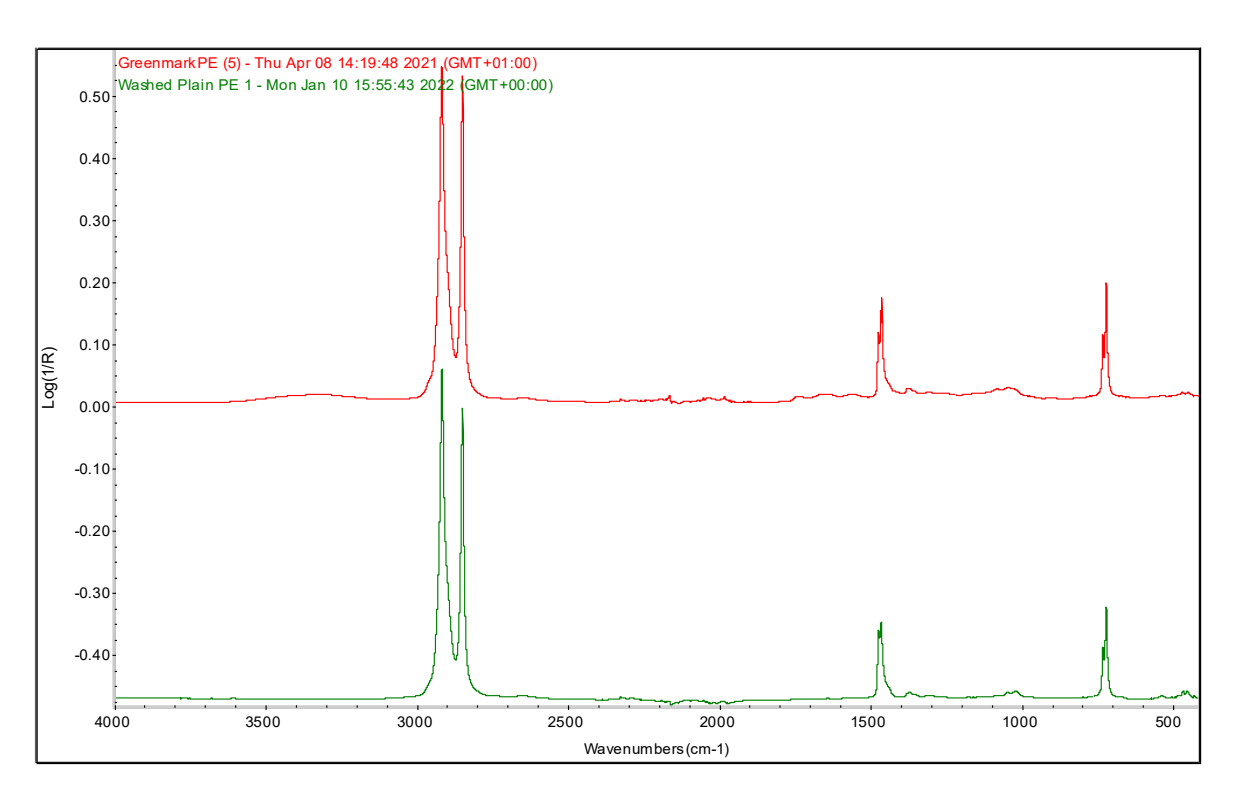


Figure 4. 1: spectra of Greenmark sachet polyethylene samples, top spectrum is the back side, the bottom spectrum is the front side

Two spectra from Greenmark PE were collected, one spectrum from the back side of the polyethylene (the inside of the sachet), opposite the ink mark, and the other from the front (the outside of the sachet) of a plain (non-ink) area. The spectra were observed in the mid-IR region (400-4000 cm⁻¹). From the spectra shown in Figure 4.1, the two spectra are similar, indicating that the ink did not penetrate through the polyethylene. If the ink was detected on the PE, one may anticipate bands in the 1900-1500 cm⁻¹ and 1450-800 cm⁻¹ regions (see

below). The reason for the presence of the low intensity bands in these areas in Figure 4.1 are unknown, but are likely contamination or possible additives. There are six dominant bands in the spectra, representing the different molecular vibrations of the samples, two strong bands between 2800 cm⁻¹ and 3000 cm⁻¹, and two weaker doublet bands at 1450 cm⁻¹ and 750 cm⁻¹. These characteristic bands closely match those in spectra of PE shown in data in the literature (33). When comparing with reference spectra in the library database the spectra also identified these samples as polyethylene. The assignment of the band vibrations are, 731-720 cm⁻¹ (C-H rocking deformation), 1473 cm⁻¹ – 1463 cm⁻¹ (C-H bending deformation), 2851 cm⁻¹ (CH₂ symmetric stretching) and 2919 cm⁻¹ (CH₂ asymmetric stretching). All five polyethylene samples obtained from different water suppliers used in this study showed similarities of composition and band vibrations (Figure 4.9). The Greenmark PE was not used for adsorption experiments due to its limited availability, as obtaining additional quantities for shredding was not feasible. Instead, other types of PE were used, as they were more readily available in greater quantities.

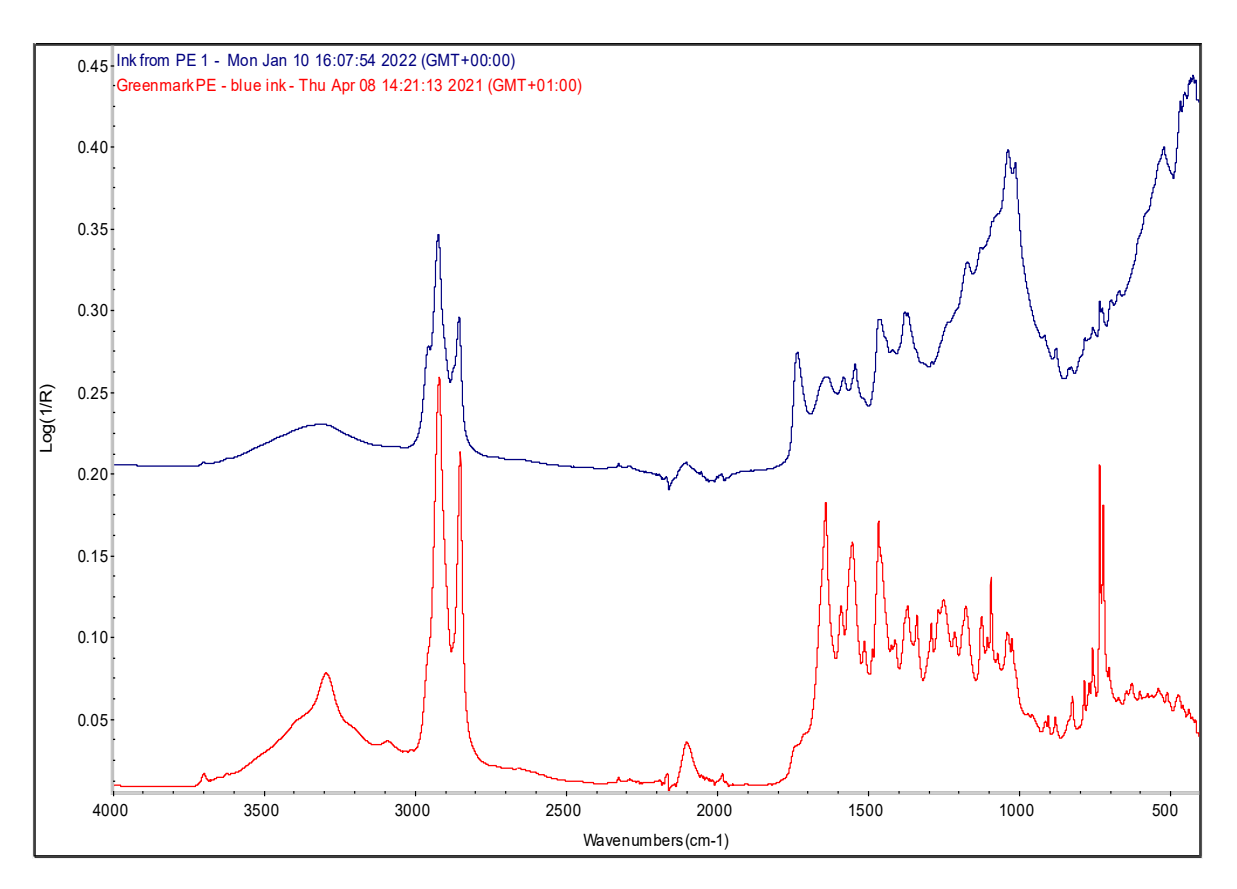


Figure 4. 2: FTIR spectra of ink (on polyethylene)

Figure 4.2 illustrates the FTIR spectra analysis of ink from Greenmark PE sachets when using two different collection methods. Ink was scraped directly from the Greenmark PE sachet and analysed (blue spectrum). The red spectrum was obtained from ink first dissolved in dichloromethane (DCM), from which the solution was applied to the ATR (attenuated total reflectance) crystal. The DCM was then evaporated, leaving the ink behind for analysis. Although different sachets were used to scrape the ink or dissolve in DCM, the sachets were from the same water supplier, and the inks were visibly the same.

It is seen in the spectra of the inks (Figure 4.2) that there are many bands, indicating that the ink is not a simple chemical or perhaps a combination of chemicals. The ink spectra are identified as hydrocarbon-based, as indicated by strong absorption bands between 2800 cm⁻¹ and 3000 cm⁻¹, corresponding to CH₂ symmetric and asymmetric stretching. The presence of a band near 1640 cm⁻¹ (C=O stretching) and another around 3300 cm⁻¹ (N-H bending) suggests the presence of an amide group, indicating a polyamide-based resin. Additionally, the band observed at approximately 1740 cm⁻¹ is likely attributed to C=O stretching in an ester group, suggesting that the ink matrix may have a polyester-based composition. The ink has hydrophilic groups, as evidenced by the N-H and C=O bonds. It could therefore change the polarity of the surface. Other components which could be ink additives or fillers are difficult to identify using FTIR alone. The red spectrum has distinct, sharp and more pronounced peaks, than the blue spectra, thus, the analysis shows that the method of sample preparation/collection significantly affects the FTIR spectra of the ink, possibly impacting the composition and the way in which the detectable functional groups interact with each other in the ink samples. Dissolving the ink in DCM and then evaporating it provides a clearer and more detailed spectrum, highlighting the ink's molecular components more effectively than direct scraping.

4.1.2. Characterisation of pristine PE using Differential Scanning Calorimetry (DSC)

The DSC results help to understand the thermal stability, melting behaviour, and crystallization kinetics of the PE samples. In the context of polyethylene, DSC measures the melting temperature (Tm), crystallization temperature (Tc), and the associated enthalpy

changes (ΔH) which are critical for understanding the thermal properties and crystallinity of the material.

Samples were washed with detergent and water to free them from any contaminants that could interfere with the analysis. The samples were cut into small, uniform pieces (3 x 3 mm) to ensure consistent results. The PE samples were placed in small aluminium pans, which were sealed with an aluminium cover before pricking with a small gauge needle just before loading into the DSC to remove any potential pressure buildup during heating. Before determination of its crystalline melting temperature, the PE sample was first melted and cooled to remove its thermal history before heating a second time.

Experiment (Measurement of Heat Flow)

During the melting phase, as the temperature increases, polyethylene undergoes a phase transition from a solid to a liquid state. This transition is typically observed as an endothermic peak on the DSC curve. The melting endotherm reflects the absorption of heat energy required to break the intermolecular forces holding the crystalline polymer chains together in the solid phase. Then, upon cooling, the melted polyethylene can recrystallise and transition back to a solid state. This crystallisation process releases heat, which is observed as an exothermic peak on the DSC curve. The crystallisation exotherm represents the energy released as the polymer chains reorganise and form ordered crystalline structures (71).

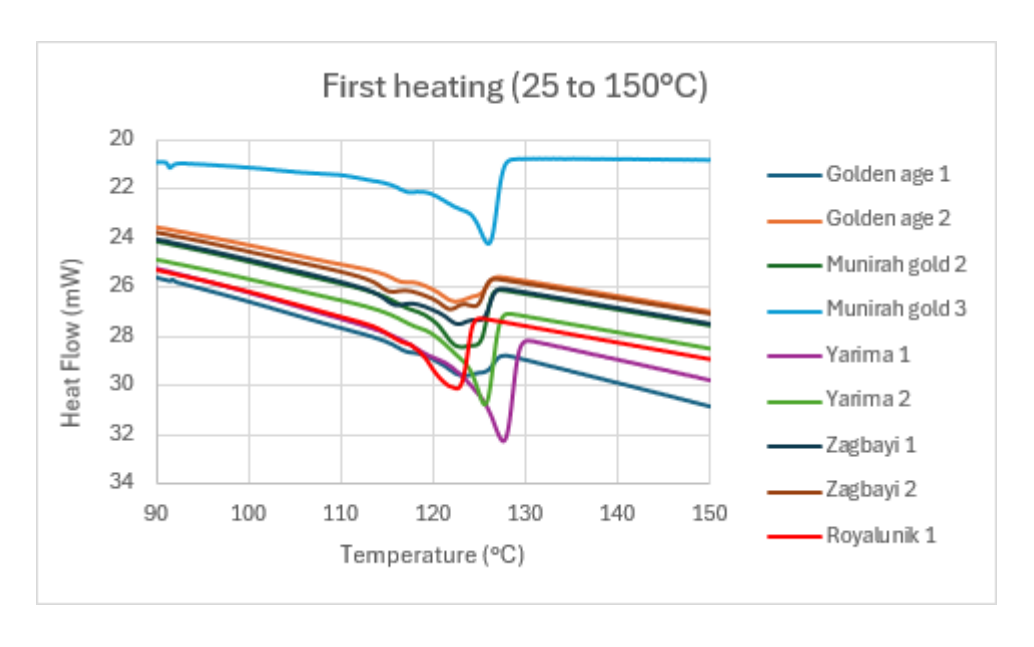


Figure 4. 3: DSC first heating curves for all the PE samples to check for uniformity/similarity and repeatability

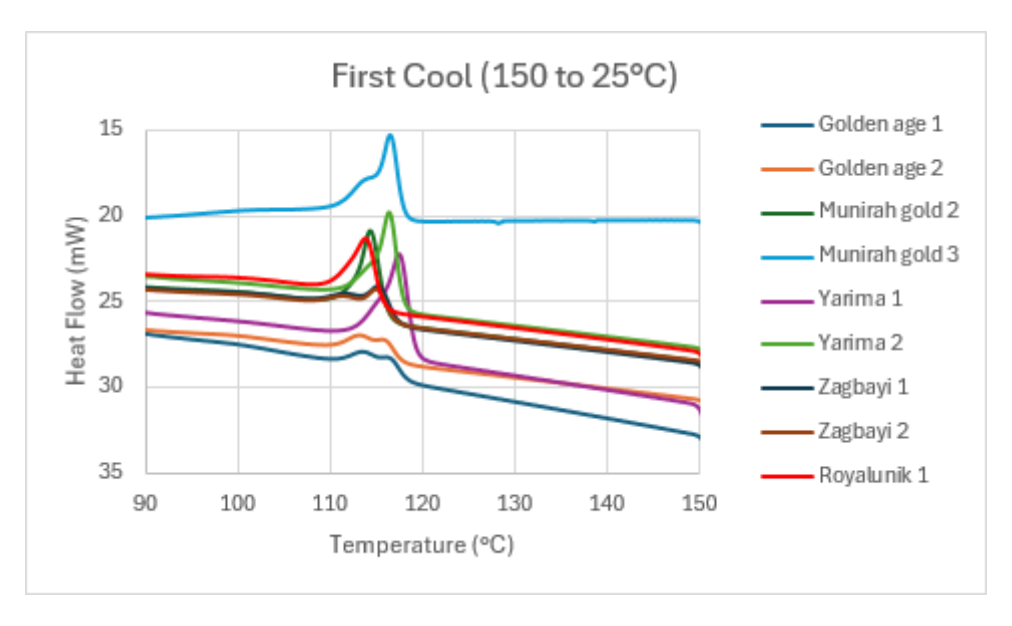


Figure 4. 4: DSC first cooling curves for all the PE samples to check for uniformity/similarity and repeatability

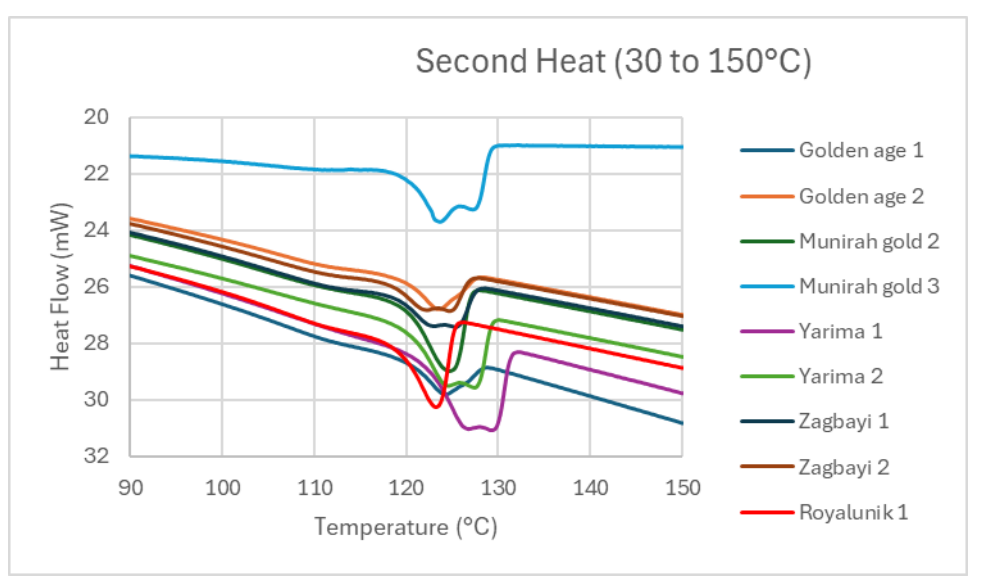


Figure 4. 5: DSC second heating curves for all the PE samples to check for uniformity/similarity and repeatability

From Figures 4.3, 4.4, and 4.5, which represent the first heating, first cooling and second heating stages, respectively of the DSC experiments. All the PE samples have different thermal histories, and different mixtures and amounts of LDPE and LLDPE.

The first melting curves (Figure 4.3) of golden-age PE samples (dark blue and orange) have different curves, indicating different thermal histories. The cooling (Figure 4.4) and second heat (Figure 4.5) are the same, indicating similar polymer contents and characteristics.

Zagbayi PE (dark green and brown) samples show similar curves from the start to the end of the first heating cycle (Figure 4.3), first cooling cycle (Figure 4.4), and second heating cycle (Figure 4.5), so have both similar thermal histories, polymer content and characteristics.

These were collected from two different sachets (Zagbayi and Golden-age) and so show there is some reproducibility between sachets.

The melting curves of Munirah gold PE samples (dark green and light blue) show a similar trend from the start of the first melting but differ at the end, then the same for the first cooling cycles and second heating cycles. It is noted that the thermal curve for Munirah Gold 3 exhibited a noticeable deviation from the other polyethylene samples, this difference is likely attributable to an instrumental baseline shift during the DSC measurement. Yarima PE samples (mauve and light green curves), show similar melting curves from the start of melting and a slight difference at the end, then the same for the first cooling cycles and second heating cycles. This could likely be attributable to minor processing variations and their thermal histories, but they contain different polymer contents and characteristics more confidently. Royalunik PE melting curve (red curve) is different from all the rest of the PE samples, from the first melting and cooling to the second melting.

The melting peaks (Figure 4.5) across all samples occur within a similar temperature range (around 115–130°C), as do the cooling peaks (Figure 4.4) within similar temperature range (110 - 120°C), reflecting the presence of polyethylene as the base polymer in all samples. Differences in peak heights are observed among different water sachet types, indicating variations in crystalline content, molecular weight or formulation (i.e. the content of LDPE and LLDPE). LDPE typically has a lower melting temperature (around 105–115°C) due to its highly branched structure, which reduces crystallinity. LLDPE has a higher melting range (120–130°C) because of its more linear structure with short chain branching, allowing for higher crystallinity (101). The sharper, more defined, higher temperature melting peaks (above approximately 115°C) correspond to LLDPE's more ordered crystalline regions as is noticed with Yarima. The broader or lower temperature melting peaks (below 115°C) reflect LDPE's diverse crystallite sizes, as branching disrupts uniform crystal formation, as shown with Golden age, and Zagbayi samples. Munirah Gold 2 and Royalunik samples display slightly

more pronounced peaks compared to others, which may indicate differences in additives, processing conditions, or molecular characteristics (101). Variations in processing conditions, and differences in thermal history (e.g., cooling rate during production) can significantly affect crystallinity and melting behaviour. Faster cooling rates lead to lower crystallinity and broader melting peaks. Slower cooling rates allow more time for crystal growth, resulting in sharper peaks at higher temperatures. Samples with higher LLDPE content are likely to show sharper, more defined peaks at higher temperatures (between 120–130°C for polyethylene), indicating greater crystallinity and a more uniform structure. Samples with higher LDPE content will exhibit broader peaks at slightly lower temperatures, reflecting lower crystallinity and more amorphous regions due to the branched structure.

Since all the PE samples exhibit similar melting and cooling temperature range characteristics, a sample of Munirah Gold 2 is used for a generalised analysis to explain the DSC melting curves observed in step 3 (second melting) as shown in Figure 4.6.

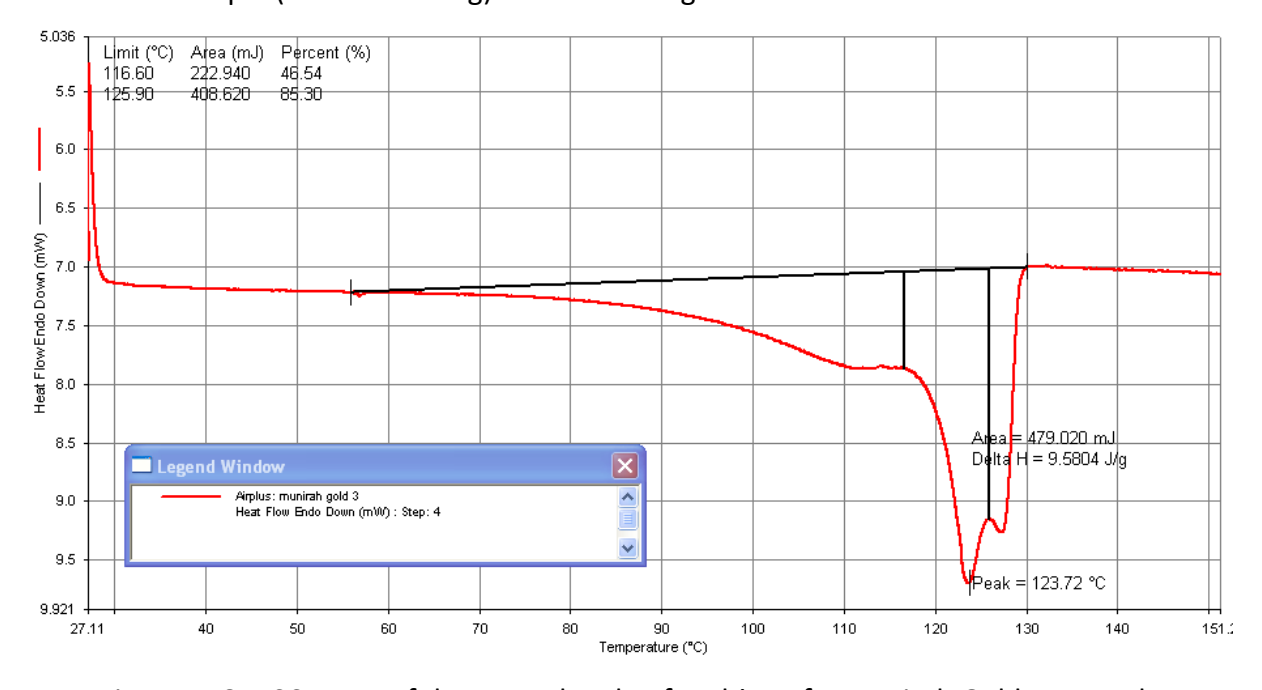


Figure 4. 6: DSC curve of the second cycle of melting of a Munirah Gold PE sample

The first melting curve typically captures the material's original/as-received state, including the thermal history from the processing conditions, thus the material was reformed during the slow cooling phase. In Figure 4.6, the second melting cycle, provides a more stabilised and comprehensive thermal response. The enthalpy of melting (ΔH) was measured at 9.5804 J/g, which reflects the energy required to melt the crystalline regions of the polymer. This suggests a moderate level of crystallinity (101), compared to other polymers as enthalpy is directly

proportional to the crystalline content. The melting transition occurred dominantly within a narrow temperature range of 116.6°C to 125.9°C, exhibiting sharp peaks and highlighting a uniform crystalline structure. The broad endothermic area and gradual slope leading up to the sharper peaks suggest the coexistence of less-ordered and more-ordered crystalline regions, with varying chain stability. This is typical of blends containing components with distinct crystallization behaviours.

These peaks strongly suggest the presence of two polyethylene types; LDPE (which typically melts in the range of 110–115°C but may show broader transitions due to its branched structure and lower crystallinity) and LLDPE, with its more linear and crystalline structure, melts at a higher temperature, typically between 120–130°C, corresponding to the observed peak at 123.72°C and the higher shoulder at 127°C. The LDPE might likely contribute to the lower-temperature shoulder observed in the range, mostly around 116–120°C, but also some to as low as 70°C.

According to Yamaguchi et al, in their work, they showed that LLDPE is miscible with LDPE in the amorphous region and that the two polymers exclude one another during crystallization (100). When compared with standard data from the literature (71, 101), the melting behaviour aligns with that of a blend containing LDPE and LLDPE. LDPE contributes to the lower-temperature transitions and broader melting range, while LLDPE contributes to the sharper, higher-temperature peaks due to its more crystalline and linear structure.

4.1.3. Characterisation of pristine PE by thermogravimetric analysis (TGA)

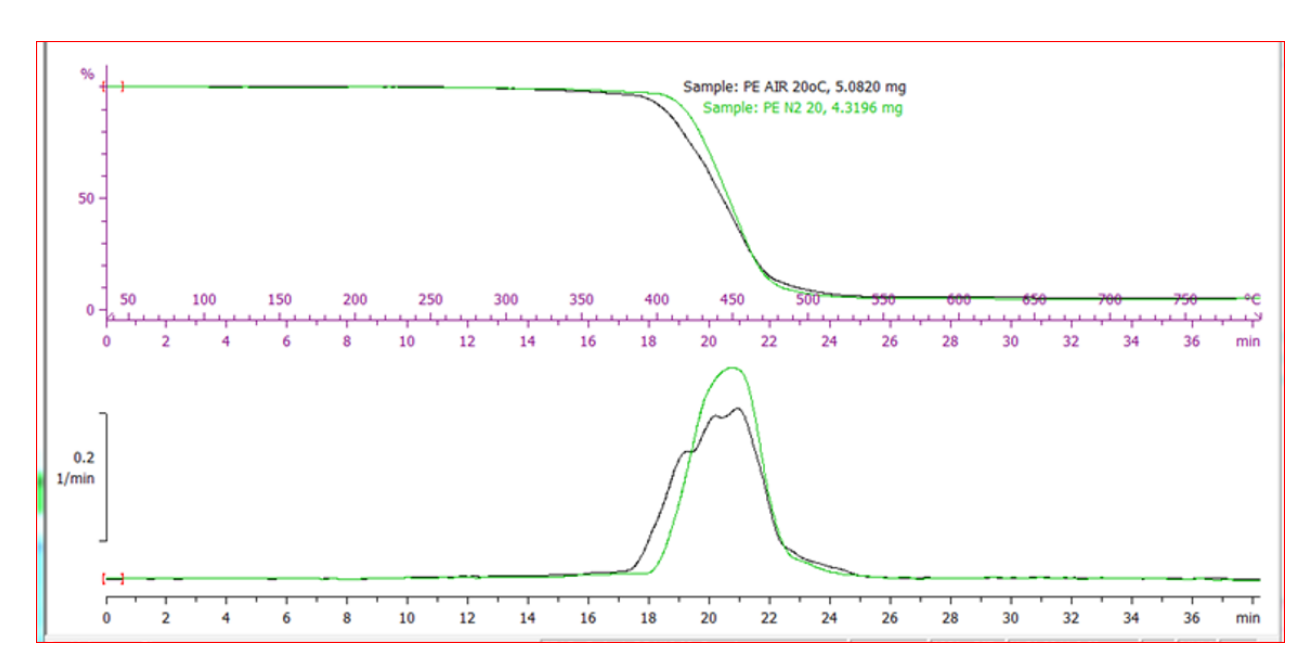


Figure 4. 7: Thermogravimetric (top) and derivative thermogravimetric (bottom) curves for Greenmark PE at a heating rate of 20°C/min under nitrogen or air

The thermogravimetric analysis (Figure 4.7) reveals that polyethylene (PE) remains thermally stable with no significant weight loss observed up to 400°C. Decomposition occurs in a single, well-defined stage, with the peak rate of degradation at approximately 450°C. This behaviour indicates high thermal stability, with a uniform degradation process confined to a relatively narrow temperature range. The absence of further weight loss beyond 500°C confirms the completion of thermal decomposition.

There are some subtle but notable differences when comparing the degradation of PE under air and nitrogen atmospheres. In the air (black line), the degradation profile between 400 °C and 480 °C exhibits more distinct, stepwise changes, suggesting multiple degradation mechanisms, likely in three main phases, but with nitrogen (green line) atmosphere it shows a single, continuous degradation stage. The initial decomposition temperature in nitrogen begins slightly and later, indicating a marginally higher thermal stability when compared to under air atmosphere.

The derivative thermogravimetric (DTG) curve highlights differences in the rate of mass loss between the two atmospheres. The air sample's degradation peak is broader, suggesting a more gradual process, due to oxidative reactions. Conversely, the nitrogen sample displays a sharper, more well-defined peak, indicative of a more rapid and uniform degradation in the

absence of oxygen. Despite these differences, the final residual mass for both conditions is similar, with a small amount of residue (non-hydrocarbon components of the PE) of about 8% mass remaining in the crucible at the end of the decomposition.

In summary, while both samples decompose within the same temperature range (400-500°C), the presence of oxygen in the air introduces additional degradation pathways, leading to a broader decomposition profile. Under nitrogen, the degradation is more rapid and concentrated, due to the inert environment which suppresses oxidative reactions. These subtle variations underscore the role of oxygen in influencing the thermal decomposition behaviour of PE.

4.2 Characterisation of ultraviolet-weathered PE water sachets

4.2.1. Characterisation of ultraviolet-weathered PE water sachets by FTIR

Accelerated ageing is usually achieved by simultaneously increasing the intensity of UV light and increasing the temperature of the exposed samples. Although the representativeness of synthetic ageing is still debated, according to the Q-lab technical bulletin (73), 340UVA provides the best correlation to actual outdoor weathering at an irradiance of 0.76 W/m² UV and 60°C, which is equivalent to noon summer sunlight. It also shows that a proportional increase in the irradiance affects the sample being tested more. Thus, to achieve faster results (double effect), for the analysis 1 experiments herein, high values of irradiance (1.55W/m²) UV and temperature of 70 °C were used for weathering of PE samples for durations of 80 hours (which is equivalent to 160 hours with double IRR).

For the analysis 2 experiments, five different samples of polyethylene films underwent the same accelerated photooxidative experiments using UV light intensity irradiance of 0.76 W/m (normal noon light), temperature 60 °C, and various time durations. Fourier transform infrared spectrometry (FTIR) utilising Attenuated Total Reflectance (ATR) with a diamond crystal was employed to assess the structural alterations induced by UV exposure. To assess the reproducibility of FTIR analyses, measurements were initially repeated multiple times for select samples, and this demonstrated consistent spectra with high repeatability. Consequently, only one spectrum was recorded for each sample.

Various areas of the samples of PE water sachets were analysed by FTIR and are identified as;

- (i) IS ink sample, spectrum collected directly from the ink inscription
- (ii) NIS no ink, spectrum collected from the front side of PE sachet

(iii) the back - spectrum collected from the plain non-ink area of the PE sachet not exposed directly to the UV bulb.

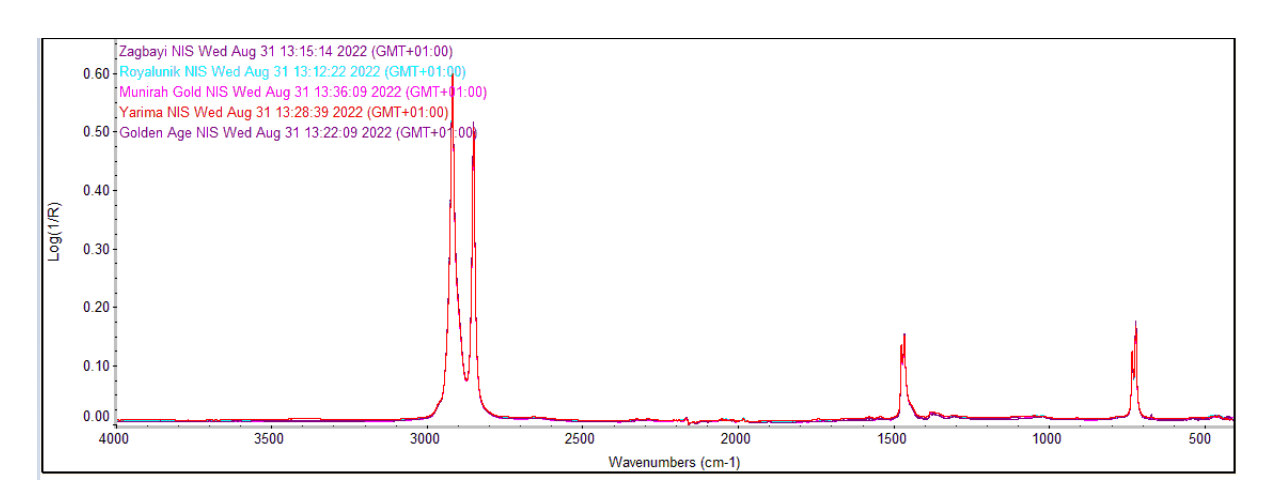


Figure 4. 8: FTIR spectra of the five PE Pristine samples

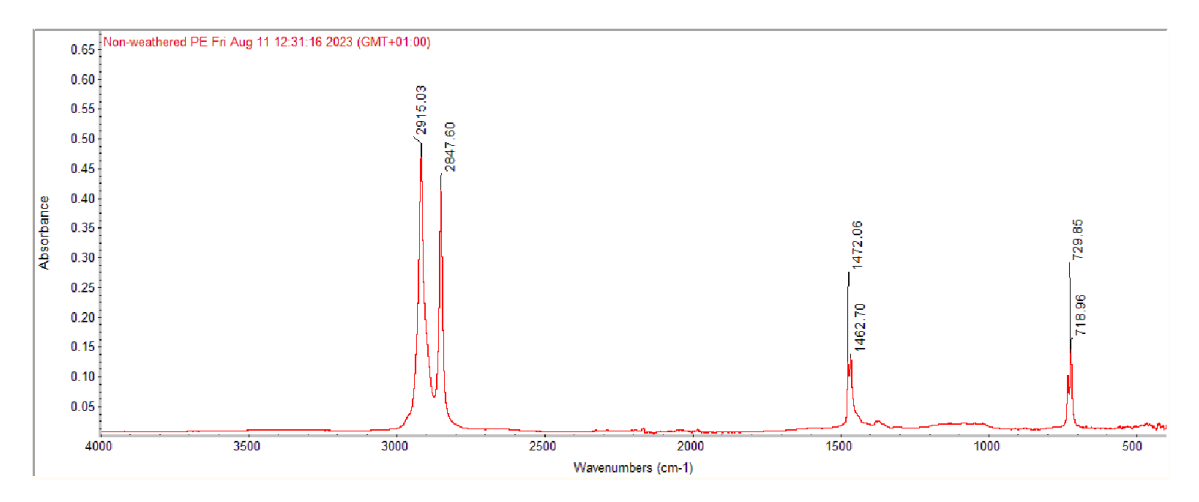


Figure 4. 9: FTIR spectrum representing all Pristine PE samples

From Figure 4.8 and Figure 4.9, the prominent bands at 2916 cm $^{-1}$ and 2849 cm $^{-1}$ represent the C-H stretching, and correspond to the asymmetric and symmetric stretching vibrations of the methylene (-CH $_2$ -) groups. Their high intensity and sharpness indicate a high concentration of methylene groups, which is characteristic of polyethylene's structure. The bands at 1470 cm $^{-1}$ and 720 cm $^{-1}$ are the C-H bending. The bands at these wavenumbers are due to the rocking vibrations of the methylene groups. The intensity of these bands confirms the long-chain hydrocarbon nature of polyethylene.

The spectra for all five pristine PE samples are nearly identical, with no significant deviations in peak position or intensity. There are no oxidative/carbonyl (C=O)/hydroxyl peaks. This confirms the pristine condition of the samples, with no oxidative degradation. This uniformity

indicates that all the samples have similar molecular compositions and structures, likely consisting of primarily linear polyethylene chains without significant impurities or variations in additives.

The flat baseline in the spectra highlights minimal background noise and no interference, ensuring that the observed peaks are clear and reliable for analysis. These spectra align well with the expected characteristics of polyethylene, particularly its high content of methylene groups and absence of functional groups associated with degradation or additives. The similarity across samples suggests consistent material quality and processing conditions.

Thus, these pristine spectra served as a baseline for identifying degradation patterns, such as the formation of carbonyl or hydroxyl groups.

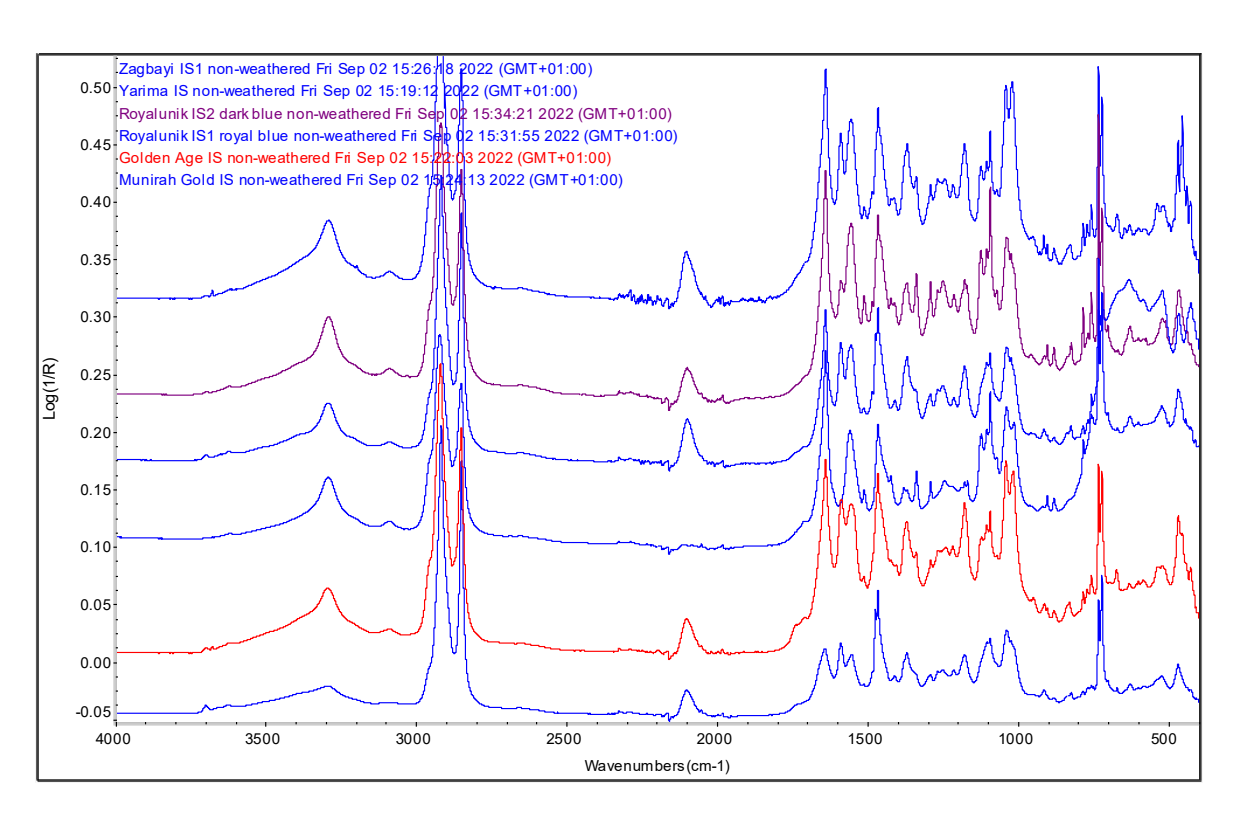


Figure 4. 10: FTIR spectra of the various inks on all the PE samples before weathering

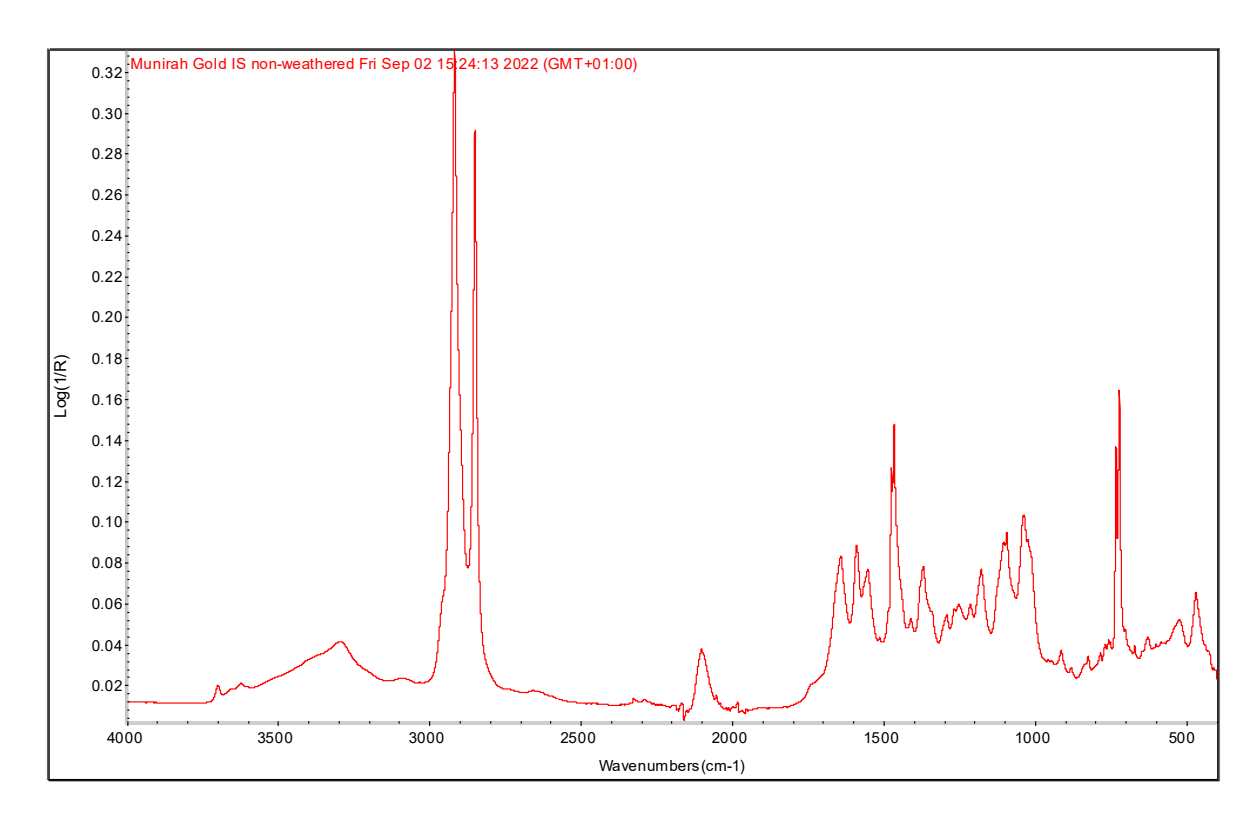


Figure 4. 11: FTIR spectra of the various inks on all the PE samples before weathering

For Figure 4.11, all the ink spectra exhibit similar broad features, indicating that the different samples likely share common materials or structural components as described in Figure 4.8 for the plain side. Some spectra, such as those of Royalunik IS1 and IS2 show higher reflectance values (stronger signals) compared to others like Munirah Gold. These differences in signal intensity could be due to variations in the surface texture, ink thickness or pigmentation as the ink colours differ from one another. The lower wavenumber region (below 1000 cm⁻¹) shows noticeable differences between the spectra, for example, the Golden Age spectrum has distinct bands that are either shifted or less intense compared to the other spectra. These variations suggest that each sample's chemical composition is slightly different.

Analysis 1: Constant irradiance, temperature, and time

This analysis was used to determine:

- (i) which PE sachet is more susceptible to oxidisation
- (ii) whether the front and back sides of the water sachets are uniformly oxidised when exposed from the front side
- (iii) whether the ink is oxidised (including visual changes reported)

Conditions used: Irradiance = 1.55 W/m^2 (this is double of the normal irradiance of daylight sunlight to achieve quicker results (81)); Temperature = 70°C ; Time = 80 hrs (80 hours with double irradiance is equivalent to 160 hours of daylight sunlight).

The results of these experiments are displayed in Table 4.1 and Figures 4.12

Spectra were collected from the different areas. Areas of bands were used to represent a quantitive change due to oxidation. The PE band areas between 650-800 cm⁻¹ were more reproducible and less effected by spectral collection procedures. These were therefore used as an internal reference to the amount of PE present and therefore, assess the extent of oxidation as shown by the band area of the C=O region.

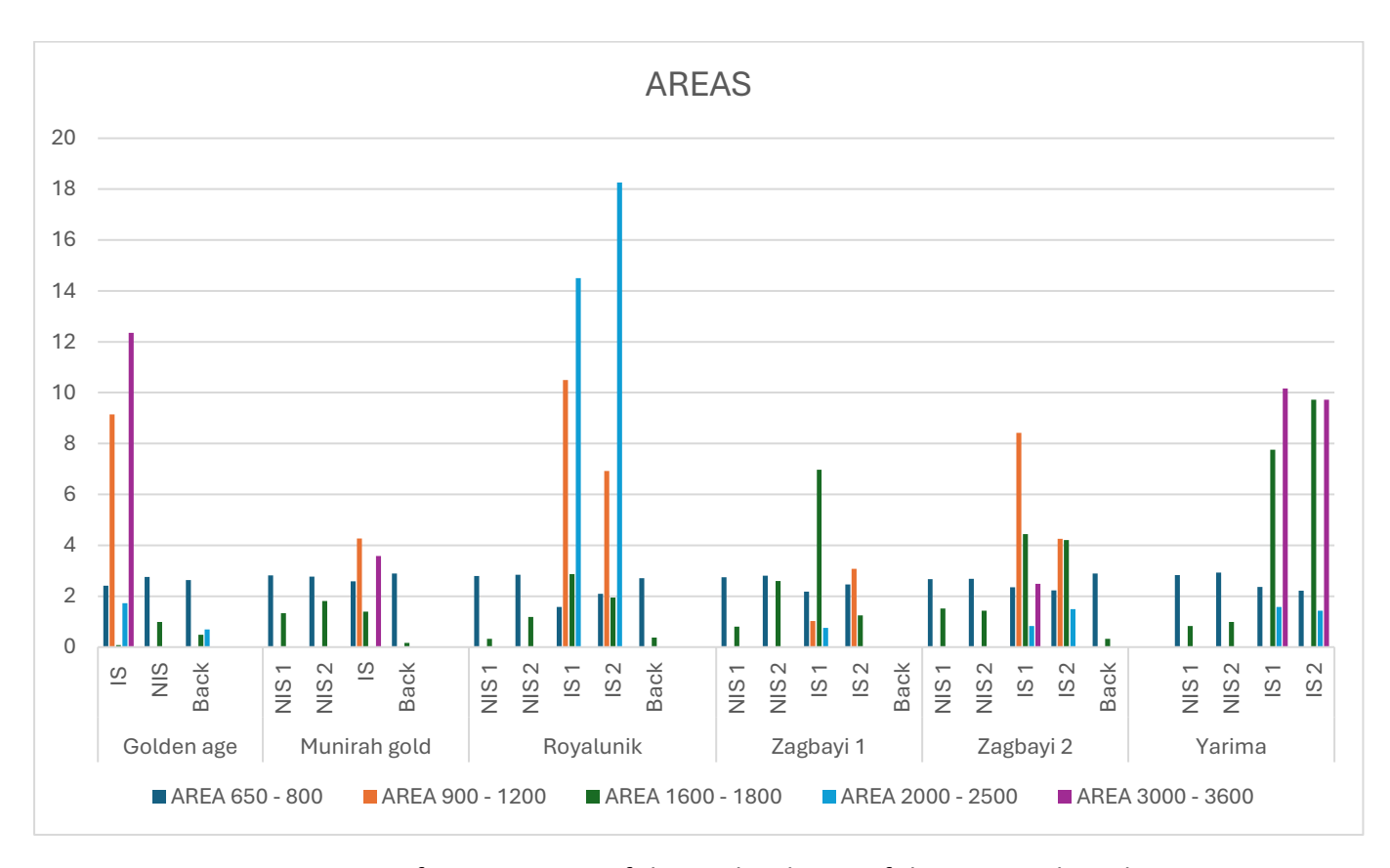


Figure 4. 12: Comparison of various areas of the oxidised sites of the UV weathered PE

From Figures 4.12 the areas around 650-800 cm⁻¹, being one of the PE characteristic bands were approximately the same, this means that the peak intensity was stable for all the PE samples.

It is worthy of note that the high oxidations that occurred on the PE took place on the ink spots, this could mean that the ink could have acted as a catalyst that boosted the oxidation on those areas. The ink oxidised more rapidly with many bands springing up around 2000-2500, 900-1200, and 3000-3600 cm⁻¹ wave numbers. The ink on Royalunik showed the highest ink oxidation, but the colour change on the PE was not very significant; this might mean that the ink was thicker on it than the rest. The ink on Golden age, and Yarima faded much faster, which means that the ink on them was not so thick.

Again, it is noticed that more oxidation took place at the front of the PE (the side facing the UV lamps) than at the back of the PE. The carbonyl formation around the area 1600-1800 cm⁻¹ wavenumbers were highest at the Yarima PE sample, followed by Zagbayi, Royalunik, Munirah gold and then Golden age, in the presence of ink.

Table 4. 1: Area ratio of the carbonyl bands with alkane bands of PE

		Area
		(Ratio)
Golden Age	NIS	2.78
	Back	5.39
Munirah gold	NIS 1	2.12
	NIS 2	1.53
	Back	17.20
Royalunik	NIS 2	2.40
	Back	7.14
Zagbayi 1	NIS 1	3.40
	NIS 2	1.08
Zagbayi 2	NIS 1	1.77
	NIS 2	1.88
	Back	8.80
Yarima	NIS 1	3.44
	NIS 2	2.98
	IS 1	0.31
	IS 2	0.23

Carbonyl area index = the maximum peak area absorbance for Carbonyl group the value of the area of the reference peak

4.1

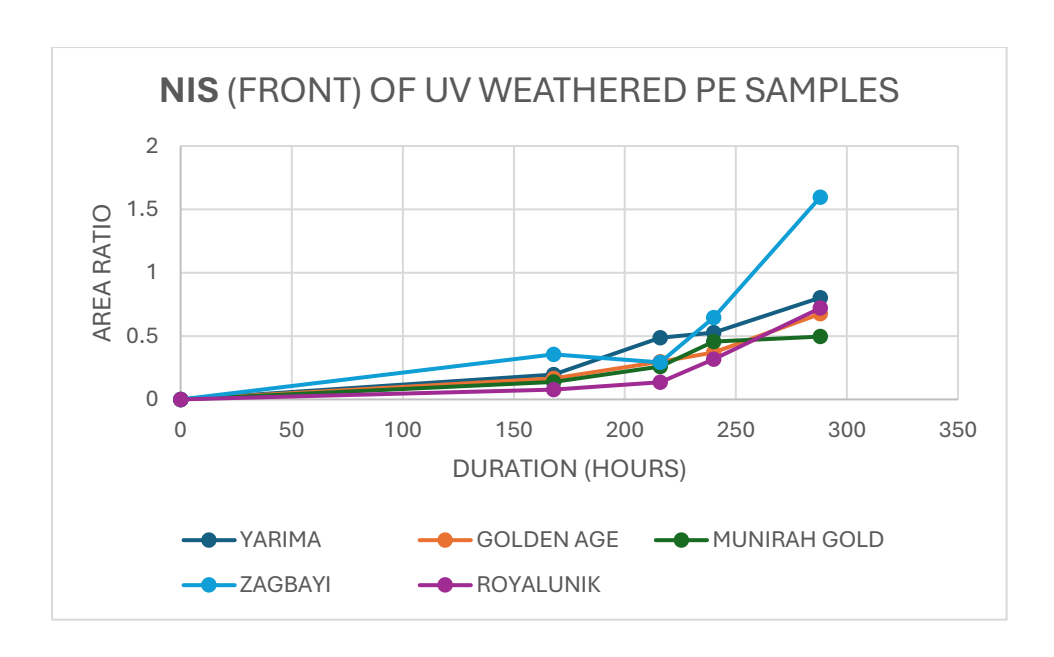


Figure 4. 13: Area ratio vs duration for all PE samples (NIS)

ANALYSIS 2

A comparison was conducted on all the inks used for the inscriptions on the various PE samples before and after weathering, for uniformity and to assess the durability, stability, and weather-resistance of the inks used on the polyethylene samples.

The weathering process was carried out under controlled conditions of constant irradiance (0.76 W/m²) and constant temperature (60°C), with varying exposure durations of 126 hours (5.25 days), 168 hours (7 days), 216 hours (9 days), and 288 hours (12 days).

The polyethylene samples tested included Golden Age, Royalunik, Zagbayi, Yarima, and Munirah Gold. To ensure repeatability and reproducibility, each polyethylene type was weathered multiple times under the specified conditions. The results were consistent, with each sample being analysed two to three times to confirm reproducibility.

A representative spectrum from each sample was selected and used as a reference to compare the behaviour and performance of the inks across all samples.

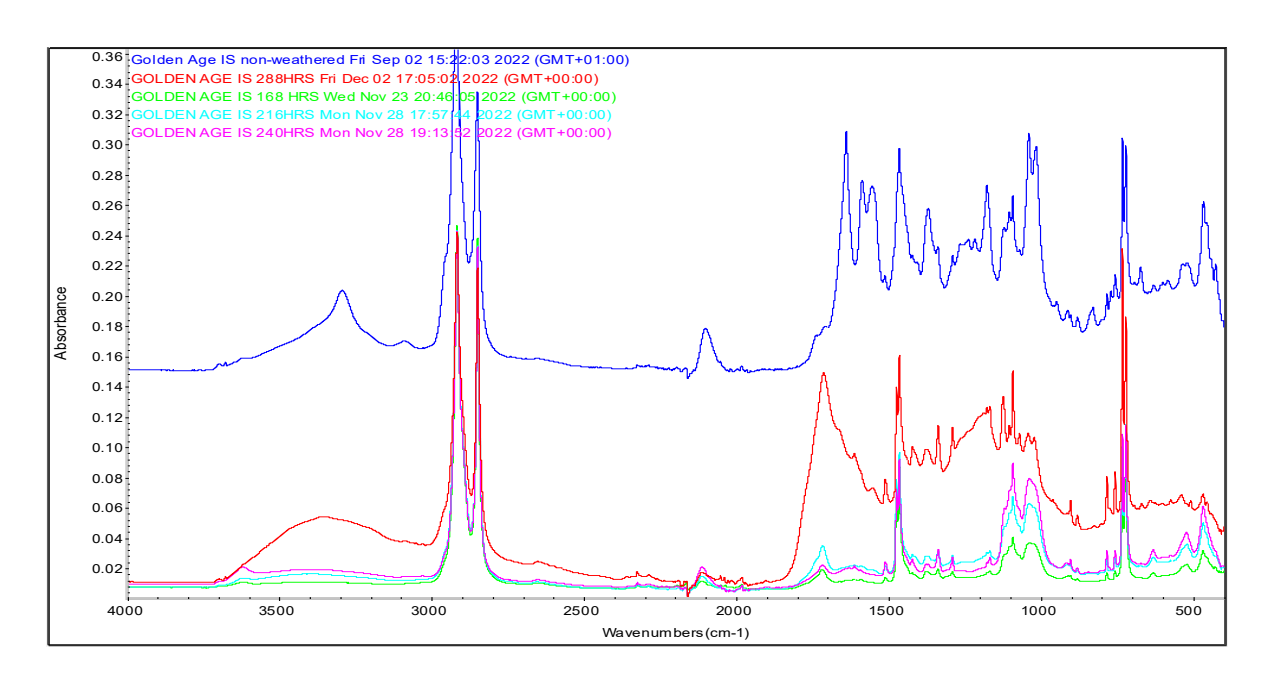


Figure 4. 14: FTIR spectra of the ink on Golden age PE before and after weathering

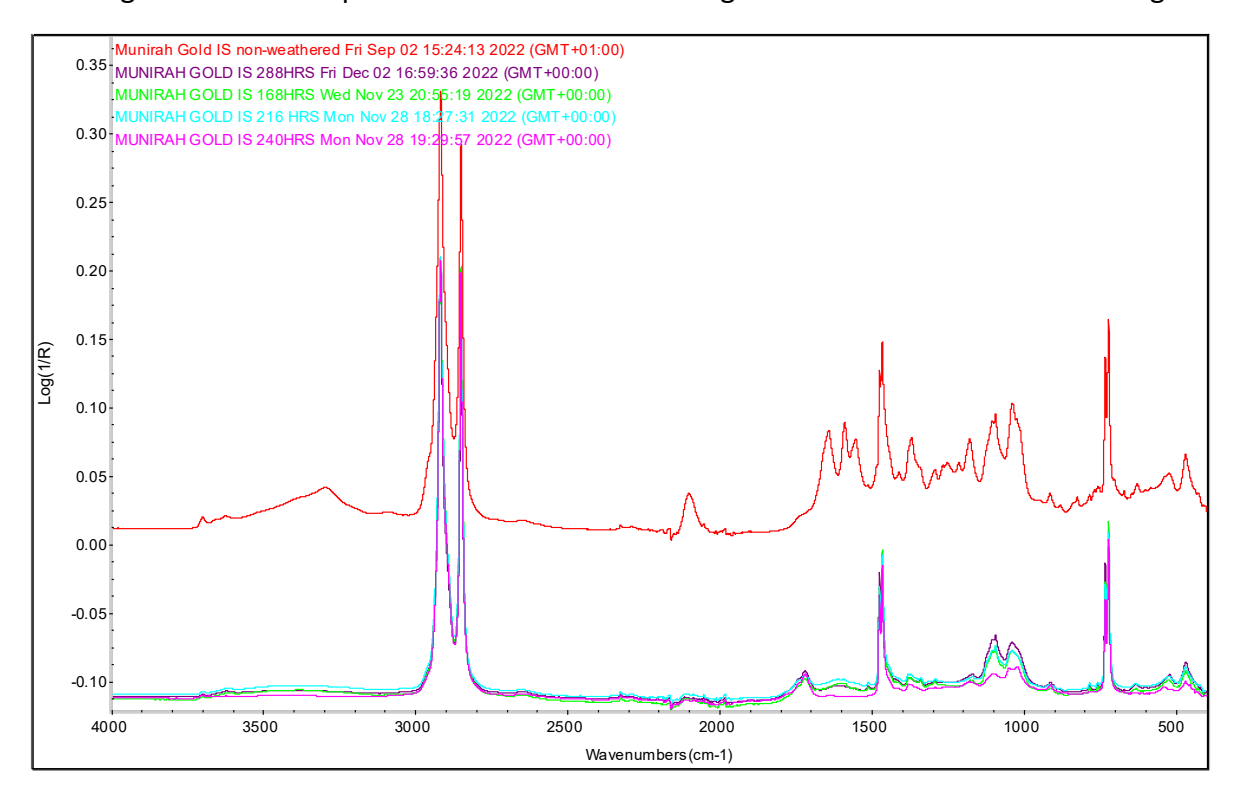


Figure 4. 15: FTIR spectra of the ink on Munirah gold PE before and after weathering

From the above Figures 4.14 - 4.15, bands due to the ink have decreased in intensity at the region of 1720cm^{-1} and 3300 cm^{-1} for all five PE samples, showing that noticeable degradation in the form of oxidation has taken place at this point for all five weathered PE samples, or the ink has washed off or both. It is visually looking washed off (Figure 4.26). There seems to be a similar rate of oxidation going on for all the PE (NIS) samples, except for the Golden age PE

sample weathered for 288 hours. This difference in the spectrum for the 288-hour sample compared to the rest may be that the Golden Age 288 hours show ink bands because the area analysed may be the area where the ink had not been washed off. The carbonyl band around 1720 cm⁻¹ is present after weathering, but it is not possible to clearly state whether it was there before any UV weathering since the ink bands could overlap it. The only way to tell would be to wash off the ink and then analyse in the same region, which might not be possible. However, it is anticipated that it is due to the UV weathering.

Comparing the changes that took place over time across the various UV-weathered PE samples

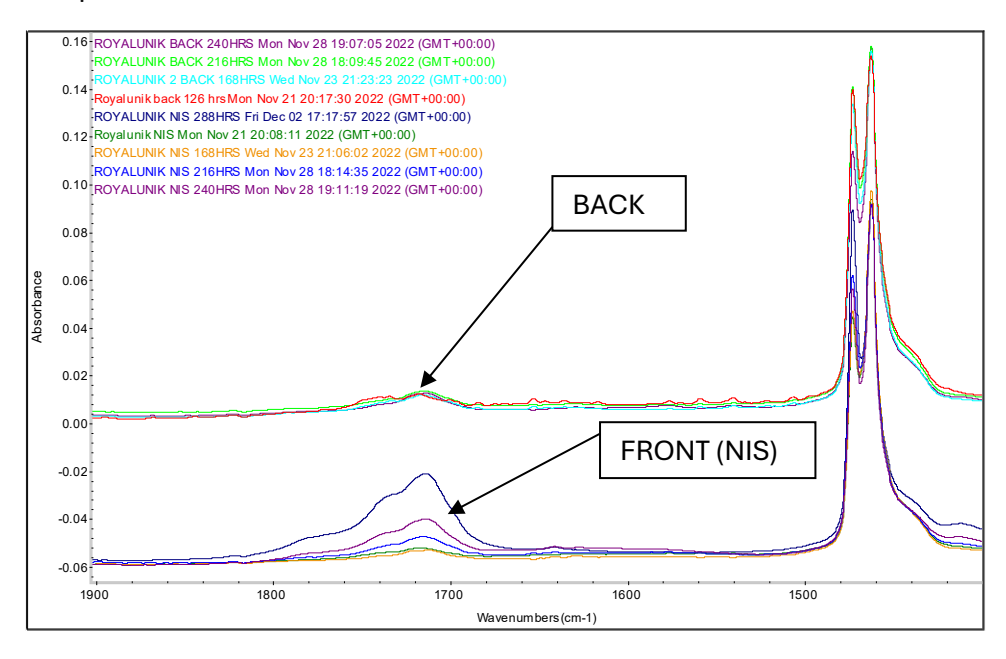


Figure 4. 16: FTIR spectra of ROYALLINK PE after UV exposure at different time intervals highlighting differences in the oxidised regions for the back and front (side facing UV bulb directly) sides of the PE

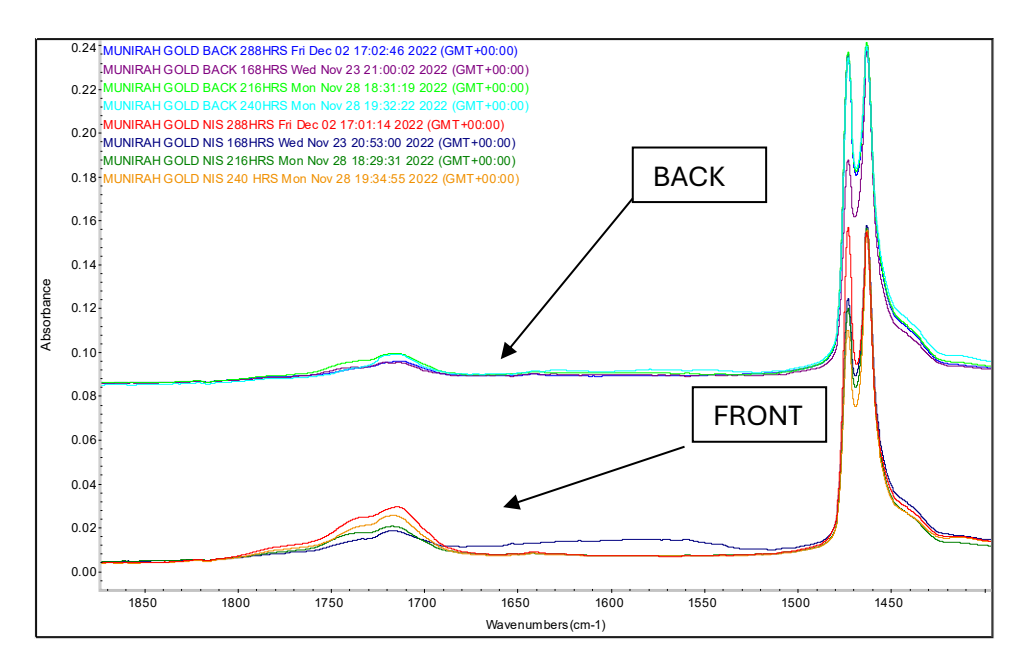


Figure 4. 17: FTIR spectra of Munirah Gold PE sample after UV exposure at different time intervals, highlighting differences in the oxidised regions for the back and front (side facing UV bulb directly) sides of the PE

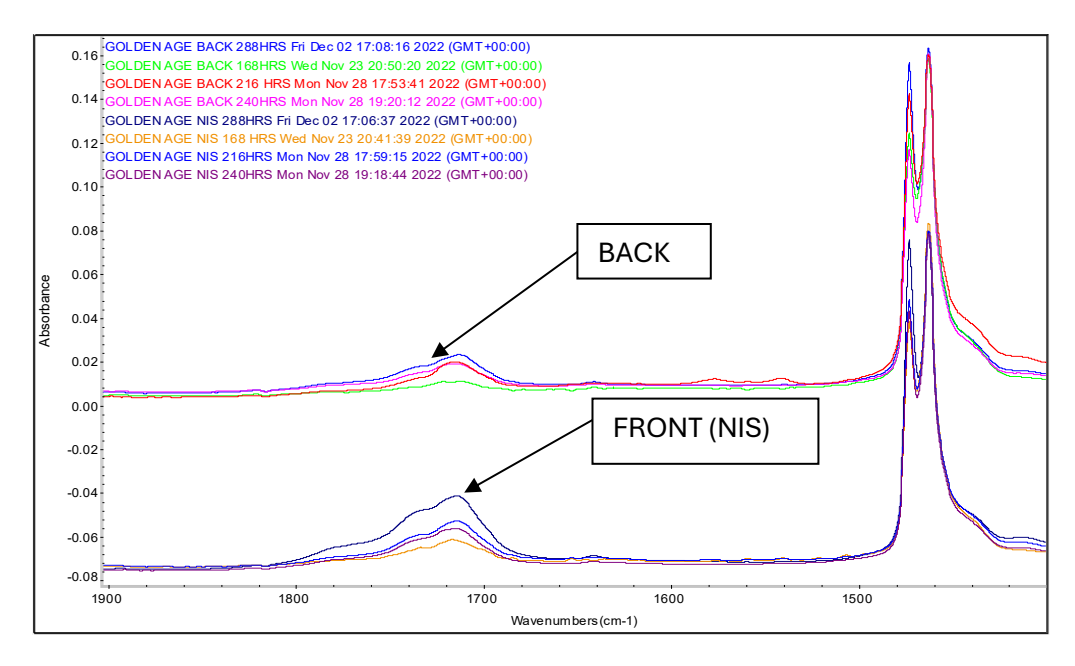


Figure 4. 18: FTIR spectra of Golden Age PE sample after UV exposure at different time intervals, highlighting differences in the oxidised regions for the back and front (side facing UV bulb directly) sides of the PE

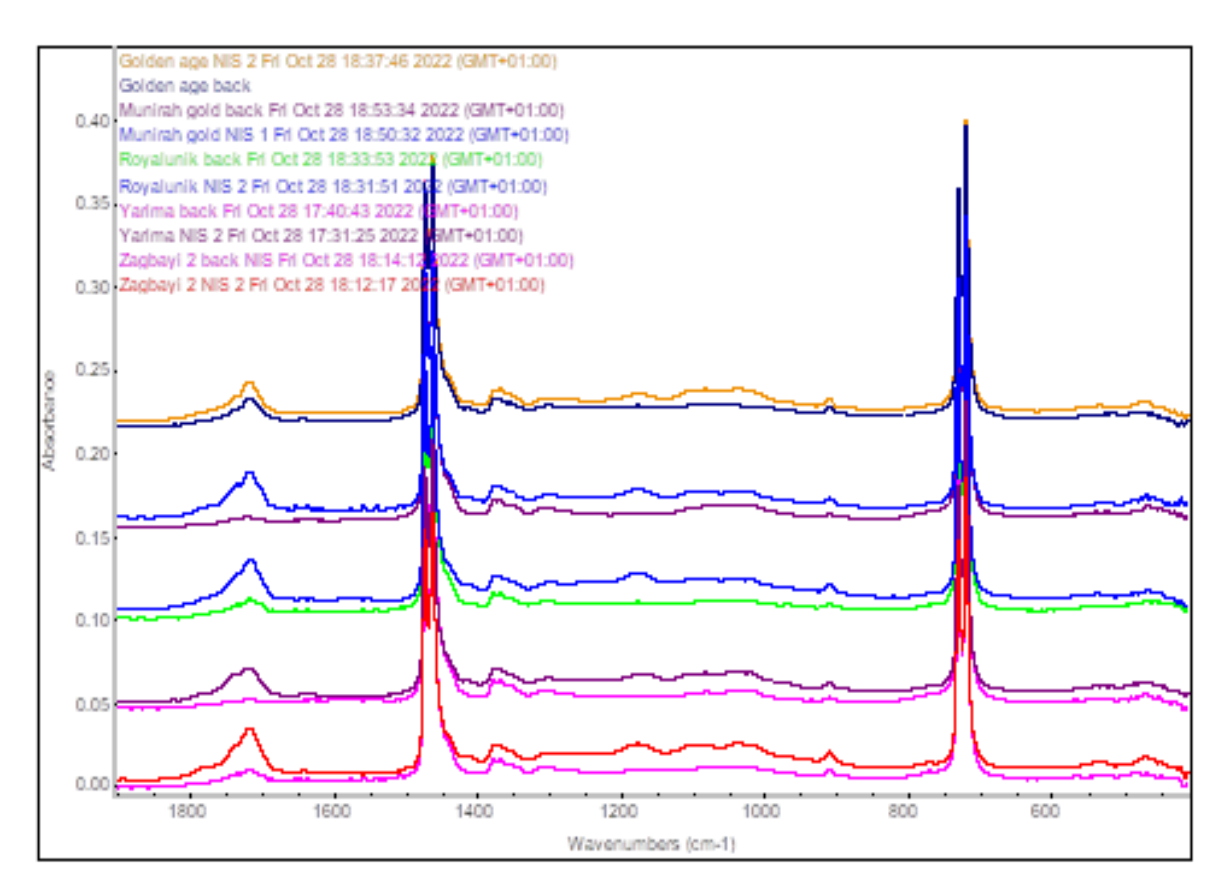


Figure 4. 19: FTIR spectra of all the PE samples after UV exposure at same time intervals (240 hours) comparing differences in the oxidised regions for the back and front (side facing UV bulb directly) sides of the PE

From Figures 4.16 to 4.19, the carbonyl band (around 1720 cm⁻¹) in the NIS (front side) FTIR spectra for all samples exhibited higher intensity than the backside. This indicates more significant oxidation on the front side, directly exposed to UV light. The direct UV exposure accelerates the oxidation process, leading to more pronounced chemical changes, such as the formation of carbonyl compounds. In contrast, the back side, which was shielded from direct UV light, experienced less oxidation over the same time intervals. The FTIR results also reveal a progressive increase in oxidation intensity over time with prolonged UV exposure, as seen by the growing intensity of the carbonyl band.

Additionally, visual observation of the PE samples showed that the ink on their surfaces washed off progressively over time, correlating with the ongoing degradation process. This is to say that UV exposure leads to both physical and chemical changes in the PE materials.

4.2.2 Natural weathered PE samples

Some PE samples (mostly different from the analysed samples) were exposed to the natural sunlight in Minna Niger state of Nigeria (Figure 4.20) for 1200 hours (50 days), from 22nd May to 13th July, 2023 and then analysed by FTIR spectroscopy to assess changes in oxidation that occurred. During sunny periods, the average irradiance was estimated at approximately 0.76 W/m². However, this value fluctuated throughout the exposure period due to changing weather conditions. On different days, the samples were exposed to heavy rainfall lasting 2-3 hours, which occurred a total of six times—four times during the day and twice at night. These alternating conditions of rain and sunlight persisted throughout the entire natural weathering process. The temperature within the period varied between average of 30°C at night and 55 °C during the day, the breeze and other natural conditions interfered. Also, during the day, the sun, is usually intense for a maximum of about five (5) hours for the day and with annual rainfall precipitation of approximately 1200 mm/year. All these non-steady exposure conditions will attribute to variability in comparison with the UV-weathering.



Figure 4. 20: A selection of the PE water sachets spread on the aluminium zinc, directly exposed to the sunlight, and supported with plastic pipes and stones to avoid being blown away by the wind

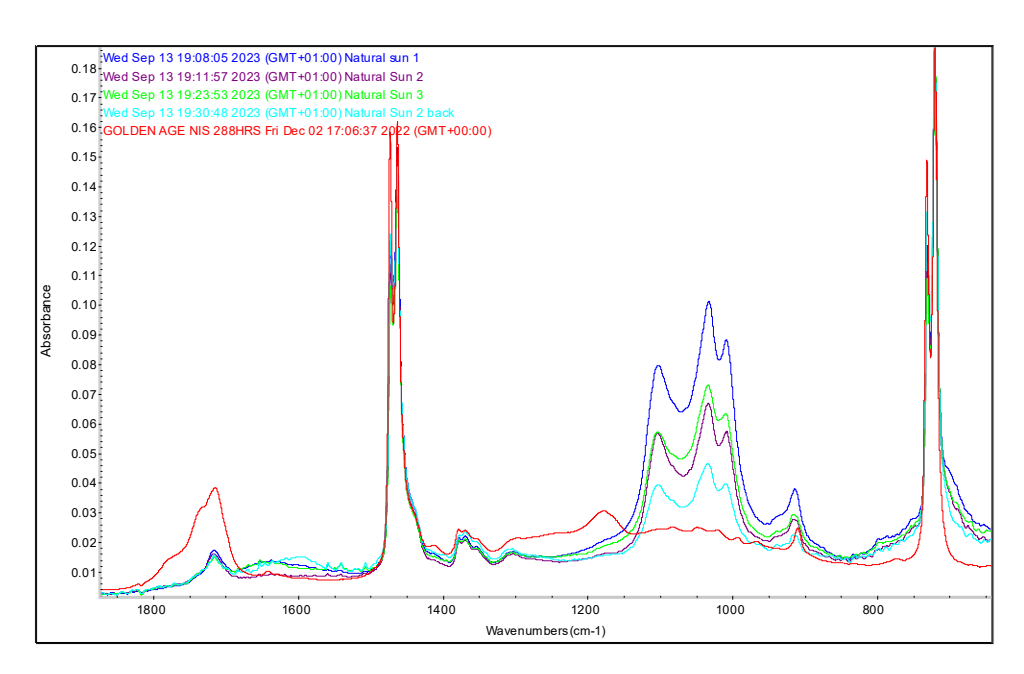


Figure 4. 21: Spectra of naturally weathered PE samples (multiple colours) compared to UV-weathered PE samples (red spectrum).

From Figure 4.21, infrared bands corresponding to oxidation around 1700 cm⁻¹ which are likely related to carbonyl (C=O) stretching vibrations are present but are less intense in the naturally weathered PE samples compared to the UV-weathered PE sample, indicating that oxidation is happening, but more slowly in natural sun exposure compared to UV-accelerated ageing. This is expected as UV light is more aggressive in breaking down polymers compared to natural sunlight. These small bands around 1700 cm⁻¹ appear to be uniform in intensity for all the natural weathered samples.

The band changes in the wavenumber region 1200-1000 cm⁻¹ for the naturally weathered PE are likely due to rusts or contamination from the aluminium zinc where the samples were spread.

The spectra collected from the front of the samples (Natural Sun 1, 2, 3) overall, show more degradation compared to those collected from the back, as expected due to greater sun exposure. The differences in the front samples, though subtle, highlight variable and possibly uneven degradation processes based on exposure conditions and the chemical nature of the PE.

Using the formula provided in equation 4.1, the area ratio for the naturally weathered PE is calculated as 0.261. By extrapolating from the graph of area ratio (Figure 4.13) and correlating these values to the UV-weathering data, it can be assumed that the naturally weathered PE corresponds to approximately 168 hours of UV weathering at a normal irradiance of 0.76

W/m² (Figure 4.22). This conclusion is supported by comparing the naturally weathered PE to the UV-weathered PE at 1700 cm⁻¹ and 1350 cm⁻¹ absorption regions, as shown in Figures 4.23, 4.24 and 4.25. The carbonyl band does look similar in intensity.

This correlation can actually link the natural weathering process to controlled UV weathering experiments, providing insight into the timeline and chemical changes occurring in PE materials.

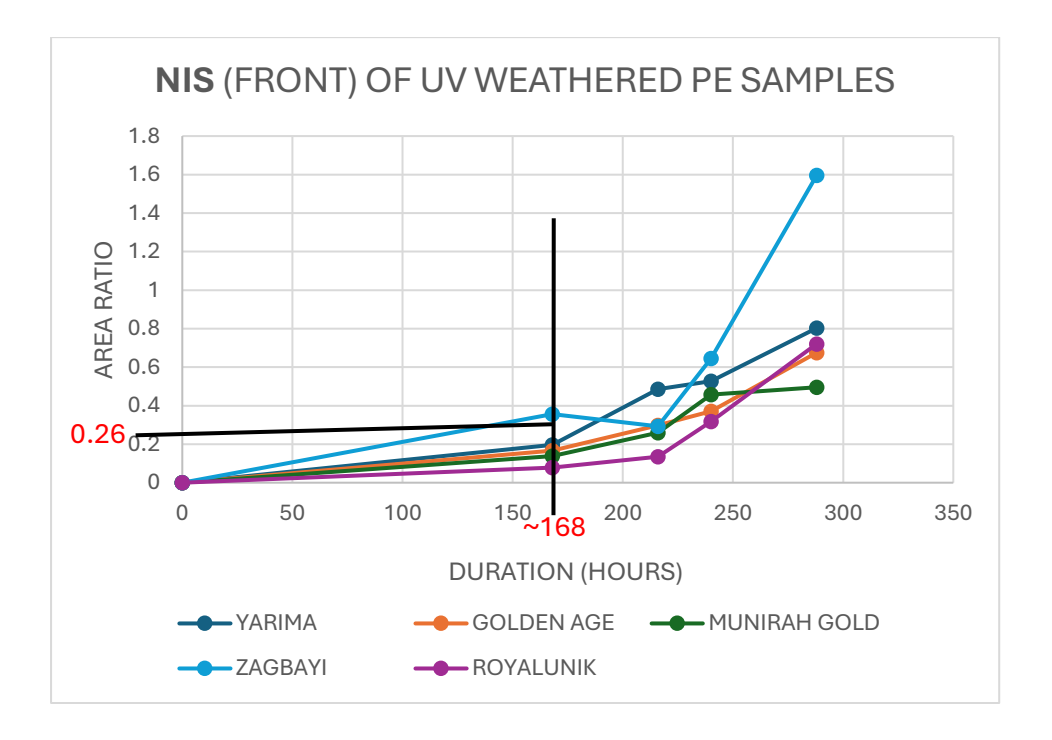


Figure 4. 22: Extrapolation of the area ratio to correlate natural weathered to UV-weathered PE

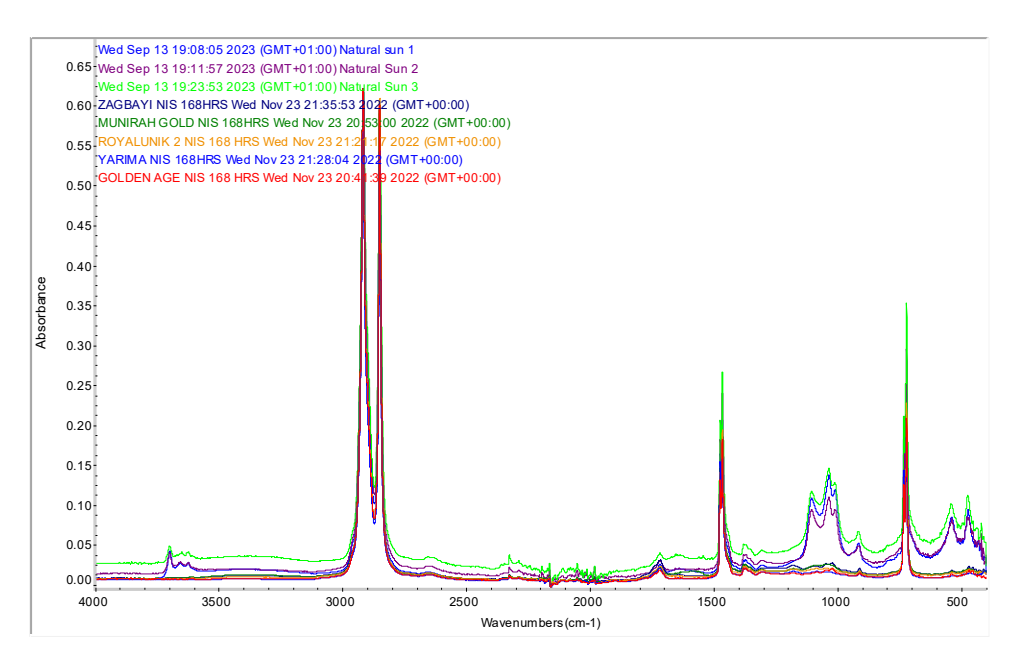


Figure 4. 23: Spectrum of natural weathered PE samples compared to UV-weathered PE samples of 168 hours

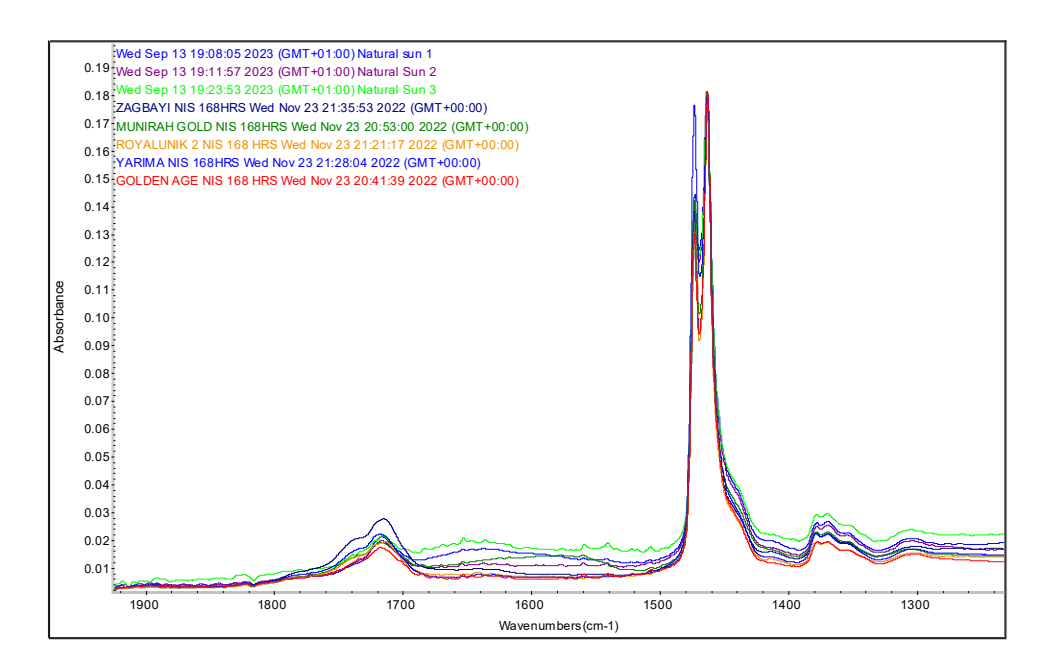


Figure 4. 24: Spectrum of naturally weathered PE samples (1200 hours) compared to UVweathered PE samples of 168 hours at the 1700 cm⁻¹ and 1350 cm⁻¹ region

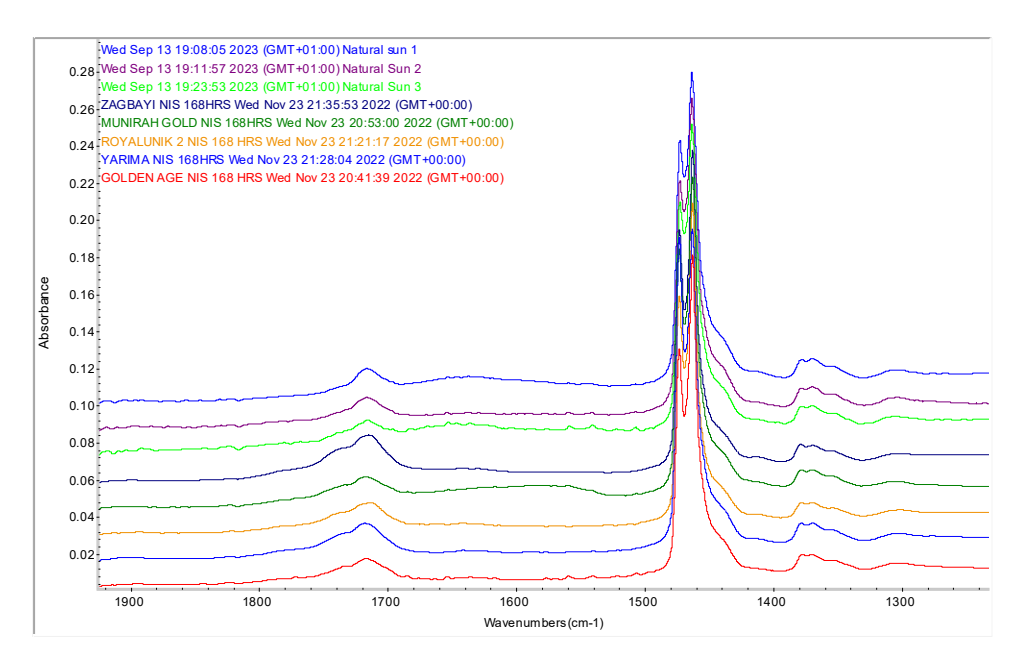


Figure 4. 25: Spectrum of natural weathered PE samples (1200 hours) compared to UV-weathered PE samples of 168 hours at the 1700 cm⁻¹ and 1350 cm⁻¹ region (zoomed image)

4.2.3 Characterisation of Polyethylene sachet with SEM

4.2.3.1 Characterisation of Ultraviolet/Natural weathered sachet PE

The visual appearance and physical texture of the UV-weathered polyethylene (PE) samples showed distinct changes with increased exposure duration (Figure 4.26). The 75-hour and 150-hour UV-weathered samples exhibited similar visual characteristics such as noticeable fading of ink inscriptions. Tactile differences revealed significantly more progressive degradation in the 150-hour sample since it felt more fragile and thinner than the 75-hour sample. Additionally, the 150-hour sample's inscriptions were more faded, and it displayed increased brittleness, tearing easily under minimal stress. In contrast, the naturally weathered PE appeared uniformly faded (but less so) and retained a dense and intact structure, suggesting less severe physical degradation than the UV-weathered samples. Rust spots were observed on the naturally weathered PE, resulting from its prolonged placement on aluminium zinc throughout the 50 days of sunlight exposure.



Figure 4. 26: (a) Pristine PE (b) Naturally weathered PE for 50 days (1200 hrs) (c) UV-weathered PE for 75 hours (d) UV-weathered PE for 150 hours

The SEM data for the surfaces of the various forms of PE were examined under back-scattered electron mode (BSE). To prevent sample charging during imaging, the samples were coated with a thin carbon layer using a carbon evaporator.

. The SEM images shown in Figure 4.27 present differences in surface structures for the different durations of UV-weathered, naturally weathered, and virgin sachet PE surfaces. Photographs of the shredded and roughened-shredded PE samples are shown in Figure 4.28. While the SEM images shown in Figure 4.29 represent the shredded and shredded-roughened PE, with the SEM data collected under secondary electron mode (SE).

From Figure 4.27, the surface of the virgin PE was smooth with few scratches, a few small particulates (observed as white spots) are present and could be a result of dirt and rough handling of the PE. Naturally weathered PE showed very few cracks and specks of dirt on the surface with 50 days (1200 hours) exposure to sunlight, day and night temperatures, seasonal variations, humidity and atmospheric contamination. When compared to Virgin PE, natural weathered PE shows a slightly more textured surface. At higher magnifications (400x and

800x), the surface exhibited some roughness and small particles or contaminants spread across the surface. This indicates that natural weathering has caused some minor surface changes. It has slight surface roughness and minor contaminants, but no significant structural damage. Ageing processes in the natural environment are generally regarded as slow (126). The small amount of debris found on the surface is likely due to dust particles and rust on the polyethylene surfaces.

The 75 hours UV-weathered PE (with double natural sun irradiance of 1.55 IRR equivalent to approx. 8 days) showed many crack patterns which support a weakness of the polymer integrity resulting from degradation. At lower magnifications (50x and 200x), the surface shows more irregularities, with visible rough patches and texture. At higher magnifications (400x and 800x), there are clear signs of surface degradation as the PE appears to have undergone some cracking or etching, which could be due to UV-induced chain scission, oxidation, or erosion. The presence of more pronounced roughness and micro-cracks indicates that UV exposure is starting to weaken the polymer structure.

The roughness and coarse structure likely increased as weathering time was prolonged. This is supposed/expected to be evidenced in the sample weathered for 150 hours (16 days). The SEM analysis, repeated for confirmation, yielded consistent results. The 150 hours of UV-weathered PE showed a surface structure with a smooth surface only, the crack pattern did not appear on the surface. This could be because the longer exposure time (150 hours) might have caused more extensive degradation of the surface, leading to the formation of a smoother surface as the cracks may have coalesced or flattened out, or that there was variability in the polymer content causing the sample exposed for 150 hours to degrade differently because it had a different thermal history and crystallinity. Rabek, in his work on polymer photodegradation (90), demonstrated that crack formation is mainly due to continuous photo-oxidative degradation. Furthermore, cracks serve as extensions of fractures, acting as stress concentrators and fracture initiation points (102). Fernando et al. in their work discussed how thermal effects during UV exposure can lead to surface reorganization and smoothening (127).

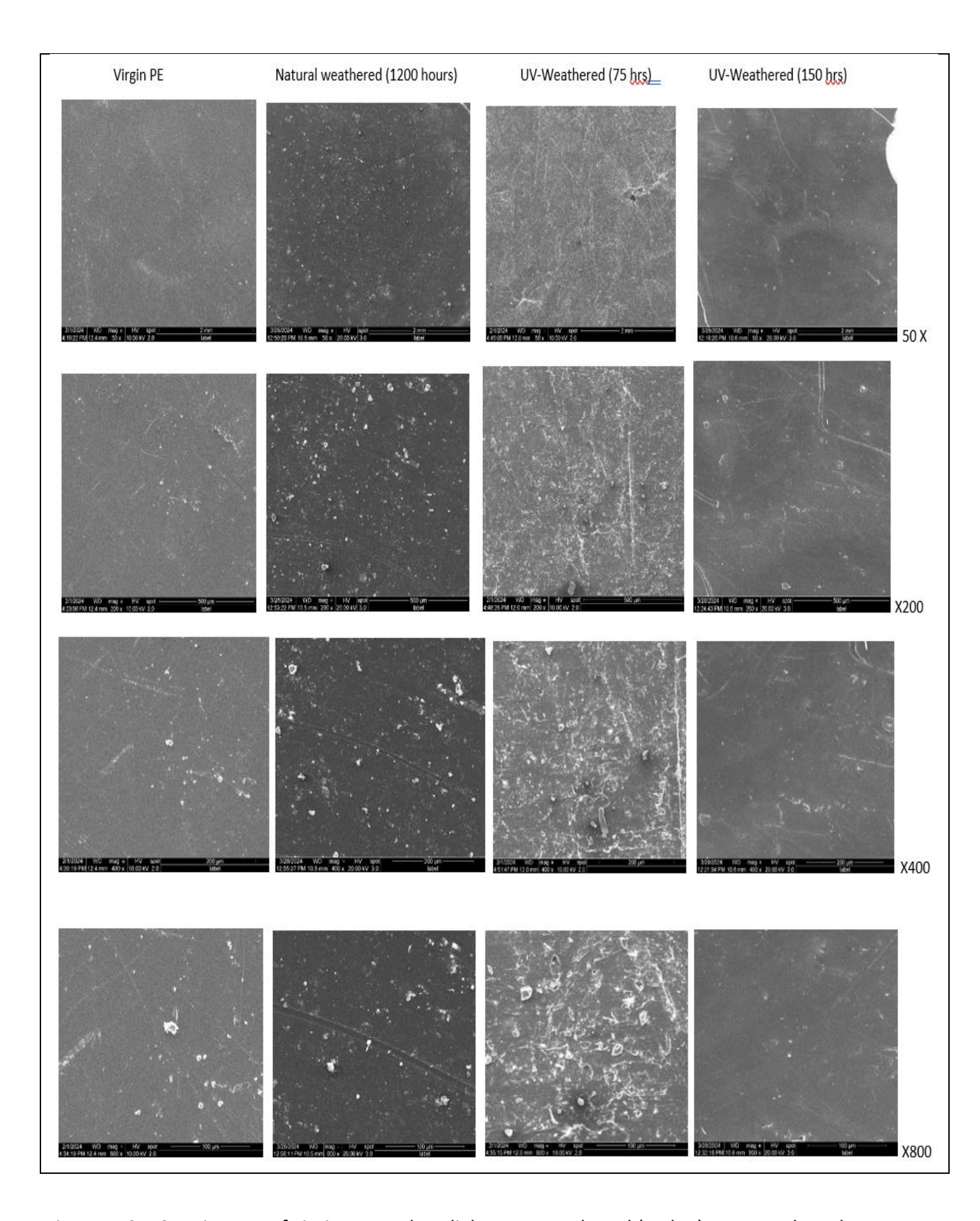


Figure 4. 27: SEM images of virgin, natural sunlight, UV- weathered (75 hrs), UV Weathered (150 hrs) PE samples





Figure 4. 28: (a) Shredded PE consisting of large flakes body with elongated strands (b) Shredded-roughened PE

Figure 4.28 shows photographs of Shredded PE and Shredded-Roughened PE. The shredded PE primarily consists of a central body with elongated, mostly curly strands. For detailed SEM analysis, the shredded PE was categorised into two components, large flakes and strands. In contrast, the shredded-roughened PE appears predominantly straightened, as the curly strands were either broken off or flattened during the mechanical roughening process. It is textured with soft-like fluffy coarse/rough surface. The colour is lighter than the shredded PE as some of the ink inscription on the surface may have been scrapped off during the mechanical roughening process. The rougher surface may also scatter light differently giving a lighter colour.

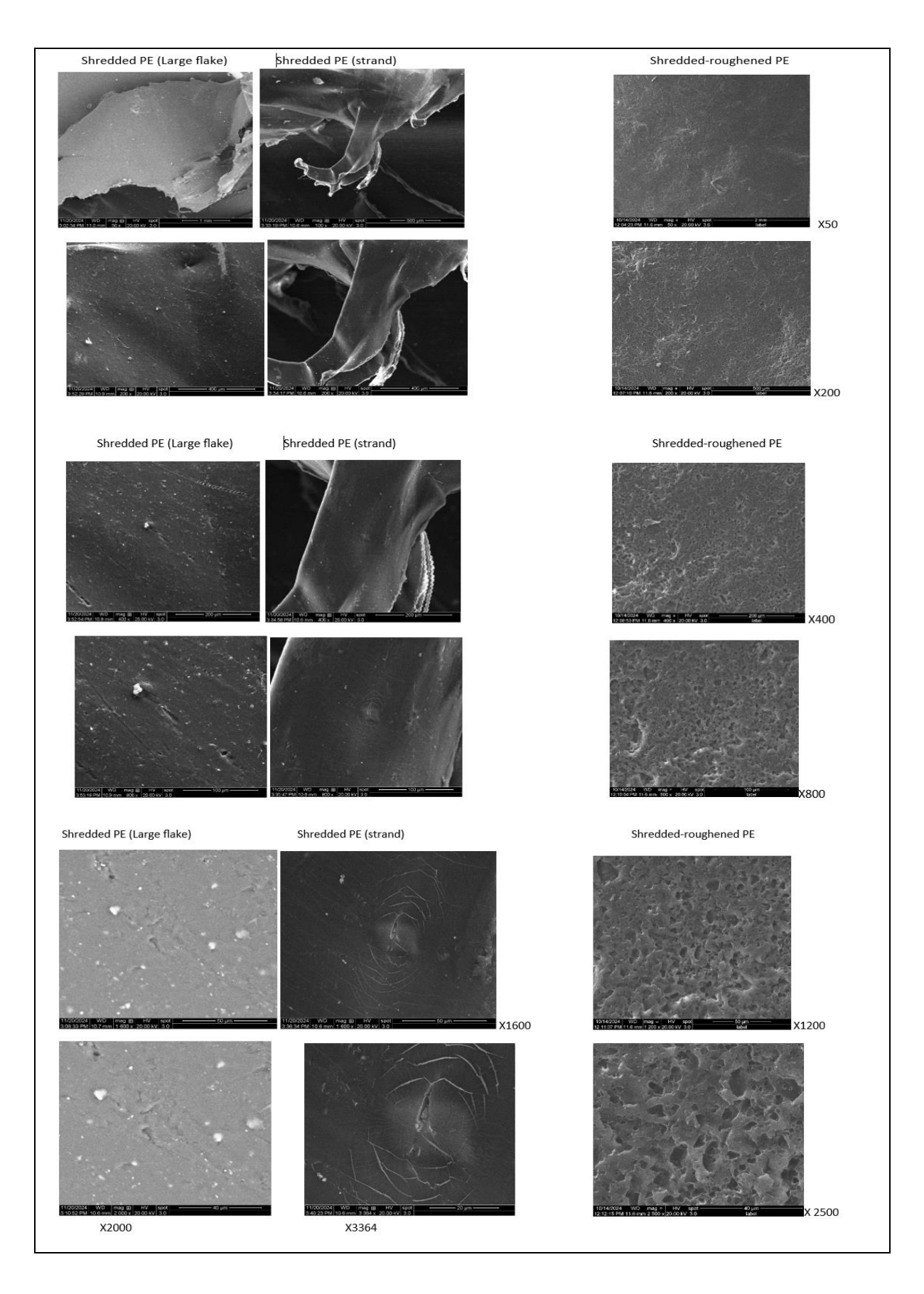


Figure 4. 29: SEM images of Shredded, and shredded-roughened PE samples

From Figure 4.29, the shredded large flakes display smooth, relatively flat surfaces with minor surface undulations, scratches, and tiny holes/perforations. At lower magnifications (X50, and X200), the surface is predominantly smooth, with only minor evidence of localised roughness or scratches, but at higher magnifications (X800, X1600, and X2000), finer surface features become visible, such as shallow pits or grooves, introduced during the shredding or mechanical processing. This means that these large flakes were produced with minimal surface alteration to the PE surface.

The Shredded PE Strand samples exhibit elongated, fibrous shapes with noticeable curling or bending, characteristic of strand-like structures. At lower magnifications, the surfaces of the strands appear smooth but less flat than the large flakes, with visible tears /distinct stress marks, introduced during mechanical shredding. At higher magnifications, the strand surfaces show more clearly the distinct stress marks and elongated grooves, indicating the stretching or pulling forces experienced during shredding.

The shredded-roughened PE displays a significantly rougher texture compared to both the flakes and strands. The SEM images reveal a highly irregular, uneven-jagged surface with prominent peaks, valleys, and random pits both at the lower and higher magnifications with interconnected voids/porous cavities network structure. This shows that the roughening process significantly altered the surface topography.

4.3. Effect of different instruments used for the shredding

Using different instruments for shredding PE water sachets can have varying/significant effects on the resulting particle size range ratios. For instance, a shredder with sharp blades may produce smaller particles than a shredder with dull blades, and the speed and force at which the shredding is done can also affect particle size. Generally, the smaller the particle size, the greater the surface area. Thus, factors such as blade sharpness, shredding speed, and force can all play a role in determining the particle size. In addition, the polyethylene feedstock preparation and the nature of the polyethylene can also affect or influence how it responds to the shredding process leading to varying particle size distributions. For instance, the weathered and non-weathered polyethylene gave varying particle size range ratios with same equipment and set condition.

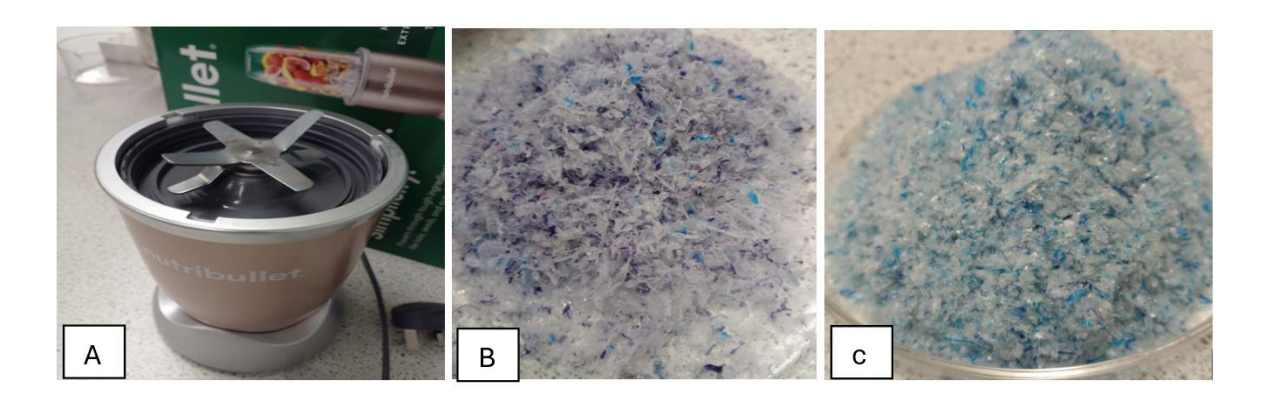


Figure 4. 30: (a) Blades from the Nutribullet 900 series blender used for the shredding procedure (b) sample of shredded pristine PE (c) sample of UV weathered PE

The blades in the Nutribullet (Figure 4.30 (a)) are dull and for pristine polyethylene produced particles that stretched at the ends, as a result of the mechanical stretching as the blades tore up the PE and due to generated heat during the grinding procedure. Figure 4.30 (c) shows the sample of a UV-weathered PE, shredded with the Nutribullet. It produces more of smaller particle-sized cuttings (2.8mm≤x≥2.0mm) and in a shorter period with the weathered PE (than the non-weathered PE, Figure 4.30 (b) which produced more of larger particles, 8mm≤x≥ 6.3mm). This difference is because the UV-weathered PE has been weakened and degraded due to exposure to UV radiation, making it easier to shred into smaller pieces.

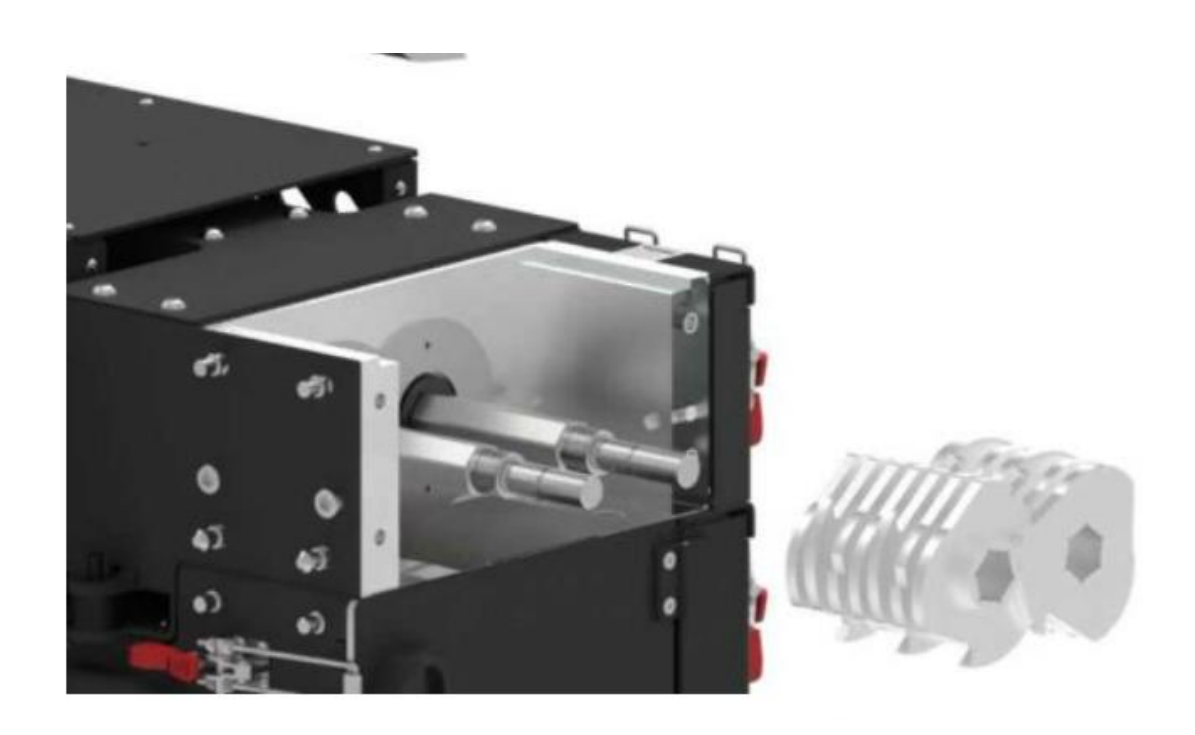


Figure 4. 31:3devo Shredder view showing many blades (Source: 3DEVO)

A 3DEVO Grinder primarily uses a combination of chopping and shearing actions to process plastic materials. The grinder's blades chop the plastic into smaller pieces, while the shearing action helps achieve a uniform particle size. This dual mechanism ensures efficient and consistent grinding of the plastic feedstock. In the initial stages of this research, the 3Devo grinder was critical in the PE preparation, as the sample of the shredded PE (Figure 4.32) produced is more uniform and believed pivotal in maintaining a controlled adsorption experiment. However, its repeated mechanical breakdown during the study posed significant setbacks, as its unavailability forced alternative shredding methods for further experiments.

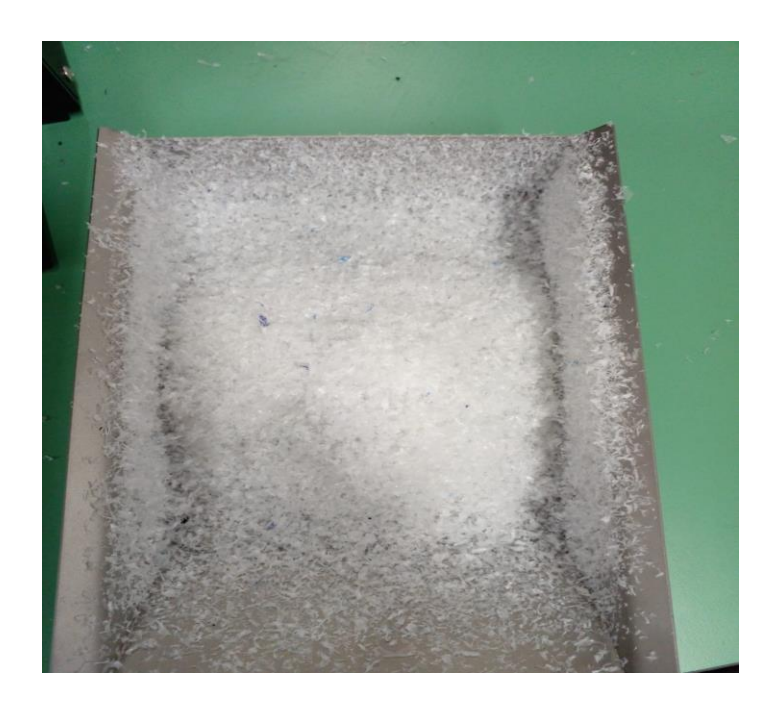


Figure 4. 32: showing the finely shredded pristine PE from the 3Devo shredder

4.3.1 The FTIR analysis showing the effects of shredding and roughening on PE

Shredding and roughening are essential preparatory steps that alter the surface characteristics of polyethylene (PE). Shredding reduces the material to smaller, uniform pieces, increasing the surface area. Roughening, on the other hand, introduces additional surface irregularities and microstructures. These modifications potentially enhance the accessibility of reactive sites and the material's adsorption properties. The FTIR analysis provides crucial insights into how these physical changes affect the material's molecular vibrations and structural integrity.

cm^{cm}

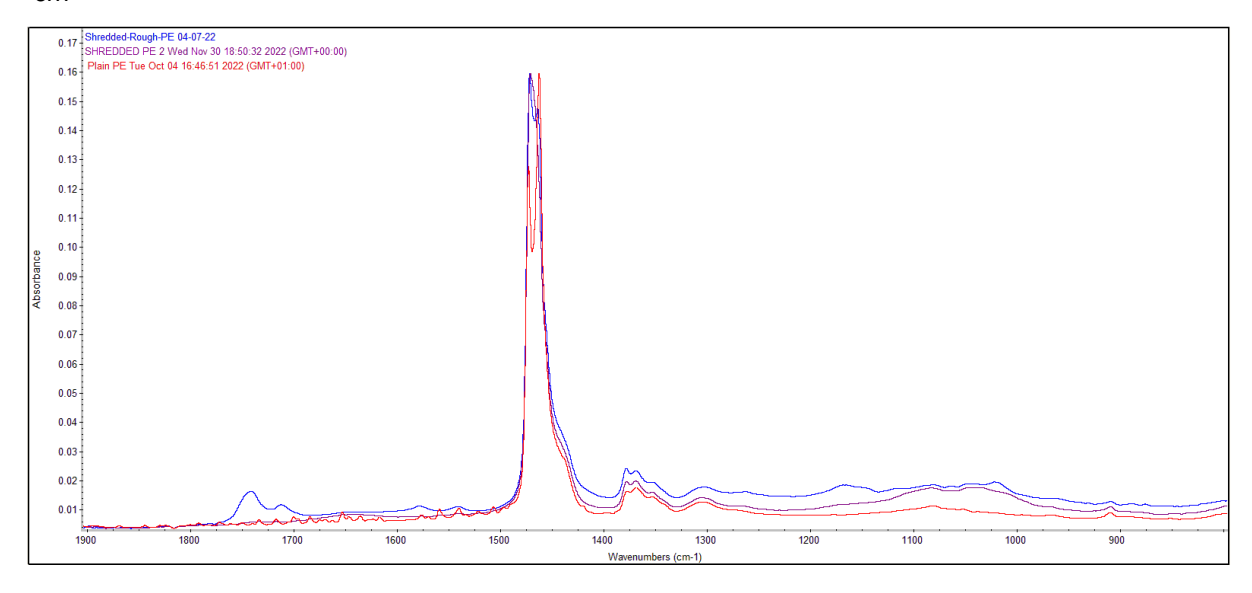


Figure 4. 33: Overlaid FTIR spectra comparing the plain, shredded, and shredded-roughened PE samples assessing similarity or deviation across samples between 800 cm⁻¹ – 1900 cm⁻¹

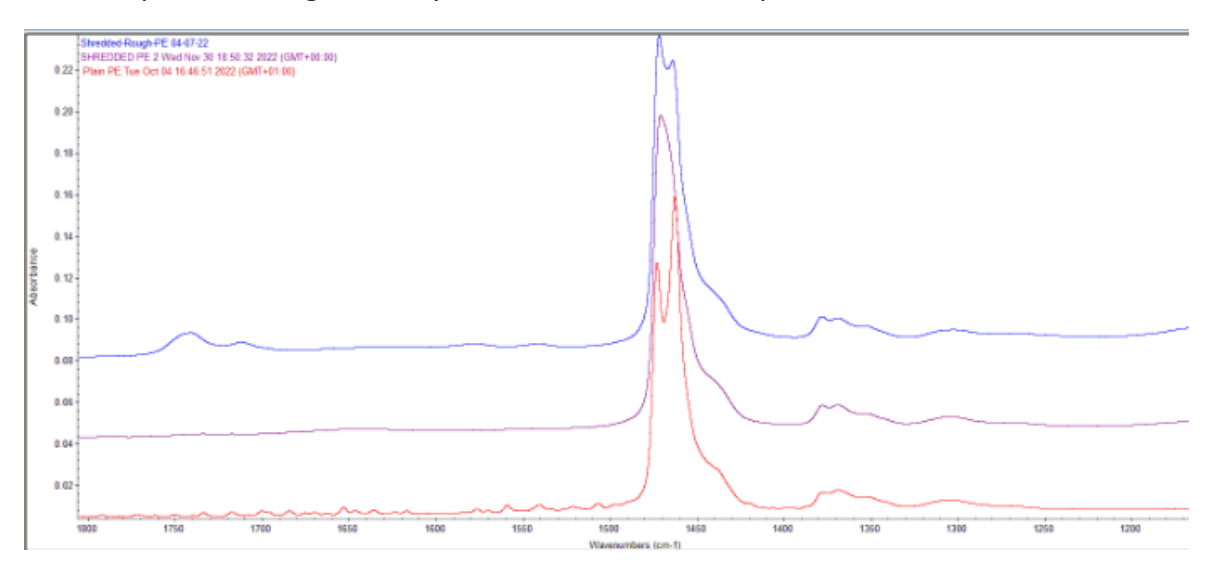


Figure 4. 34: Stacked FTIR spectra of the plain, shredded, and shredded-roughened PE samples, plotted separately to better distinguish spectral differences

The vibrations at 1350 cm⁻¹ often correspond to bending vibrations of -CH₃ groups. Polyethylene may contain small amounts of branches or impurities with methyl (-CH₃) groups, contributing to this absorbance.

The bands around 1460 cm⁻¹ (on the shredded-roughened and plain PE) are attributed to the symmetric stretching vibrations of -CH₂- groups. Its presence reinforces the evidence of intact polyethylene chains, but it is noticed that the shredded PE displays a single broadband (likely

from the broadening of the two bands merging to show one band) while the roughened PE shows two bands, but at different ratio intensities. This might indicate a difference in the structural ordering of PE chains between the samples. The roughening process may have affected the molecular structure in a way that introduces variations in the vibrational environment of the methylene groups within the polymer chains. There could be changes in crystallinity, thus different polymer chain arrangements leading to differences in vibrational energies. This could be due to C=O groups changing the interaction between polymer chains, i.e. spreading the chains further apart and thus changing vibrational energies.

The band noticed on the roughened PE at 1750 cm⁻¹, which corresponds to C=O stretching vibrations, indicates oxidative degradation and carbonyl group formation. The localised heat at surfaces during mechanical rubbing and roughening would be a strong contributor to this observation.

4.4. Characterisation of the Crude oil

Two forms of oil, natural crude oil and synthetic crude oil were characterised to identify their chemical compositions, physical properties, and behaviour.

4.4.1 Oil Characterisation by GC-MS

The GC-MS equipment was used to identify the various compositions of the oils. However, GC-MS analysis is limited to detecting volatile components within the oil, specifically those that volatilise at temperatures between 25°C and 350°C, the operating range of the instrument.

4.4.1.1. GC-MS – pristine (natural and synthetic oils)

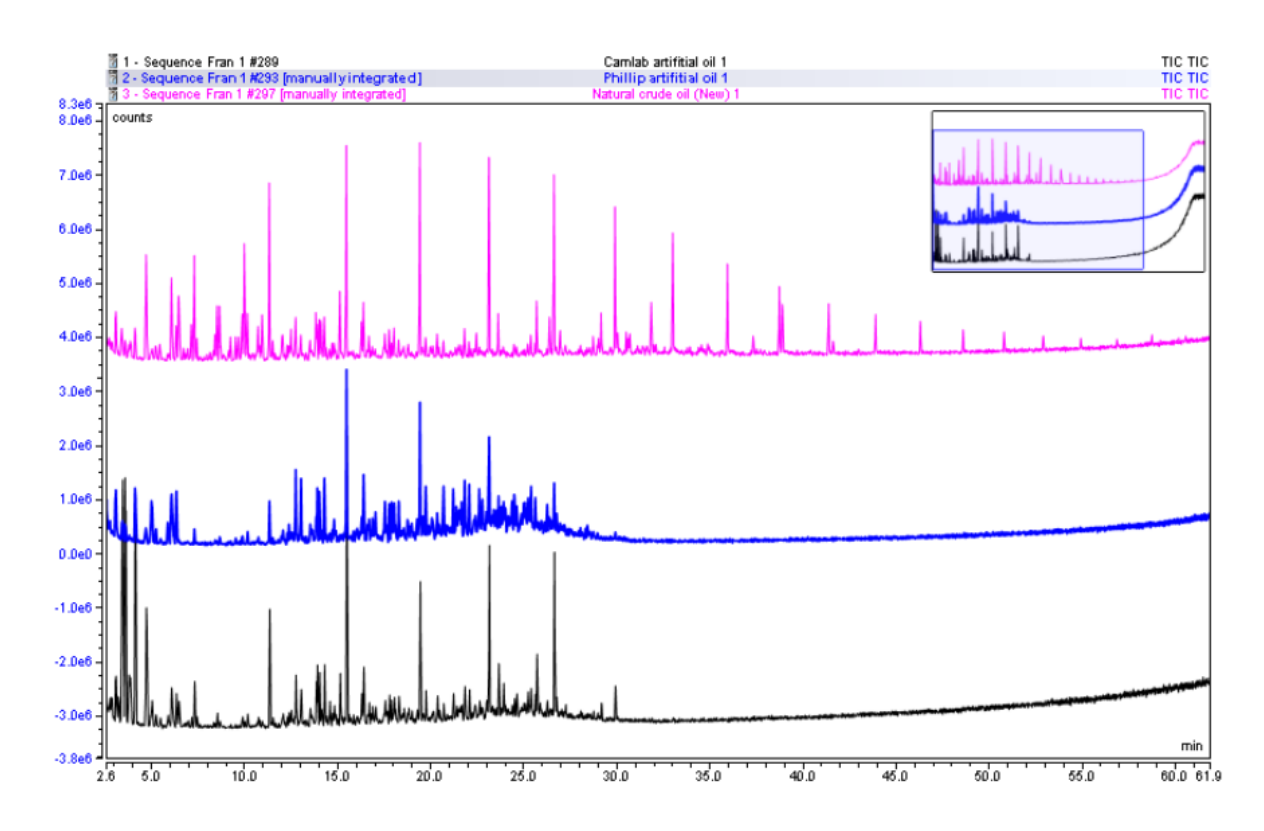


Figure 4. 35: GCMS chromatographs of the fresh natural crude oil 1 (top chromatogram) and Synthetic crude oil (Phillip (middle chromatogram) and Camlab (bottom chromatogram) samples

Figure 4.35 shows the GC–MS analysis of crude oil, Phillips oil, and Camlab oil. It revealed distinct differences in their chemical compositions, which were clearly reflected in their chromatographic profiles, also shown in Appendix A1-A4. In this study, only chromatographic peaks with areas exceeding 1500 counts per minute were considered for integration and reporting. This threshold was applied to ensure that only reliably detectable and quantifiable compounds were included in the analysis. Out of these three oil samples, crude oil displayed the most complex and diverse profile, characterised by a wide range of hydrocarbon peaks that spanned from short-chain (C10) to long-chain (C40) alkanes and aromatic hydrocarbons, as well as their derivatives. This means that crude oil contains a wide range of hydrocarbon molecules with varying chain lengths and structures. These were detected using key diagnostic ions, for example, m/z 57 (total area of 2,411,911 counts/min) and m/z 71 (total area of 680,926 counts/min), which are commonly used to track alkanes in mass spectrometry (169, 170). The resulting chromatogram for crude oil showed numerous, strong peaks spread

across a broad range of retention times, indicating that it contains both volatile and less volatile hydrocarbons within the detection limit of GC-MS. Camlab oil also contained C10-C40 alkanes also detected by the diagnostic ions, m/z 57 (total of 489,719 counts/min) and 71 (total area of 121,569 counts/min), and also detectable component m/z 57 in Phillip oil (total of 396,381 counts/min), and m/z 71 (80,098 counts/min).

Additionally, crude oil contained high concentrations of aromatic hydrocarbons, such as naphthalene (m/z 128, with total area of 25,118 counts/min) and its alkylated derivatives (e.g., m/z 142, total area of 35,501 counts/min, m/z 156, total area of 28,718 counts/min and m/z 170, total area of 7,849 counts/min). These compounds are typically found in raw, unrefined petroleum and indicate the presence of polycyclic aromatic hydrocarbons (PAHs), which are significant environmental pollutants due to their toxicity and persistence. The presence of both parent and alkylated PAHs shows that the crude oil is unrefined and naturally sourced (169), likely representing a real-world contaminant scenario.

In contrast, Phillips oil and Camlab oil showed no integrated peaks for the aromatic hydrocarbons, and its alkylated derivatives. They may be lacking them or have them in undetectable quantities).

In this analysis, the mass spectra of several chromatographic peaks were found to exhibit mass ions at both m/z 57 and m/z 71. These peaks likely represent structurally complex hydrocarbons, such as branched or cyclic alkanes, that fragment to produce both ions. This dual-fragment pattern underscores the chemical complexity of these oils and highlights the limitations of straightforward hydrocarbon classification based solely on individual ion monitoring. While these peaks were most prevalent in the crude oil sample, they were observed only to a limited extent in the Camlab and Phillip oils, consistent with their simpler and more refined hydrocarbon compositions.

The term "no integrated peaks" (shown in Appendix A1-A3) indicates that no measurable signals were recorded for the compound(s) in question within the defined retention time and mass-to-charge (m/z) range. This suggests that the compound was either absent or present at trace levels below the detection limit. For example, while crude oil showed multiple integrated peaks for naphthalene and its alkylated derivatives, Phillips oil and Camlab oil

showed no integrated peaks, indicating a lack of detectable PAH content in those samples under the specified criteria.

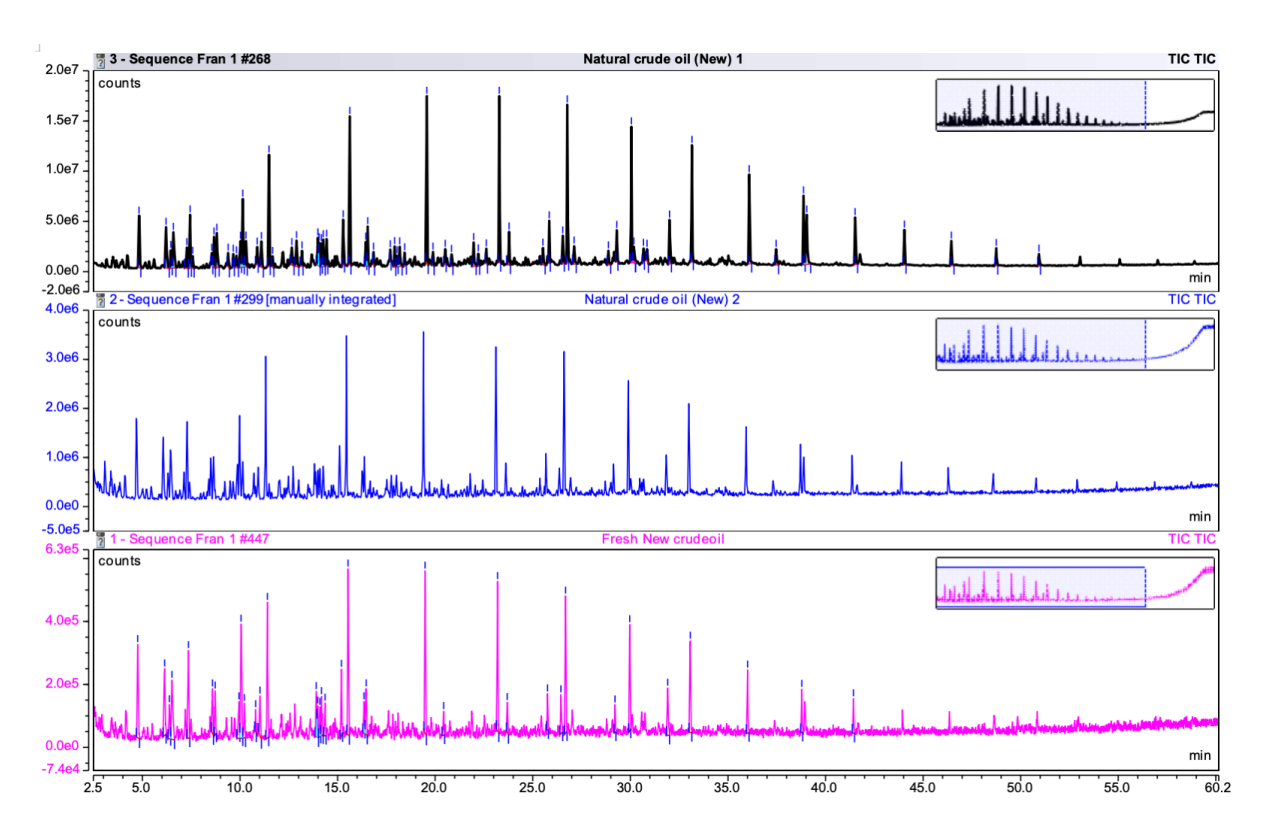


Figure 4. 36: Chromatograph showing a complex composition of 3 natural crude oils (Bonny light) from the same source but at different times

Figure 4.36 shows three chromatograms comparing the chemical composition of natural crude oil samples taken from the same source but at different times (natural crude oil 1 – November 2021, natural crude oil December 2022, fresh new crude oil – July 2023). Each chromatogram (in black, blue, and pink) displays multiple peaks of varying heights, representing different chemical compounds present in the oil samples. Each sample exhibits a complex pattern of peaks, with some notable differences between them, suggesting temporal variations in the crude oil composition from this source.

Table 4. 2: Select components identified by GCMS from the Crude oil and their associated intensities, retention time, peak area and molecular structure

For simplicity and to provide an example, only a select number of the natural crude oil components are identified here. Those selected relate to having the highest peak areas (Table 4.2).

	Name of molecule	Intensity (ion count)	Retention time (mins)	Area (count min)	Molecular structure
1	Thiophene-2- carboxylic acid, 2,4,6- trichlorophenyl ester C ₁₁ H ₅ Cl ₃ O ₂ S	5.0e ⁶	8.72	36730	
2	Karahanaenona C ₁₀ H ₁₆ O	1.5e ⁷	19.72	676916	
3	Decahydro-1,1,4a,5,6- pentamethylnaphthalen e C ₁₅ H ₂₈	4.0e ⁷	29.16	411943	
4	3,7,11,15-Tetramethyl- 2-hexadecen-1-ol C ₂₀ H ₄₀ O	5.5e ⁷	31.85	2601064	J. J
5	Hexadecane, 2,6,10,14- tetramethyl- C ₂₀ H ₄₂	1.5 e ⁷	41.64	55838	
6	2,4a,7-Trihydroxy-1- methyl-8- methylenegibb-3-ene 1,10-carboxylic acid 1- 4 lactone C ₁₉ H ₂₂ O ₆	5.0e ⁶	50.82	67446	НО

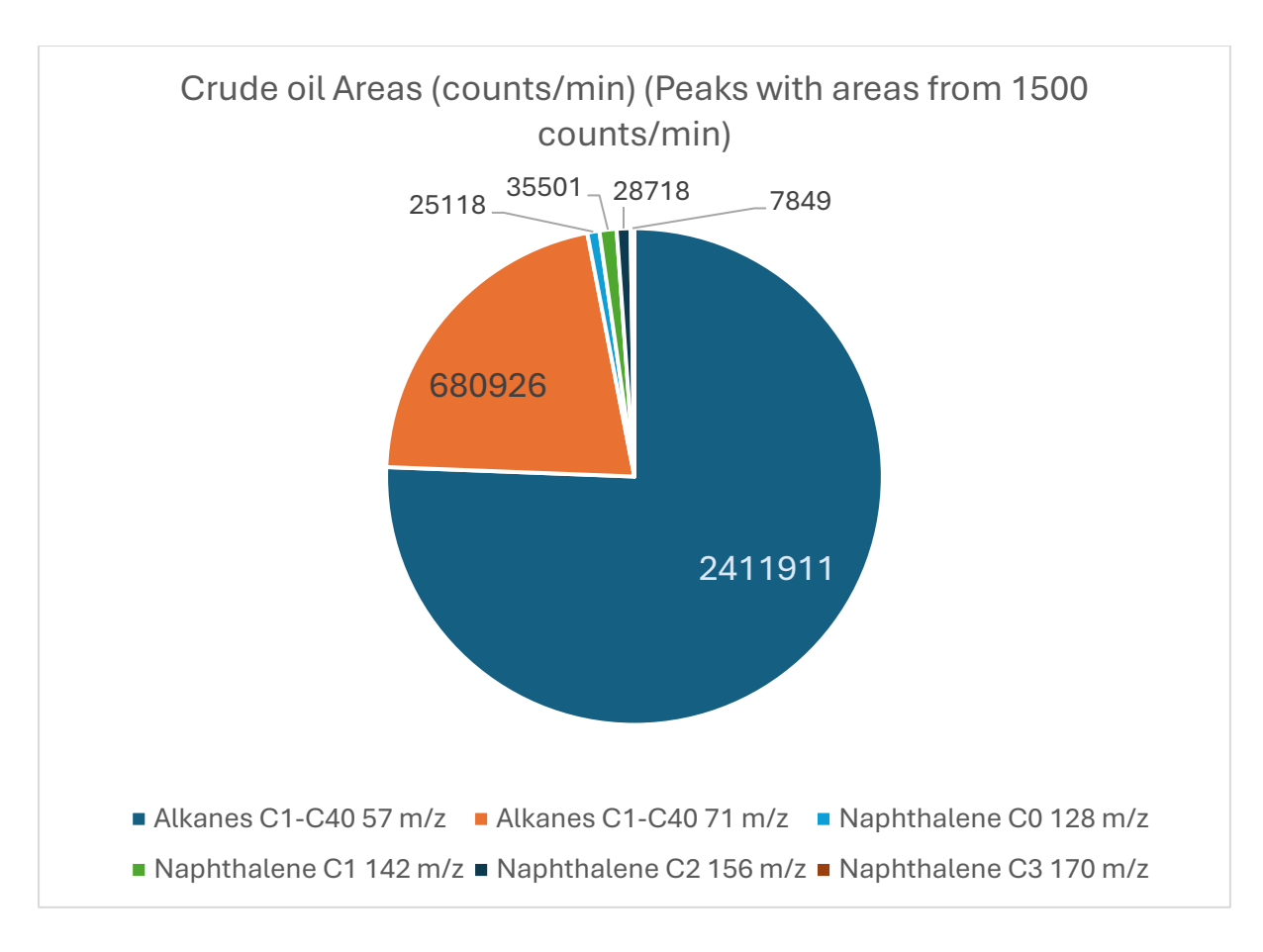


Figure 4. 37 Pie chart showing the distribution of hydrocarbon types in crude oil based on GC-MS peak areas from 1500 counts/min

Figure 4.37 shows that the crude oil sample contains a wide range of hydrocarbon compounds, compared to those of the Phillips and Camlab synthetic oils (Appendix A4). Alkanes are the dominant category, represented by m/z 57 (straight-chain alkanes) and m/z 71 (branched/cyclic alkanes), with several peaks exhibiting both ions. These "mixed" peaks were assigned based on the dominant fragment. Additionally, the crude oil also contains a substantial fraction of aromatic hydrocarbons, including naphthalene and its alkylated derivatives (e.g., m/z 128, 142, 156, and 170). These polycyclic aromatic hydrocarbons (PAHs) are typical of raw, unrefined petroleum and contribute significantly to the total hydrocarbon area. Their presence reinforces the classification of the crude oil as unrefined and chemically diverse, containing both volatile and semi-volatile components across a wide retention range. The overall composition reflects the complex and unrefined nature of crude oil.

For quantitative representation in the pie chart (Figures 4.37 and Appendix A4), which illustrates the relative proportions of hydrocarbon types, each mixed peak was assigned to only one category to avoid duplication. In this analysis, the classification of these ambiguous

peaks is based on the dominant ion fragment (either m/z 57 or m/z 71) with the peak being attributed solely to the category associated with the stronger signal. This ensures that each peak contributes only once to the total, preserving the integrity of the proportional analysis and allowing for a more accurate visual representation of the hydrocarbon distribution.

Phillip oil sample exhibits the simplest profile among the three samples, dominated almost entirely by straight-chain alkanes (m/z 57). Only a small number of peaks corresponding to m/z 71 were observed, and no aromatics were detected.

Camlab oil sample displays a relatively simple hydrocarbon profile dominated by alkanes, as determined by GC–MS analysis. Only peaks with integrated areas equal to or exceeding 1500 counts per minute were included to ensure analytical reliability. The detected hydrocarbons were classified based on their mass spectral fragments: m/z 57 for straight-chain alkanes and m/z 71 for branched or cyclic alkanes. No aromatic hydrocarbons were detected above the threshold, suggesting either their absence or presence at concentrations below the detection limit. A small number of mixed peaks (showing both m/z 57 and 71) were observed and classified according to the dominant ion. The overall composition reflects a synthetic or refined origin, with fewer total compounds and lower chemical diversity compared to crude oil. Camlab oil displays a simpler hydrocarbon profile than crude oil and the total area of both m/z 57 and m/z 71 ions present, are significantly lower than those in crude oil. No aromatic hydrocarbons were detected above the quantification threshold, suggesting the oil has undergone partial refinement or is sourced from a lighter petroleum fraction.

In conclusion and comparison of the 3 oils, the comparative pie chart illustrates the relative abundance of hydrocarbons in each oil type. Crude oil accounts for the highest total GC–MS area, followed by Camlab which is slightly higher than Phillip oils. Both Camlab and Phillip oils exhibited similar GC–MS profiles, characterised by relatively low chemical complexity, absence of aromatic hydrocarbons, and a dominance of alkanes detected via m/z 57 and 71. These similarities, including minimal mixed fragmentation peaks and lower total ion areas, reflect their synthetic nature and distinguish them clearly from the unrefined and chemically diverse crude oil sample.

4.4.2. GC-MS - Weathered oils

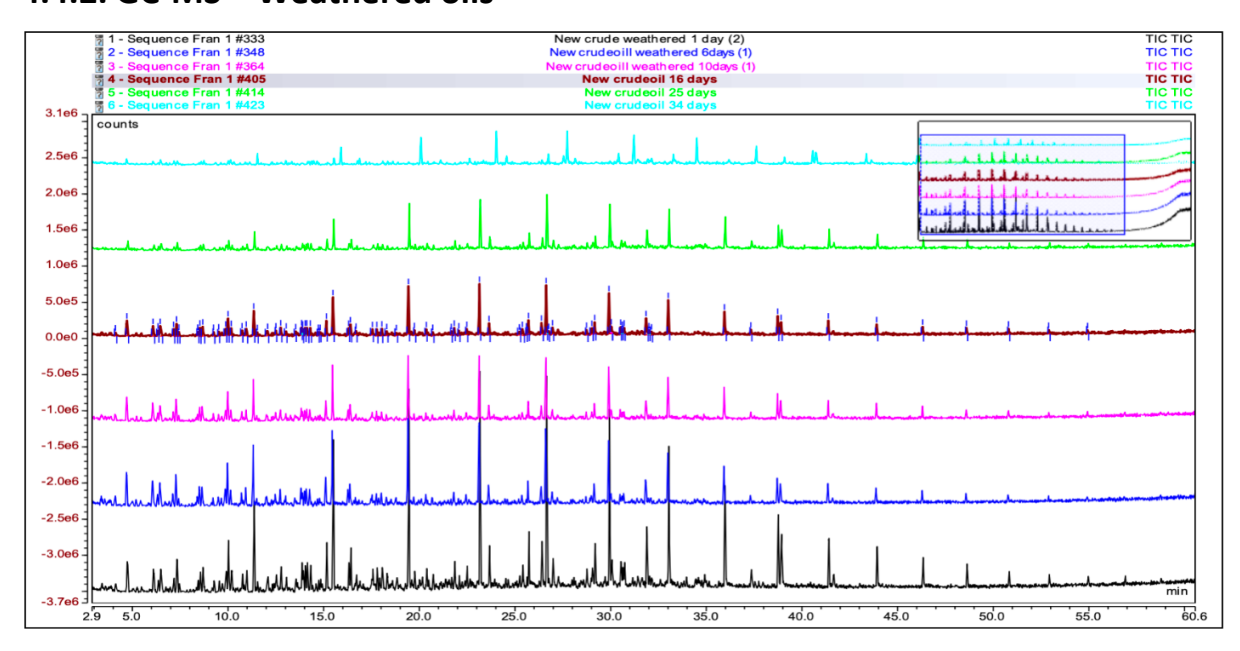


Figure 4. 38: Chromatograph showing intensity changes of weathered crude oil 2 on various days

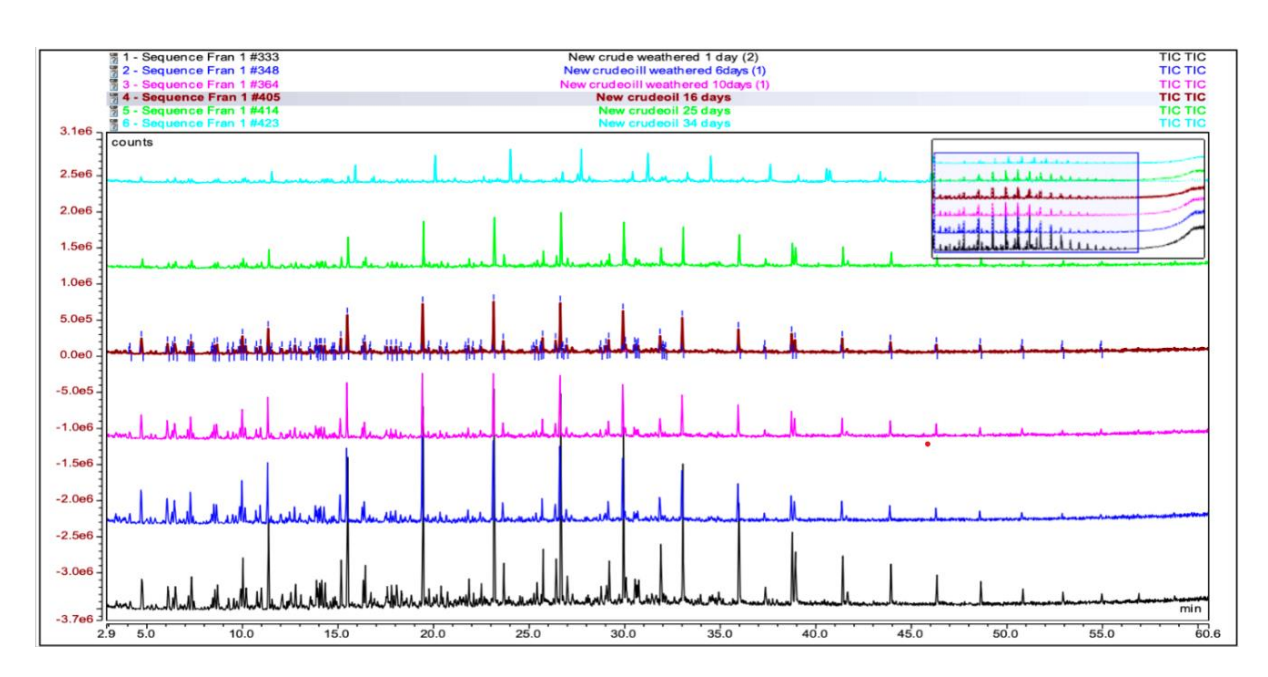


Figure 4. 39: Chromatograph showing intensity changes of weathered Phillip synthetic oil on various days

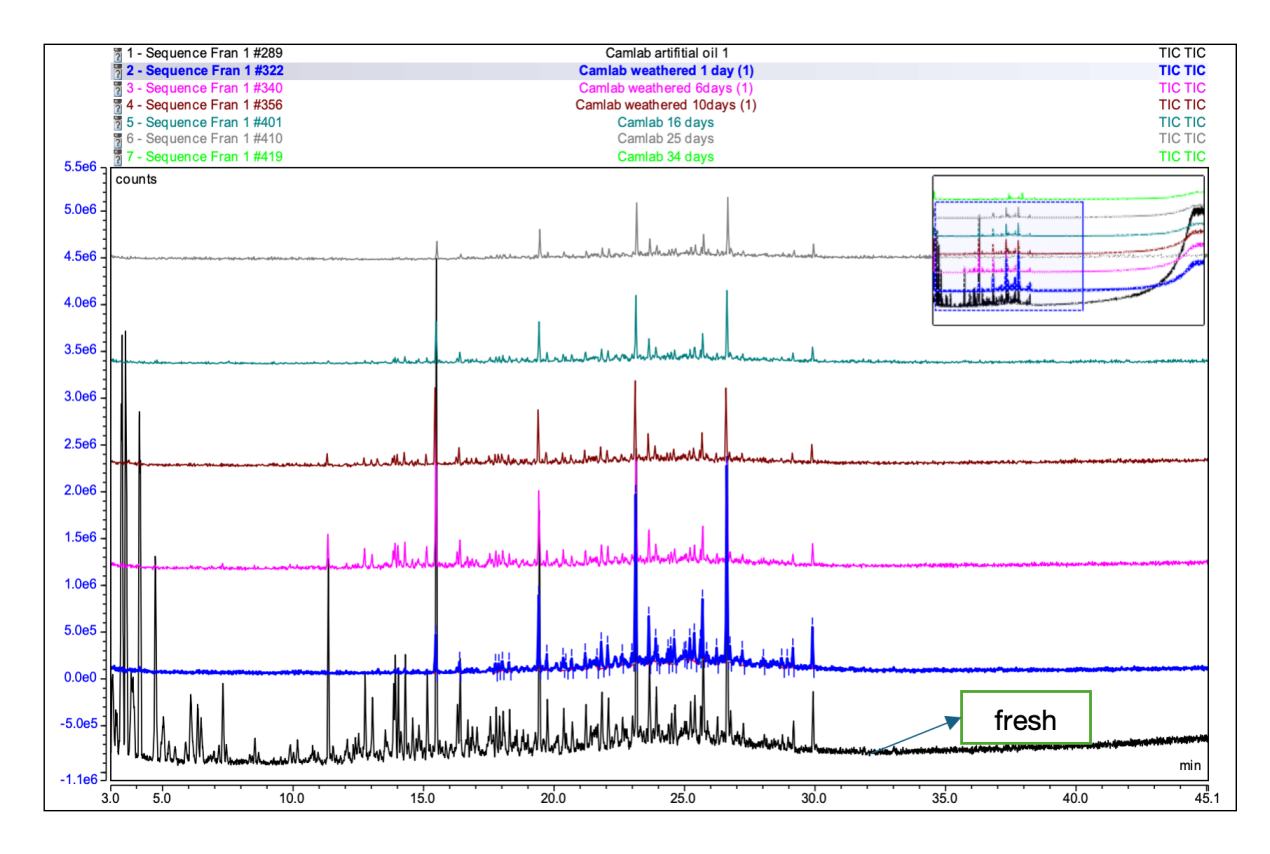


Figure 4. 40: Chromatograph showing intensity changes of weathered Camlab synthetic oil on various days

From Figures 4.38, 4.39 and 4.40, it is noticed that when the oil is exposed to the atmosphere from day one, there is a noticeable disappearance of some peaks or decrease in the intensity of several peaks detected by the GCMS in the lower temperature region (3 to 15 minutes), suggesting the loss or reduction of certain volatile components. As the number of days increased, more volatile hydrocarbons continued to evaporate. This is evident from the decreasing number of peaks and lower intensities over time, some peaks have merged or disappeared entirely, indicating chemical transformations such as oxidation, evaporation of lighter hydrocarbons, and possible microbial degradation.

The overall shape of the chromatogram has changed, with fewer peaks and a shift towards compounds that are more resistant to weathering/evaporation, likely heavier, less volatile hydrocarbons. Exposure to air can lead to the oxidation of hydrocarbons, forming new compounds that may not be as volatile or detectable by GC-MS. At room temperature, a confirmatory practical test (inside the fume cupboard) substantiated this weight loss by weighing 20 g of oil for each sample. Noticeable weight losses were recorded each day (Appendix A3) and about 3 g (crude oil 3), 4.1g (Camlab) and 5.45g (Phillip) of weight loss was recorded for 65 days.

4.4.3 Characterisation of oils with TGA

Thermogravimetric analysis (TGA) is a thermal analytical technique used to characterise a substance by monitoring its weight loss as a function of temperature. This method offers a detailed representation of the sample's composition and decomposition behaviours. It is expected that the weight loss at lower temperatures (35-325°C) would present the fraction of components observed by the GCMS analysis, while at higher temperatures, the loss would reflect the decomposition of heavier fractions, including the oils' non-volatile components and thermally stable residues.

4.4.3.1. TGA - Oils

TGA results from various crude oils (Crude oil 1, 2 and 3)

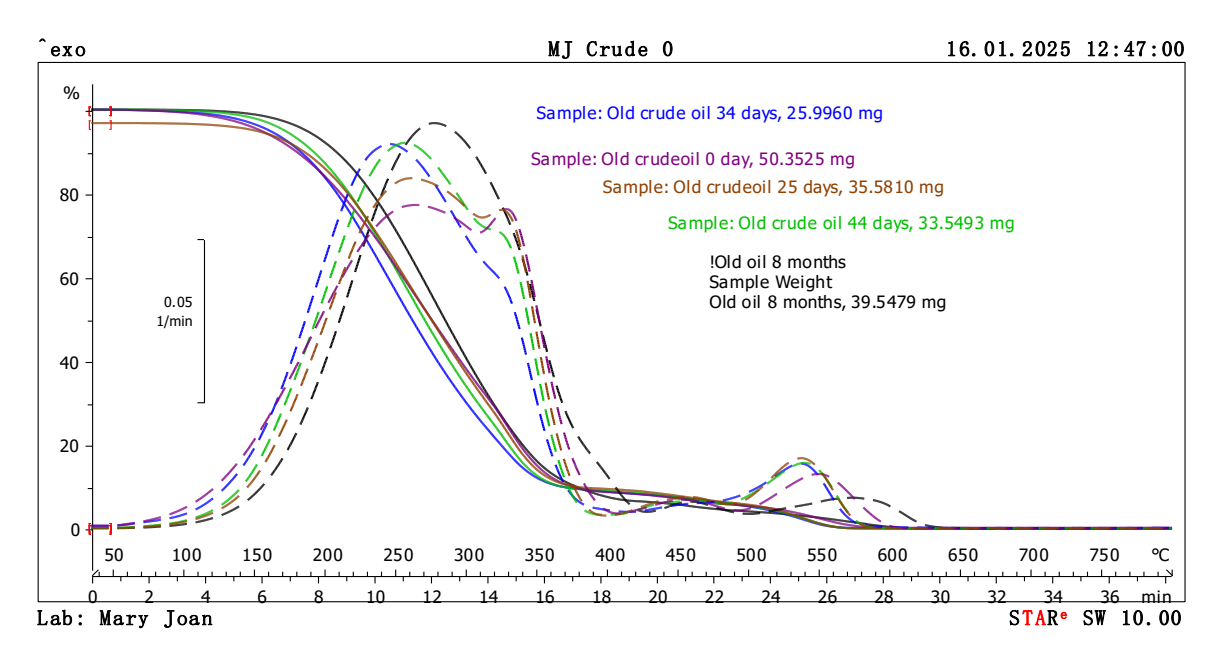


Figure 4. 41: TGA graph of Crude oil 1 weathered for various days

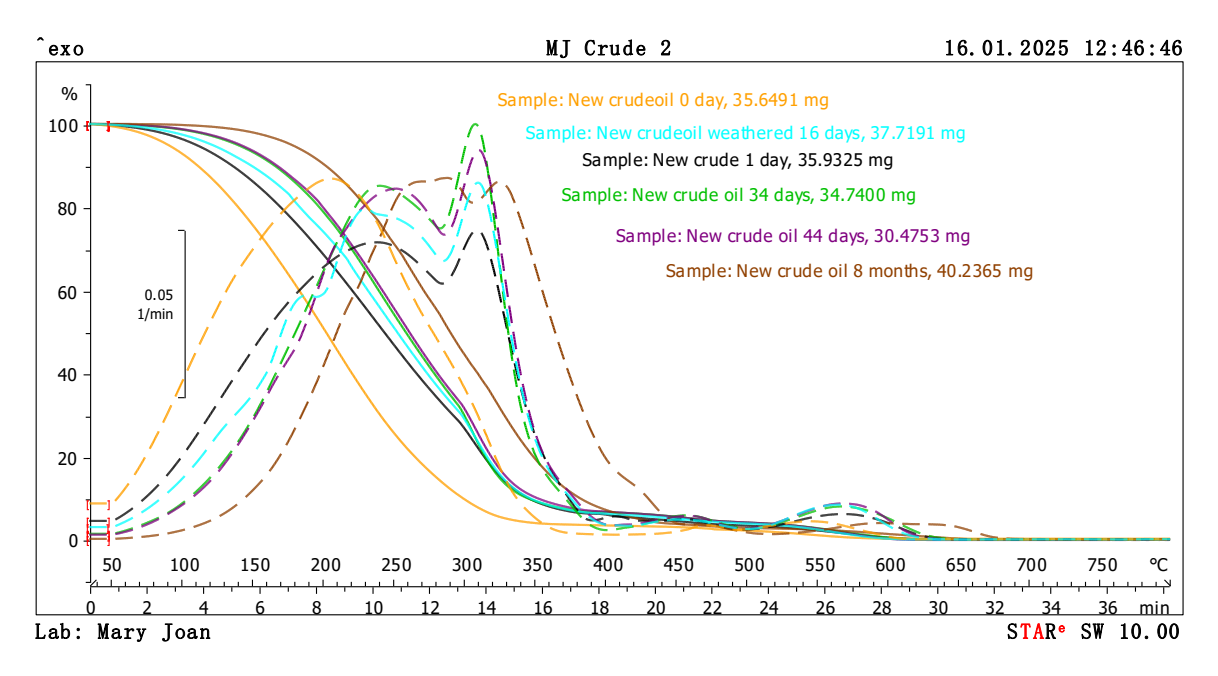


Figure 4. 42: TGA graph of Crude oil 2 weathered for various days

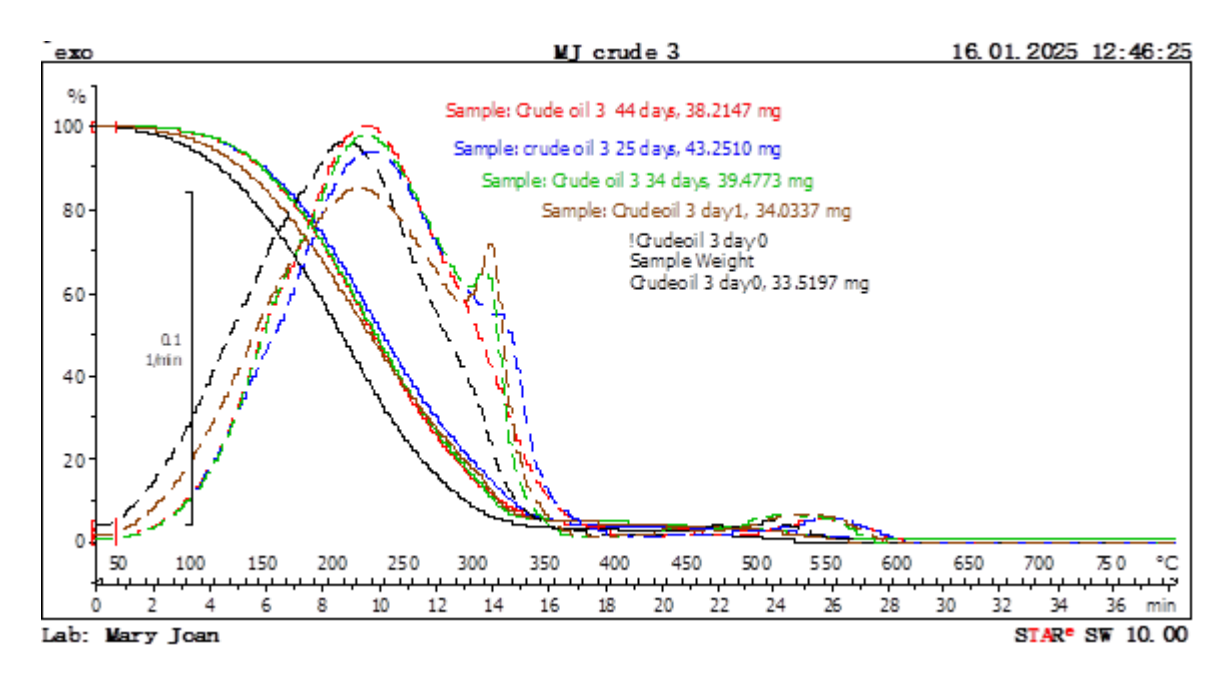


Figure 4. 43: TGA graph of Crude oil 3 weathered for various days

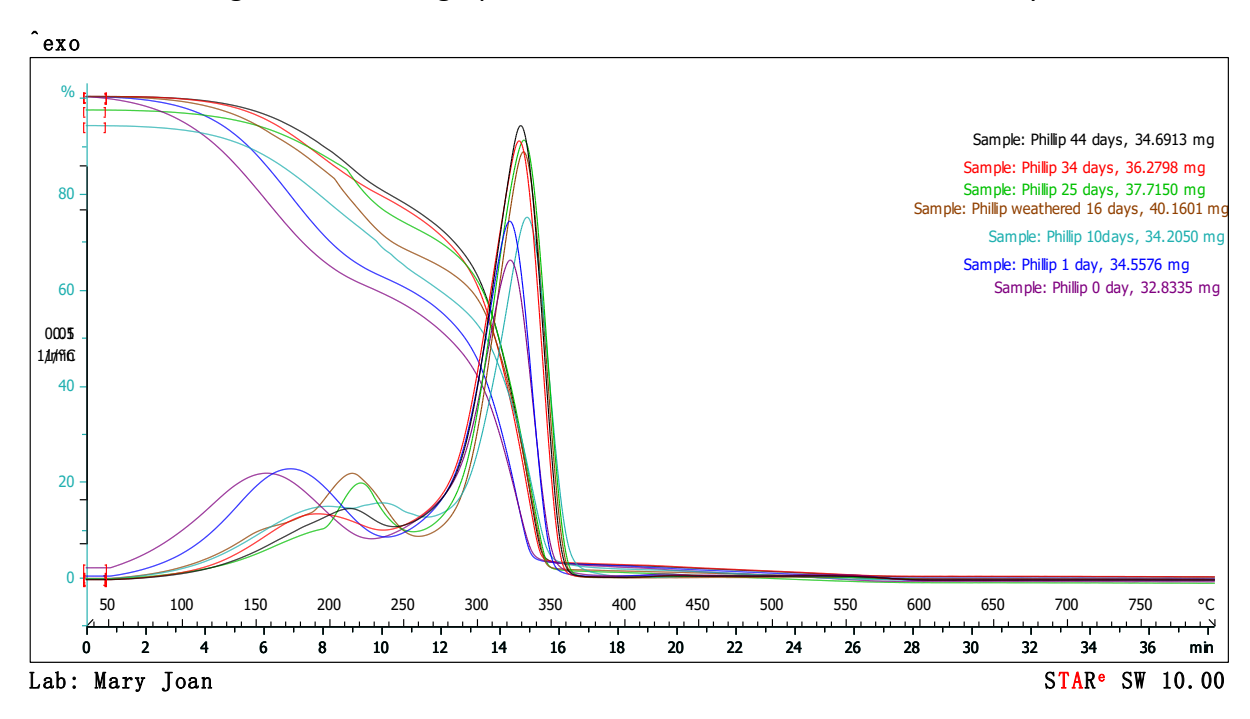


Figure 4. 44: TGA graph of Phillip oil weathered for various days

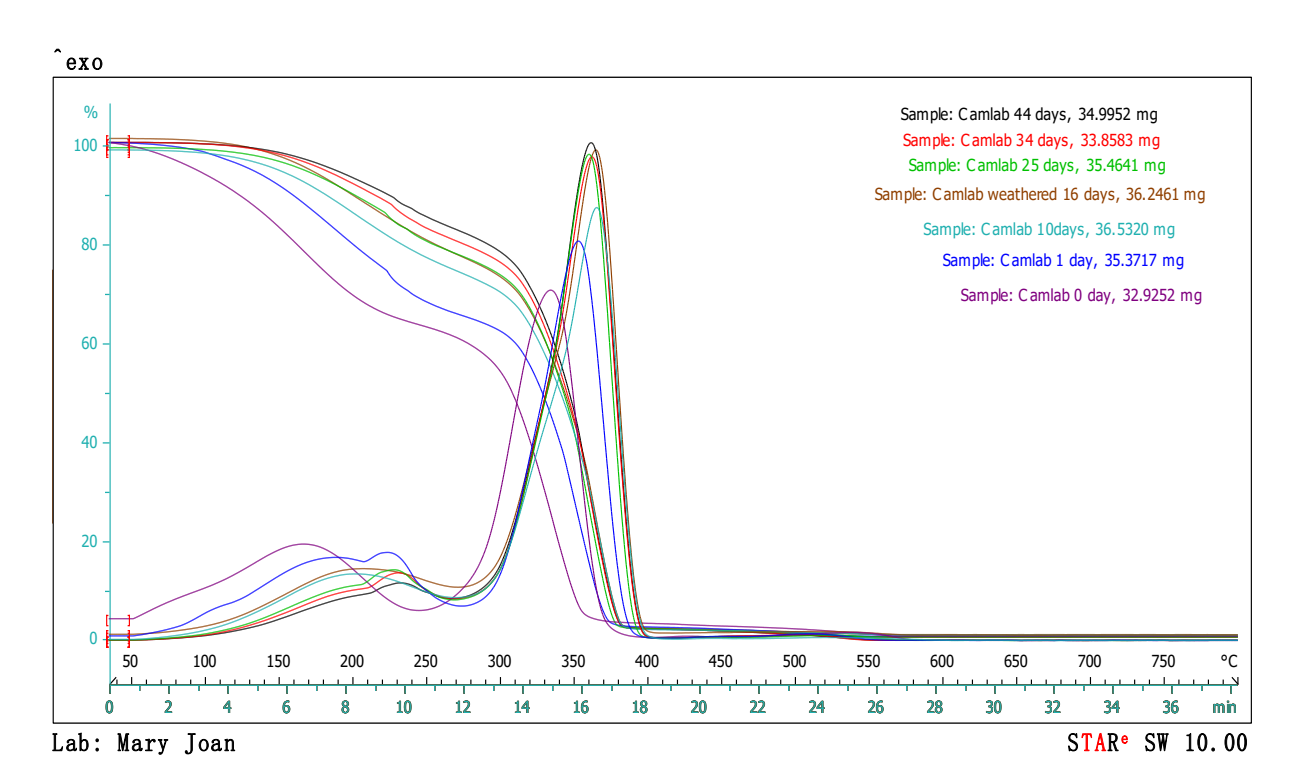


Figure 4. 45: TGA graph of Camlab oil weathered for various days

From Figures 4.41–45, the total weight loss for the oils diminishes with increased weathering days, this shows that the oils' composition changes over time as volatile fractions evaporate, and heavier fractions dcompose (130).

Day 1

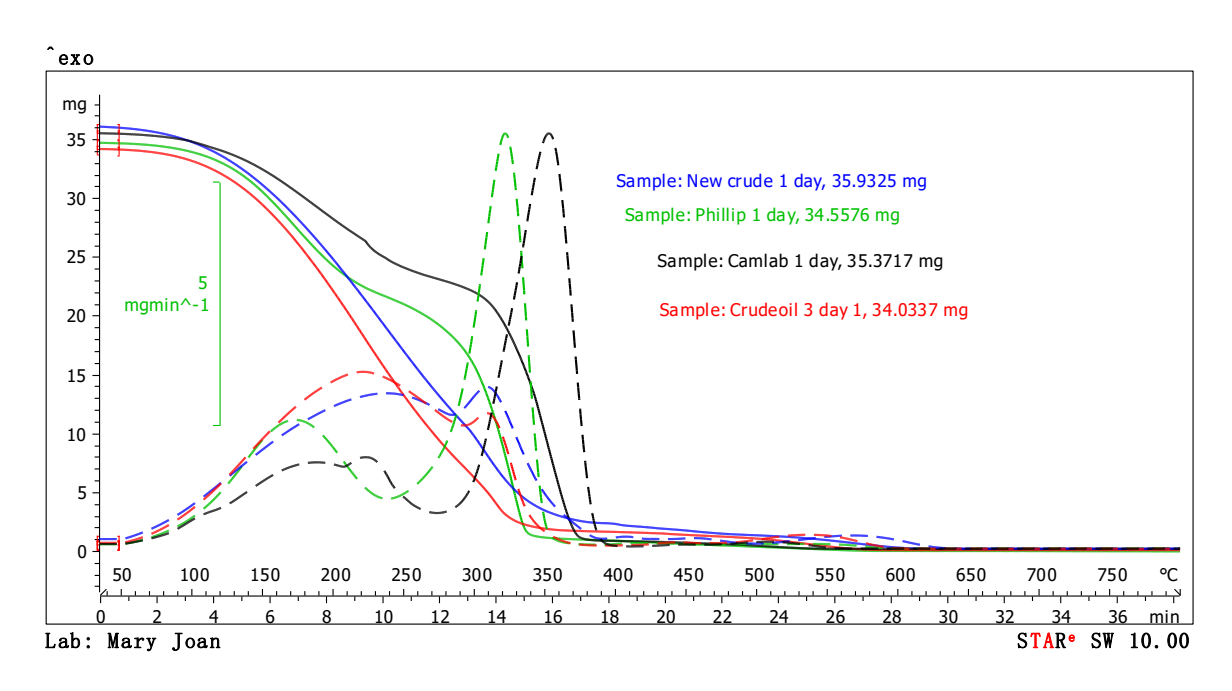


Figure 4. 46: TGA graph of Camlab, Phillip synthetic oils, and Crude oils 2 and 3 weathered for one day

Figures 4.46 show that both the synthetic (Camlab, Phillip) and natural crude oils (2 and 3) have different characteristic compositions as also shown by their GCMS chromatographs. The synthetic oils displayed three main stages of weight loss ($50 - 250^{\circ}$ C; $250 - 400^{\circ}$ C and 400- 550° C) and were different to the natural crude oils which have two main stages of weight loss ($50 - 400^{\circ}$ C and $400 - 550^{\circ}$ C). The mass loss profiles (and hence composition) change as the oils are exposed to various temperatures. At the lower temperatures there is loss of volatile components.

Although there are three main weight losses for the synthetic oils and two for the crude oils, the three temperature regions were chosen for further comparative analysis. The three weight loss regions within the oils can adequately represent the light, medium and heavy temperature fractions (68, 103).

From Figure 4.46 Phillip and Camlab synthetic oils (green and black curves). exhibited lower mass loss rates than crude oil at low temperatures but the opposite was true at high temperatures (above 250 °C)., which might suggest that they contain less volatile (lighter) components. More graphs of comparative analysis for different oils at different days are in Appendix A4.



Figure 4. 47: TGA graph of 3 crude oils showing the weight loss changes within the 2 major temperature regions (above) and 3 temperature regions (below) as weathering days increase

From Figure 4.47, showing the compositions in the 2 major temperature ranges (blue curve, $50-400\,^{\circ}\text{C}$ and orange curve, $400-650\,^{\circ}\text{C}$), all three crude oils show relatively stable behaviour around 95-98% weight loss. Amongst the 3 crude oils, the new crude oil 2 showed the most significant weathering effects with a 5% decrease in lighter fractions, while the old crude oil 1 showed remarkable stability with almost no change, and crude oil 3 showed about 2% weight loss in the lighter region. For the heavier fractions ($400-650\,^{\circ}\text{C}$), all the crude oils showed minimal changes within 1-2% and remained relatively stable throughout.

The three temperature regions were calculated to be able to compare the crude oils with the Synthetic oils. For the three crude oils in the 3 temperature regions, all the crude oils contain significant volatile compounds shown by the weight loss in the $50 - 250^{\circ}$ C temperature range. The crude oil 1 has the most stable light fraction weight loss between approximately 72-75% weight loss. Crude oil 2 and 3 show more gradual weight loss over time in this temperature range, with a gradual decline from 74 - 62% weight loss.

For the medium range (250-400°C range), old crude oil 1 was more stable around 20%. Crude oil 2 contained around 20 - 25%, while crude oil 3 gradually contained from around 25% to approximately 35% as the weathering days increased, making it very unstable among all the 3 crude oils. This increase in weight loss could be due to increasing content or possible concentration of the medium components as the lighter ones evaporated.

For the high-temperature range (400-650°C), all the crude oils showed very low weight loss, around 10% or less.

This result indicates that Crude Oil 1 demonstrated greater stability, likely due to its prolonged usage and repeated handling in the laboratory, which may have allowed for partial weathering or stabilisation over time. In contrast, Crude Oil 3 appeared to be the least stable, as it was freshly received and had undergone minimal exposure or aging before the tests. Crude Oil 2 exhibited stability characteristics between those of Crude Oil 1 and Crude Oil 3, reflecting its intermediate level of handling or exposure.

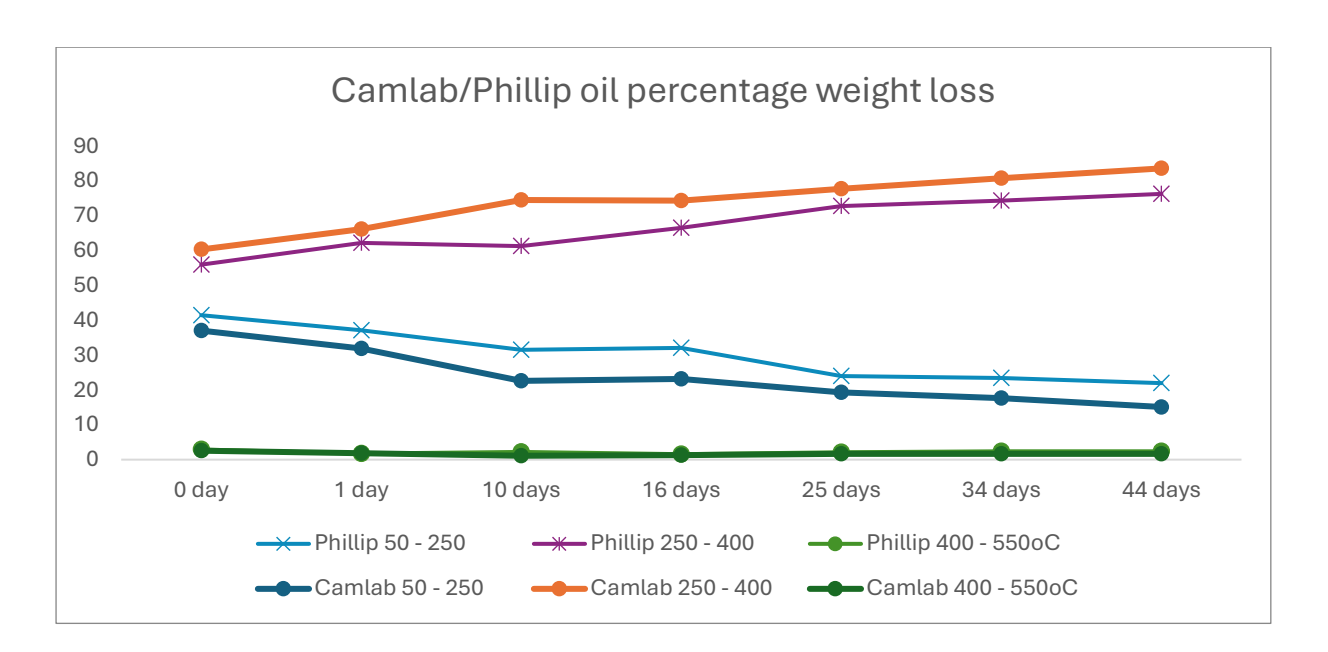


Figure 4. 48: TGA graph of Camlab and Phillip synthetic oils showing the weight loss changes within the 3 major different temperature ranges as weathering days increase

From Figure 4.48, the percentage weight loss patterns of Camlab and Phillip crude oils were similar over the range of temperatures and increasing number of days of exposure. They show that the two synthetic crude oils have similar compositions and could be classified the same, though the Camlab oil had a slightly higher medium mass fraction relative to the lighter fraction compared to Phillip oil. The weight loss in the lowest temperature region (light fraction) decreased from 41 to 21% for the Phillip oil and around 37 – 15% for the Camlab oil as the weathering time increased resulting from the more volatile components of the oil evaporating. The percentage weight loss in the middle-temperature region (medium fraction) increased from 60 to 83% for the Camlab and 55 – 76% for Phillip oil as the weathering time increased resulting from a corresponding loss in the light fraction. The percentage weight loss changes with weathering in the high-temperature region for the two Synthetic oils representing the heavy fraction was negligible and was noticed to vary between 1-2%.

Comparison of Synthetic oils with Natural Crude Oils in the 3 temperature regions (50-250°C, 250-400°C and 400-550)

Comparing Figures 4.47 (below) and 4.48: For the low-temperature region (50-250°C), crude oils showed much higher initial weight loss (70-74%) and maintained this throughout the weathering compared to synthetics oils (37-41%) which showed more decline in this range.

This shows that crude oils retain more volatile components. For the mid-temperature region (250-400°C), synthetic oils show higher weight loss (60-83%) vs crude oils (23-33%). Synthetic oils show an upward trend while crude oils were more stable across the weathering days. Only Crude Oil 3 showed some increase in this range. This suggests that Camlab and Phillip synthetic oils have more medium-temperature components.

For the high-temperature region (400-550°C), both synthetic and crude oils show similar behaviour, very low content (2-7%), and high stability over the weathering duration. This might indicate similar heavy fraction of content.

The significant difference also amongst these oils is that synthetic oils show faster compositional changes during weathering, showing a more pronounced shift from light to medium-temperature components. Crude oils generally showed more stability. This comparison highlights that synthetic oils have significantly different thermal stability and composition profiles compared to natural crude oils, which means that they might behave differently during handling.

This trend was verified by Physical weight loss experiment of 20g sample for the different oils in the fume cupboard for 65 days (with crude oil 3 and the 2 synthetic oils) as shown in Appendix A3. The weight losses in the Camlab and Phillip oil progressed more in the early days of the sample exposure to the atmosphere. This is contrary to the result of the TGA, which showed that it is likely that the natural crude oil contained more lightweight fractions because of the high percentage of weight loss in the lower temperature region. This contrasting behaviour shows that the oils can behave differently under controlled heating and natural/real-life conditions. This occurrence could be explained by the disappearance of peaks in the lower-temperature region in GCMS showed that the lighter fractions of the crude oils could persist for a longer periods more than the synthetic oils. These volatile components evaporate readily under controlled conditions of heating and are detected as a significant light fraction in these tests. The physical weighing under room temperature is influenced by atmospheric conditions, as molecular diffusion which interacts with external factors, such as viscosity, temperature, and airflow, to dictate how quickly volatile components evaporate (108, 109, 110). From Figure 4.35, the synthetic oils (Camlab and Phillip) showed fewer peaks which indicates that they have fewer components than the natural crude oil and are often manufactured to have a narrower molecular weight distribution with less viscous components. This also may contribute to why volatiles escaped more freely at room temperature in the synthetic oils, leading to a faster weight loss as seen in the Appendix A3 results. This could also mean that evaporation was taking place faster in the synthetic oils as temperature or the weathering days increased.

4.5 Rheology of Natural crude oil

Natural crude oil samples were placed in 250 mL beakers and exposed to open-air conditions in the laboratory's fume cupboard for 41 days, allowing the samples to undergo weathering. This setup was to mimic natural evaporative processes, enabling the study of rheological changes over time and optimising strategies for oil spill response for both pristine and weathered crude oil. Rheological measurements were performed multiple times for each sample to ensure consistency and reproducibility of the results. From the collected data, two representative graphs for each sample were selected for this discussion. It is noted that at lower shear rates, the data exhibit sporadic behaviour due to the low viscosity of the crude oil and the sensitivity limits of the rheometer at these values.

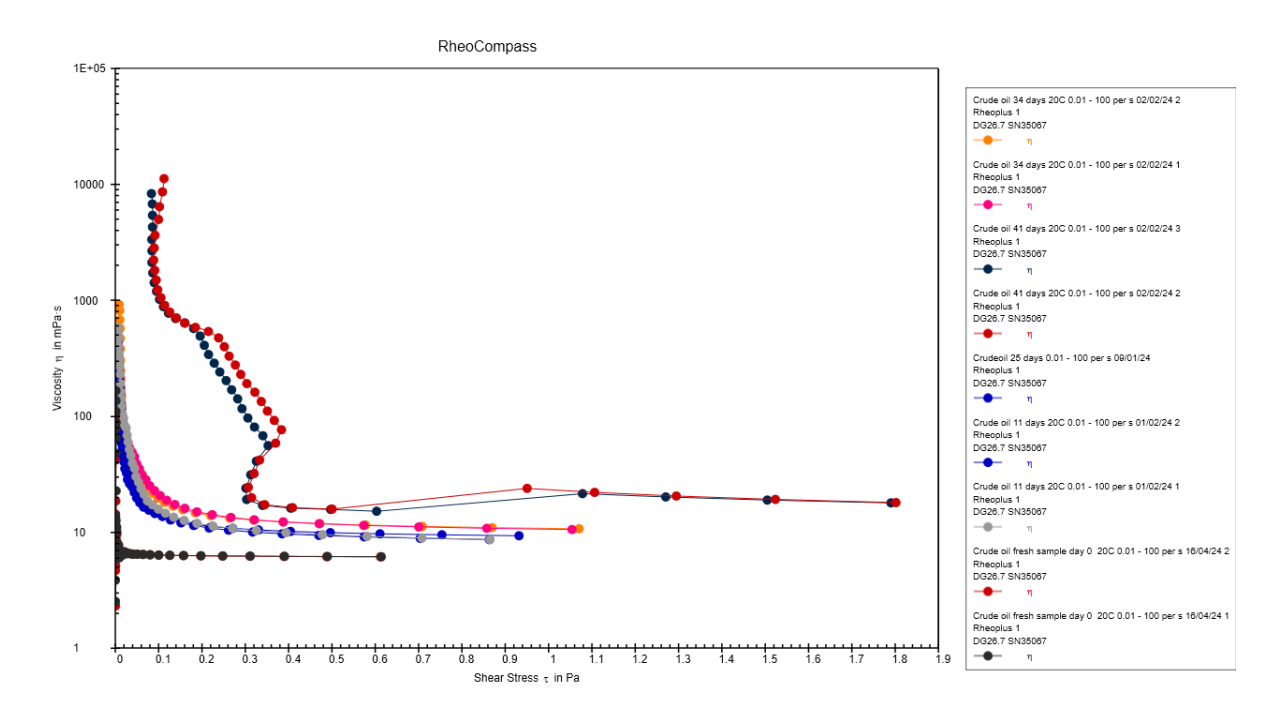


Figure 4. 49: Rheology graph of pristine and weathered natural crude oil at a constant temperature of 20 degrees centigrade

Figure 4.49 shows the rheological analysis of both pristine and weathered crude oil samples at a constant temperature of 20°C, providing insights into the flow behaviour of the samples as weathering progresses. The pristine crude oil (day 0) displays the lowest viscosity and the highest sensitivity to shear stress. At low shear stress values, the viscosity drops significantly, reflecting a Newtonian-like behaviour at these conditions. This indicates that the pristine oil contains a higher proportion of light, volatile hydrocarbons, which contribute to its low resistance to flow. As weathering progresses from day 0 onwards (day 11 to day 41), the crude oil becomes more viscous and less responsive to shear stress. This change is due to the

evaporation of lighter fractions and the relatively higher concentration of heavier hydrocarbons. By day 41, the shape of the curve is unexpected between 0.3 to 0.4 shear. This could be as a result of compositional changes/phase separation, wall slip/ boundary effect or instrument /measurement artifacts which could contribute to this unexpected deviation. To pinpoint the exact cause could need further investigation in future work.

The loss of lighter fractions is also shown by the TGA graphs (Appendix A4), the physical weathering measurements carried out (Appendix A3) and the GCMS graph (Figure 4.38). Despite this increase in viscosity, all weathered samples eventually stabilise at a viscosity range of approximately 8-25 mPa·s at low shear stress (around 0.3-0.5 Pa). This rheological analysis shown in Figure 4.49 underscores the dynamic nature of crude oil as it weathers over time. The transition from a low-viscosity, shear-sensitive fluid to a more viscous, shear-stable material highlights the importance of understanding crude oils physical behaviour under environmental conditions.

4.6. Contact angle measurement and Surface energy

Contact angle measurements provide insights into how liquids interact with the surface, indicating whether the PE samples are hydrophobic, hydrophilic, or oleophilic. This experiment aims to evaluate how surface modification (roughening) and environmental degradation (UV-weathering) influence wettability and surface energy.

Contact angle measurements were carried out using water, diiodomethane, and pristine crude oil on the different forms of polyethylene to determine their surface wettability. Contact angle and surface energy calculations were carried out on; Virgin PE, roughened PE, and weathered PE (75 hrs and 150 hrs).

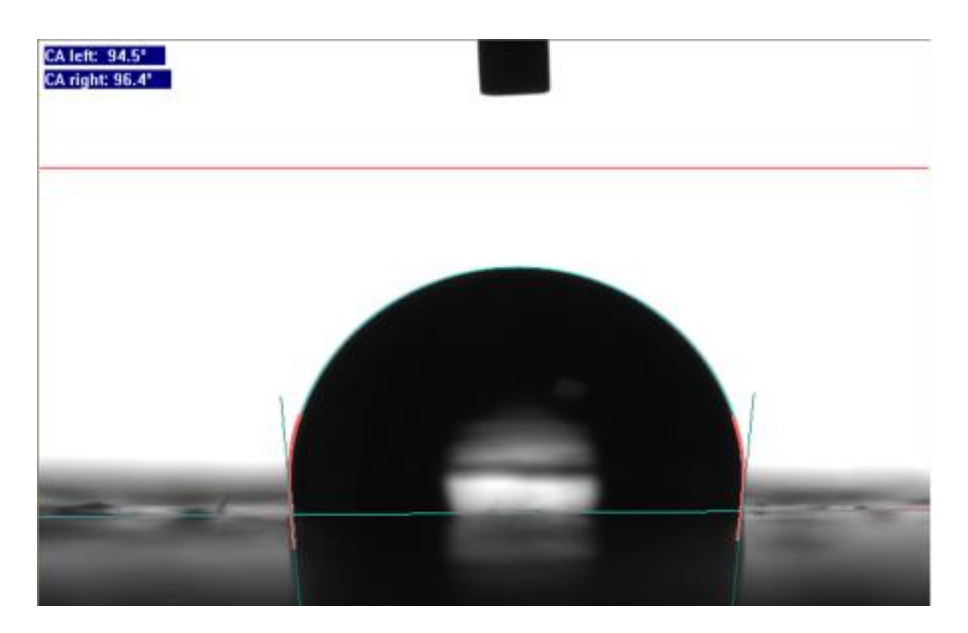


Figure 4. 50: A screenshot of contact angle measurement for a water droplet on a polyethylene surface using the SCA20 software

Water, diiodomethane, and crude oil were used as the fluids in this experiment. Water represents a polar liquid and tests the hydrophilicity/hydrophobicity or wetting behaviour of the surface. Diiodomethane (non-polar liquid) is used to determine the dispersive component of the surface energy and crude oil is used to test the oleophilic or oleophobic nature of the surfaces of these PE samples. Three repeat measurements were done to achieve the standard deviation.

Table 4. 3: Contact angle measurements of various forms of PE samples

	Virgin/ Pristine	Roughened PE	UV weathered PE	
	PE		75 hrs	150 hrs
Water contact angle	94.5	81.4	88.7	73.6
(WCA)				
Standard deviation for	4.8	3.9	5.1	1.7
WCA				
Diiodomethane	61.6	54.5	54.2	
contact angle (DCA)				53
Standard deviation for	3.6	5.8	2.4	0.8
DCA				
Crude oil contact	26.2	0	0	0
angle (CCA)				

Standard de	viation for	0.6	-	-	-
CCA					
Surface	energy	27.3	33	31.7	36.3
(dyn/cm)					

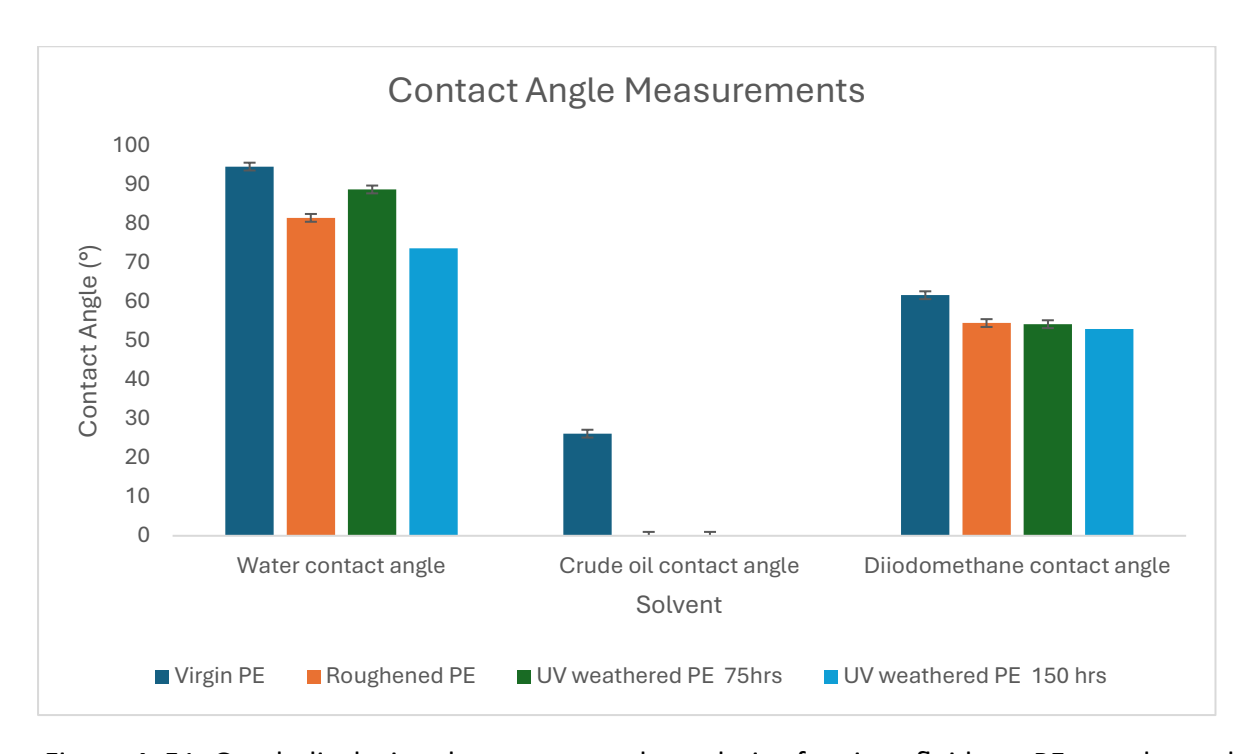


Figure 4. 51: Graph displaying the contact angle analysis of various fluids on PE samples and their error bars

(Note: Crude oil contact angle for roughened PE = 0, 75 hour and 150 hour weathered PE samples = 0)

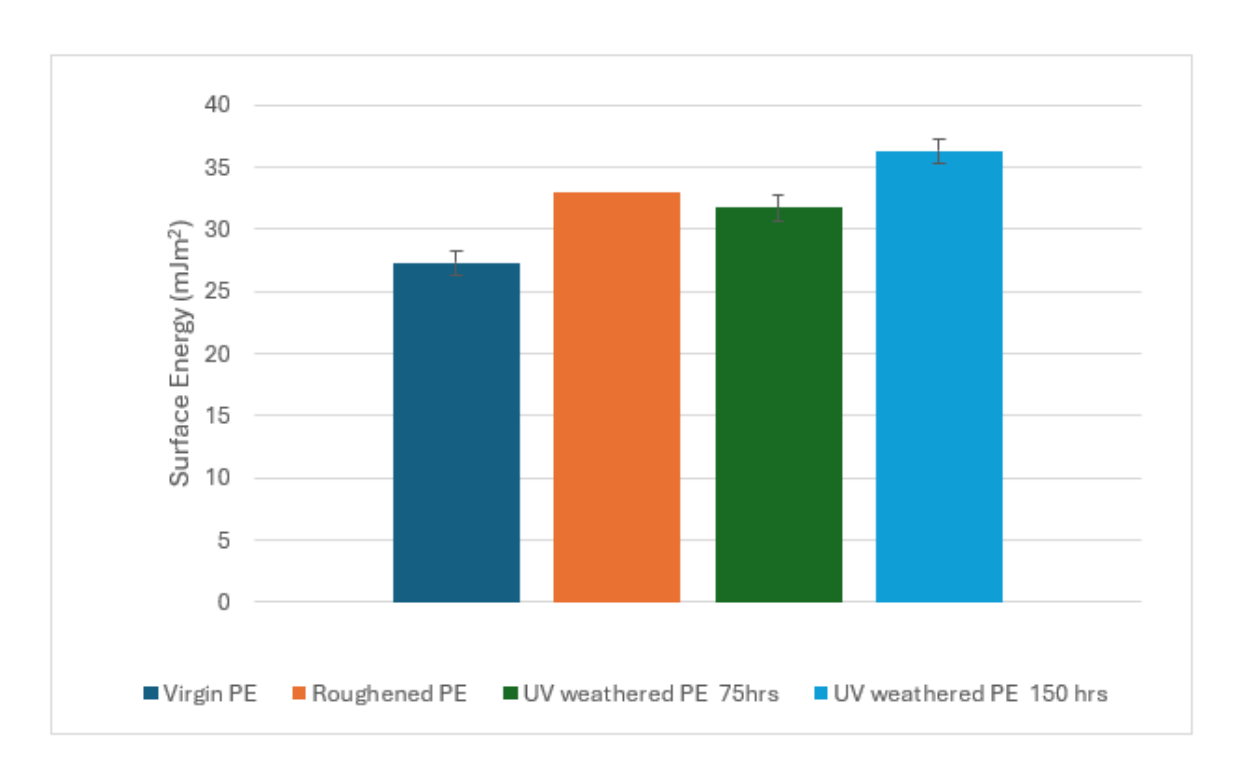


Figure 4. 52: Graph displaying the surface energies of various PE types on various fluids and their error bars

The contact angle values for polyethylene (PE) samples in the above table 4.3 and graphs (4.51 and 4.52) indicate the wettability characteristics of the various PE sample surfaces. The Virgin PE with a water contact angle of 94.5° appears to be more hydrophobic than the rest, while UV-weathered PE (150 hrs) with a water contact angle of 73.6° is the least hydrophobic. This means that as PE undergoes roughening and UV weathering, the water contact angle decreases, indicating increased wettability (or decreased hydrophobicity). Altering the PE surface topography, for example, roughening can change the interaction between the liquid and the PE. Rough surfaces may enhance wettability by increasing surface area or altering the wetting mechanism (e.g., transitioning between Wenzel and Cassie-Baxter states) (115, 116). UV radiation, oxygen, and moisture exposure during weathering can induce surface oxidation, chemical degradation, and morphological changes. These effects often increase surface polarity, making the surface more hydrophilic. Roughening has a lower effect than 75 hours of UV exposure, which could be explained by the rougher surface texture of the former as evidenced by the SEM images. The 150-hour UV exposure surface was less rough than both the roughened and 75-hour UV exposure samples, as evidenced by the SEM images but still showed lower water contact angles. The surface oxidation must therefore be a strong factor in modifying the hydrophobicity of the surface.

For the diiodomethane contact angle, the virgin PE also has a higher contact angle value (61.6°) than the rest, it decreases with roughening and UV weathering, following the same trend for the water contact angle (but to slightly differing extents), suggesting an increase in surface energy.

For the crude oil contact angle, the virgin PE has a contact angle value of 26.15° and a zero contact angle value for the rest, suggesting complete wetting and strong affinity of these surfaces for crude oil.

The surface energy increases with roughening and UV weathering, indicating a higher affinity for liquids.

In summary, the virgin PE has the highest water contact angle and a relatively low crude oil contact angle, showing that the surface is hydrophobic, and oleophillic. For the roughened and UV-weathered PE, the decreased water contact angle values and zero crude oil contact angles show that these treatments significantly increase the surface's affinity for crude oil whilst making it more hydrophilic. Thus, it is expected that the surface modifications will enhance the polyethylene's ability to sorb crude oil by increasing the surface energy and wettability.

Chapter 5

5.0 Preliminary batch experiments

According to Section 3.3.4 of ASTM 726-17, the PE sorbent is classified as a type II adsorbent (loose)—an unconsolidated, particulate material without sufficient form and strength to be handled except with scoops and similar equipment. The standard also outlines some performance factors, including oil and water adsorption strength, buoyancy, and reusability tests. This chapter outlines the methods used for all these tests.

5.1 Introduction

The different preliminary experiments described in this section were conducted to establish the main adsorption experimental procedures developed and a basic understanding of the effect of influencing factors on adsorption. Different types of natural and synthetic crude oils were used. Natural Crude oil 1 (been around and in use in the lab for about 1 year), Natural crude oil 2 (6 months), Natural crude oil 3 (a few days after arrival into the UK), Phillip and Camlab artificial oils (over one year old in the lab).

Natural crude oil is a complex mixture of hydrocarbons and other organic compounds, formed naturally over millions of years from organic matter, varies widely depending on the source and contains impurities like sulphur, nitrogen and metals while artificial crude oil is produced by companies such as Phillip or Camlab and are synthesised with controlled composition that is simpler and tailored for laboratory uses.

All the oil used for adsorption experiments were exposed to the atmosphere for one day, in other words, weathered for one day before the experiment. This allows for simulating real-life conditions such as the evaporation of volatile components to some extent, temperature equilibration with the environment, slight oxidation, and degassing, all of which contribute to achieving a more stable and consistent oil sample. This stability is essential for ensuring reliable and reproducible results in the adsorption experiment, as it minimises variations in the oil's properties that could otherwise affect the outcome of the results.

5.1.1 Assessment of contact time for adsorption of crude oil

Contact time represents how long the sorbent is left in contact with the oil spill for it to be adsorbed. This time corresponds to the point at which the adsorption rate slows down or reaches equilibrium.

To establish a baseline for the determination of the contact time, adsorption experiments found in the literature were utilised and compared, even though their research was different from this research.

According to the literature, various contact times were used in different studies and were based on the material's ability to sorb the oil at equilibrium, the oil type, and the experimental goals. For emergency response scenarios for cleaning light to medium crude oils, Xu et al. (2009) developed a nanocellulose aerogel with 98% adsorption efficiency achieved with a contact time of 30 seconds. Gui et al. (2010) developed a carbon nanotube (CNT) sponge with over 90% efficiency in a 2-minute contact time, whereas Zhu et al. (2011) developed a carbon fibre/polyurethane sorbent with approximately 80% efficiency in a 3-minute contact time. Some researchers have based their work on a standard laboratory testing duration. For example, Wei et al. (2003) studied polypropylene non-woven sorbent and achieved an 80% efficiency, while Nguyen et al. (2018) worked with coconut-activated carbon and obtained an 85% efficiency, both within a 20-minute contact time. Based on the above, the PE sorbent contact time needed was estimated to be between one minute and 30 minutes since the oils are light or medium-weight and the PE has a relatively low surface area.

Deionised water, and Phillip artificial oil were used for this procedure as it is assumed that Phillip oil is ideal for adsorption studies due to its controlled composition, low contaminants, consistent viscosity, thermal stability, ease of handling, non-degradability, and compatibility with sorbent materials, all of which ensure reliable and reproducible experimental outcomes.

5.1.1.1 Experimental procedures for determining the contact time

Materials and equipment:

Phillip oil sample, deionised water, shredded PE (sieve size : ≤2.36 mm, ≥1.80 mm), glass beakers (≥250 mL), analytical balance (±0.01 g precision), stop watch, sieve or mesh, measuring cylinders and electric oven.

Experimental design:

Parameter	Value
Mass of Oil	10.0 g
Water Volume	100 mL
Oil-to-Water Ratio	1:10 (w/v)
Mass of PE	0.5 g (shredded, dry weight)
Contact Times	1, 2, 3, 4, 5, 10, 15, 20, 25, 30 minutes
Sorbent Size	≤2.36 mm ≥1.80 mm

Procedure

To prepare the oil-water mixture, about 10g of oil was added to 100 mls of water in ten (10) different beakers, and labelled with different time intervals, 1, 2, 3, 4, 5, 10, 15,20, 25, and 30 minutes. About 0.5g of ≤2.36 mm≥ 1.80 mm shredded PE (10 portions) were weighed out for each trial. A timer was started as the pre-weighed adsorbent was added to the first beaker, and were given a slight, short, single rolling shake by hand to ensure good contact between the oil and the adsorbent. At the designated time interval, the adsorbent were lifted from the oil-water mixture using sieves. The adsorbents were then allowed to drain for 5 mins (tilting the sieves at an angle of about 45° to remove any excess and help remove any trapped water). The adsorption capacity was calculated using the equation as stated in section 3.3.1. The procedure is repeated and recorded at each time interval. Different oil-to-water ratios and varying amounts of adsorbent were used to carry out same experiment to determine the optimal contact time for maximum oil adsorption. This time is typically when the adsorption rate significantly slows down or reaches equilibrium.

Experimental Units Summary:

Time Intervals	10 time points (1-30 minutes)
Replicates per condition	3
Blanks 3	Oil + water
Controls 3	Water + PE
Total experimental units	30
Total tests completed	30

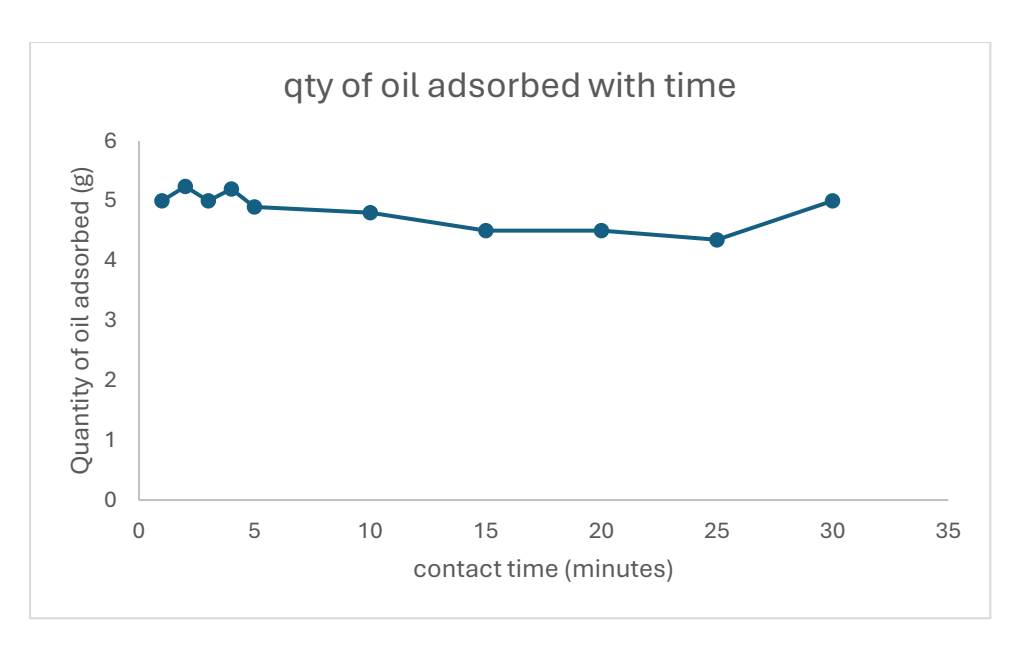


Figure 5. 1: Graph of contact time versus adsorbed oil (Phillip oil)

From Figure 5.1, the adsorption rate of oil on PE was high, as indicated by the steep increase in the quantity of oil adsorbed (5g/g) after the first time interval of one minute, the oil was filling the most accessible adsorption sites quickly. This shows that the adsorbent material readily adsorbs the oil molecules quickly during the initial stages of its contact time. Approximately 5.8 grams average was observed at around the 1-5-minute mark, and about 4.6 grams observed at around the 25-minute mark. Estimating from the graph, the average adsorption capacity appears to be around 5 grams. The variability in the adsorption values suggests some level of minor inconsistencies or error in the experimental procedure maybe there was not a uniform method of removing the adsorbent from the oil-water mixture as it was manually done or the angle of tilting of the sieve was not uniform as it was assumed, for the complete drainage before measurement and calculations, however, the values remain within a relatively narrow range, which could imply that the experiment is reasonably reproducible, but not perfectly so.

In general, the data indicates that contact time will not significantly affect the amount of oil adsorbed beyond the initial stages, because, despite the increase in contact time, the quantity of oil adsorbed remains almost constant. This shows the adsorption process reaches a saturation point quickly, and any additional contact time will not result in more oil being adsorbed.

Based on these results, a contact time of 5 minutes was chosen for all the experiments, since it is assumed that maximum adsorption capacity would have been reached. The faster the oil is trapped, the less likely it will be dispersed and get away farther into the sea. This is an added advantage of the PE adsorbent.

5.1.2 Adsorption experiments with PE square sheets

These experiments were performed to assess the amounts of oil adsorbed on a large flat surface film of PE and its integrity over time. This was in comparison to shredded PE with a smaller surface area that tended to curl when in contact with oil, which is discussed later. 5 g of natural crude oil 1 was weighed into a plastic vial, 30 mm² sheet of PE was first weighed and then dipped into the oil and allowed a contact time of 5 minutes. The PE film was removed using tweezers, excess oil on the PE was allowed to drain off for approximately 1 minute back in to the vial, and then pegged on a tripod stand to allow further drainage for 30 minutes (as shown in Figure 5.2) before a second weighing. The effect of contact time on the adsorption of crude oil onto the surface of PE was investigated at different time intervals (2 mins, 1 hr, 2 hrs, 3 days, 1 week, and 2 weeks). The swelling of PE during these experiments was also investigated.

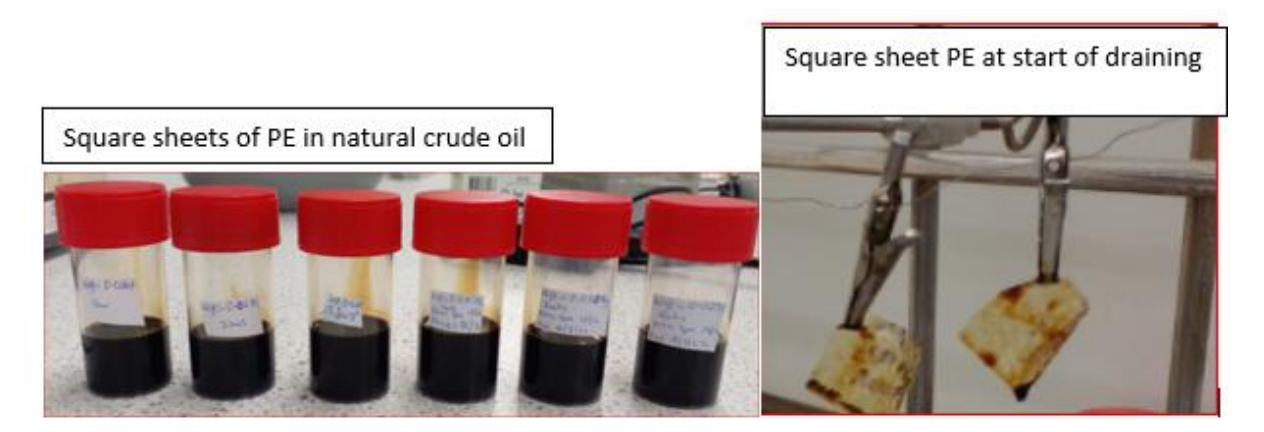


Figure 5. 2: Adsorption experiment with square PE to check the effect of contact time and film integrity

Table 5. 1: Weights of crude oil adsorbed on and amounts drained off square-shaped PE at various time intervals

Duration	Weight	Weight of PE	Weight of	Weight of oil	Weight of oil
	of PE (g)	after draining	oil adsorbed	drained (g) per	drained (g) per g
		for 30 mins (g)	(g)	sq. shaped PE	of sq. shaped PE
2 minutes	0.029	0.079	0.050	0.026	1.72
1 hour	0.027	0.071	0.044	0.031	1.63
2 hours	0.029	0.073	0.044	0.026	1.52
3 days	0.028	0.070	0.042	0.032	1.50
1 week	0.030	0.078	0.048	0.013	1.60
2 weeks	0.031	0.083	0.052	0.063	1.67
Average	0.029	0.073	0.045	0.032	1.61

From the results shown in Table 5.1, there was no significant change in the weight of crude oil adsorbed by square shaped PE film for the various contact time intervals. This confirms that the adsorption is very fast and contact time beyond 5 minutes is not likely to be a quantitative factor that will influence the adsorption exercise. The various square-shaped PEs adsorbed on average about 1.6 times their own weight. On average, 0.029 g of square shaped PE adsorbed 0.045 g of crude oil, thus the adsorption capacity per gramme of PE is 1.61 g/g. Comparing this result with that observed in experiment 5.1.1 with shredded PE, the curling of shredded PE significantly enhances its adsorption capacity compared to square-shaped PE, this is primarily due to increased surface area because curling naturally increases the surface area of the PE exposed to the oil, unlike the flat surface of square-shaped PE, curled PE provides more contact points for oil adsorption, which allows it to hold more oil. The curled structure also creates more interstitial spaces or voids where oil can be trapped. These spaces act like small reservoirs, further enhancing the material's ability to adsorb and retain oil. Furthermore, it can be said that the curled and irregular structure of the shredded PE promotes capillary action, drawing the oil into the material more. More importantly, in this experiment, it was observed that there was no swelling of the PE (in the X, Y or Z direction), meaning only adsorption took place.

5.1.3 Determination of the quantity of adsorbent to be used for adsorption experiments

Determining the mass of adsorbent to be used is critical in maximising oil adsorption capacity while minimising material use. From the literature, previous researchers conducting small-scale batch experiments using similar materials for oil adsorption had used a wide range of sorbent weights of between 0.05 - 0.5 g, depending on scale, sorbent type, and oil to water ratios. This forms the basis for tests carried out to determine the sorbent quantity to be used. Zhu et al. (117) investigated using electrospun polyvinyl chloride (PVC)/polystyrene (PS) fibers as sorbents for oil spill cleanup. The sorbent dosage used in their experiments ranged from 0.05 to 0.2 g of fabric on 1:20 ratio of oil-water mixture. Banerjee et al (93) used oil-water mixture ratio of 1:100 for most of their crude oil adsorption works and Ranjit Gurav et al (118) in their work, Adsorptive removal of crude petroleum oil from water (with floating pinewood biochar decorated with coconut oil-derived fatty acids) used 6g of crude oil to 100ml of water. The experimental variables are detailed below:

Parameter	Range/values used
PE Sorbent weight	0.5 g, 1 g, 2 g, 5 g
Oil type	Camlab oil Phillip oil, Natural crude oil
Oil to water ratio	1:10 (e.g. 10 g of oil in 100 ml water)
Oil mass	10 g, 20 g, 30 g, up to 50 g (scaled with sorbent mass)
Water volume	100 ml, 200 ml, 300 ml and up to 500 ml scaled with oil mass
Sorbent size	≤2.36 mm ≥1.80 mm
Contact time	5 minutes

Experimental Procedure

In these preliminary experiments, oil-water mixture of 1:10 was used, and all the adsorption procedure as described in section 5.1.1.1 . About 10g - 50g of oil (increased progressively as the quantity of sorbent increased), 0.5g - 5g of $\le 2.36 \ge 1.80$ mm PE particle size, 5 minutes contact time, and based on literature a range of sorbent dosages were explored to determine the most effective for maximising the adsorption capacity. Different oils (natural crude 3, Phillip and Camlab artificial crude oils) were used for the experiment.

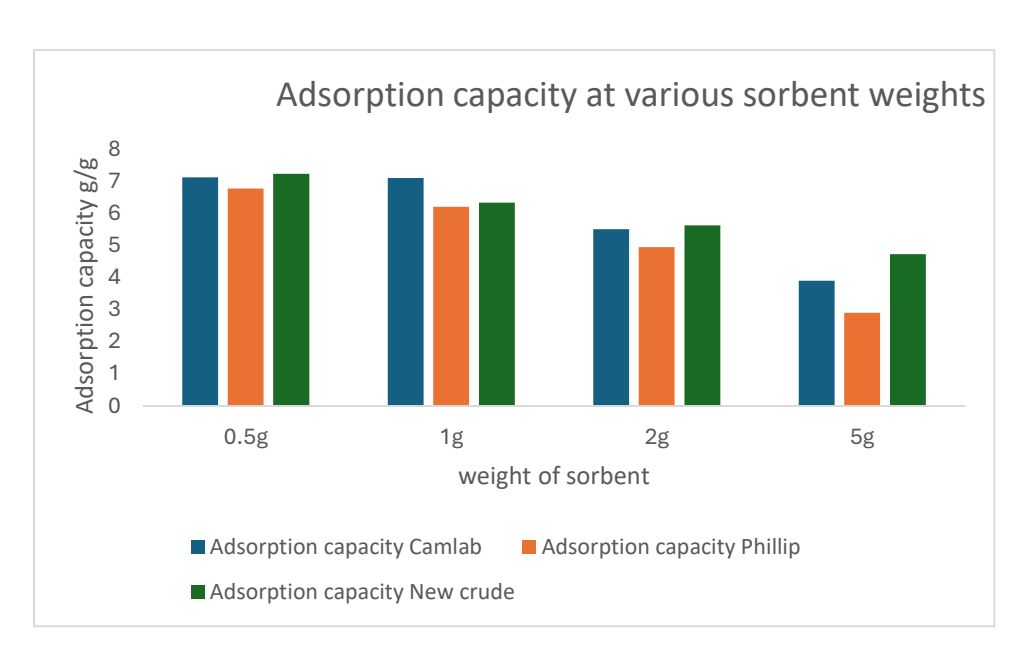


Figure 5. 3: Adsorption capacity (g/g) of Camlab oil, Phillip oil, and new crude oil as a function of PE sorbent weight (0.5–5 g).

Figure 5.3, shows the adsorption capacity (g/g) of Camlab oil, Phillip oil, and new crude oil as a function of PE sorbent weight (0.5–5 g). Each test was performed in triplicate with 10 g of oil under identical conditions. Adsorption capacity was calculated after 5 minutes of contact time followed by a 5-minute drain period. Results show decreasing capacity with increasing sorbent weight.

There are differences in adsorption capacity between the three types of oils (Camlab, Phillip, and natural crude 3) across different sorbent weights. At lower sorbent weights (0.5g and 1g), all three oils show relatively high and similar adsorption capacities 6.5-7g/g, with Camlab and Natural crude oil 3 slightly outperforming Phillip oil. As sorbent weight increases (2g and 5g), the adsorption capacities for all oils decrease, but at different rates. Camlab showed the steepest decline, while new natural crude oil 3 maintains the highest adsorption capacity at higher sorbent weights. These differences observed could be due to several factors; the natural crude oil 3 might be more viscous or because it has more light fractions than the Camlab and Phillip (as shown in Figure 4.36) and thus adhere better to the sorbent material even at higher weights. The general decrease in adsorption capacity across the board could be that, as sorbent weight increases, the total surface area for adsorption increases, but not necessarily linearly, or there might be a point of saturation or diminishing returns where adding more sorbent does not proportionally increase adsorption capacity. There might be

an influence of packing density, (the way the adsorbent is arranged in the oil-water mixture can influence the accessibility of its surface area and the uniformity of fluid interaction), can affect how easily fluids can move through the sorbent, impacting the rate and extent of adsorption. Also, there could be the effect of self-weight pressure (i.e. the weight of the adsorbent itself), especially when stacked in a sieve or oven, can create localised pressure on the lower layers. This pressure may compress the adsorbent, reduce surface accessibility, or during handling, such as lifting the adsorbent off the mixture, this weight-induced pressure can also contribute to squeezing out additional oil, particularly from compacted layers, thereby influencing the observed oil capacity decrease. This could explain the general downward trend for all oils as sorbent weight increases

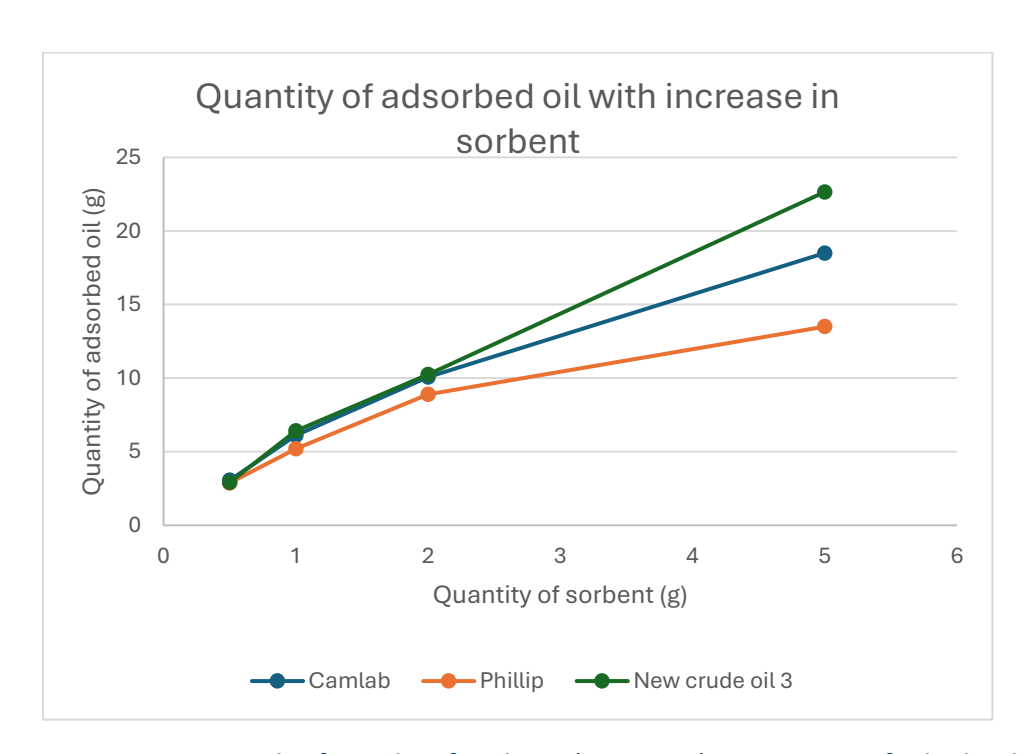


Figure 5. 4: Graph of weight of sorbent (0.5g – 5g) vs quantity of oil adsorbed using a fixed 50g of various oils (Camlab, Phillip and New crude oil 3)

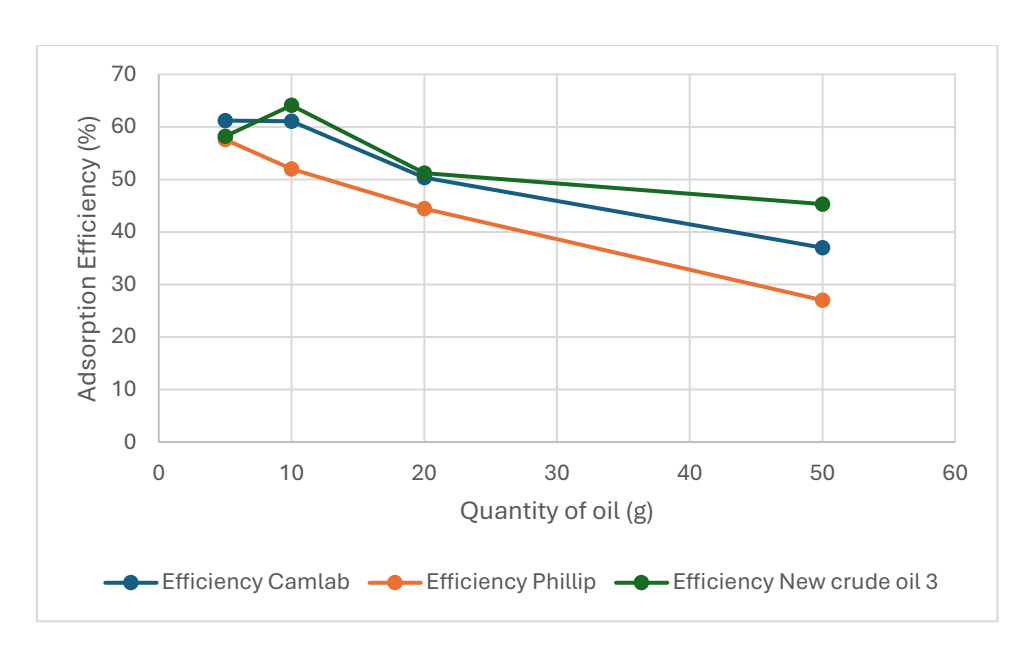


Figure 5. 5: Adsorption efficiency (%) of Camlab, Phillip, and new crude oil 3 as a function of sorbent quantity (5–50 g)

Figures 5.4 and 5.5 present data on the quantity of adsorbed oil and adsorption efficiency for oils (Camlab, Phillip, and New crude oil 3) using varying quantities of the sorbents with 5g-50g of oil. Each data point represents the average of triplicate experiments. Adsorption efficiency was calculated as the percentage of oil adsorbed relative to the initial oil quantity, following a 5-minute contact time and 5-minute drainage.

Figure 5.4 shows the quantity of oil adsorbed by each sorbent as the amount of sorbent increases from 0.5 g to 5 g. The graph displays an increasing trend for all three sorbents, indicating that more oil is adsorbed as the quantity of sorbent increases. However, the rate of increase reduced at higher sorbent quantities.

Comparing Figures 5.3 and 5.4, we can observe that while increasing the sorbent quantity leads to more oil being adsorbed overall, the adsorption capacity per unit weight of sorbent decreases (from 7g/g - 3g/g). This suggests that using larger amounts of sorbent may not be as effective in terms of adsorption capacity per unit weight as shown in Figure 5.5. The adsorption efficiencies decreased from about 61% to 37% as the sorbent quantity/weight increased. Based on these tests and the literature, 0.5 g of PE was selected as the baseline sorbent mass for all further experiments. This dose offered high adsorption efficiency, practical handling, and consistency with previous studies, particularly for short-contact-time batch experiments.

5.1.4 Shredding of PE and particle size distributions of sorbents

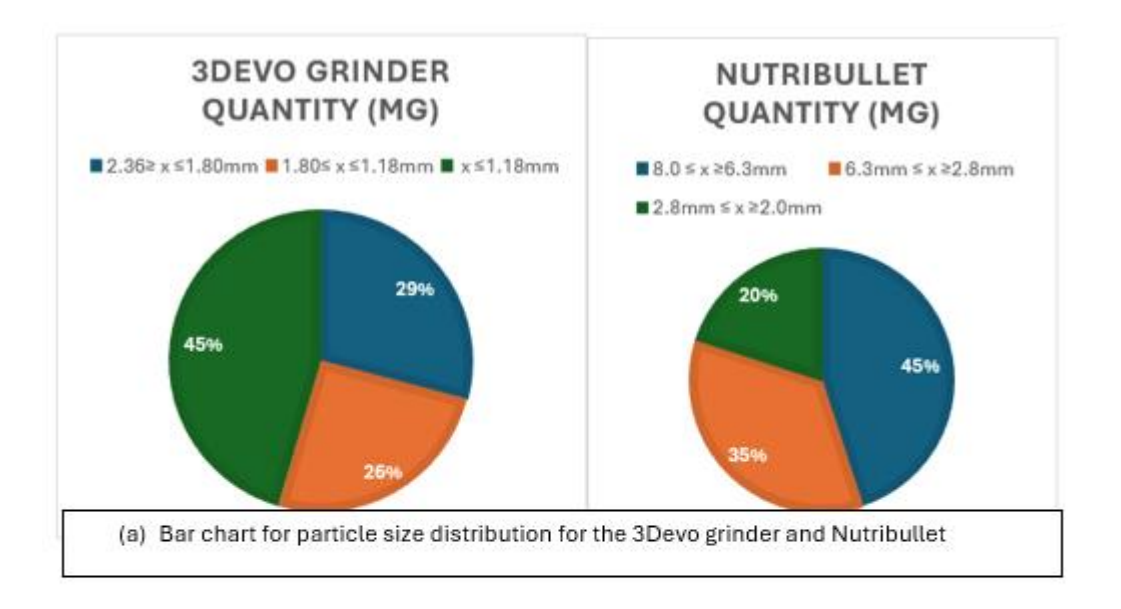
Different shredding instruments and conditions significantly affect the particle size distribution of polyethylene water sachets after shredding. Factors such as blade sharpness, shredding speed, force, feedstock preparation, and the nature of the polyethylene (e.g., weathered vs. non-weathered) influenced the resulting particle sizes and surface areas.

Initially, the three particle sizes produced by the 3devo shredder $(2.36 \ge x \le 1.80 \text{mm}, 1.80 \ge x \le 1.18 \text{mm})$ and square-shaped PE of 30mm x 30mm were used at the start of the preliminary experiments. The 3devo shredder was used to create these shredded particle size ranges but it broke down several times (although it was proposedly designed for shredding many types of polymer including film, the shredder over heated and burned out the motor), so another shredder (Nutribullet blender) was introduced, and this gave bigger particle sizes of $8.0 \le x \ge 6.3 \text{mm}$, $6.3 \text{mm} \le x \ge 2.8 \text{mm}$, $2.8 \text{mm} \le x \ge 2.0 \text{mm}$ and these were used for the final adsorption experiments. The particles produced by the 3devo shredder were used in the preliminary experiments

For the 3Devo, the cut PE particles (roughly ≥30mm≤50mm) were fed into the machine once (single pass). It was added at a controlled rate (8-10g), with a preset temperature range of 80 °C.

For the NutriBullet, the cup is filled to 50-75% capacity, with a fixed speed of 20,000 RPM and a blending time of 30 seconds to 1 minute. After blending for 4-5 times, the particles often reach a plateau where the do not further reduce.

For quantification of particle size distribution, about 100g of sorbent, which had been shredded using the 3devo grinder or the Nutribullet blender, was size graded using mesh sieves, and the mass of the particle sizes was recorded.



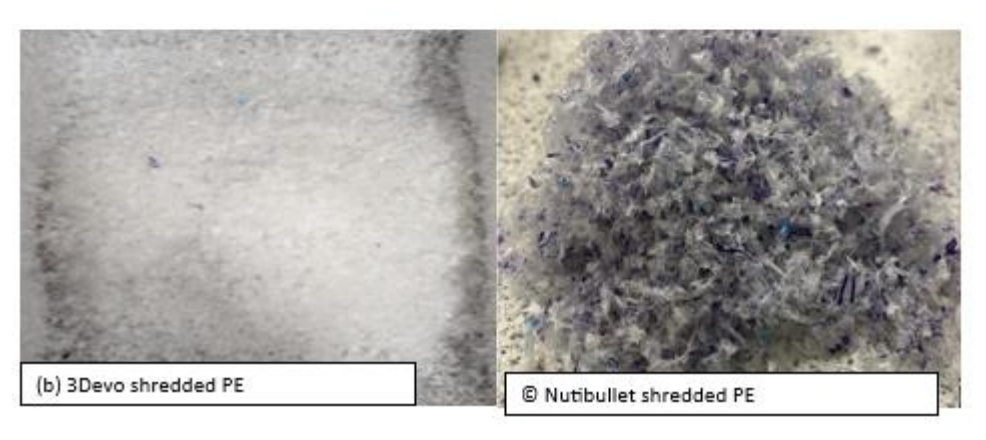


Figure 5. 6: Particle size distribution of the shredded PE of 3Devo and Nutribullet shredders The pie charts in Figure 5.6(a) illustrate the particle size distribution of the sorbent for two different shredders: the 3DEVO Grinder and the Nutribullet blender. The Nutribullet blender produces much larger shredded particle sizes (Figure 5.6 c). The 3DEVO Grinder has sharper blades than the Nutribullet, thus the 3DEVO Grinder gave a significantly higher proportion (45 wgt % of total weight) of the smallest size (x \le 1.18 mm), indicating more efficient size reduction into finer particles (Figure 5.6 b). The 3DEVO grinder also produced medium-sized particles (1.80 \le x \le 1.18 mm) constituting 26 wgt %, while the larger particles 2.36 \ge x \le 1.80 mm) made up 29 wgt %. The Nutribullet blender with dull blades, produced a higher proportion of larger particles (45%, 8.0 \le x \ge 6.3 mm), the second highest proportion of medium-sized particles (6.3mm \le x \ge 2.8 mm) constituting 35 wgt % and the lowest proportion of smallest particles (in the range of 2.8mm \le x \ge 2.0mm (20 wgt %), indicating overall a coarser grinding than the 3DEVO grinder.

5.1.5 Determination of sorbent oven drying time after adsorption

It was noted after the adsorption experiments that water droplets were observed within the oil/sorbent mixture, therefore to establish the true amount of oil adsorbed the water was removed by evaporation in an oven.

The drying time of 240 minutes at 60°C was established using a constant weight method approach by monitoring the weight of a Shredded PE sample (1g) after soaking with water, draining excess water and exposure to an oven temperature at 60°C for various time intervals until a constant weight was obtained, indicating that all moisture had been removed. To verify, additional measurements are taken to ensure no further weight change. The sorbent drying time is the duration required to reach this constant weight.

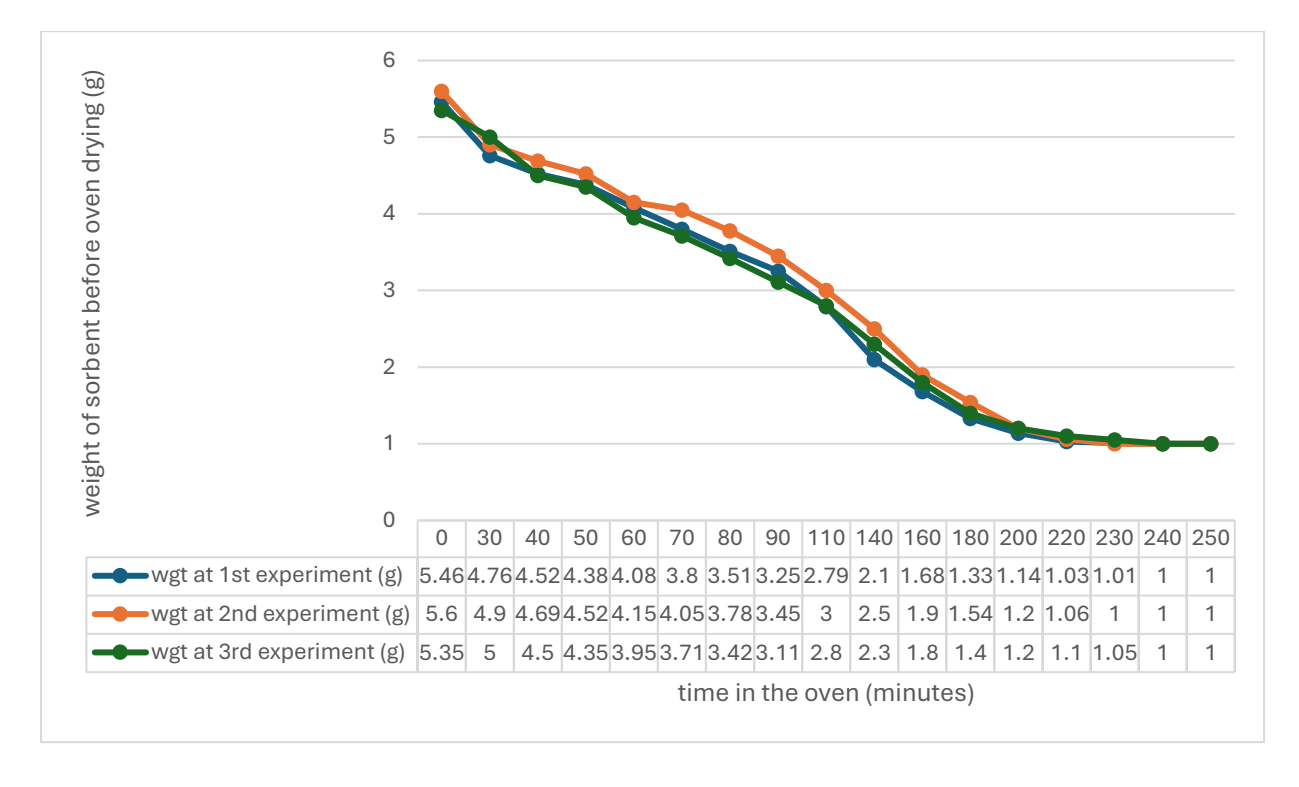


Figure 5. 7: Graph showing how the constant weight time (drying time) was determined Figure 5.7 shows a plot of the weight of the soaked and drained sorbent before (5.46 g, 5.60 g and 5.35 g) and during oven drying over time for three separate experiments. There was a rapid decrease in weight at the onset of the experiment and as the sorbent continued to lose its moisture its weight eventually gradually stabilised. The weight became constant around 240 minutes for all three experiments showing that the sorbent reached its final dried state. The results are consistent across all three experiments, indicating reliable and repeatable drying conditions.

5.1.6 To determine the extent of evaporation of crude oil in the oven at a constant temperature of 60 degrees.

To check the rate and extent of evaporation of Crude Oil 3 when subjected to a constant temperature of 60°C over 240 minutes, and to verify the reproducibility of the results.

Procedure

10 g of Crude Oil 3 was weighed into a 50 ml beaker, using an analytical balance. The oven was preheated to a stable temperature of 60°C. The beaker containing the crude oil 3 sample was placed inside the oven and the timer started. At predetermined time intervals (e.g., 1 min, 2 min, 5 min, 10 min, 20 min, 40 min, 60 min, 90 min, 120 min, 150 min, 180 min, 220 min, and 240 min), the beaker is removed from the oven, allowed to cool to room temperature and then weighed. For reproducibility, the entire procedure was repeated using a fresh 10 g

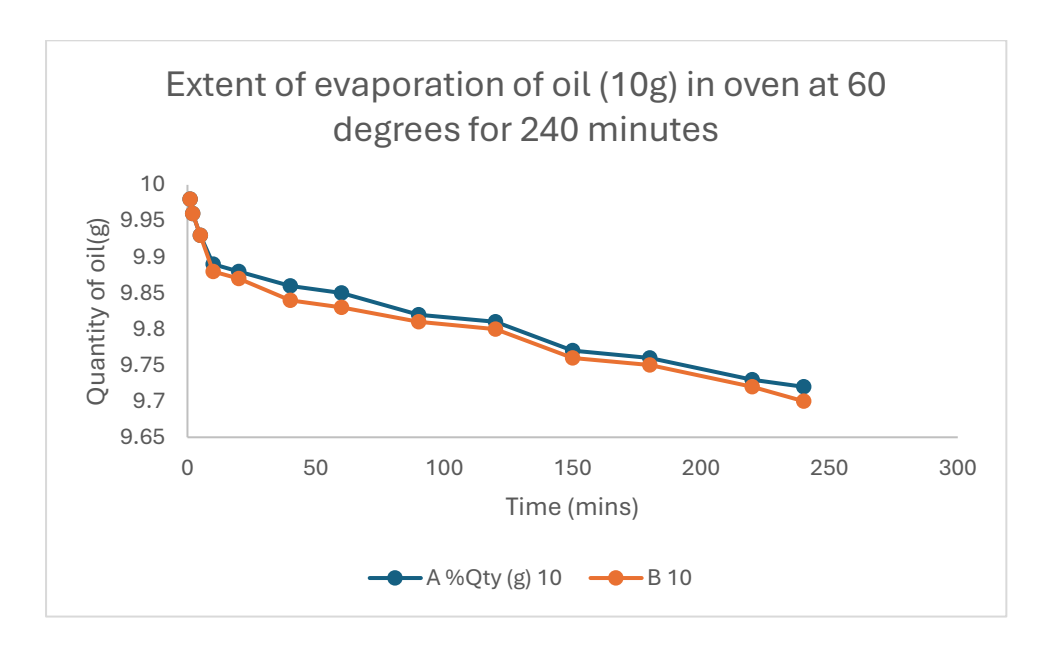


Figure 5. 8: Evaporation curve of the oil after 240 minutes at a temperature of 60 degrees centigrade

Figure 5.8 show the extent of evaporation of 10 g of crude oil over 240 minutes at a constant temperature of 60°C in the oven. The experiment highlights the multi-component nature of crude oil, where different components evaporate at different rates depending on their volatility. At 60°C, the temperature is sufficient to evaporate the lighter components quickly, but the heavier components take much longer, showing that crude oil contains a mixture of substances with varying boiling points. The initial rapid weight loss from 10 g to 9.88g

between 0-20 minutes is due to the evaporation of the very volatile components reducing by 1.2% - 1.3% by weight, followed by a slower, more gradual loss after 20 minutes, as the remaining oil consists of heavier, less volatile compounds. Beyond 150 Minutes, the graph shows a consistent, but much slower decrease in the quantity of oil. This suggests that the oil has reached a phase where only the most resistant, high-boiling-point components are left, which evaporate very slowly. Although the oil continues to evaporate, the curve starts to level off slightly towards the end of the experiment, indicating that the evaporation process is nearing completion for the given temperature and time. The oil is approaching a steady-state where further weight loss would be minimal if the experiment continued under the same conditions. By the 240 minutes, the weight loss of the crude oil was about 2.8% - 3%. The similarity in the behavior of the two data sets indicates consistency and reliability in the experimental process.

5.2 ASTM procedure for the sorbent tests

5.2.1 Dynamic degradation test from ASTM F726-17

This procedure is designed to test water take-up and to determine oleophilic properties of an adsorbent sample under dynamic conditions. This test is performed at $23 \pm 4^{\circ}$ C as described in the ASTM 726 test procedure.

The experiment was performed with the 3 different sizes of shredded PE (2.36 \le x \ge 1.80, 1.80 \le x \ge 1.18 mm and x \le 1.18 mm).

Procedure 1: To determine water uptake by shredded PE in the presence of water alone

4g of shredded PE sample (all three different samples were used separately) was first weighed and then placed in a 400 ml plastic container with 200ml and then sealed with the container's cap. The container was then placed on its side and mounted on a shaker table, Gyratory Water Bath shaker (Model G76D; Figure 5.9), set at a frequency of 150 cycles per minute and an amplitude of 2.5 cm for 15 min. After the contents of the jar are allowed to settle for 2 min. Observations about the condition of the adsorbent and the condition of the water are recorded. If 10 % or more of the adsorbent material has sunk, then the adsorbent is considered to have failed this test. The contents of the jar are strained through a mesh basket to catch the adsorbent samples (tilted to let water drain), which are then weighed after a 30 s drain period. The water pick-up ratio is calculated from the weight measurements.

Procedure 2: To determine water uptake by shredded PE in the presence of water and oil

1g of shredded PE (1.80 ≤x≥ 1.18mm) sample was first weighed and then placed in a 400 ml plastic container with 200ml of water 1g of crude oil and then sealed with the container's cap. The container was then placed on its side and mounted on a shaker table, Gyratory Water Bath shaker (Model G76D; Figure 5.9), set at a frequency of 150 cycles per minute and an amplitude of 2.5 cm for 15 min. After the contents of the jar are allowed to settle for 2 min. Observations about the condition of the adsorbent and the condition of the water are recorded. If 10 % or more of the adsorbent material has sunk, then the adsorbent is considered to have failed this test. The contents of the jar are strained through a mesh basket to catch the adsorbent samples (tilted to let the water-oil mixture drain), which are then weighed after a 30 sec. drain period and placed in the oven for 240 minutes, to remove all water. The amount of water adsorbed could then be calculated from the weight measurements.

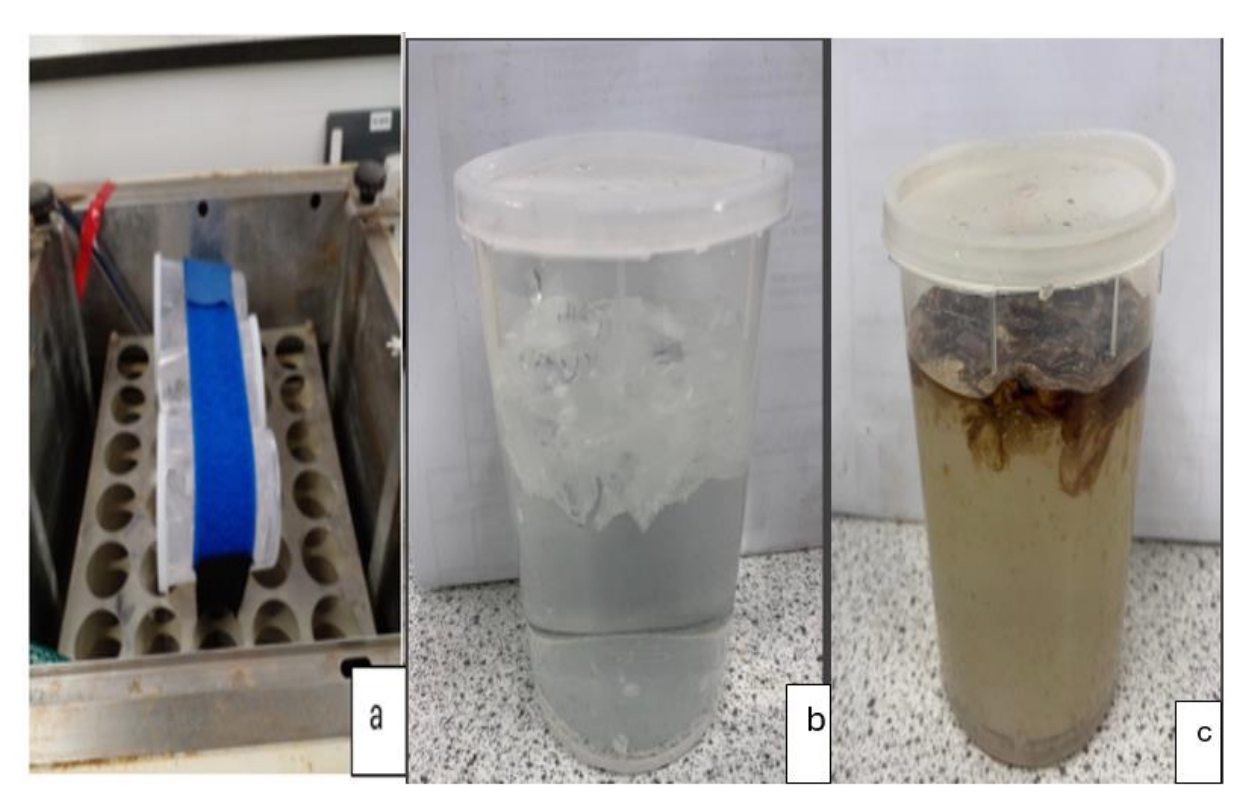


Figure 5. 9: (a) Sorbent in the Gyratory Water Bath shaker (Model G76D) during test (b) and (c) sorbent left to settle after the test

Calculation:

Using the data obtained from the above experiment, water adsorbency is calculated as a ratio of water adsorbed to dry adsorbent weight as follows:

water adsorbency = SW/SO

where:

SO = initial dry adsorbent weight,

SW = (SWT - SO) net water adsorbed, and

SWT = weight of adsorbent samples with water after the Dynamic Degradation test.

The experiment was repeated multiple times to ensure reproducibility and from the experiment carried out, the following was deduced.

Table 5. 2: Water adsorbency calculations

	Procedure 1	Procedure 2		
Shredded PE size	2.36 ≤x≥ 1.80mm	1.80 ≤x≥	X ≤	1.80≤x≥1.18mm
		1.18mm	1.18mm	
Initial wgt (So)	4g	4g	4g	1g
Wgt of PE after	22.47g	19.42g	27.88g	6.14g
exp (SwT)				
After oven-	-	-	-	5.47g
drying net water				
adsorbed (Sw)				
Net water	18.47g	15.42g	23.88g	0.67g
adsorbed (Sw)				
Water	4.60g/g	3.86g/g	5.97g/g	0.67g/g
adsorbency				
(Sw/So)				
%tage of	0	0	0	0
adsorbent sunk				
after experiment				

Procedure 1:

for PE 2.36 ≤x≥ 1.80mm

Water adsorbency = (22.47 - 4.0)/4.0

= 18.47/4.0

=4.6g

Therefore, adsorbency for PE particle size 2.36 ≤x≥ 1.80mm is 4.6g/g

for PE 1.80 ≤x≥ 1.18mm

Water adsorbency = (19.42 - 4.0)/4.0

= 15.42/4.0

=3.855g

Therefore, adsorbency for PE particle size 1.80 ≤x≥ 1.18mm is 3.855g/g

for PE \leq 1.18mm Water adsorbency = (27.88 – 4.0)/4.0 = 23.88/4.0 =5.97g Therefore, adsorbency for PE particle size \leq 1.18mm is 5.97g/g

Procedure 2 (after oven-drying of loaded sorbent with oil-water mixture) for PE 1.80 \leq x \geq 1.18mm Water adsorbency = (6.14 - 5.47)/1 = 0.671

Thus adsorbency for the PE particle size 1.80 \leq x \geq 1.18mm used to adsorb a mixture of oil and water = 0.67g/g

From the results obtained in Table 5.2 and from observations in the absence of oil, the PE behaves differently, as it adsorbs some water. The smallest particle size adsorbed 23.88g of water and with the highest water adsorbency of 5.97g/g. The medium-sized particles 1.80 ≤x≥ 1.18mm performed best in terms of minimising water adsorption, which is generally desirable for oil sorbents. While in the presence of oil and water, the PE gives preferential treatment to the oil as it adsorbs more oil than the water. The water adsorbency in the presence of water alone is 3.855g/g, while in the presence of both oil and water, the water adsorbency was 0.671g/g. This shows the selectivity of oil over water in a mixed environment by PE, and also, PE retains oil efficiently while allowing water to be excluded. A lot of experimental evidence/studies have directly tested PE-based sorbents in oil-water separation applications, confirming their oleophilic properties (5, 23, 106, 122, 131, 156).

Overall, after the experiment, all the particle sizes did not record sinking, and it was observed that the PE particles were uncurled while dispersed and stretched out in the oil-water mixture while adsorbing oil-water and still maintaining their structural integrity. This might be as a result of the force of the shaking effect in the water bath shaker or when dispersed in water, PE particles may experience some surface tension effects that cause them to uncurl or stretch as they interact with the oil-water molecules or can be attributed to the high degree of elasticity and flexibility of its polymer chains, however, because the material does not adsorb much water, it does not become waterlogged or sink.

5.3 Final adsorption experiment

5.3.1 Adsorption Protocol with Shredded PE

The standard protocol involved all adsorption experiments at room temperature. Crude oil (5g-10g) was added to 100 ml deionised water in a 250 ml glass beaker. The mixture was given a slight, rolling shake for about 10 seconds. Immediately after shaking, the oil floated to the water's surface (Figure 5.8). Onto this floating crude oil, a definite weight of the sorbent (0.5g-1.0g) was added, given a rolling shake for 10 seconds and allowed to stand for a contact time of 5 minutes. The sorbents were lifted from the water using 1mm x 1mm hole stainless steel mesh. The sorbents were then allowed to drain for 5 mins (with about 2 times intermediate tilting to remove trapped water and excess oil), weighed, and put in the oven at 60° C for 240 minutes to enable any adsorbed/trapped water in the sorbents to dry after the sorbents were re-weighed.

5.3.2 Assessment of oil contamination in water after clean-up

This experiment is a preliminary and one-off assessment designed to analyse the amount of oil contamination dissolved in the water after the adsorption experiment. The methodology procedures were not perfect as residual oil sources could contribute to the results (though best efforts were made not to). The water onto which the oil had been spilled was analysed for contamination by extraction with Dichloromethane (DCM) and GC-MS analysis. The remediated water was poured into a clean separation funnel, and an appropriate volume of DCM was added to provide a 1:1 volume ratio with water. The separation funnel was vigorously shaken, periodically venting to release any built-up pressure. The mixture was then allowed to stand undisturbed until two distinct separate layers formed. DCM being denser settled at the bottom, while the aqueous layer remained on top. The DCM layer was carefully drained into a clean, dry beaker. The extraction process was repeated 2-3 times with fresh DCM and the aqueous layer to ensure maximum extraction of any residual oil. The DCM extracts were combined in a single container. The extracted oil in DCM was analysed using GC-MS to determine the quantity and composition of any oil present.

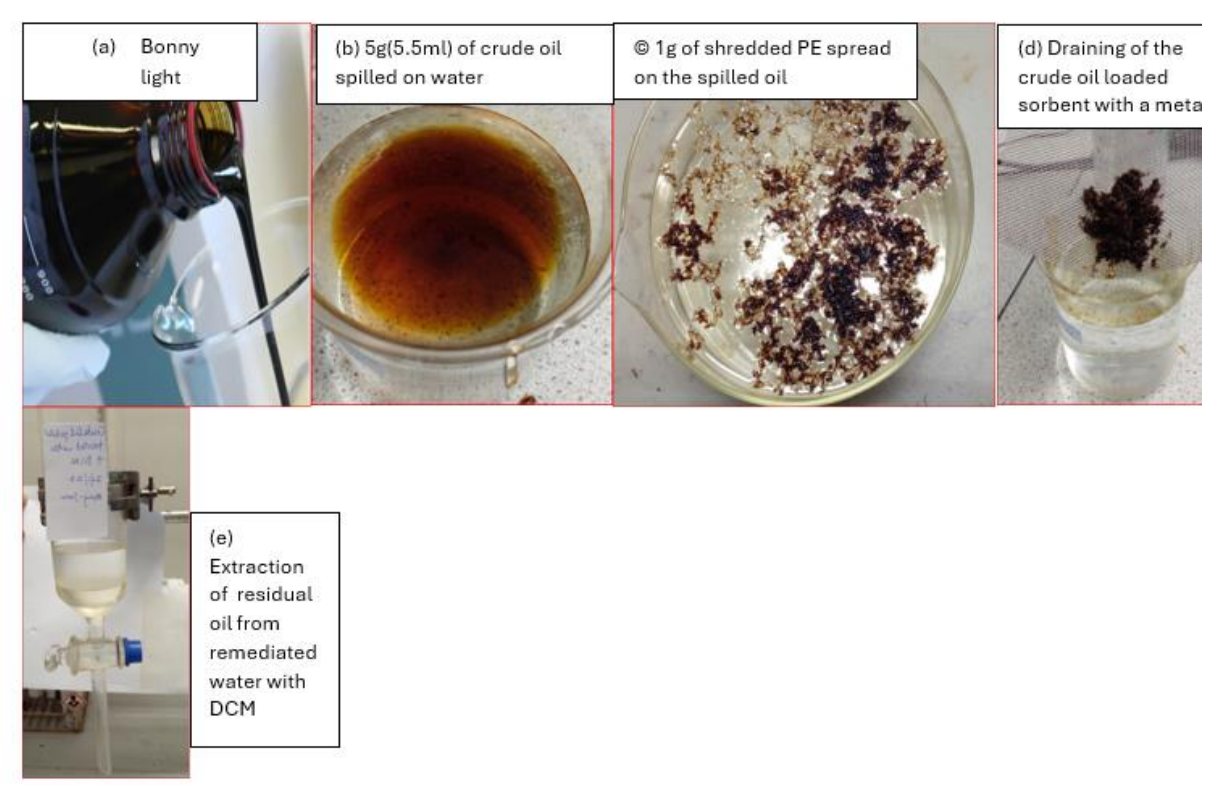


Figure 5. 10: Adsorption experiment with crude oil and Shredded PE sorbent, and extraction of residual oil from remediated water with DCM

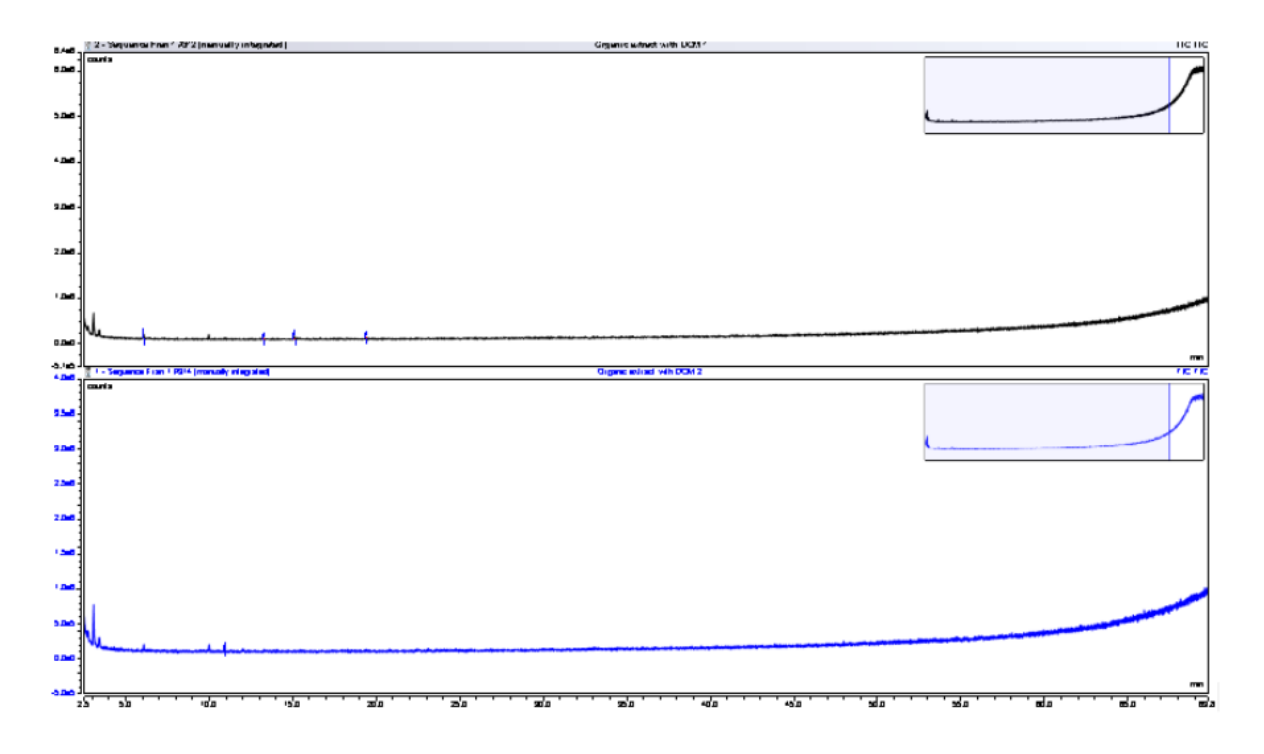


Figure 5. 11: GCMS chromatograph showing the results of DCM extract composition of two remediated water samples after adsorption experiments

From Figure 5.11, the two chromatographs show very similar patterns, indicating consistency in the sorbent's cleaning performance. Thus, considering the large amount of oil initially poured onto the water, only small amounts could be detected by the GCMS within the water. The few small peaks present in both chromatographs, when compared with the chromatograph of natural crude oil in Figure 4.37, suggest that the polyethylene sorbent was highly effective at removing most of the oil from the water surface, particularly the lighter, more volatile compounds, as detected by the GC-MS. The organic extract with DCM 1 and organic extract with DCM 2, showed small peaks of Cyclobutane, 2-propenylidene, Chloroacetic acid, 1-cyclopentylethyl ester, Benzene, (1-methylethyl) and Decane at retention times of 6, 13, 15 and 19 minutes respectively for the 2 chromatographs.

5.3.3. Desorption procedure and reusability of sorbent

In the desorption procedure, as described in ASTM 726, squeeze-type with mop or roller-type wringer are advised, but these were not available in the lab, as an alternative flexible net (Figure 5.12c) was used, which was deemed appropriate for the application. The sorbent was no longer reused when the oil coated shredded PE particles clumped/aggregated together (Figure 5.12e) and could not effectively redisperse on the water surface (Figure 5.12f).

Two methods were practiced,

- (i) oven-dried sorbent method: In this method, after the adsorption procedure, the sorbent is dried in an oven after each sorption use, removing water and thus allowing amounts of oil adsorbed to be calculated.
- (ii) non-oven dried sorbent method: In this method, after the sorbent was used to sorb oil-water mixture, it was squeezed to remove the oil and water mixture and reused immediately without oven-drying for another round of sorption.

5.3.3.1 Method 1 for Desorption procedure and reusability of sorbent (oven-dried-sorbent)

After the adsorption experiments were carried out, as described in the adsorption protocol Section 5.3.1, the loaded sorbent was removed from the water surface, weighed, and put into

the oven to remove the water then weighed again (to determine the amount of water removed), squeezed in a flexible nylon net (fine filter fabric mesh water strain 1mmx1mm) to remove the adsorbed oil and then measure (Figure 5.12).



Figure 5. 12: Recycling process (a − f)

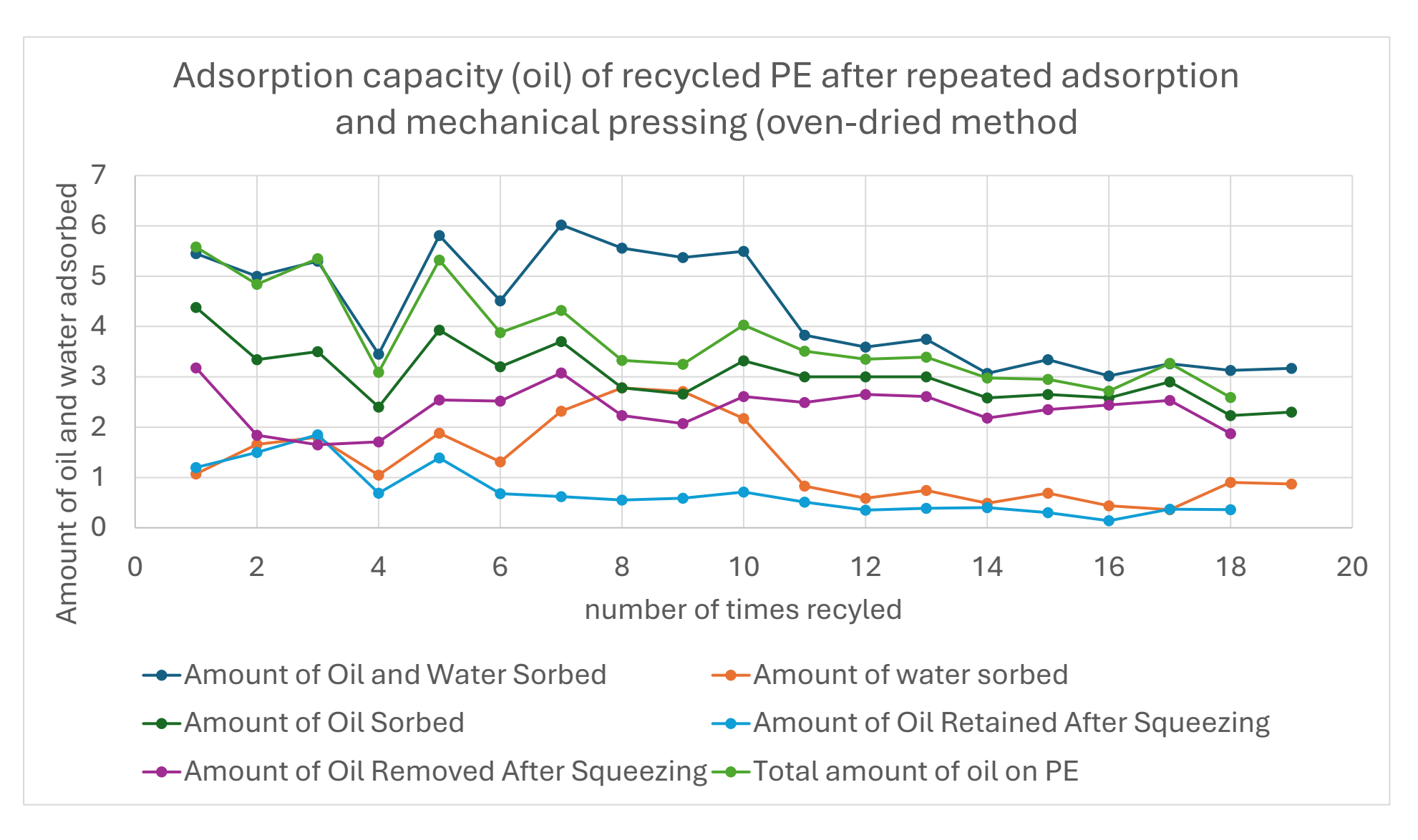


Figure 5. 13: Adsorption capacity (oil and water) of recycled PE after repeated adsorption and mechanical pressing

Figure 5.13 presents the adsorption behavior of recycled polyethylene sorbent in terms of oil and water sorption across multiple cycles of reuse. The sorbent is dried in an oven after each use, removing water but leaving oil behind. The dark blue curve which represents the total combined amount of oil and water adsorbed by the PE in each cycle and the leaf green curve which represents the amount of oil sorbed, initially fluctuates, with an overall slight decline over the first few cycles. There are significant dips around cycles 4, and 6 (between 3.4g and 4.5g for the amount of oil and water adsorbed, and between 2.4g - 3.4g for the amount of oil sorbed), which might be a result of experimental variability (inconsistencies in the drying or squeezing process), but later gradually stabilises to about 3 g and 2.5 g respectively and consequently decreases with more cycles. The orange curve which represents the amount of water adsorbed by the PE (difference between the dark blue and the leaf green curves) appears relatively stable (between 1.3g -1.7g of water sorbed) but shows a sudden increase at cycles, 7, 8 and 9 (between 2.3g – 2.7g) potentially due to variations in how effectively the PE sorbent particle was drained after it was lifted from the oil-water mixture as the curled PE might have trapped some water not visible to see and also this might lead to more water being left behind after each drying and squeezing process. These spikes gradually settled and subsequently decreased to about 0.8 g with more cycles. For the light blue curve and light green curve which represent the amount of oil retained on the PE after mechanical squeezing and the total amount of oil on PE respectively, a spike occurred at cycles 3 and 5. This incident might suggest that during this cycle, the PE sorbent had an unusual interaction with the oil, and trapped more oil (on the PE surface as the PE was still springy, or a reduction in the mechanical pressure applied during squeezing, leading to higher oil retention on the PE (1.8 g – 1.39 g), but this normalised in subsequent cycles showing a stable range of oil quantity on the PE sorbent (between 0.14g - 0.7g retained on PE after squeezing). The mourve curve which represented the amount of oil removed after squeezing, showed a reasonable amount of oil, about more than half of the adsorbed oil being squeezed out from the PE after sorption (4.4 g adsorbed, and 3.2 g was squeezed out). There was a drop in the amount of oil being removed in cycles 2- 4 (1.8 g), which could be as a result of inconsistent or less pressure application. After this drop, the amount of oil squeezed out was consistent afterwards and gradually correspondingly decreased as sorbed oil (leaf green curve) with more cycles. This indicates that in the initial uses of the PE sorbent, a reasonable amount of oil could be effectively squeezed out, suggesting the PE is still relatively efficient at adsorbing and releasing oil as the PE is still curly and springy. After around 10 cycles, just like the other curves, it stabilizes at a lower level, suggesting that the amount of oil removed after squeezing has become stabilised. This likely corresponds to a point where the PE sorbent has reached a consistent level of oil retention, with little additional or less oil being squeezed out in subsequent cycles or the stabilization could indicate that the PE has likely reached its limit for effective oil adsorption.

The combined behaviour of all the curves reflects the efficiency of the PE sorbent in adsorbing/releasing oil after repeated cycles and its general decline. The light blue curve (amount of oil retained on PE after squeezing) and the dark blue curve (total amount of oil and water sorbed) reinforce the idea that the sorbent's overall capacity is diminishing with repeated use.

This general trend seems like during the first few cycles the PE stays curly and not compressed and thus leading to more oil being retained and suggests that the sorbent loses efficiency with repeated use but eventually reaches a point (after 10th cycle) where its performance remains relatively consistent, as it seems that the curly PE has been stretched out and thus maintains a more uniform performance. It could also be noted that manual squeezing introduces variability, potentially causing fluctuations seen in the earlier cycles.

5.3.3.2 Method 2 for Desorption procedure and reusability of sorbent (non-oven dried)

After the adsorption experiments were carried out, as described in the adsorption protocol, the loaded sorbent was squeezed in a flexible nylon net (fine filter fabric mesh water strain 1mm x 1mm) to remove the adsorbed oil/water mixture. The desorbed sorbent was re-used immediately for another round of adsorption procedure, without being dried in the oven.

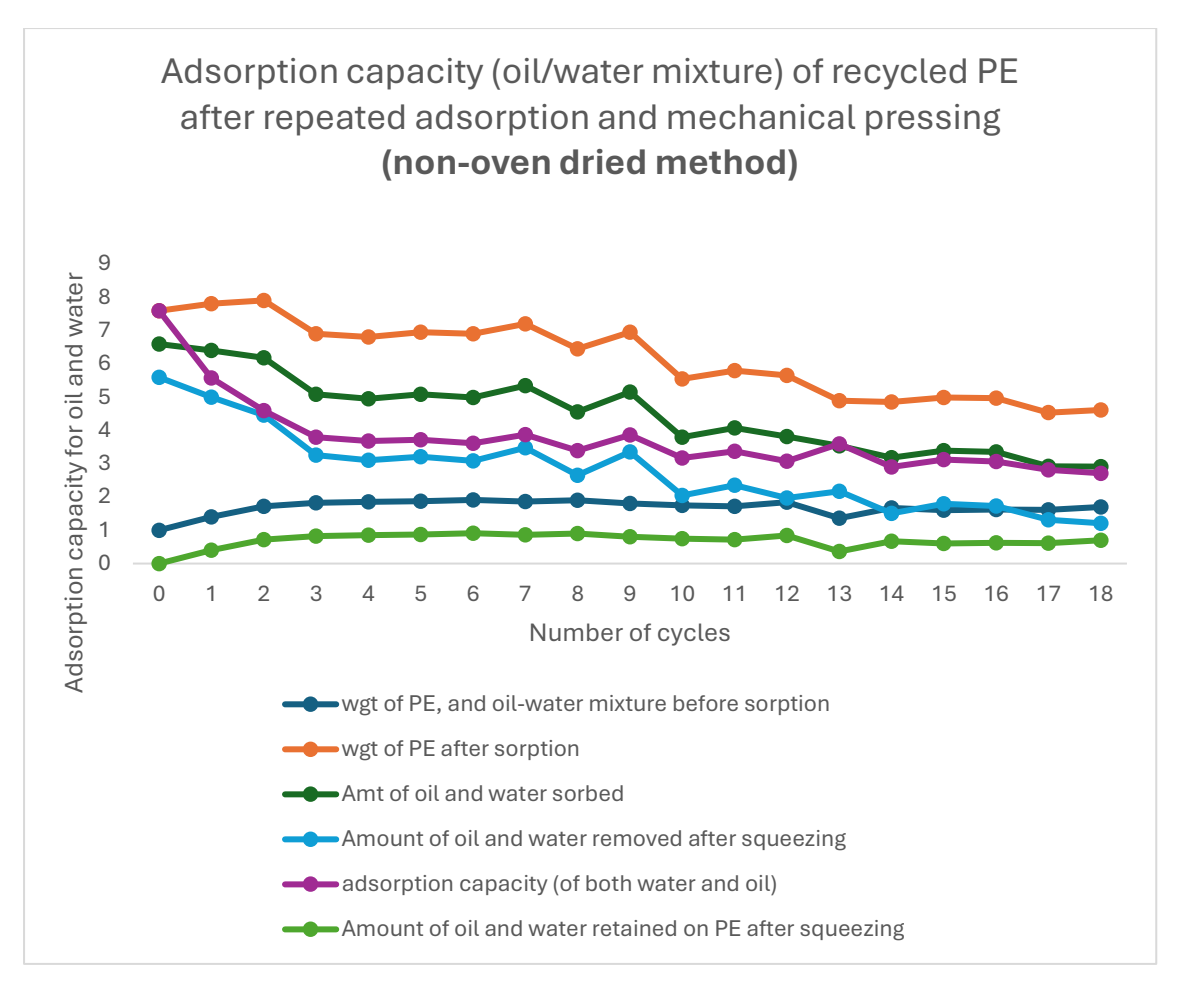


Figure 5. 14: Desorption procedure and reusability of sorbent (using a non-oven-dry adsorbent method)

From Figure 5.14, the weight of the PE sorbent before sorption (dark blue curve) remains relatively constant (between 1 g and 1.7 g) throughout the cycles, indicating that the PE sorbent continually contains a uniform amount of oil and water after squeezing (as also noted in the light green curve) over repeated use $(0.4 \, \mathrm{g} - 0.7 \, \mathrm{g})$. The weight of the PE sorbent after sorption (orange curve) starts high (7.8 g) and shows a gradual decrease over the cycles (4.6 g), indicating a reduction in the sorption capacity over time. However, it does stabilise after 13 cycles as also exhibited in method 1 (oven-dried, Figure 5.13). The amount of oil and water removed through squeezing (light blue curve) follows a similar decreasing trend to the sorbed mixture amount. The retained amount of oil-water after squeezing shows a slight decrease over time, indicating that the PE sorbent becomes less effective at retaining the mixture after repeated cycles. It is generally noticed that after around 12 - 13 cycles, there is some stabilisation in terms of adsorption by the sorbent, indicating that the sorbent reaches a steady state in terms of adsorption capacity and retention. This might be due to some

structural changes (stretching out or thinning out) in the PE sorbent as a result of repeated use and pressure during desorption.

This non-oven-dried method seems simpler and less energy-intensive, but as water is retained, it could affect oil sorption in subsequent cycles as more active sites are taken up by water.

Generally, from Figures 5.12 and 5.13, the PE sorbent exhibits some effectiveness even after 18 cycles, showing it can still adsorb and retain oil, albeit at a reduced capacity, thus it can be said that the recycled PE sorbent demonstrates good reusability, maintaining significant oil adsorption capacity even after multiple cycles of use and mechanical pressing.

It starts with a high initial adsorption capacity, and while it decreases, the sorbent remains functional over multiple cycles.

However, some inconsistencies are expected in this manual squeezing desorption procedure because it is not an automated or standardised extraction method. There are potential human errors, for example; there may be inconsistent pressure application during squeezing from sample to sample depending on the operator's strength/fatigue, which might result in incomplete extraction of the fluids, and again, the use of flexible polymer nets and nitrile or latex gloves introduces potential for oil retention due to the high affinity between hydrocarbons and these non-polar polymeric materials leading to non-accurate measurement of the oil adsorbed by sorbent or extracted from it during the desorption process.

Chapter 6

6.0 Optimisation of conditions for oil adsorption by the developed sorbents

6.1 Introduction

This chapter describes an I-optimal design approach (a type of statistical design of experiment (DoE)) to finding the optimal experimental conditions for the most efficient and effective removal of crude oil from contaminated water.

I-optimal design is one of the response surface methodologies used to evaluate the significant factors of a process or study to obtain optimal conditions. I-optimal designs are flexible and can be tailored to any problem with fewer experimental runs. The response surface methods like I-optimal designs, are used for finding optimum conditions. Finding the optimal conditions can be achieved by maximising or minimising a response or by approximating the response to a targeted value (80). In subsequent experiments, only Phillip and Natural crude 3 oils were selected for further testing. Camlab oil was excluded because its adsorption behaviour and physical properties were found to be similar to those of Phillip oil. Therefore, Phillip oil was chosen as the representative synthetic oil for the remainder of the study.

6.2 Optimisation of Philips and Natural crude oils removal from water: I-optimal design

The methodology for the adsorption experiments used to carry out the optimisation studies has been previously described in Section 3.3.1 and was based on batch adsorption procedures. To optimise the removal of crude oil from water using PE, six potential factors were initially examined for their influence: adsorbent quantity (g), size of adsorbent, adsorbent type, pH of the oil-water mixture, contact time, and oil dosage. Preliminary screening experiments were conducted to evaluate the statistical and practical significance of each of these variables on the oil removal efficiency.

pH of the oil-water mixture: Tests across a range of pH values (e.g., acidic from 3 to 10, alkaline) showed minimal variation in oil uptake by PE, indicating that PE's hydrophobic

nature dominates over any surface charge effects that would be pH-dependent. As a result, pH was deemed non-influential and excluded.

Contact time: Initial preliminary experiment conduction in section 5.1.1.1 revealed that oil adsorption onto PE reached equilibrium within a relatively short period (often within 5 minutes). Beyond that, there was little to no increase in adsorption. This plateau in performance indicated that, under the experimental conditions, contact time had a negligible effect within the tested range, leading to its removal as a critical factor. Following this analysis, only four factors were retained for the final I-optimal design: Adsorbent quantity (g), Size of adsorbent, Adsorbent type (e.g., plain, shredded, roughened) and Oil dosage (g). These four factors significantly influenced adsorption performance within the tested levels and were thus used to build the predictive model and analyse optimisation outcomes. They were further examined in more detail via optimisation analysis using I-optimal design.

The screening experiment was undertaken where one factor was varied and other factors remained constant, often referred to as one-factor-a-time (OFAT). OFAT is good for initial screening to identify significant factors but is not practical for optimisation. This justifies using RSM like I-optimal designs for optimisation of these significant factors previously identified from the screening experiment, because it is more powerful and efficient for fine-tuning the significant factors identified earlier, leading to better and faster optimisation.

The I-optimal experiments were carried out in two sets, the first with non-weathered PE sorbent and two types of oil (Philip artificial crude oil and natural crude oil) and the second set performed with UV-weathered PE sorbent and the same two oil types (Philip artificial crude oil and natural crude oil).

For the first set of experiments, two numeric factors; adsorbent quantity and quantity of oil, and two categorical factors; adsorbent types (shredded (W) and shredded-roughened (X)) and size of PE (2.8 mm \le x \ge 2.0mm, 6.3 mm \le x \ge 2.8 mm and 8.0 mm \le x \ge 6.3mm) were all used for the optimisation studies. These PE sizes are not categorised as numerical factors because they are discrete ranges. A numeric factor would imply that you can vary their values freely within a linear range, but here, they are limited to predefined ranges thus are better represented as categorical factors. In this research, these ranges are sometimes referred to using the first figure in each range for simplicity. For example, the range 2.8 mm \le x \ge 2.0 mm

is referred to as 2.8 mm, 6.3 mm \le x \ge 2.8 mm is referred to as 6.3 mm and 8.0 mm \le x \ge 6.3mm is referred to as 8.0 mm.

In the scenario herein, for the first set of tests, 27 experimental runs were created including seven replicates using Design-Expert® software version 13. After the experiments were carried out, the responses were generated as shown in Appendix B1 – B2.

For the second set of tests, which focused on UV-weathered polyethylene (PE), the initial aim was to process it similarly to the non-weathered PE from the first set of tests by employing shredding and shredding-roughening techniques to enhance its surface properties for sorption applications. However, a different approach had to be taken because the desired shredded-roughened surface could not be achieved with UV-weathered PE. This limitation is due to the advanced degradation of the UV-weathered PE, which had already undergone significant structural breakdown (Section 4.2), making it unsuitable for the same mechanical treatment as non-weathered PE, as the material exhibited brittleness/fragility in the structure, unlike fresh or non-weathered polyethylene, which can withstand roughening processes. The weathered PE lacks the required tensile strength and flexibility to handle such treatments. Only the shredding process was still feasible because it simply involved shredding the material into smaller pieces, but the roughening (which would require mechanical abrasion or deformation) was not achievable without further grinding the material into fine powder.

Therefore, only UV-weathered and then shredded type of PE was used, and the "adsorbent type" as a categoric factor was not included in this second set of experiments. Here, the two categoric factors are the time of UV-weathering (0, 75, and 150 hours) and sizes of the PE (size of PE ($2.8 \text{ mm} \le x \ge 2.0 \text{mm}$, $6.3 \text{ mm} \le x \ge 2.8 \text{ mm}$ and $8.0 \text{ mm} \le x \ge 6.3 \text{mm}$)). These were incorporated in addition to two numeric factors as indicated in the first set of experiments, and 32 experimental runs were generated including eight replicates. After the experiments were carried out for each type of oil (Phillip Synthetic and Natural crude oil) for the second set of experiments, the responses were generated as shown in Appendices B3 – B4.

Every factor level combination was used in a randomised order. This design enabled it to fit a second-order polynomial model with main factors, two-factor interactions, and quadratic terms. These quadratic terms will capture the curvature in the relationship between the

responses (adsorption capacity and adsorption efficiency which has been previously defined in Section 3.3.1) and the experimental factors.

In summary, the equation model was defined as:

$$Y = \beta + aA + bB + cC + dD + abAB + acAC + adAD + bcBC + bdBD + cdCD + aaA^2 + bbB^2$$
 6.1

where Y is the measured response, e.g., adsorption capacity (g/g) or efficiency (%) for the specific PE sorbent associated with every variable level combination, β is the intercept (mean value), and A, B, C and D are the main factors. For the first set of experiments i.e. shredded and shredded-roughened, A = mass of PE; B = mass of oil; C = type of PE and D = particle size of PE. For the second set of experiments i.e. UV-weathered and shredded; A = mass of PE; B = mass of oil; C = size of PE and D = time of UV-weathering. AB, AC, AD, BC, BD, and CD are the two-factor (binary) interactions. A² and B² are the quadratic numerical (quantitative) factors, and a, b, c, d or ab, ac, ad, bc, bd, cd or aa, bb are the coefficients of the main factors, interaction factors, and quadratic numerical factors, respectively. Analysis of variance (ANOVA) was carried out to describe the coefficients of the quadratic equation. The significance of the adsorption variables was evaluated using the P-value and F-value, with the lack-of-fit test serving as a supporting measure to assess the adequacy of the fitted model. For optimisation of adsorption parameters, a numerical optimization method was employed to determine the optimal adsorption conditions based on the desirability function.

Model reduction (refining the model to be as simple and efficient as possible while still providing reliable and meaningful predictions) was applied where appropriate, by eliminating non-significant terms based on statistical analysis to enhance the accuracy and predictive power of the proposed quadratic model (using Design-Expert® software, version 13.0). This step ensures that only the most relevant factors and interactions are retained, without compromising the model's ability to describe the system.

6.3 Results

6.3.1 I-optimal experimental designs

The experiments utilised both Phillip synthetic oil and natural crude oil. Comprehensive results and analyses for both sets of experiments are provided separately in the Appendix.

This section highlights the key findings from experiments using Phillip synthetic oil, offering specific examples of the analyses performed.

6.3.1.1 Experiments with Phillip Synthetic Oil

The experimental results from the first set for adsorption capacity (g/g) and adsorption efficiency (%) of Phillip oil from the 27 experimental runs, along with the corresponding predicted values from the Design Expert software, 13, are presented in Appendix B1. Design Expert 13 also provided the mathematical relationships between the four independent factors studied (adsorbent quantity, oil quantity, adsorbent type, and adsorbent size) and the responses (adsorption capacity and efficiency). The equations (discussed below) describing response 1 (adsorption capacity) are presented in Equations 6.2 to 6.7, while those for response 2 (adsorption efficiency) are shown in Equations 6.8 to 6.13.

For Factors 1 and 2 (adsorbent quantity and oil quantity), both the theoretical masses (as provided by the I-optimal design) and the experimentally measured masses are included in the appendices B1 – B4 for clarity and reproducibility. All mass values are reported using significant figures consistent with the precision of the balance used for weighing the oil and PE particles.

Table 6. 1: The ANOVA table for the two-factor interaction model for Response 1; Adsorption capacity for Phillip oil on shredded (W), and shredded-roughened PE (X)

Source	Coefficient of estimate	Sum of Squares	df	Mean Square	F-value	p-value	
Model		38.19	14	2.73	31.92	< 0.0001	significant
A-Mass of PE	-0.1909	0.3908	1	0.3908	4.57	0.0537	
B-Mass of oil	-0.0560	0.0229	1	0.0229	0.2676	0.6144	
C-Type of PE	0.9579	22.02	1	22.02	257.71	< 0.0001	
D-Size of PE	0.6354/-0.5918	5.66	2	2.83	33.10	< 0.0001	
АВ	0.2494	0.4303	1	0.4303	5.04	0.0445	
AC	-0.0537	0.0336	1	0.0336	0.3927	0.5426	
AD	-0.3748 /0.2089	0.8421	2	0.4210	4.93	0.0274	
ВС	-0.1363	0.2238	1	0.2238	2.62	0.1316	
BD	-0.3004 /0.0476	0.7262	2	0.3631	4.25	0.0402	

CD	0.4712/-0.0741	3.36	2	1.68	19.68	0.0002	
Residual		1.03	12	0.0855			
Lack of Fit		0.5441	7	0.0777	0.8074	0.6164	not significant
Pure Error		0.4814	5	0.0963			
Cor Total		39.22	26				

Standard deviation 0.2923; Mean 4.94; CV% 5.92; R2 0.9739; Adjusted R2 0.9433; Predicted R2 0.7984; adeq Precision 19.9723

The ANOVA in Table 6.1 for the two-factor interaction (2FI) model for Response 1: Adsorption capacity, shows the significance of the factors and their interactions with one another.

The overall model is highly significant with a p-value less than 0.0001, indicating that most of the factors included in the model significantly affect the adsorption capacity, and that the analysis is very reliable. The mass of PE, A (p-value = 0.0537) has some influence but is not significant and the mass of oil, B (p-value 0.6144) is not significant. The type of PE, C (p-value <0.0001), the size of PE, D (p-value < 0.0001), interactions AB (p-value = 0.0445), AD (p-value = 0.0274), BD (p-value = 0.0402), and CD (p-value = 0.0002) are highly significant, indicating they have a strong effect on the adsorption capacity. Interactions AC (p-value = 0.5426) and BC (p-value = 0.1316) are not significant, indicating they do not significantly affect the adsorption capacity. R² value of 0.9739 means the model explains about 97.39% of the variability in adsorption capacity, which also suggests that about 97.39% of the experimental data could be matched with the predicted value, which is very good.

The Lack of Fit is insignificant (p-value = 0.6164) meaning the model fits the data well. Adeq Precision above 4 indicates an adequate signal. This high value of 19.9723, confirms that the model is highly reliable and has good predictive capabilities, suitable for making informed decisions based on experimental data and optimising the adsorption process.

In conclusion, the adsorption capacity is most influenced by the type and size of the PE sorbent used, with significant contributions from how these factors interact with each other and the mass of PE and oil. The model is statistically robust, accounting for substantial variation in the dependent variable.

The final equations in terms of actual factors for the adsorption capacity (Y) are shown here. There are 6 equations derived for Y (adsorption capacity) from the outcome of this experiment. The equations in terms of actual factors can be used to predict the response for given levels of each factor.

$$Y(W, 2.8mm) = +8.717 - 5.04A - 0.39B + 0.40AB$$
 6.2

$$Y(W, 6.3 \text{mm}) = +5.24 - 2.271 \text{A} - 0.25 \text{B} + 0.40 \text{AB}$$
 6.3

$$Y(W, 8.0mm) = +5.62 - 2.88A - 0.17B + 0.40AB$$
 6.4

$$Y(X, 2.8 \text{mm}) = +12.72 - 5.47 \text{A} - 0.5 \text{B} + 0.4 \text{AB}$$
 6.5

$$Y(X, 6.3 \text{mm}) = +8.148 - 3.14A - 0.36B + 0.40AB$$
 6.6

$$Y(X, 8.0 \text{mm}) = +7.89 - 3.31 \text{A} - 0.28 \text{B} + 0.40 \text{AB}$$
 6.7

Each equation represents a different scenario with varying particle sizes of either shredded PE (W) or shredded-roughened PE (X), as well as the mass of PE (A), the mass of oil (B), and the influence of the response variable. For instance, Equation 6.2 is generated thus; Y(W, 2.8mm) is Shredded PE (W), and particle size $2.8mm \le x \ge 2.0 \text{ mm}$. The intercepts are the baseline responses when A, B and AB are zero.

Across all equations, increasing the mass of PE (A) consistently decreases the response, Y, indicating a strong negative effect, increasing the mass of oil (B) generally has a smaller negative effect on the response compared to the mass of PE. The positive interaction term (AB) suggests that the combined increase in both the mass of PE and the mass of oil leads to a slight increase in the response, mitigating some of the negative effects of increasing each factor individually.

Comparing the shredded and shredded-roughened PE, showed that the shredded-roughened PE (X) with smaller particles (2.8mm \le x \ge 2.0 mm) generally has a higher baseline response (intercept) compared to shredded PE (W), indicating that roughened PE might be more effective in its application. The smallest particle size (2.8mm \le x \ge 2.0 mm) for both types, tends to have the highest negative impact on the responses, implying that the smaller particles might be more effective in adsorption but are also more sensitive to increases in the mass of PE and oil.

In conclusion, the interaction between the mass of PE and oil slightly enhances the response, suggesting that optimization of both factors is crucial for maximizing the sorbent's performance.

Figure 6.1a displays the normal probability plot of studentised residuals for adsorption capacity (g/g), which is used to assess the normality of residuals, an essential assumption in ANOVA and regression models. This plot helps determine whether the residuals follow a normal distribution by checking if the points align approximately along a straight line without significant deviation. If the distribution is not normal, a nonlinear pattern may emerge, which can often be corrected through an appropriate transformation (80). As observed, nearly all data points lie on a straight line for both responses, indicating that the residuals are normally

distributed. Figure 6.1b illustrates the correlation between actual and predicted values of adsorption capacity (g/g). This plot displays the relationship between the predicted values from the model and the actual observed values. The actual values are the measured values of the adsorption capacity obtained from the experiment carried out as shown in Appendix B1, which was determined experimentally, while the predicted values were generated by using Equations 6.3 to 6.8. As can be seen, the predicted values for adsorption capacity for Phillip oil adsorption, obtained from the model, are in good agreement with the actual experimental data, because the points generally followed the straight line, suggesting that the residuals are approximately normally distributed. Since there are no significant deviations from the line, it indicates that the model's assumption of normality is reasonable. Moreover, different sizes of the PE did not seem to introduce any noticeable pattern or deviation from normality, there is a consistent spread of points across different sizes of PE particles, indicating that the model performs well across the different sizes. It should be noted that these models predict data that was used to develop the model, and this may introduce some inherent bias for these models (80). This model would need to be validated with a confirmatory experiment.

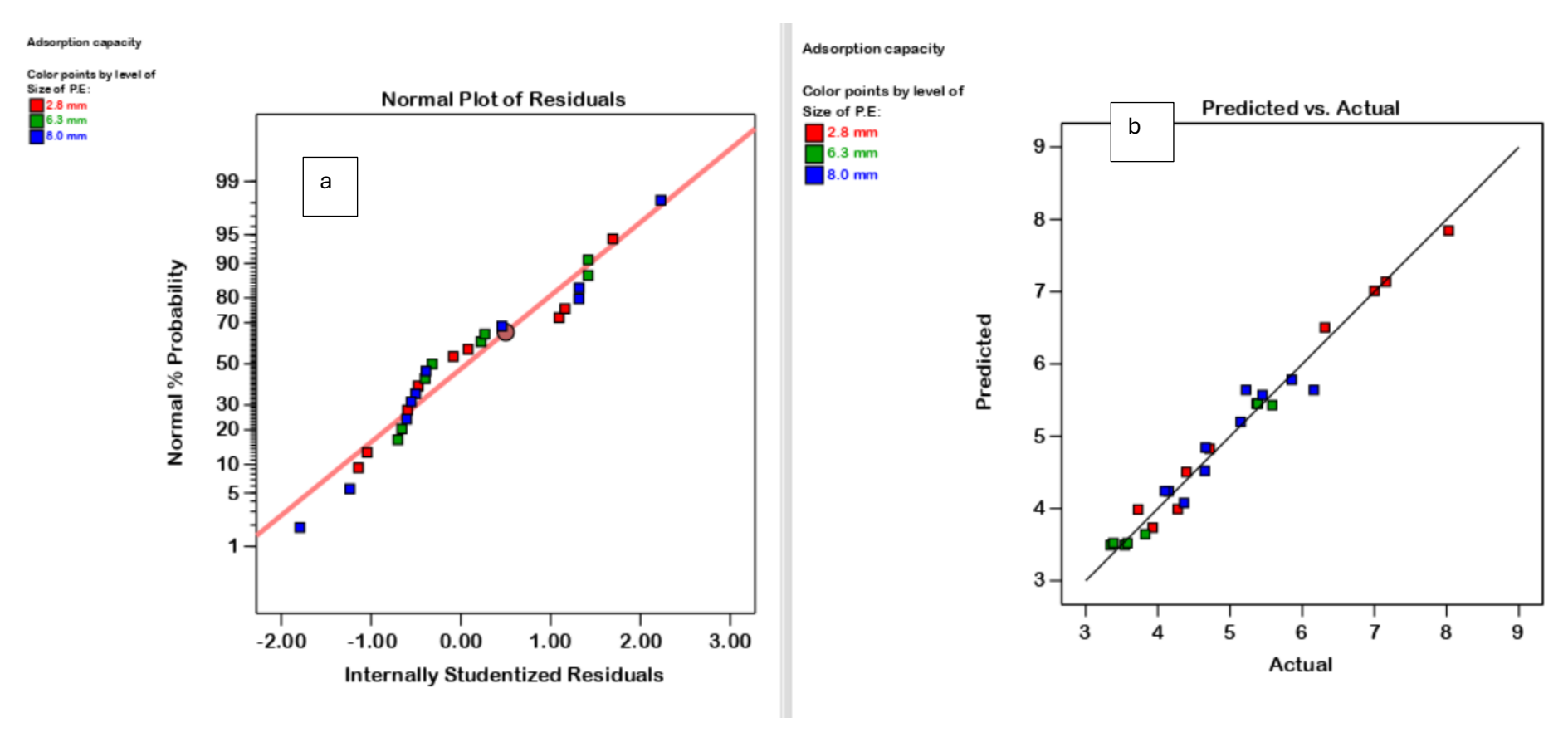


Figure 6. 1: Normal probability plot of studentised residuals(a) and correlation between actual and predicted values (b) of adsorption capacity for Phillip oil

Note: These graphs were plotted and obtained from Design-Expert®13, and similar trends were obtained for both responses (adsorption capacity and adsorption efficiency Figure 6.5) for both the first and second sets of experiments, i.e., those carried out with the shredded,

shredded-roughened, and UV-weathered PE and both Phillip synthetic and Natural crude oils. The figures are represented in the appendices B1 – B4.

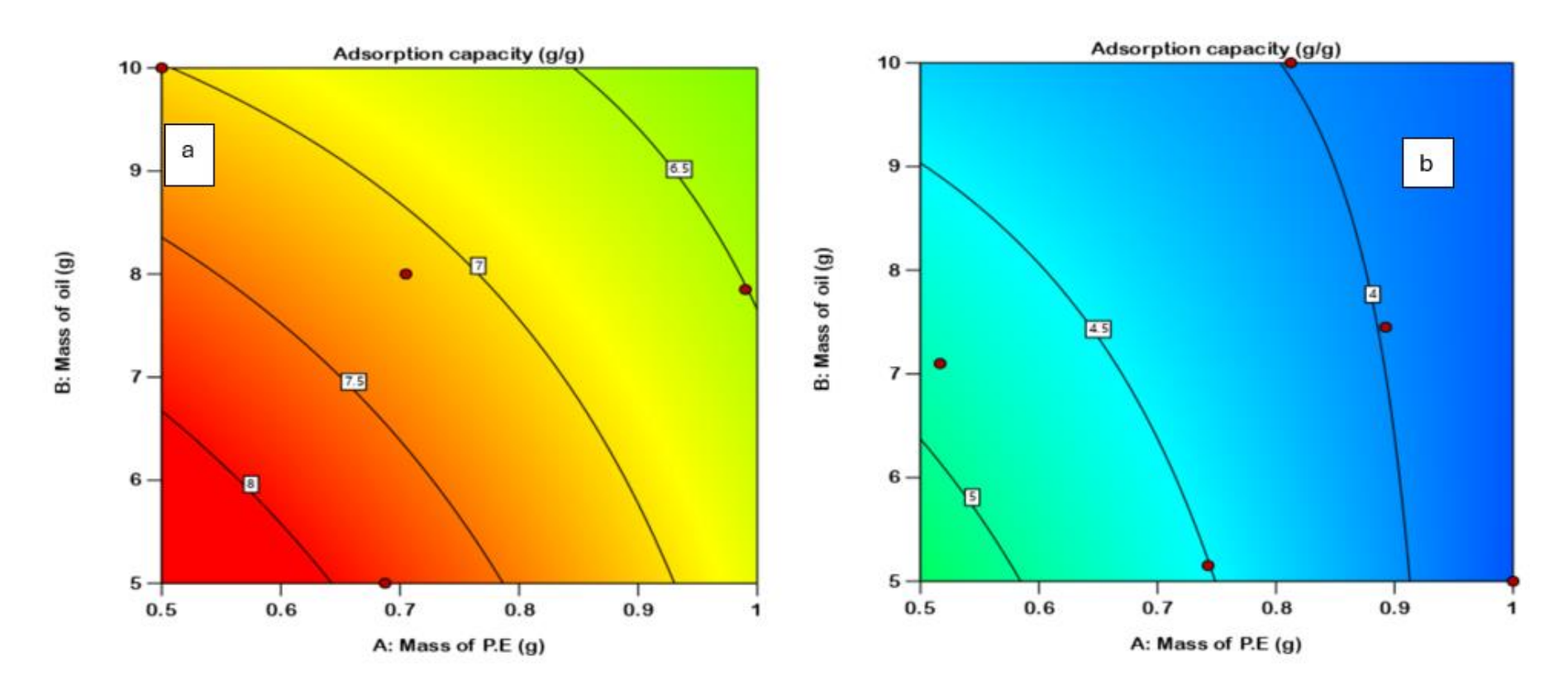


Figure 6. 2: (a) Adsorption capacity of Phillip oil with shredded-roughened PE Particle size 2.8 mm \le x \ge 2.0 mm (b) Adsorption capacity of Phillip oil with shredded PE Particle size 2.8 mm \le x \ge 2.0 mm

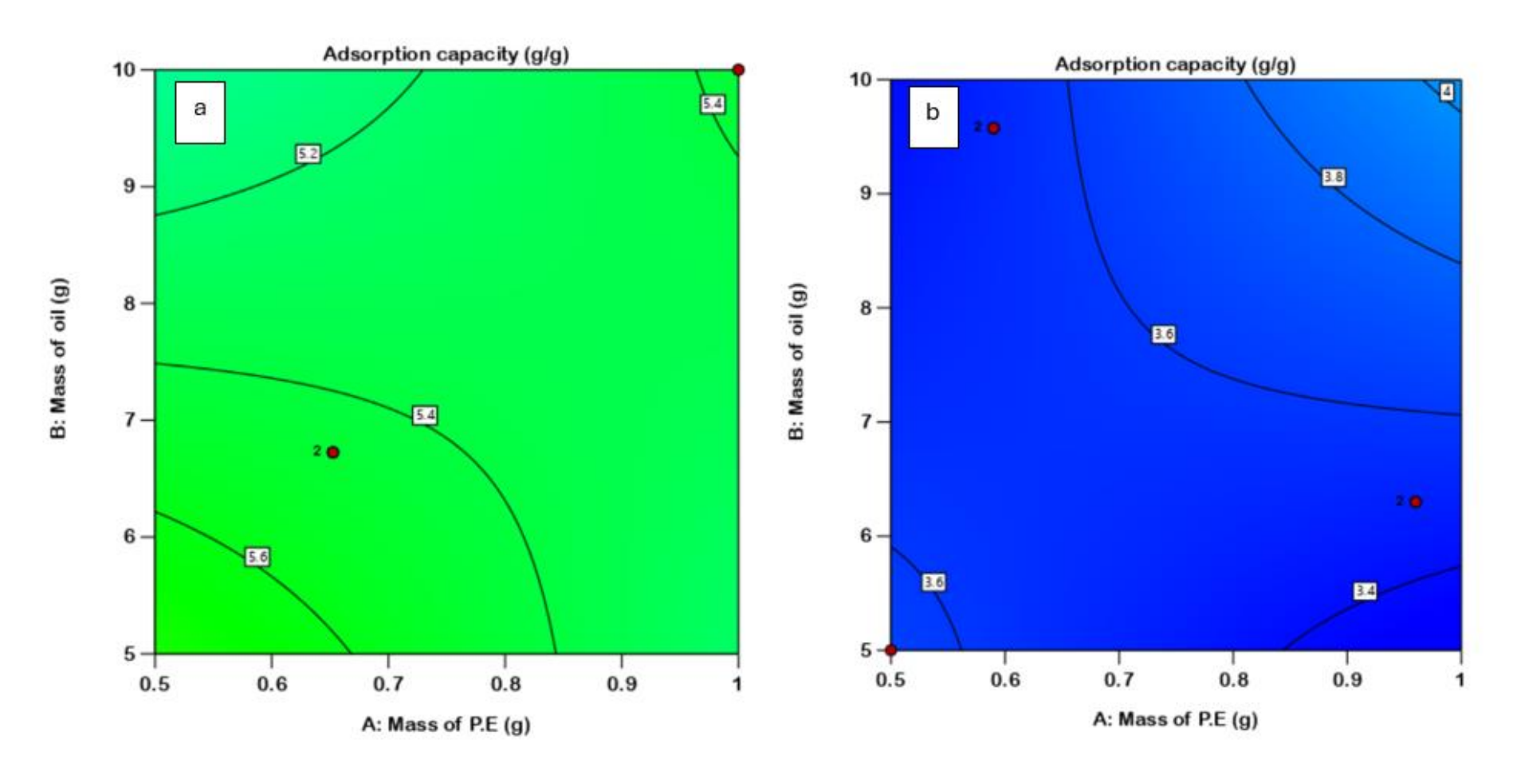


Figure 6. 3: (a) Adsorption capacity of Phillip oil with shredded-roughened PE Particle size 6.3 mm \le x \ge 2.8 mm (b) Adsorption capacity of Phillip oil with shredded PE Particle size 6.3 mm \le x \ge 2.8 mm

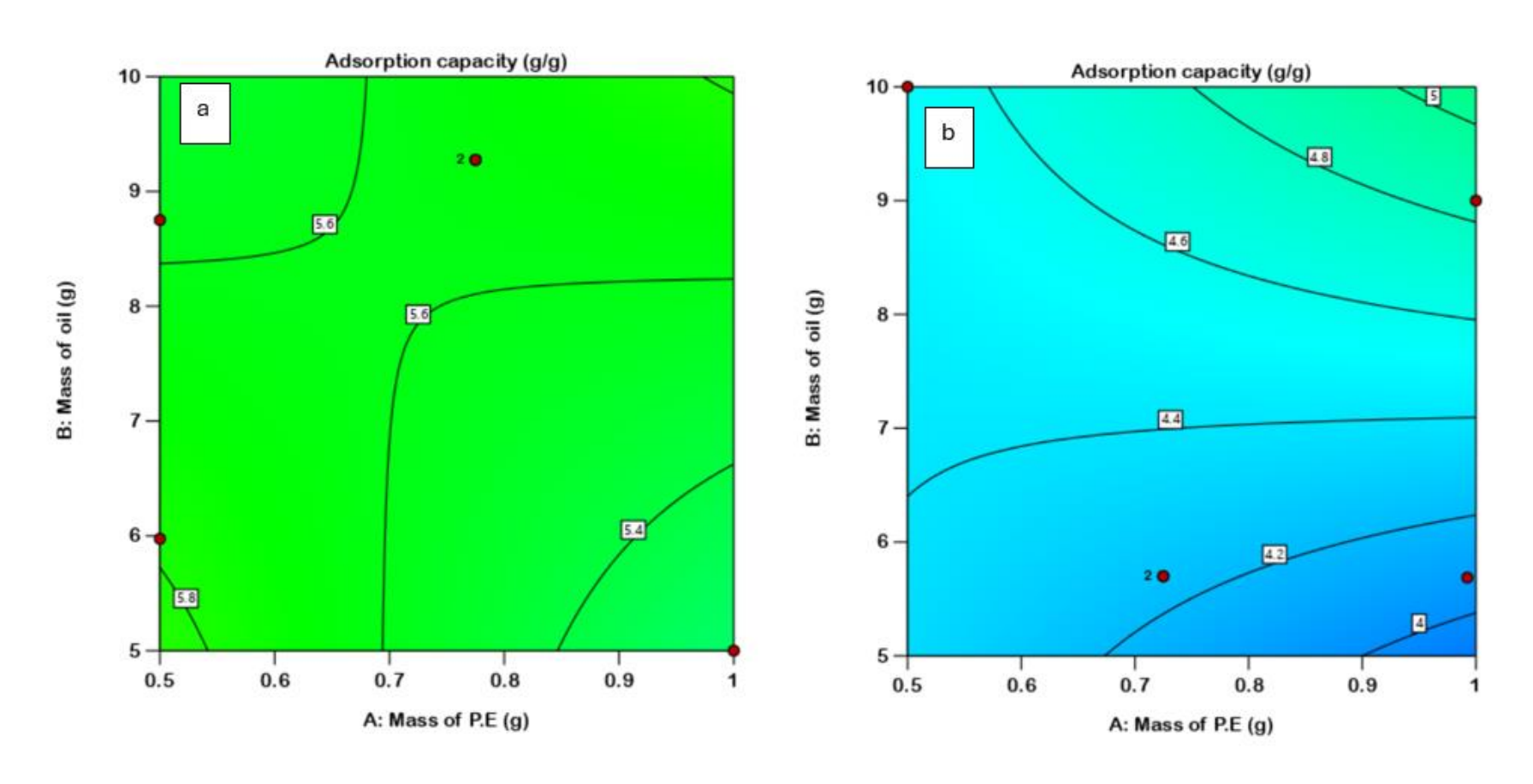


Figure 6. 4: (a) Adsorption capacity of Phillip oil with shredded-roughened PE Particle size 8.0 mm \le x \ge 6.3 mm (b) Adsorption capacity of Phillip oil with shredded PE Particle size 8.0 mm \le x \ge 6.3 mm

From the graphs above (Figures 6.2, 6.3, and 6.4), the adsorption capacity of Phillips oil with shredded PE (W) particle size of 2.8 mm \le x \ge 2.0 mm, ranges from approximately 4.0 g/g to 5.0 g/g. The highest capacity was observed at lower oil mass 5 g and lower PE mass of 0.5 g. The trend shows a decrease in adsorption capacity with increasing oil mass and increasing PE mass. This might be because every PE particle has many available adsorption sites (related to surface area). As oil mass increases, the increasing oil mass can contribute to a decrease in adsorption capacity through several mechanisms, like the squeezing-out effect, and saturation of adsorption sites. Beyond this point, no additional oil can be adsorbed, even if more oil is added. This trend is also influenced by the physical and chemical properties of the oil and PE, such as viscosity, surface tension, and surface roughness.

For the roughened PE (X) particle size of 2.8 mm \le x \ge 2.0 mm, the adsorption capacity ranges from approximately 6.5 g/g to 8.0 g/g. Again, higher capacities were observed at lower oil masses and lower PE masses. The trend shows an ncrease in adsorption capacity with a decreasing quantity of PE and oil masses.

The adsorption capacity of Phillips oil with shredded-roughened (X) PE particle size of 6.3 mm $\leq x \geq 2.8$ mm ranges between 5.2 g/g and 5.6 g/g, and slightly increases with an increase in the mass of PE when the mass of oil is between 9-10 g. The oil mass has a minor effect on the adsorption capacity, with a small decrease observed. The shredded PE (W) graph predominantly shows blue colours, indicating a lower adsorption capacity compared to shredded-roughened PE. The contour lines show adsorption capacities ranging from approximately 3.4 g/g to 4.0 g/g. The adsorption capacity slightly increases with an increase in the mass of PE (at higher oil masses), and the mass of oil also has a small influence on the adsorption capacity in that it slightly increases within increasing mass of oil. Thus, shredded-roughened PE (X) displays a higher overall adsorption capacity and is slightly more sensitive to changes in the mass of PE and oil compared to shredded PE (W) for PE particle size 6.3mm $\leq x \geq 2.8$ mm. Though both types of PE show similar trends in adsorption capacity to changes in the mass of PE and oil, the shredded-roughened PE consistently performed better.

For the particle size of 8 mm \le x \ge 6.3 mm, the graph shows a uniform green colour for the shredded-roughened PE (X), indicating an adsorption capacity of around 5.6 g/g across the entire range of PE mass and oil mass. The contours are less distinct and appear flatter, indicating minimal variation in adsorption capacity. This means that the adsorption capacity

remains relatively constant regardless of the mass of PE and oil, suggesting a steady performance of shredded-roughened PE in this configuration, offering a stable and predictable performance with a consistent adsorption capacity. While the graph of the shredded PE (W) displays a gradient from blue to green to a lighter shade of blue, indicating a range of adsorption capacities from around 4.0 g/g to 5.0 g/g. The contours are more pronounced and show significant variation in adsorption capacity as the mass of PE and oil changes. In other words, the adsorption capacity increases with the mass of oil and PE, thus suggesting more variability and fluctuation with shredded PE.

In conclusion, all three sets of graphs show ranges of adsorption capacities ranges from approximately 3.35 g/g to 8.03 g/g. For smaller particle sizes (2.8 mm \le x \ge 2.0 mm and 6.3 mm \le x \ge 2.8 mm), shredded-roughened PE (X) generally offers higher and more consistent adsorption capacities, and with increasing PE and oil masses compared to shredded PE (W).

In Section 5.3.3, the shredded PE (W) is described as having key physical properties like increased surface area, springiness, and mechanical robustness, all of which boost its oil adsorption capacity. The flexibility of shredded PE (W) allows it to conform to oil more effectively, enabling better oil adsorption and retention. However, when PE is shredded and then, roughened (shredded-roughened), additional benefits arise due to the increased surface area and surface roughness. The roughening process further enhances the material's surface energy as shown previously in Table 4.3, and provides more sites for oil molecules to adhere to. According to studies like those of Aparna et al. (98), roughened polymer films increase the interfacial energy between the polymer surface and the adsorbate, leading to better adhesion and adsorption on the surface. This is also applicable in this work as the shredded-roughened PE offers micro-cavities and voids, trapping more oil molecules (than the shredded PE) and enhancing van der Waals forces and other surface interactions, increasing the material's oil retention and minimising the likelihood of oil dripping off after removal from an oil spill. The shredded-roughened PE also shows increased porosity, which allows it to trap more oil, further increasing its adsorption capacity. Compared to other materials such as cellulose fibre used by Teas et al. (18) to adsorb crude oil, which demonstrated high oil adsorption capacities (5 g/g), shredded-roughened PE exhibited similar results. According to Hoang et al. (99) in their work "Advanced super-hydrophobic polymerbased porous absorbents for the treatment of oil-polluted water", to optimize the porous sorbent's hydrophobicity, they discovered that for a porous material to sorb effectively it should possess a surface energy value in the range of 30 mN/m (30 dyn/cm). The roughened PE used in this experiment has a surface energy of 33 dyn/cm and the rest of the PEs (shredded only, UV-weathered) exhibited within same range (33 dyn/cm ±3 as shown in Table 4.3).

Similar results were exhibited with the adsorption capacity for the natural crude oil (see Appendix B20 and B22). The shredded-roughened PE demonstrated significantly higher oil adsorption capacities with various particle sizes compared to its shredded-only counterparts, this increase in adsorption capacity can be attributed to the enhanced surface roughness, which provided more active sites for oil interaction, outperforming the shredded-only samples.

Table 6. 2: The ANOVA table for the reduced quadratic model for Response 2; Adsorption Efficiency for Phillip oil on shredded (W), and shredded-roughened PE (X)

Source	Coefficient of estimate	Sum of Squares	df	Mean Square	F-value	p-value	Remark
Model		49.72	11	4.52	62.50	< 0.0001	significant
A-Mass of P.E	-0.1909	10.88	1	10.8	150.46	0.0001	
B-Mass of oil	-0.0560	15.59	1	15.59	215.61	0.6144	
C-Type of P.E	0.9579	15.11	1	15.11	208.91	< 0.0001	
D-Size of P.E	0.6354 /-0.5918	3.29	2	1.65	22.77	< 0.0001	
ВС	-0.1363	0.6131	1	0.6131	8.48	0.0107	
BD	-0.3004 /0.0476	0.5304	2	0.2652	3.67	0.0505	
CD	0.4712 /-0.0741	2.12	2	1.06	14.65	0.0003	
B^2		0.7621	1	0.7621	10.56	0.0054	
Residual		1.08	15	0.0723			
Lack of Fit		0.8482	10	0.0848	1.79	0.2698	not significant
Pure Error		0.2367	5	0.0473			
Cor Total		50.81	26				

Standard deviation 0.2689; Mean 6.36; CV% 4.23; R2 0.9739; Adjusted R2 0.9630; Predicted R2 0.9221; Adeq Precision 31.2195

Table 6.2 represents an ANOVA (Analysis of Variance) for a reduced quadratic model aimed at analysing the adsorption efficiency of Phillip oil. The model utilises a square root transformation with a constant of 0.5 to stabilize variance and normalise the data.

The overall model is highly significant (F-value = 62.50, p < 0.0001). This indicates that the predictors included in the model explain a significant portion of the variability in adsorption efficiency. The mass of PE (A) is highly significant (F-value = 150.46, p < 0.0001), and is a critical factor affecting adsorption efficiency. Mass of oil (B) is highly significant (F-value = 215.61, p < 0.0001), and plays a significant role in adsorption efficiency. The type of PE (C) is highly significant (F-value = 208.91, p < 0.0001), and has a substantial impact on the adsorption efficiency. The size of PE (D) is significant (F-value = 22.77, p < 0.0001), it influences adsorption efficiency but to a lesser extent compared to other factors.

BC interaction (mass of oil and mass of PE) is significant (F-value = 8.48, p = 0.0107). This interaction shows that the combined effect of the mass of oil and PE is significant.

BD interaction (mass of oil and size of PE) is marginally significant (F-value = 3.67, p = 0.0505). This suggests a potential interaction effect between the mass of oil and the size of PE particles. It shows a nearly significant effect on the outcome being measured. This result is extremely close to being statistically significant at the conventional p=0.05 level. This suggests that oil mass and PE size might have a combined effect, but the evidence falls just short of the traditional threshold for claiming a definitive interaction effect.

CD interaction (type of PE and size of PE) is significant (F-value = 14.65, p = 0.0003). These values indicate that the interaction between the type and size of PE particles significantly affects adsorption efficiency.

 B^2 (Quadratic effect of mass of oil) is significant (F-value = 10.54, p = 0.0054). This suggests a non-linear relationship between the mass of oil and adsorption efficiency. The residual mean square (MS) value is 0.0723 and it represents the variation in adsorption efficiency not explained by the model. Since the adsorption efficiencies range between 0 and 1 (or 0% and 100%), a residual MS of 0.0723 is relatively small. This means the model is doing a good job at explaining most of the variation in adsorption efficiency, with only a small portion (7.23% variance) unaccounted for.

The lack of Fit is not significant (F-value = 1.79, p = 0.2698). This indicates that the model fits the data well.

Model Fit Statistics:

R² (Coefficient of Determination) is 0.9739: R² measures the proportion of the total variability in the response variable (adsorption efficiency) that is explained by the model. It ranges from 0 to 1 (0% to 100%), and higher values indicate better model performance. With a value of 0.9739, it means the model explains 97.39% of the variability in the adsorption efficiency. This value is quite high, suggesting that the model does an excellent job of capturing the relationship between the factors and the response (adsorption efficiency). Even though with a high R², it doesn't guarantee only with its value that the model is good, because it can be inflated if unnecessary factors are included, that is why Adjusted R² is also evaluated.

Adjusted R²: 96.30%, which accounts for the number of predictors in the model and adjusts the R² value accordingly, slightly lower than the regular R² obtained. The small drop (from 97.39% to 96.30%) shows that the factors in the model are relevant and contribute meaningfully to explaining the variability.

Predicted R² of 92.21%, is a strong indicator showing the model has a good predictive capability and also trained to avoid overfitting. The predicted R² measures the model's ability to anticipate new, unseen data. It is calculated by removing data points from the model, predicting their values, and comparing the predictions to actual values. It also ranges from 0 to 1. So with a value of 92.21%, which is slightly lower than Adjusted R².

The gap between Adjusted R² and Predicted R² could suggest that the model does not generalise well, but here the gap is small (4.09%), confirming a good balance between fit and prediction.

Adeq Precision of 31.2159, confirms that the model provides a strong and reliable/adequate signal and that the model can be used to navigate the design space confidently. It is indicative that it has sufficient response to identify optimal conditions. The general rule of thumb is that an adeq precision greater than 4 indicates an adequate signal.

In conclusion, this ANOVA table reveals that the adsorption efficiency of Phillip oil is significantly influenced by the mass of PE, the mass of oil, the type of PE, and the size of PE.

The model is statistically significant, fits the data well, and has good predictive capability. The interactions between different factors and the quadratic effect of the mass of oil also play important roles in adsorption efficiency.

Final Equations in Terms of Actual Factors for the Adsorption efficiency (Q);

There are 6 equations derived for Q (adsorption efficiency) from the outcome of this experiment. The equations in terms of actual factors can be used to predict the response for given levels of each factor.

$$\sqrt{(Q + 0.5)}_{W, 2.8mm} = +10.58 + 3.64A - 1.62B + 0.077B^{2}$$

$$6.8$$

$$\sqrt{(Q + 0.5)}_{W, 6.3mm} = +8.842 + 3.634A - 1.46247B + 0.077B^{2}$$

$$6.9$$

$$\sqrt{(Q + 0.5)}_{W, 8.0mm} = +9.52 + 3.64A - 1.4B + 0.077B^{2}$$

$$6.10$$

$$\sqrt{(Q + 0.5)}_{X, 2.8mm} = +14.14 + 3.64A - 1.79B + 0.077B^{2}$$

$$6.11$$

$$\sqrt{(Q + 0.5)}_{X, 6.3mm} = +11.77 + 3.64A - 1.64B + 0.077B^{2}$$

$$6.12$$

$$\sqrt{(Q + 0.5)}_{X, 8.0mm} = +11.72 + 3.64A - 1.62B + 0.077B^{2}$$

$$6.13$$

The adsorption efficiency is transformed using the square root to linearise the model. Here, $\sqrt{(Q+0.5)}$ is the square root of the transformed adsorption efficiency. A, represents PE's mass and B represents oil mass. The type of PE shredded (W) or shredded-roughened (X) and the size of PE particles (2.8 mm \le x \ge 2.0 mm, 6.3 mm \le x \ge 2.8 mm, and 8.0 mm \le x \ge 6.3 mm \le x \ge 2.8 mm) are considered. The equations took the general form:

$$\sqrt{(Q + 0.5)}$$
 = intercept + 3.64A + coefficient of B + 0.077B²

The intercept and coefficients change depending on the type and size of PE particles. Higher intercepts are seen in shredded-roughened PE than shredded PE, indicating that roughened PE generally starts with a higher baseline adsorption efficiency. All equations have a negative coefficient for *B* indicating that increasing the oil mass decreases the adsorption efficiency.

The coefficients for B vary slightly between the types and sizes of PE, with shredded-roughened PE having slightly higher negative values. This indicates that the influence of the oil mass on adsorption efficiency is more pronounced (or negative) for shredded-roughened

PE. The coefficient for A remains constant at +3.64 across all equations, suggesting that increasing the mass of PE consistently increases the adsorption efficiency regardless of the type and size of PE. The quadratic term is the same for all equations, indicating a consistent quadratic relationship between oil mass and adsorption efficiency. In conclusion, the shredded-roughened PE (X) generally provides higher adsorption efficiency across all sizes compared to shredded PE (W). The size of PE particles has a subtle but noticeable impact on the adsorption efficiency. For both shredded and shredded-roughened PE, increasing the size from $2.8 \text{ mm} \le x \ge 2.0 \text{ mm}$ to $8.0 \text{ mm} \le x \ge 6.3 \text{ mm}$ slightly increases the efficiency.

The equations can be used to predict the adsorption efficiency by inputting the specific masses of PE and oil, allowing for optimization of the adsorption process.

Figure 6.5a represents the normal probability plot of studentised residuals for adsorption efficiency (g/g). As can be seen, almost all data lie on a straight line for the adsorption efficiency, and therefore, it can be assumed that they are normally distributed. Figure 6.5b represents the correlation between actual and predicted values of adsorption efficiency (g/g). The actual values are the measured values of the adsorption efficiency obtained from the experiment carried out as shown in Appendix B1, which was determined experimentally, while the predicted values were generated by using Equations 6.8 to 6.13. As can be seen, the predicted values for adsorption efficiency for Phillip oil adsorption, obtained from the model, are in good agreement with the actual experimental data, because the points generally followed the straight line, suggesting that the residuals are approximately normally distributed. Since there are no significant deviations from the line, it indicates that the model's assumption of normality is reasonable.

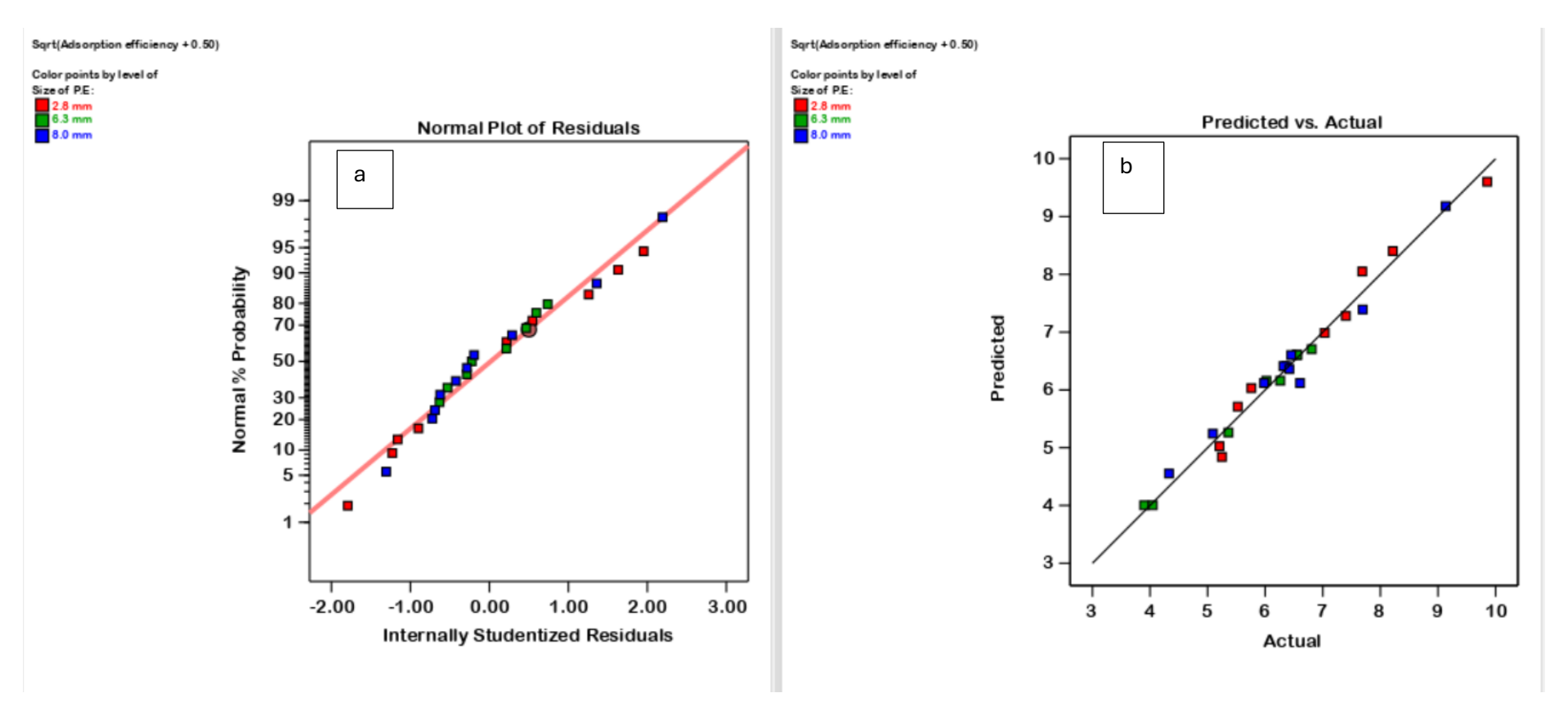
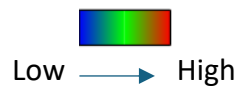


Figure 6. 5: Normal probability plot of studentised residuals(a) and correlation between actual and predicted values (b) of adsorption efficiency for Phillip oil



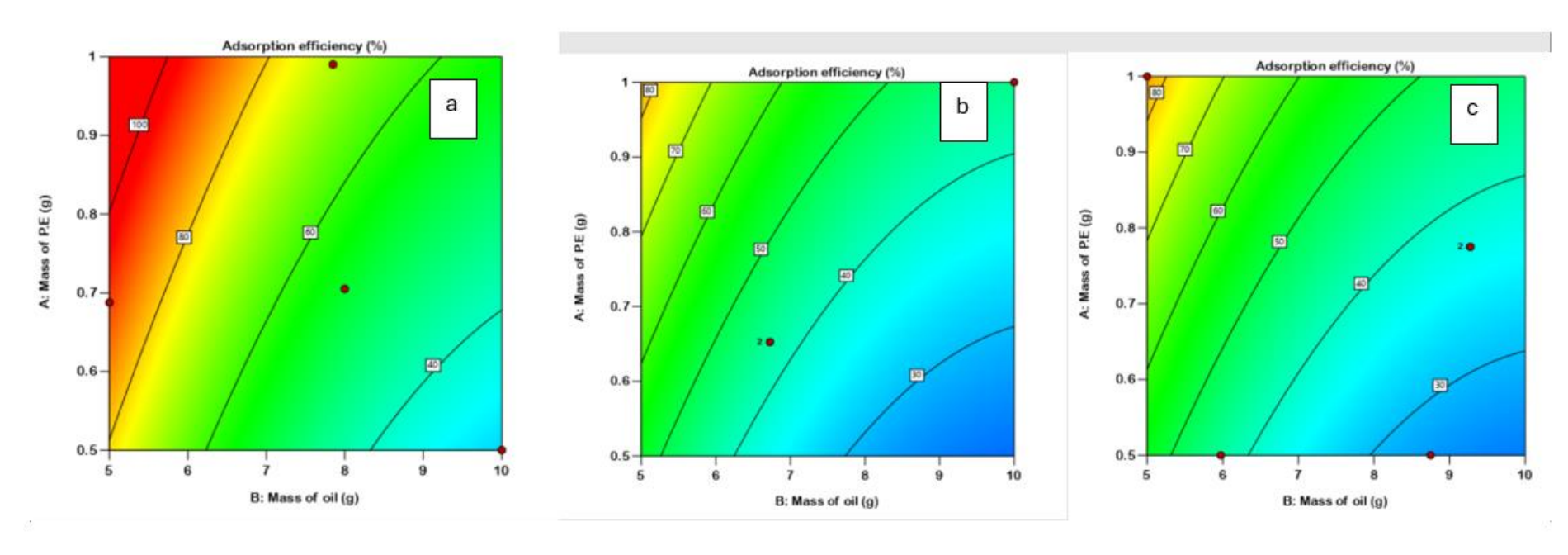


Figure 6. 6: (a) Adsorption efficiency of Phillip oil with shredded-roughened PE (X) Particle size 2.8 mm \le x \ge 2.0 mm (b) Adsorption efficiency of Phillip oil with shredded-roughened PE (X) Particle size 6.3 mm \le x \ge 2.8 mm (c) Adsorption efficiency of Phillip oil with shredded-roughened PE (X) Particle size 8.0 mm \le x \ge 6.3 mm

This software used a predefined colour scheme to visually represent the range of values in all the data collected. A Jet colour scheme was selected for this analysis, where blue represents low responses, green (for medium), yellow (high), and red (very high up to 100% in the case of efficiency).

Figure 6.6 contains three contour plots (a, b, and c), each representing the adsorption efficiency of Phillip oil using shredded-roughened PE (X) under the three different particle sizes used in the adsorption experiment.

For graph a, the particle size 2.8 mm \le x \ge 2.0 mm which is the smallest particle size range, shows the adsorption efficiency is highest (100%) when the mass of PE is above 0.7 g and the mass of oil is around 5-6 g (red region). As the mass of oil increases beyond 6 g, the adsorption efficiency decreases gradually. Similarly, reducing the mass of PE below 0.7 g also decreases adsorption efficiency. In other words, the smaller PE size particles result in higher adsorption efficiency for lower oil masses, particularly in the 5–6 g range.

For graph (b), the particle size 6.3 mm $\le x \ge 2.8$ mm, shows that the adsorption efficiency peaks at about 70% in the plot's top left region when PE's mass is around 0.8 g, and oil mass is around 5 g. Efficiency decreases as both PE and oil mass increase (green and blue regions), particularly beyond 6-7 g of oil. Compared to graph (a), this particle size range leads to lower adsorption efficiency overall, indicating a reduction in effectiveness as the particle size increases.

For graph c, the particle size 8.0 mm \le x \ge 6.3 mm which is the largest particle size range, has an adsorption efficiency similar to the particle size 6.3 mm \le x \ge 2.8 mm, maxing out around 70% when the PE mass is 0.9 g and oil mass is 5-6 g. As PE's mass decreases or oil's mass increases, the efficiency drops significantly (green and blue regions). The larger particle size seems to limit the adsorption efficiency, with efficiency remaining below 70% even under optimal conditions.

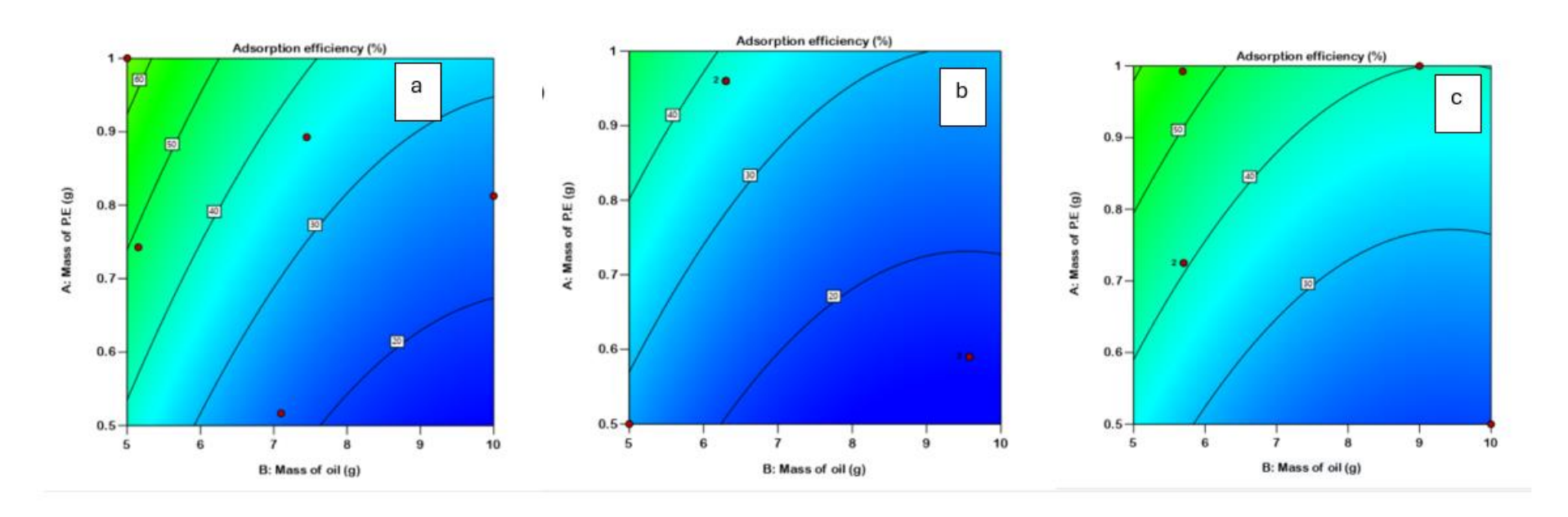


Figure 6. 7: (a) Adsorption efficiency of Phillip oil with shredded PE (W) Particle size 2.8 mm \le x \ge 2.0 mm (b) Adsorption efficiency of Phillip oil with shredded PE (W) Particle size 6.3 mm \le x \ge 2.8 mm (c) Adsorption efficiency of Phillip oil with shredded PE (W)) Particle size 8.0 mm \le x \ge 6.3 mm

Figure 6.7 shows the contour plots (a, b, and c) representing the adsorption efficiency of Phillip oil using shredded PE (W) for different particle size ranges.

For plot a, particle size of 2.8 mm \le x \ge 2.0 mm, the adsorption efficiency can reach 60% under specific conditions as a specific combination of oil and PE mass (for example, outside of which range efficiency quickly decreases; higher oil mass than 5 g and lower PE mass than 1 g. The variability highlighted by the many contour lines shows it is highly sensitive to changes. This means that this particle size demonstrates the highest possible adsorption efficiency of 60% under a narrow range of conditions.

Plot b (6.3 mm \le x \ge 2.8 mm): Efficiency starts lower than in Plot A, with a maximum of 40% achieved at higher PE mass (1 g) and low oil mass (5 g). Efficiency declines as oil mass increases, indicating a sharper dependency on oil mass.

Plot c (8.0 mm \le x \ge 6.3 mm): The maximum adsorption efficiency reaches 50%, and this happens over a slightly wider range of conditions (compared to Plot A). The efficiency here is more consistent and does not drop as steeply as in Plot A when conditions deviate from the optimum. This is shown to be less sensitive because of the fewer contour lines. This makes Plot c more robust for adsorption efficiency across varying operational parameters.

In conclusion, it can be said that the larger particle size range $8.0 \text{ mm} \le x \ge 6.3 \text{ mm}$ appear better for adsorption efficiency from this data, because the efficiency declines less steeply as oil mass increases, indicating better performance across the varying oil-PE combinations. From Figures 6.6 and 6.7 it can be seen that shredded-roughened PE has better efficiency compared to shredded only PE.

6.3.1.2 Optimisation of parameters for Phillip oil adsorption by the polyethylene sorbent

A numerical optimisation method was employed to determine the optimal conditions for adsorption capacity and efficiency across different adsorbents. This method identifies the optimal point that maximises the desired conditions based on the desirability function. The desirability function, a multiple-response approach, computes an objective function ranging from 0 to 1, representing values from undesirable to target conditions. The concepts of desirability and solutions are used to assess how well the settings of input factors achieve a

desired response or set of responses. This tool allows for the combination of favourable conditions to achieve optimal experimental settings that best meet all objectives. The numerical optimisation approach, implemented using Design Expert® 13.0 software, adjusts the values of PE size, PE weight, oil weight, and PE type within their specified ranges while selecting each specific response (the adsorption capacity or efficiency) and maximising (optimising) and prioritising it over the other to achieve the specific condition that will yield the best response. Thus, for this study, simultaneous optimisation of both responses were performed, integrating adsorption capacity and adsorption efficiency into the process. The optimal conditions for each response were determined using a numerical optimisation tool, which was adjusted by modifying the significance (importance) assigned to each response. Appendix B12 presents the optimised conditions for the adsorption of Philip oil by nonweathered PE, where adsorption capacity was prioritised over adsorption efficiency, with importance values set at 5 and 1, respectively. The model chose shredded-roughened PE (X) against shredded only as the type of PE sorbent, 2.8 mm (i.e. 2.8 mm \leq x \geq 2.0 mm) as the particle size range and the lowest adsorbent dose within the range of 0.5 g, as the best for Phillip oil uptake. It also selected optimal values of 6.7 g of oil in between the lower and the upper limits of the oil quantities (5 g and 10 g respectively). At these conditions, the adsorption capacity was 8.0 g/g with corresponding adsorption efficiency of 54.8%, and desirability values of 0.9.

Appendix B13 shows the optimisation of the conditions for the adsorption of Phillip oil by non-weathered PE, when the adsorption efficiency was prioritised over adsorption capacity (importance = 5 and 1, respectively). The model chose shredded-roughened PE (X) of particle size 8.0mm (i.e. $8.0 \text{ mm} \le x \ge 6.3 \text{ mm}$), mass of PE as 1.0g, mass of oil as 5.0g. At these conditions, the efficiency value was 83.8% with corresponding capacity value of 5.2 g/g and desirability value of 0.8. In addition, some confirmatory experimental runs were performed to confirm the robustness of the predicted model under these optimal conditions as selected by the model. A confirmatory test bridges the gap between model-based optimization and real-world application. It validates that the chosen optimal settings (derived from the model) are accurate, reliable, and practical when implemented in real experiments or production environments. As shown in Table 6.3, the results obtained from the confirmatory experiments were within the accuracy and precision of the design space (95% for both prediction and

confidence intervals), which indicates adequate predictability of the model for the responses (adsorption capacity and efficiency) analysed.

6.4: I-optimal experiments with the Natural crude oil

The response variables (adsorption capacity (g/g) and adsorption efficiency (%)) for natural crude oil, derived from 27 experimental runs (shredded and shredded-roughened), and from 32 experimental runs (UV-weathered PE) are detailed in Appendix B2, and B4 respectively, along with the corresponding predicted values generated by the Design Expert software. The software also provided mathematical models describing the relationships between the five independent variables studied; adsorbent quantity, oil quantity, adsorbent type, UV time of weathering and adsorbent size as the case may be (Appendices B5-B8). Based on the actual factors, the equations representing adsorption capacity and efficiency are presented in Appendix B9 and B11. Optimised conditions for the crude oil adsorption and efficiency for both non-weathered and UV-weathered PE are shown in Appendices B16, B17, B18 and B19.

The graphs in Appendices B20–B29 illustrate the relationship between various forms of PE and natural crude oil in terms of adsorption capacity and efficiency.

A confirmatory experiment was also carried out to validate the robustness of the predicted model under these optimal conditions as selected by the model. The results of the tests are shown in Table 6.4.

As can be observed in Table 6.4, for the adsorption capacity for natural crude oil with PE particle size 2.8 mm \le x \ge 2.0 mm (adsorbent X), the predicted value for the adsorption capacity was 5.9 g/g \pm 0.3, with confidence interval (95% - range 4.8 g/g to 7.0 g/g) and the confirmatory experimental result was 5.9 g/g. This result falls within the confidence interval, confirming that it matches the model's prediction. Also, that of adsorption efficiency with 8.0 mm \le x \ge 6.3 mm, (adsorbent X), with predicted efficiency value of 76.2% \pm 2.2%, and the experimental value of 71.9% was achieved. This value is within the confidence interval (95% = range 71.5% to 80.8%), but it is slightly lower than the predicted mean. The result is acceptable because it is within the predicted range. Likewise, for the adsorption capacity with 6.3 mm \le x \ge 2.8 mm, (adsorbent UV-weathered 0hr), predicted efficiency value of 6.0 g/g \pm 0.3 and a confirmatory experimental value of 5.1g/g was achieved. This value is within the confidence interval value of 5.1 g/g and 6.8 g/g as recommended by the model.

The predicted adsorption efficiency for shredded polyethylene (PE) in crude oil adsorption was 73.1%, with an uncertainty margin of ±5.1%, and a confidence interval of 61% to 85%.

However, the mean confirmatory experimental adsorption efficiency achieved was only 50.7%, falling significantly outside the predicted range. This observed efficiency is lower than expected by 10.3 percentage points, indicating a notable discrepancy between the model's predictions and actual experimental results.

Several factors may explain this difference. One possible reason is the unstable nature of the natural crude oil sample used in the experiment. Although the oil had been capped securely when stored in the lab for over a year since the original I-optimal experiment, it is known that over time, crude oil can lose lighter fractions, altering its composition and maybe adsorption behaviour.

Another possible factor is material variability, the PE used in the confirmatory experiment came from a different batch than the one used for the original optimisation, this could lead to differences in particle characteristics and adsorption performance due to differences in PE content. For adsorption studies, it is common for predictions to work better for adsorption capacity and rather than efficiency (124,125)), which is reflected here because the model gave a wider confidence interval for efficiency (61% - 85%). A wider confidence interval suggests that the model predicted efficiency with greater uncertainty. This often happens because efficiency is influenced by more complex, interconnected factors (e.g., mass transfer, binding strength, fluid dynamics). Adsorption capacity predictions, in contrast, tend to be more reliable because they depend more on adsorbent quantity and adsorbate concentration, which are easier to model accurately. Thus, the model's inherent uncertainty for efficiency highlights that deviations in experimental results were more likely to occur for efficiency compared to capacity. Additionally, some unaccounted-for experimental error may have occurred during the confirmatory test.

It is also worth noting that the desirability value for the adsorption efficiency of UV-weathered PE in crude oil adsorption was the lowest among the tested responses, at 0.7. This suggests that the model itself indicates room for improvement in either experimental conditions or adsorbent properties to achieve higher efficiency. Specifically, the current conditions and PE characteristics may not fully optimise adsorption efficiency, particularly for PE particles with a size range of 6.3 mm \le x \ge 2.8 mm. This particle size may be more sensitive to certain factors compared to others, potentially affecting adsorption performance.

Since the particle size range is wide, it may be that the combined size range in this batch have a more uneven distribution of particle sizes (i.e. may be more of the smaller particle sizes). From the previous experiment for the efficiencies, it is noted that larger particle sizes are better for adsorption efficiency so if this batch range contains more of the smaller particle sizes (closer to 2.8 mm), it could result in a lower efficiency result because they may behave more like the smaller size range. Conversely, if there were predominantly larger particles (closer to 6.3 mm) they might exhibit better efficiency.

6.5 Experiments with the UV-weathered PE

For the second set of experiments with the UV-weathered PE, the response variables (adsorption capacity (g/g) and adsorption efficiency (%)) for Philip and natural crude oil, derived from 32 experimental runs (UV-weathered PE) are detailed in Appendix B3 and B4, respectively, along with the corresponding predicted values generated by the Design Expert software. The software also provided ANOVA (Appendix B7, B8) and mathematical equations describing the relationships between the four independent variables studied: adsorbent quantity, oil quantity, UV time of weathering and adsorbent size. The equations representing adsorption capacity and efficiency are presented in Appendix B10 and B11 based on the actual factors. Appendix B14, B15, B18 and B19 show the optimisation of the conditions for the adsorption of Phillip oil and Natural crude oil by UV-weathered PE when adsorption capacity and efficiency were considered over one another and vice versa respectively.

A confirmatory experiment was also carried out to validate the robustness of the predicted model under these optimal conditions as selected by the model. The results of the tests are shown in Tables 6.3 and 6.4.

6.5.1 Effects of UV weathered PE on adsorption of Philip oil and crude oil

Appendix B20 – B29 showed different interactions of the oils with various particle sizes and comparison amongst themselves (various particle sizes).

From 2D plots as seen for $2.8 \text{mm} \le x \ge 2.0 \text{ mm}$ and $6.3 \text{ mm} \le x \ge 2.8 \text{ mm}$ size ranges, there is an increase in adsorption capacity with some UV weathering (75 hours), but then it decreases

with more UV weathering (150 hours). The larger size range is similar for 0 hour and 75 hours weathering, but still a decrease with 150 hours UV weathering.

For adsorption efficiency and capacity there is a similar trend in that there are increases with an increasing mass of PE and a decreasing mass of oil. There is a slight improvement in efficiency for the smaller (2.8mm $\le x \ge 2.0$ mm) and middle-(6.3 mm $\le x \ge 2.8$ mm) size ranges with 75 hr UV weathering and then a definite decrease in efficiency with UV weathering of 150 hours. There's no difference when increasing 75 hours for the larger particle size (8 mm $\le x \ge 6.3$ mm) but does also decrease when increasing to 150 hours of UV-weathering.

These changes could be attributed to the varying contact angles, surface energies and degradation level of these PEs. UV weathering causes surface oxidation, leading to the formation of hydrophilic functional groups (e.g., hydroxyl and carbonyl groups), as shown in the FTIR analysis. At 75 hours of UV exposure, it is assumed that these groups enhanced adsorption by improving surface wettability and interaction with oil molecules, with the increase in surface energy as shown in Table 4.3. However, prolonged UV exposure (150 hours) results in over-oxidation and severe degradation, weakening the PE structure and disrupting the hydrophilic-hydrophobic balance, which reduces oil adsorption.

SEM analysis (Figure 4.31) reveals that moderate UV exposure (75 hours) increases surface roughness, creating more adsorption sites to anchor oil to its surface, but the 150-hour UV-weathered PE exhibits a smoother surface, indicating a loss of adsorption sites due to degradation.

There are large differences in adsorption capacities and efficiencies between crude oil and Phillips oil when investigating UV weathering. The adsorption capacity and efficiencies are much higher with crude oil. For instance, for the small particle size ranges, the highest adsorption capacity and efficiency values with the Phillip oil were 3.9 g/g and 40%, while that for the natural crude oil were 6.5 g/g and 70%, for the medium size particle size for the 75-hour UV-weathering for Phillip oil was 3.7 g/g and 38% and for crude oil was 5.5 g/g and 80% and for the largest particle size for the Phillip oil was 3.4 g/g and 36% and crude oil was 5 g/g and 70%.

Crude oil might likely be adsorbed better by UV-weathered PE because it contains a complex mixture of hydrocarbons with a broader range of polar and non-polar components, including heavier fractions, as shown in the TGA analysis (e.g., resins and asphaltenes) (115). These polar components can form stronger interactions with the hydrophilic functional groups introduced on the UV-weathered PE surface, enhancing adsorption. Phillips oil (a refined or lighter oil) has a narrower composition and may have fewer polar components may result in weaker interactions with the oxidised PE surface. Again, natural crude oil typically has a higher viscosity than refined oils like Phillips oil. This increased viscosity may allow crude oil to better adhere to and coat the roughened surfaces of UV-weathered PE, improving adsorption capacity and efficiency. Phillips oil, being less viscous, may flow more freely and have reduced retention on the PE surface, thus lacking the same level of interaction, leading to lower adsorption capacity and efficiency.

Table 6. 3: Results of confirmatory experiments for analysed Optimal-I design model for adsorption of Philip synthetic oil

Response	Adsorbent type	Adsorbent size	Target	Predicted mean	Desirability	Confirmation experiment	Confidence interval (95%)	
							Low I	high
Adsorption capacity (g/g)	X	2.8 mm ≤ x ≥ 2.0 mm	Maximise	8.005 g/g ± 0.29	0.857	7.52667g/g	7.35587	8.65307
Adsorption efficiency	x	8 mm ≤ x ≥ 6.3 mm	Maximise	83.83% ± 4.938	0.832	79.062%	73.64%	94.53%
Adsorption Capacity	O hr UV- weathered	2.8 mm ≤ x ≥ 2.0 mm	Maximise	3.825g/g	0.794	3.46	2.85	5.399
Adsorption efficiency (%)	O hr UV- weathered	8 mm ≤ x ≥ 6.3 mm	Maximise	57.05% ± 4.808	0.818	48.10%	47.21%	66.87%

X = Shredded-roughened PE; for confirmation experiment, each of the values obtained represents the average of three (3) different experimental samples carried out

Table 6. 4: Results of confirmatory experiments for analysed Optimal-I design model for adsorption of Natural crude oil

Response	Adsorbent	Target	Predicted	Desirability	Confirmation	Confidence interval (95%)	
					experiment	Low	High
Adsorption capacity (g/g)	X (2.8 mm \le x \ge 2.0 mm)	Maximise	5.85g/g ± 0.245	0.873	5.933g/g	4.75g/g	6.968g/g
Adsorption efficiency (%)	X (8 mm ≤ x ≥ 6.3 mm)	Maximise	76.15% ±2.22	0.844	71.90%	71.52%	80.77%
Adsorption capacity (g/g)	Ohr UV-weathered (2.8mm ≤ x ≥ 2.0 mm)	Maximise	5.96g/g ± 0.319	0.952	5.133g/g	5.08g/g	6.825g/g
Adsorption efficiency (%)	Ohr UV-weathered (6.3 mm \leq x \geq 2.8 mm)	Maximise	73.1%±5.087	0.724	50.7%	61%	85%

X = Shredded-roughened PE; for confirmation experiment, each of the values obtained represents average of three (3) different experimental samples carried out

From Tables 6.3 and 6.4, the results of the confirmatory tests with the UV-weathered PE samples can be used to compare the experimental test results of set 1. The PE samples that were chosen by the model 0 hr UV-weathered (2.8mm $\le x \ge 2.0$ mm) and 0 hr UV-weathered (6.3 mm $\le x \ge 2.8$ mm) are effectively the same as those done in set 1 in that they are shredded non-weathered PE (W) and have the same particle size ranges.

For the set 1 experimental result, using 1 g of shredded PE of particle size 2.8mm $\le x \ge 2.0$ mm to adsorb 5 g of Phillip oil could achieve a maximum adsorption capacity of 5 g/g according to the model. The confirmatory experimental result with a prediction of 3.82 g/g achieved an adsorption capacity of 3.96 g/g. Again, the set 1 experimental result using 0.5 g of particle size 8mm $\le x \ge 6.3$ mm of PE on 10 g of Phillip oil achieved a maximum adsorption efficiency of 40%, and the confirmatory experimental result with a prediction of 57% achieved 48.1% (falls within the confidence interval of 47% and 57%. 1 g of particle size of 2.8mm $\le x \ge 2.0$ mm PE was used to adsorb 5 g of crude oil and achieved 4.6 g/g in the first set of experiments and the confirmatory result with a prediction of 5.96 g/g was able to accomplish an adsorption capacity of 5.1 g/g. 1 g of particle size of 6.3mm $\le x \ge 2.8$ mm PE was used to adsorb 5 g of crude oil and achieved an adsorption efficiency of 60% but the confirmatory experiment achieved 50%, with the model prediction of 73%.

This analysis shows that the confirmatory experimental results largely align with the model's predictions, though some discrepancies exist. The model's predictions for adsorption capacity and efficiency in most cases are reasonably close to the experimental results, particularly for Phillips oil adsorption (where values fall within the confidence intervals). For crude oil adsorption efficiency (e.g., $6.3 \text{ mm} \le x \ge 2.8 \text{ mm}$ particle size), the model's prediction deviates significantly from the experimental value (73% predicted vs. 60% from set 1 tests vs. 50% achieved in the confirmatory test). This suggests that the model might have overestimated adsorption efficiency for certain conditions. The model can be referred to as being reasonably dependable for providing general predictions of adsorption behaviour but may require refinement to improve accuracy in specific scenarios, particularly for medium particle sizes $(6.3 \text{ mm} \le x \ge 2.8 \text{ mm})$ and for crude oil adsorption.

Chapter 7

7.0 Column Adsorption

A preliminary column adsorption experiment for oil with polyethylene sorbents was carried out as an insightful practical step toward understanding the real-life application options of PE for oil adsorption on a larger scale, particularly with guidance from the optimised conditions identified in Chapter 6. These optimised conditions (Table 7.1), specifically quantitative factors were scaled up to five times (5X). This serves as a practical test to see if the adsorption capacities and efficiencies predicted by the model are achievable when the system is under a more substantial load.

Assumptions made when scaling from Batch to Column Experiment

- The physical and chemical characteristics of the PE sorbent are assumed to remain unchanged, especially under similar environmental conditions.
- ii. It is assumed that both the batch and column experiments were conducted at similar temperatures.
- iii. It is assumed that there is operational consistency between both systems
- iv. The packed bed in the column is assumed to be homogeneously packed, with uniform distribution of the PE adsorbent, minimising channelling or voids that might affect flow or adsorption kinetics.

Table 7. 1: Optimised conditions for the adsorption of Phillip and Natural crude oils

Type of oil	Response	Type of adsorbent/ particle size	Quantity of PE	Quantity of oil	Model predicted outcome	
	Adsorption	Х			8.005 g/g ± 0.29	
	capacity (g/g)	2.8 mm ≤ x ≥ 2.0 mm	0.5	6.65356	0.003 6/6 ± 0.23	
	Adsorption	Х			83.83% ± 4.938	
Dhillin cynthotic	efficiency (%)	8 mm ≤ x ≥ 6.3 mm	1	5	03.03/0 ± 4.330	
Phillip synthetic oil	Adsorption	O hr UV-weathered			2 925 a/a	
Oii	capacity (g/g)	2.8 mm ≤ x ≥ 2.0 mm	0.5	10	3.825g/g	
	Adsorption efficiency (%)	O hr UV-weathered	0.9955	5.29357	57.05% ± 4.808	
		8 mm ≤ x ≥ 6.3 mm				
	Adsorption	Х	0.5	10	F 0F - /- + 0 24F	
	capacity (g/g)	2.8 mm ≤ x ≥ 2.0 mm	0.5	10	5.85g/g ± 0.245	
	Adsorption	Х	1	F	76.15% ±2.22	
Natural crude oil	efficiency (%)	8 mm ≤ x ≥ 6.3 mm	1	5		
	Adsorption	O hr UV-weathered		10	F.O.C. / . O.O.10	
	capacity (g/g)	2.8 mm ≤ x ≥ 2.0 mm	0.5	10	5.96g/g ± 0.319	
	Adsorption	O hr UV-weathered	1	5	73.1%±5.087	
	efficiency (%)	6.3mm ≤ x ≥ 2.8 mm				

7.1 Introduction

The column, or continuous adsorption method, is commonly used to evaluate the performance of adsorbent materials in large-scale adsorption systems. Fixed-bed adsorption is the most widely used and frequently documented among the various techniques available in the literature. A contaminated solution (adsorbate) flows through a stationary bed of adsorbent material in a fixed-bed column setup. As the solution passes from the top of the column to the bottom, adsorption occurs when the solute particles adhere to the surface of the adsorbent.

In a fixed-bed adsorption system, the column is divided into three main zones that change over time as adsorption progresses. These zones are: saturation, adsorption and non-work zones.

Saturated Zone: This is the top section of the column where the adsorbent (material capturing the contaminant) has reached full capacity and can no longer adsorb more solute from the solution. In this zone, all adsorption sites are occupied, and the solute flows through without being captured.

Adsorption Zone (Mass Transfer Zone): Below the saturated zone is the adsorption or mass transfer zone. Here, the adsorbent is actively capturing oil from the solution, with the solute binding to available sites on the adsorbent. Over time, as more solute is captured, this zone moves downward toward the bottom of the column.

Non-Work Zone: This is the bottom section of the column where the adsorbent is not yet adsorbed or saturated and still has the capacity to adsorb the solute. Initially, this zone does not experience much interaction with the solute because the adsorption process is focused in the adsorption zone above.

As the experiment progresses, the adsorption zone gradually shifts downward while capturing oil from the solution. This movement reduces the size of the non-work zone, and the saturated zone expands downward. When the adsorption zone reaches the bottom of the column, breakthrough occurs. This means the adsorbent in the entire column is nearly full, and solute particles start to escape through the effluent (the solution leaving the column). At this point, the solute concentration in the effluent begins to rise quickly, indicating that the column's capacity to remove solute is decreasing.

The adsorption exhaustion point is reached when the effluent concentration reaches 90–95% of the influent concentration (the initial concentration entering the column). This signals that the adsorbent is almost entirely saturated and that the column is no longer effectively removing the solute (80).

7.2 Materials

The experiments were conducted at room temperature using a 50 cm polypropylene column with an internal diameter of 1.5 cm. The adsorption tests involved Phillip synthetic oil and natural crude oil as the target oils, using polyethylene (PE) sorbents in two forms: shredded (W) and shredded-roughened (X), which were prepared with the optimized particle sizes.

7.3 Methodology

7.3.1. Preparation of the PE sorbent (Particle Sizing and Surface treatment)

These were based on the optimised particle sizes, sorbent quantities, and corresponding surface treatments, such as shredded-roughened (X), Shredded (W), or UV-weathered (0-hour weathered, also denoted as W), selected by the model (detailed in Appendix B12–B15 of Chapter 6). The particle sizes were prepared following the procedure outlined in Section 3.1.1.1.

7.3.2 Packing Method

The PE sorbents were used in two different scaled-up quantities: 5 g and 2.5 g. The sorbent was carefully added into a 50 cm-long column (with a diameter of 1.5 cm) and compressed using a spatula to create a uniformly packed bed of consistent height for each set. Efforts were made to ensure that the bed heights in the column were approximately the same for both sets. For the 5 g set, the height was approximately 18 cm, while for the 2.5 g set, it was approximately 10 cm. Packing density calculations are shown in Appendix C2.

7.3.3 Preparation of the Oil-Water Mixture

The method for preparing the oil-water mixture, as described in Section 3.3.1, was followed, with the specified quantity of oil in the optimised conditions scaled up by a factor of 5. The oil-water mixture was thoroughly mixed by stirring to give a uniform distribution, then allowed to settle back to a separated mixture before being passed through the column.

.

7.3.4 Column Loading and Flow Initiation

The prepared oil-water mixture was slowly poured into the top of the column, allowing it to flow vertically from top to bottom, ensuring initial contact with the PE adsorbent. The time is noted from when the mixture is poured into the column and outflow time when water, oil-water and oil start to drop from the base of the column. The flow was allowed to continue until it stopped.

7.3.5 Sorbent removal after oil adsorption measurement

The saturated PE adsorbent was carefully removed from the column by pushing it from the inlet through the outlet. The sorbent was placed on a sieve at a 45° angle for 5-10 minutes to allow drainage of any easily removed oil. The drained sorbent was weighed, placed in a glass dish, and oven-dried to remove any trapped water. Oil adsorption quantification followed the procedure outlined in Section 3.15.

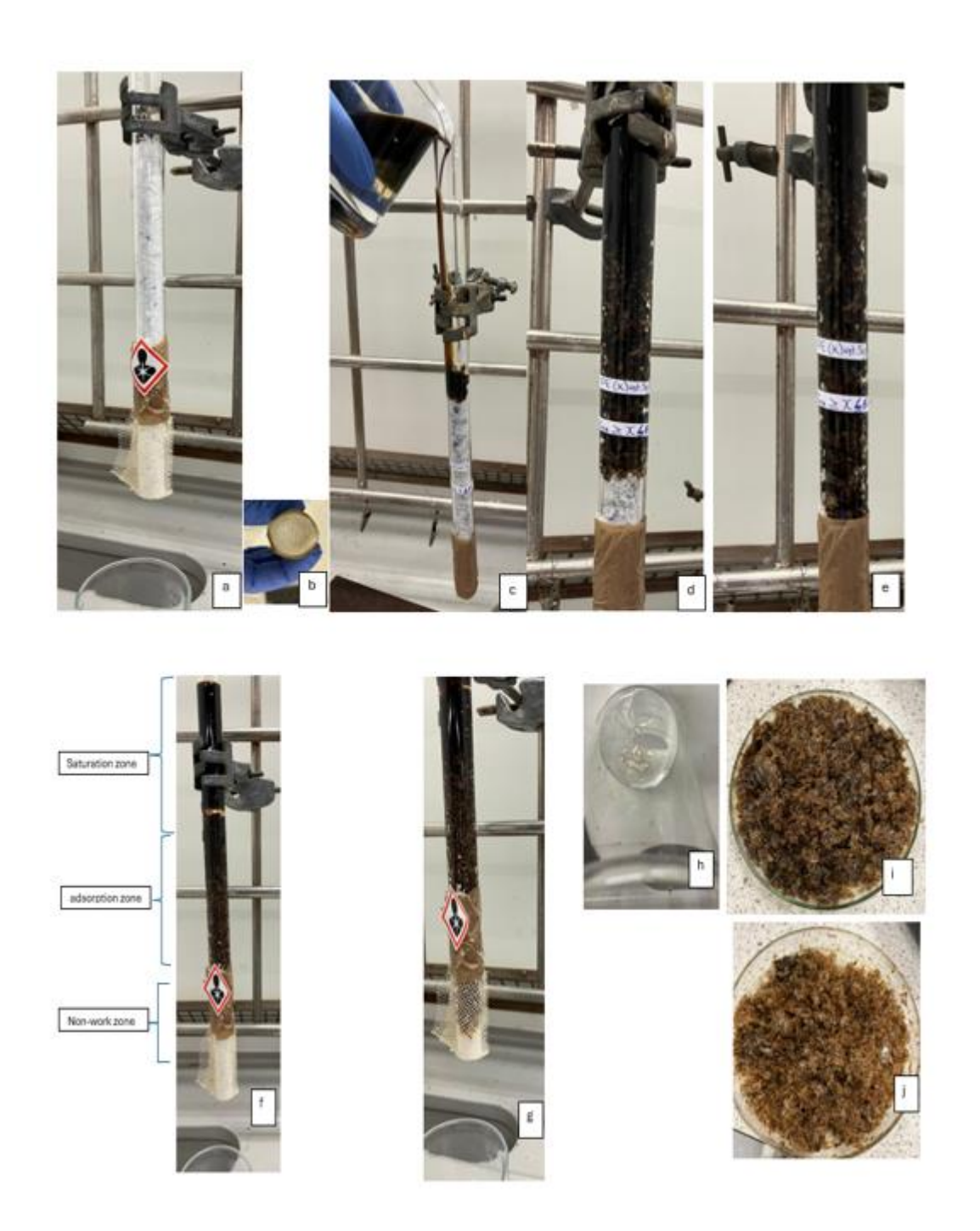


Figure 7. 1: (a) Column filled with PE sorbent and secured with a flexible sieve net at base (b) base of column (c) Oil-water mixture pouring into the column (d)- (g) gradual movement/shift of the adsorption zone downwards and the shrinking of the non-work zone (h) water exits first from the column (i) adsorbent removed from the column and spread in a glassware before put in oven (j) adsorbent after oven-drying.

7.3.6 Result of column experiment

The results are summarised in Appendix table C2.

Figure 7.1 (a-j) illustrates the process/stages of the preliminary column adsorption experiment using polyethylene (PE) as the adsorbent to remove oil from the prepared oilwater mixture. The column is packed with PE sorbent material and secured with a flexible net at the base, to prevent particle loss while allowing liquids to flow through unobstructed. A close-up view of the column's base (b) shows the dimensions of the sieve net supports. Achieving a uniform packing density throughout the column was challenging and this could impact the accuracy and efficiency of the results. Thus, it is assumed that there was non-uniform packing of the column because the adsorbent material was hand packed.

The oil-water mixture was gently poured into the top of the column, to initiate the adsorption process. As the mixture flowed downward through the PE sorbent bed, an adsorption zone formed and gradually shifted downward, visibly accumulating oil within the sorbent. The PE sorbent selectively adsorbed the oil due to its hydrophobic nature, allowing water to flow freely and exit at the base. The shrinking of the non-work zone and the downward movement of the adsorption zone, as captured in the images, confirmed the ongoing adsorption process and the oil retention within the PE bed.

7.3.7 Observations in the column experiment

The water exits the column at the bottom first (between 2-4 minutes for the shredded PE (W) and between 7-10 minutes for shredded-roughened PE) before a mixture of oil-water is observed. This occurs first in a reduced oil concentration, which gradually leads to increased oil-water concentration. Finally the oil starts to drop within a short period (2-3 minutes) after water drop (assumed saturation/break-through point). From the start to end, the drops come fast at the start, gradually slow down, and finally stop after some time. This aligns with the principle of hydrophobic adsorbents preferentially adsorbing oil while allowing water to pass through, thus, this selective behaviour is attributed to the hydrophobic nature of polyethylene (PE), which repels water molecules while forming stronger interactions with oil molecules, as noted in prior studies on polymer-based sorbents for oil removal (95, 96). The delayed appearance of oil in shredded-roughened PE compared to shredded PE highlights the role of surface modifications in enhancing adsorption capacity as was described in Chapter 6 (Figures 6.3 – 6.5) with batch adsorption, where shredded-roughened PE consistently out-

performed the shredded PE in terms of adsorption capacity. This also aligns with the result of the contact angle characterisation of the roughened PE in Section 4.2.4 which shows that it is expected that the surface modification will enhance the polyethylene's ability to sorb crude oil by increasing the surface energy and wettability. This surface roughening increases the surface area and provides more active sites for oil adsorption, which may have led to better oil retention and slower breakthroughs (98). So, the gradual increase in oil concentration at the column outlet until the breakthrough point reflects the progression of the adsorption zone, a characteristic observed in fixed-bed column studies. This progression indicates that the adsorption sites within the sorbent bed are gradually becoming saturated, which is critical for predicting the operational limits of the column. Similar trends have been reported in column experiments using other hydrophobic materials, where the saturation of the sorbent correlates with the movement of the adsorption front (98, 105, 106, 80).

After holding the PE in a sieve inclined at approximately 45 degrees for 5 minutes to drain excess oil, it is observed that only a few drops of mostly oil (less than 0.5 g) is drained, unlike during batch experiments the oil-water mixture (more than 1g) drains. This suggests that the dynamic flow in the column setup facilitates stronger interactions between the oil and the PE sorbent. Prior research has shown that continuous flow systems, such as columns, promote better contact between the adsorbate and adsorbent, enhancing retention and reducing free drainage. In contrast, static conditions in batch experiments may allow for easier detachment of loosely bound oil. This is because the column setup likely does not adsorb as much loosely held oil in the first place as the dynamic flow conditions flush out or prevent the attachment of loosely held oil, being weakly attached cannot resist the shear forces or pressure gradients present in a column system. In contrast, the batch system allows loosely bound oil to adhere temporarily because there is no flow to disrupt this weak attachment, thus this explains the greater amount of oil lost during drainage. This finding aligns with previous studies emphasising the superior efficiency of dynamic systems for oil-water separation (104, 107).

The manual packing of the column, leading to non-uniform packing density, could have introduced variability in the adsorption process. Non-uniform packing can cause preferential flow paths (channelling) and reduce contact between the oil-water mixture and the sorbent, as highlighted by Zhang et al. (106). This effect could explain the inconsistencies in flow rates and the accumulation of oil-water mixtures in the column headspace. Furthermore,

channelling can result in uneven saturation of the sorbent bed, reducing the effective utilization of the PE sorbent.

Table 7. 2: Comparing the predicted values of the model for the oils in a batch experiment with the scaled-up values in the column adsorption experiment

Type of oil	Response	Type of adsorbent/	Target	Model	Desirability	Column	Confidence interval (95%)	
		particle size		Predicted values (batch experiment)		adsorption result	Low	High
Phillip synthetic oil	Adsorption capacity (g/g)	X 2.8 mm ≤ x ≥ 2.0 mm	Maximise	8.005 g/g ± 0.29	0.857	7.62	7.35587	8.65307
	Adsorption efficiency (%)	X 8 mm ≤ x ≥ 6.3 mm	Maximise	83.83% ± 4.938	0.832	60.24%	73.64%	94.53%
	Adsorption capacity (g/g)	O hr UV-weathered 2.8 mm \leq x \geq 2.0 mm	Maximise	3.825g/g	0.794	6.28 g/g	2.85	5.399
	Adsorption efficiency (%)	O hr UV-weathered 8 mm ≤ x ≥ 6.3 mm	Maximise	57.05% ± 4.808	0.818	58.48%	47.21%	66.87%
Natural crude oil	Adsorption capacity (g/g)	X 2.8 mm ≤ x ≥ 2.0 mm	Maximise	5.85g/g ± 0.245	0.873	8.6 g/g	4.75g/g	6.968g/g
	Adsorption efficiency (%)	X 8 mm ≤ x ≥ 6.3 mm	Maximise	76.15% ±2.22	0.844	62.88%	71.52%	80.77%
	Adsorption capacity (g/g)	O hr UV-weathered 2.8 mm \leq x \geq 2.0 mm	Maximise	5.96g/g ± 0.319	0.952	7.12 g/g	5.08g/g	6.825g/g

Adsorption	O hr UV-weathered	Maximise	73.1%±5.087	0.724	46%	61%	85%
efficiency (%)	6.3mm ≤ x ≥ 2.8 mm						

Phillip oil:

For Phillip oil, the smaller particle size (X) of 2.8 mm \le x \ge 2.0 mm, the model predicted the value of 8.005g/g±0.29, while the column adsorption result is 7.62 g/g. The confidence interval (95%) of the batch result is (7.35587, 8.65307), which encompasses the column result, suggesting consistency between batch and scaled-up column results. For 0hr UV-weathered PE (W), with the same particle size, the predicted adsorption capacity is significantly lower at 3.825g/g in the batch, with the column result at 6.28 g/g. This suggests that there is a positive effect using the column for the adsorption. This agreement indicates that the column system maintains comparable adsorption performance, validating the model's reliability.

The predicted adsorption efficiency for the larger particles sizes (X) of 8 mm \le x \ge 6.3 mm, is 83.83%±4.938 in batch experiment, with a scaled-up efficiency of 60.24%. in the column experimental result. This is significantly lower than the batch result, suggesting that the efficiency reduces when scaled up or other factors which occurred during the column adsorption might have affected its efficiency. Unlike for the 0hr UV-weathered PE with larger particles, the batch efficiency is 57.05%±4.808, and the column result is 58.48%. There is an alignment between the predicted value of the batch and the column adsorption efficiency.

Natural Crude Oil:

The adsorption Capacity predicted by the model for the smaller particle size of $2.8 \text{ mm} \le x \ge 2.0 \text{ mm}$ (X) in batch is $5.85 \text{g/g} \pm 0.245 \text{ but } 8.6 \text{ g/g}$ was achieved in the column experiment. This difference indicates that column conditions improve adsorption for natural crude oil. The same for the 0hr UV-weathered PE of the same size, the predicted adsorption capacity in the batch is $5.96 \text{g/g} \pm 0.319 \text{ but } 7.12 \text{ g/g}$ was achieved in the column experiment, indicating a consistent increase in adsorption capacity as well.

For the predicted adsorption efficiencies for both the 8 mm \le x \ge 6.3 mm (W) and 6.3mm \le x \ge 2.8 mm 0hr UV-weathered PE in batch (76.15%±2.22 and 73.1%±5.087 respectively) in batch, with a column result of 62.88% and 46% respectively for the two particle sizes. This suggests reduced efficiency in scaled-up experiments. The significant drop implies that column adsorption efficiency decreases drastically in the column adsorption, possibly due to the methodology problem.

These results show that batch adsorption experiments can predict scaled-up column performance to some extent, but discrepancies exist, especially in adsorption efficiency. This difference might be due to factors like flow dynamics, channelling effects, or incomplete contact in columns. Moreover, these experiments are larger scale than the batch, so gravity and compression from above could squeeze out oil.

7.3.8 Formular used for the calculations for the values on the Table 7.1

(i) Flow rate (Q):

$$Q = \frac{V}{t}$$

Where Q = flow rate (ml/min or L/h)

V= Volume of liquid passing through (ml or L)

t = time (minutes or hours)

(ii) Packing density

$$\rho p = \frac{m}{V}$$

where ρp = packing density (g/cm³ or kg/L)

m = Mass of adsorbent material (g or kg)

V = Volume of the packed bed in the column (cm³or L)

If the packed bed height is uniform, the volume is calculated as:

 $V = A \times h$

Where A = Cross-sectional area of the column (cm³) which can be calculated as:

$$A = \pi \times (\frac{d}{2})^2$$

Where d = column internal diameter

Hh = height of the packed adsorbent bed (cm)

Thus packing density $\rho p = \frac{m}{A x h}$

Chapter 8

8.0 Discussion of Results, Conclusion, Limitations, Challenges and Further Work

8.1 Introduction

The primary aim of this study is to understand and evaluate the efficacy of polyethylene as an oil adsorbent for removing crude oil from the water surface, focusing on its adsorption capacity, efficiency, selectivity, and reusability. This study also aims to identify and analyse the critical factors influencing PE's adsorption behaviour, including surface area, hydrophobicity, and oil-to-adsorbent interactions. Ultimately, the findings will contribute to developing optimised PE-based adsorbents with enhanced performance for environmental remediation of oil spills.

The discussions in this chapter will be focused mainly on the discoveries of the characterisation of the polyethylene materials used in the study (including physical and chemical properties), analysis of both synthetic and natural crude oils used (including their chemical and thermal characteristics), and their interactions with the PE. The batch experiments are also discussed, as they provided critical insights that informed the design and optimisation of the final experimental framework. Additionally, the chapter covers the results of the Design of Experiments (DOE), focusing on the process optimisation for adsorption capacity and efficiency. Column adsorption studies was carried out using the optimised conditions obtained from the batch experiment to evaluate performance under continuous flow conditions and assess scalability. Observations, limitations, challenges encountered during the study, and suggestions for future work are also briefly addressed.

8.2 Characterisation of Polyethylene

Characterising wastewater sachets PE is crucial for understanding its composition and evaluating its structural, physical, thermal, and surface properties. These properties play a significant role in determining its effectiveness and efficiency in oil adsorption. By analysing these attributes, we can better assess how PE interacts with oil and optimise its performance for adsorption applications.

Pristine water sachets PE exhibited strong, characteristic FTIR bands such as methylene group vibrations (e.g., 2916 cm⁻¹ and 2849 cm⁻¹ for asymmetric and symmetric C-H stretching). No signs of oxidation or degradation were observed, confirming that the samples were in pristine condition. The wastewater sachets PE being analysed were discovered to be made up of 2 types of PE, LLDPE and LDPE, at almost the same ratio. This was revealed in the characterisation of polyethylene from the DSC thermal analysis, where the melting peaks observed between 115°C and 130°C corresponded to the distinct thermal behaviours of LDPE and LLDPE. LDPE, with its highly branched structure, exhibited lower melting peaks, while the higher melting peaks were attributed to the more crystalline and linear structure of LLDPE. These findings indicate that the PE samples are blends of these two polymer types, contributing to their unique structural and thermal properties. Their thermal properties also revealed inconsistent melting and crystallisation peaks across samples, indicating variations in LDPE and LLDPE contents.

UV-Weathered PE characterised by FTIR, revealed significant structural changes as revealed by their spectra. They showed the emergence of carbonyl and hydroxyl bands, indicating oxidation. These were more pronounced on the front (UV-exposed) side compared to the back. SEM analysis revealed surface degradation in UV-weathered samples, including microcracks and etching, which intensified with prolonged exposure up to 75 hours of double irradiation, which is equivalent to 2x of normal irradiation. The 150-hour UV exposure sample displayed smoother surfaces, potentially due to further degradation, smoothing out earlier cracks. It was identified in the work of Fernando et al on how thermal effects during UV exposure can lead to surface reorganisation and smoothening (127). Also, Rabek in their work on polymer photodegradation showed that prolonged UV exposure of polyolefins leads to complete degradation and erosion of the surface layer (90)

Natural Weathered PE (50 days in sunlight) characterised by FTIR, revealed slower and less pronounced oxidation compared to UV-weathering, with weaker carbonyl bands in their FTIR spectra; thus, surface changes were minimal. Comparatively, natural weathering did not achieve the same extent of degradation or oxidation as the controlled UV-weathering experiments. The SEM analysis also confirmed this as the surface of natural PE had fewer and minor cracks but visually had some colour fading but not as much as the UV weathered PE. Natural weathered PE exhibited subtle colour fading of ink, and changes in

transparency/opaqueness due to the scattering of light on the cracks. This is due to slower oxidation and degradation under natural conditions, compared to the more intense discolouration observed in UV-weathered PE. The pronounced colour fading in UV-weathered PE are attributed to faster oxidation and the formation of degradation products like carbonyl groups, which are less prominent in naturally weathered samples due to lower intensity and variability of sunlight exposure. Another reason for studying UV weathering is that the water sachets (for use as an adsorbent) that were recovered from the environment may have been exposed to sunlight and so may be oxidised before use or before shredding.

Correlation between the natural and UV weathered PE, using an extrapolation method on the area ratio graph of the FTIR analysis for the oxidised region, demonstrated that naturally weathered PE (50 days or 1200 hours in sunlight) corresponded to approximately 168 hours of UV exposure, based on the carbonyl band intensities. Both natural and UV-weathered samples showed a progressive increase in oxidation over time, but the UV-weathering process was significantly faster and more uniform.

SEM analysis highlighted more pronounced surface degradation in UV-weathered PE, supporting the accelerated impact of controlled UV exposure compared to naturally weathered under environmental conditions.

8.3. Effect of shredding and roughening of PE

Oil adheres and forms a thin film on the surface of the PE and remains on the surface of the PE. Since PE is non-porous, surface modification is key to improving adsorption performance. Oil adheres to the surface via van der Waal forces, hydrophobic interactions and surface roughness, forming a thin film rather than being absorbed into the material, as PE lacks internal pores, meaning oil retention occurs only on the surface. There was little evidence of oil penetration or adsorption into the bulk of the polymer since the sample dimensions did not change after soaking in the oil for 28 days.

The physical surface properties of PE, such as its roughness and texture, play a significant role in determining its oil adsorption capacity. Treatments like shredding and roughening modify the surface morphology, enhancing adsorption effectiveness by increasing the available surface area and interaction sites.

Shredding breaks down the PE into smaller, particles with some cracks and curly fibrous strands, while roughening introduces irregularities and increases surface heterogeneity. These treatments are observed to be critical in achieving optimal particle structure for improved adsorption behaviour. As can be seen in the SEM images of the shredded and shredded-roughened PE samples (Figure 4.28), they reveal distinct differences in surface structure, providing insights into the different effects of shredding and roughening treatments. This experiment showed that Shredded PE primarily consist of two structural components: large flakes and strands. The large flakes exhibit relatively shallow pits and grooves, indicating localised stress during mechanical processing. The strands show elongated, fibrous structures with noticeable curling and bending. Stress marks and elongated grooves are also visible, resulting from the mechanical forces applied during shredding. These structural differences showed that shredding induces varying degrees of mechanical deformation, depending also on the equipment used. Depending on the blade design and mode of operation, different shredders may exhibit variations in their structural components.

Shredded PE performed significantly better than larger flat square-shaped PE sheets due to their ability to curl. The shredded PE had a higher adsorption capacity (5-7 g/g) compared to flat PE sheets (1.61 g/g). This was assigned to the curling effects on the shredded PE, which creates more surface area and interstitial spaces for oil trapping.

The shredded-roughened PE, however, demonstrates a significantly rougher texture with prominent peaks, valleys, and random pits visible even at lower magnifications. Higher magnifications reveal a network of microtraps, connected voids and porous cavities, showing that the roughening process significantly alters the PE's topography more than just shredding.

There is also oxidation during the roughening of the PE as shown in the FTIR spectrum at 1720 cm⁻¹ (Figure 4.33) thus increasing its surface energy (Table 4.3), and enhanced adsorption ability over shredded only PE.

Thus, shredding and then roughening increased surface irregularity, which enhanced the material's surface area and potentially introduced additional active sites. It also increased surface energy, making it more suitable for adsorption applications as observed in all the results from both batch and column experiments.

8.4. Effects of Weathering on Surface Morphology

The SEM analysis reveals significant differences in surface morphology between UVweathered, naturally weathered, and mechanically roughened PE samples. UV exposure causes rapid and advanced degradation, including chain scission, oxidation, and surface erosion, as evidenced by cracks and roughness at 75 hours, followed by smoother, more degraded surfaces at 150 hours. In contrast, naturally weathered PE shows only minor surface changes over 1200 hours due to lower UV intensity and environmental factors. The naturally weathered PE (1200 hours with assumed normal IRR = 0.76 W/m²) shows minor surface changes compared to the virgin PE, with only slight roughness. This indicates that natural weathering progresses more slowly than accelerated UV degradation due to lower UV light intensity and certain environmental factors. The slower progression of natural weathering suggests that its effects on surface morphology are less pronounced. So potentially being exposed in the environment, it can still be used for adsorption as the effect of the exposure to the environment did not affect it much after 1200 hours (50 days). The SEM data demonstrates that mechanical roughening produces a more consistent increase in surface irregularity and active sites than natural or UV weathering. While weathering introduces degradation features such as cracks and pits, these effects are less predictable and depend on exposure time and environmental conditions. Shredded-roughened PE, therefore, offers a more controlled approach to enhancing adsorption performance compared to natural or UVinduced modifications.

8.5 Particle Size Distribution and effects on adsorption

Particle size distribution is also a crucial factor influencing PE's adsorption effectiveness. From the results of the experiments (batch and column), smaller particle sizes offer higher surface area-to-volume ratios, facilitating better oil interaction and adsorption capacity. For the shredded PE, particle size characterisation revealed a range of particle sizes, resulting in a mixture of smaller flakes, strands, and larger irregular particles (Figure 4.28). This variability in particle size is likely a result of the shredding process, which generates uneven mechanical stresses across the polymer. In contrast, shredded-roughened PE displayed more uniform particle size shapes, with more consistently uniform particles compared to the shredded-only PE. The roughening process appears to standardise the size to some degree, potentially through secondary fragmentation of larger particles during the treatment process. There tend

to be some flattening out of the curled and stretched-out areas making the PE bigger than the supposed size. In preparation of the PE, after shredding, sieving, and roughening, the PE was used straight after for adsorption, there was no particle size separation again. This has demonstrated superior adsorption performance in both batch and column experiments (as discussed in Chapters 5, 6 and 7). The SEM findings support this, as shredded-roughened PE exhibited a more textured and porous surface at both micro and macro scales, enhancing its adsorption potential.

In column adsorption experiments, the impact of particle size distribution in PE sorbents reveals complex interactions between surface treatment, oil properties, and system dynamics. The data shows that shredded-roughened PE (X) consistently outperforms shredded PE (W) in adsorption capacity, with values of 7.62 g/g versus 6.28 g/g for Phillip oil, and 8.6 g/g versus 7.12 g/g for natural crude oil at 2.8 mm \leq x \geq 2.0 mm particle size. This superior performance of X-type PE is attributed to enhanced surface properties through roughening treatment.

The efficiency of the system varies with particle size and oil type. For larger particles (8mm) \leq x \geq 6.3 mm, shredded-roughened PE achieved 60.24% efficiency with Phillip oil and 62.88% with natural crude oil, while shredded-only PE showed 58.48% and 46% respectively. This indicates that surface roughening maintains its advantage even at larger particle sizes, though the overall efficiency tends to be lower than with smaller particles.

Flow dynamics and flow-through times were markedly different between oil types and surface treatments. With Phillip oil, smaller particles (2.8mm) process more quickly. Shredded-roughened PE requires 4.5 minutes while shredded (W)-type needs 2.5 minutes. However, with natural crude oil, adsorption times increase significantly. It took shredded-roughened PE about 30 minutes and shredded-only PE (3.5 minutes), respectively. This substantial difference suggests that oil type and viscosity can interact strongly with surface treatment effects.

For larger particles, the time differential becomes even more pronounced with natural crude oil, where shredded-roughened PE of particle size $8mm \le x \ge 2.0$ mm requires 45 minutes and shredded-only PE of particle size $6.3mm \le x \ge 2.0$ mm requires 5 minutes. This further indicates that the combination of surface roughening and larger particle size creates more

complex flow paths, leading to longer flow-through times and potentially better oil-sorbent contact.

The packing density remains relatively consistent between material types (0.157 g/cm³ for 5g samples and 0.1415 g/cm³ for 2.5g samples), suggesting that the performance differences arise primarily from surface characteristics and particle size rather than packing variations. However, the manual packing process may have introduced some variability in these results.

These findings demonstrate that particle size effects cannot be considered in isolation, especially in column adsorption, but should be evaluated alongside surface treatment, oil properties, and operational parameters to optimise the system's performance. The enhanced performance of roughened surfaces comes at the cost of longer flow-through times, presenting a trade-off between efficiency and throughput that must be considered in practical applications.

8.6 PE chemical composition, hydrophobicity and oil selectivity

Polyethylene is a non-polar polymer composed of long chains of hydrocarbons, giving it a chemically inert nature and low surface energy. This molecular structure inherently promotes oil selectivity due to the compatibility between the non-polar nature of PE and oil molecules. Oils, being primarily composed of hydrocarbons, exhibit stronger van der Waals interactions with PE surfaces compared to water, a polar substance. This selectivity forms the basis of PE's effectiveness in separating oil from oil-water mixtures.

The FTIR results for pristine PE in Figure 4.9 confirm the absence of polar functional groups, emphasising their chemical inertness and hydrophobic nature characterised by strong bands around 2916 cm⁻¹ and 2848 cm⁻¹, corresponding to the symmetric and asymmetric stretching vibrations of methylene (-CH₂) groups. These non-polar functional groups contribute directly to its hydrophobic properties. Conversely, some surface modifications (roughening and UV-weathering) exhibited bands around 1720 cm⁻¹, attributed to carbonyl (-C=O) groups formed through oxidation. This suggests that while PE retains its hydrophobic base structure, roughening and prolonged weathering introduces polar functional groups, which may reduce its hydrophobicity and impact oil selectivity over time (Figures 4.33, 4.34 and 4.21). Also, the spectral bands (Figures 4.14 and 4.15) at 1640 cm⁻¹ (C=O stretching) and 3300 cm⁻¹ (N-H

bending) indicate an amide band, suggesting that the ink markings on the PE is a polyamide-based ink resin, while the 1740 cm⁻¹ band (C=O stretching) suggests a polyester-based matrix, with hydrophilic groups (N-H and C=O) that may alter the surface polarity, as seen in the preliminary experiments (sections 5.2 and 5.3) where the shredded PE adsorbed some water droplets. In the presence of only water, water is more likely to be adsorbed to the ink marking than the PE, the water adsorption on the markings could be at the molecular level though cannot be proved. but in the presence of both oil and water, the oil dominates over the water and is adsorbed unto both the PE and the markings. Thus, the overall structure remains dominated by non-polar chains, retaining sufficient hydrophobicity for effective oil adsorption. This selective behaviour reinforces PE's preference for oil over water. Water repellence prevents water from spreading across the PE surface, ensuring that oil molecules dominate the adsorption process even in the presence of water. Together, these hydrophobic and water-repellent properties are critical in driving PE's selective adsorption behaviour, enabling higher oil uptake while minimising water adsorption.

The contact angle values in Table 4.3 further illustrate the wettability characteristics of various PE samples, while pristine PE has a high contact angle value ($>90^{\circ}$), surface roughening and UV weathering decrease the water contact angle by introducing morphological changes (micro- and nanoscale surface irregularities) and surface oxidation, thereby increasing wettability and surface polarity. These modifications raised its surface energy, making the surface more hydrophilic, but also enhanced its oleophilic properties with increased PE's affinity for crude oil (crude oil contact angle for pristine PE = 26° , while roughened and weathered PEs were all 0° , and the contact angle for diiodomethane were all reduced), ultimately improving its ability to sorb crude oil efficiently.

The results from Chapter 5 (batch adsorption) and Chapter 7 (column adsorption) further emphasise the role of PE's chemical composition and hydrophobicity in oil selectivity. In the batch system, the PE's nonpolar nature ensured consistent oil adsorption in static conditions. Shredded-roughened PE outperformed shredded-only PE, with smaller particle sizes showing higher adsorption capacities due to increased surface area, structural irregularities and enhanced hydrophobic interactions. Under dynamic flow (column), the hydrophobic properties of PE ensured the effective separation of oil and water. Shredded-roughened PE delayed oil breakthrough and demonstrated higher oil retention than shredded-only PE,

linking surface modifications to improved performance. This supports the scalability of PE's hydrophobic and selective behaviour, validating its use in real-world oil-water separation systems, especially for the removal of oil spilt on water surface.

The hydrophobic nature of PE is complemented by its thermal and mechanical resilience, which ensures consistent performance across various environmental conditions. Thermal analysis in Chapter 4, including DSC and TGA analysis, demonstrated that PE maintains a temperature stability of up to 300°C. Mechanically, PE is a robust material that withstands the stresses of shredding, roughening, and repeated adsorption cycles (of up to 18) as shown in the preliminary batch experiments. This high mechanical and thermal tolerance is essential for practical applications, such as oil spill remediation, where both mechanical and thermal ruggedness is needed. We should also consider that as the environmental temperature increases, the PE flexibility might be affected.

Additionally, while roughening improves adsorption capacity, it may also increase the risk of structural degradation during prolonged use because of the abrasion it was subjected to during the roughening process. Though not verified but assumed, the roughened PE might not be able to be recycled as much as the 18 cycles of shredded-only PE. Rabek et al. (90) stated in their review that all polymeric materials have a limited lifespan, particularly when exposed to harsh environmental conditions such as high temperatures, UV radiation, humidity, and chemical exposure.

8.8 Characterisation of Crude Oils

The GC-MS results revealed that both natural and synthetic crude oils consist of a number of complex compositions, with synthetic oils losing their lighter fractions faster than natural crude oils, as shown by the reduction and disappearance of peaks within the GC-MS limits. TGA analysis indicated that natural crude oil contains a higher percentage of light fractions, while synthetic oils have more medium-weight components, with both exhibiting similar high-temperature fractions. Over time, total weight loss decreases as volatile fractions evaporate and heavier fractions degrade. Interestingly, physical weighing showed faster weight loss in synthetic oils at room temperature, likely due to their composition or properties, despite having fewer volatile components as indicated by TGA. This highlights the need to consider

both analytical techniques and real-world conditions for a comprehensive understanding of crude oil behaviour. After spillage, the composition of oil will change and thus their properties and how they are adsorbed. This is an important factor in determining how effective the PE will be (alongside other factors).

The rheological analysis (Figure 4.53) highlights how crude oil viscosity changes with weathering over time. Pristine crude oil exhibited low viscosity and Newtonian-like behaviour due to its high content of light, volatile hydrocarbons. As weathering progressed, lighter fractions evaporated, leading to increased viscosity and a transition toward non-Newtonian behaviour, where the oil became more responsive to shear stress. By the later stages of weathering, heavier hydrocarbons dominated, causing the oil to thicken significantly. These changes underscore the dynamic nature of crude oil during weathering, affecting its flow properties and handling.

8.9 Optimisation of Adsorption Parameters

The I-optimal design was used to evaluate key factors (adsorbent quantity, particle size, adsorbent type, and, for UV-weathered PE, the time of weathering) influencing adsorption capacity and efficiency. This study revealed that strong interactions exist between these factors, significantly affecting the sorbents' performance (adsorption capacity and efficiency).

8.9.1 Effect of Using Non-Weathered PE

For Phillip Oil, shredded-roughened PE exhibited higher adsorption capacities (up to 8 g/g) and efficiencies (up to 100%) compared to shredded-only PE (6.5g/g and 70% respectively). For Natural Crude Oil, shredded-roughened PE exhibited a lower adsorption capacity of about 6 g/g and efficiency up to 72%., than its performance with Phillip oil.

For both Phillip and natural crude oils, the model's best conditions for adsorption capacity involved shredded-roughened PE, smaller particle sizes, and low adsorbent doses. The smaller particle sizes (2.8 mm \le x \ge 2.0 mm) were more effective for adsorption capacity, while larger sizes (8.0 mm \le x \ge 6.3 mm) provided better efficiency.

The shredded-only PE performed well in the experiment though with lower values because the slightly modified surface (curls and cracks) contributed largely to the adsorption of oil as the cracks and the cup-like curls provide more surface area and sites for oil anchorage. These features helped trap oil and improve the adsorption performance compared to smooth, unmodified PE. Also, the van der Waal forces play a significant role in the interaction between the hydrophobic PE surface and the non-polar oil molecules, as it supports the attachment of oil to the irregular shapes and edges of shredded PE particles to enable it physically trap oil, contributing to its adsorption capacity.

Since shredded-only PE is not weathered, it does not experience structural degradation, and this structural integrity can support consistent oil adsorption performance, although at a lower level than the shredded-roughened and UV-modified PE.

8.9.2 Effect of Using UV-Weathered PE

Although the model selected 0-hour UV weathering as the optimal condition, it is interesting to note that moderate UV exposure (75 hours at double irradiance, IRR = 1.55 W/m², equivalent to 150 hours at normal irradiance) enhanced adsorption performance for both oils. This improvement was attributed to increased surface energy and roughness, as confirmed by contact angle measurements, FTIR, and SEM analyses. However, prolonged weathering (150 hours at double irradiance, equivalent to 300 hours at normal irradiance) led to performance decline due to over-oxidation and structural degradation, resulting in surface erosion.

Adsorption capacity was generally higher for natural crude oil (up to 6.5 g/g) compared to Phillip oil (up to 3.9 g/g). Similarly, efficiency was higher for natural crude oil (up to 80%) compared to Phillip oil (up to 60%). Thus, natural crude oil consistently showed better adsorption results with UV-weathering, due to its higher viscosity and complex hydrocarbon mixture, which formed stronger interactions with the oxidised PE surface.

The model's selection of 0-hour UV weathering as optimal (Appendix B18, B19) suggests that maybe the non-weathered PE maintained its structural integrity and adsorption ability better than UV-weathered PE in the given conditions. Although moderate UV exposure (B24, B25, B26, B27) improved adsorption performance, the variability in results across different exposure times may have led the model to prioritise the most consistent and stable adsorption condition, which was non-weathered PE (0-hour UV-weathered PE). The same adsorption performance for B28 and B29 for 0hr and 75 hr UV-weathered. From the data, the

highest observed adsorption performances were with the 75 hour UV-exposure in most of the graphs for the range of factors investigated (B24, B25, B26, B27).

In conclusion, the sorbent design must balance mechanical modifications, chemical stability and material integrity to maximise adsorption effectiveness. The studies have highlighted the role of increased surface area and roughness in improving oil retention, moderate weathering enhances adsorption, and prolonged weathering will lead to surface degradation and reduced efficiency. Also, oil type, sorbent particle size and dosage affect adsorption. The model will need refinement as it accurately predicted Phillip oil adsorption but overestimated crude oil efficiency, especially for medium-sized particles.

Moderate UV weathering in a control lab setting can be related to natural weathering by considering the intensity and duration of the UV radiation under real environmental conditions. Since natural weathering occurs under fluctuating sunlight exposure with slower oxidation and less surface degradation, an equivalent laboratory UV exposure can be estimated based on solar irradiance levels and cumulative UV dose over time.

8.10 Preliminary column adsorption with optimised conditions scaled up from batch experiment

The scaled-up column experiment (equivalent to 5X the optimised batch conditions) using shredded (W) and shredded-roughened (X) PE sorbents revealed distinct sequential separation patterns. Shredded-roughened PE delayed oil breakthrough and improved adsorption capacity due to its surface modification, which increased active sites and enhanced oil retention. The column's dynamic flow increased oil-PE sorbent interactions, which might have resulted from reduced free-oil drainage observed in batch systems after the experiment (the free-oil drainage accumulated in a cup-like curl drains in the column experiments would drain after the sorbent in a batch experiment is lifted from the mixture, put in a sieve and tilted at an angle to let excess fluids out).

These results confirm the selective oil-water separation capability of PE and highlight the impact of surface roughening on performance. This preliminary column experiment demonstrated greater adsorption capacity and more pronounced differences between shredded-only and shredded-roughened PE sorbent. It also demonstrates that the optimised conditions of the batch experiment perhaps do not fully describe effectively the column

adsorption as other factors play a part in the determination of the column efficiency, for example the column dimensions, flow rates, and sorbent packing techniques should also be optimised, to ensure consistent performance.

8.11 Comparing this work with other previous work carried out on polyethylene-based (LDPE) sorbents

The sorbents in Table 8.1 highlight the potential of waste polyethylene (LDPE) for oil spill cleanup. While LDPE powder and wax exhibit low adsorption capacities (<0.1 g/g) due to their non-porous nature, foamed LDPE sorbents (with adsorption capacities ranging from 3.4 to 12 g/g) perform better. However, foamed LDPE requires intricate crosslinking and foaming processes, which increase production costs. Additionally, these foams are difficult to clean, collapse over time, and are sensitive to organic solvents, leading to issues like swelling or dissolution, which limit their reusability and recyclability (96).

In contrast, shredded PE, though with a lower adsorption capacity (up to 7 g/g), offers superior mechanical durability and high reusability (up to 18 cycles), with no need for chemical additives. Then when mechanically roughened, it achieves up to 8 g/g adsorption capacity. This research highlights the potential of waste polyethylene (LDPE) for oil spill cleanup, offering a simpler, mechanically driven approach compared to other polyethylene-based sorbents.

This work emphasises a simpler and more scalable approach than chemically processed sorbents, making it an eco-friendly, cost-effective alternative for large-scale oil spill remediation. The lack of chemical surface treatments and the low production cost make shredded and shredded-roughened PE a promising option that strikes a balance between adsorption efficiency, reusability, and ease of preparation, positioning it as a practical and sustainable solution compared to more complex polyethylene-based sorbents. Further research on this work is needed to obtain optimised conditions for a large-scale production to increase the adsorption capacity.

Table 8. 1: Comparing this work with other previous work carried out on polyethylene-based (LDPE) sorbents

Sorbent	Preparation	Adsorption	Effect of surface	Adsorption	Scalability/cost/Environmental	Reusability	Reference
material	method	mechanism	modification	capacity	impact	(no of	
						cycles)	
Shredded-	mechanical	Surface	Shredding and then	Up to 8.6 g/g for	Scalable & low-cost (uses waste	No data	This
roughened PE		adsorption	roughening	crude oil	PE sachets) Eco-friendly		research
(LDPE + LLDPE)			introduced cracks,				work
			anchor sites, and				
			increased surface				
			energy				
Shredded PE	mechanical	Surface	Simple shredding	6 - 7.1 g/g for	Scalable & low-cost	18 cycles	This
(LDPE + LLDPE)		adsorption	introduced cracks	crude oil	Eco-friendly		research
			and fibrous cup-like				work
			extensions				
Shredded 75-hr	Physical	Surface	Increased surface	Up to 6.5 g/g for	High energy cost for processing,	No data	This
UV-weathered		adsorption	energy and roughness	crude oil	and might not be eco-friendly		research
(IRR = 1.55			improved adsorption				work
W/m²)							

Shredded 150 hr	Physical		Surface	Smoothed surface,	Up to 3.5 g/g for	High energy cost for processing,	No data	This
UV-weathered			adsorption	over-oxidation and	crude oil	and might not be eco-friendly		research
PE				structural				work
(IRR = 1.55				degradation led to				
W/m²)				performance decline,				
				though there was				
				higher surface energy				
Recycled LDPE	Chemical		Capillary	Chemical crosslinking	4 - 5g/g	Moderate cost,	No data but	(132)
Processed into			action and	and foaming	for crude oil	Less eco-friendly due to	can be reused	
foam			absorption	increased porosity		chemical additives		
(foam 1)			(possesses	and absorption				
			around 75	capacity				
			vol% of					
			pores)					
Recycled LDPE-	Chemical	and	Capillary	Cross-linking and	8-12 g/g for crude	Scalable but limited by	10 cycles	(132)
based foams	thermal		action and	thermal	oil	availability of waste foams.		
initially used for			absorption	enhancement				
various			(96 vol% of	increased the				
packaging			pores)	porosity				
(foam 2)								

LDPE powders	Plasma	Surface	Plasma treatment	<0.10g/g for crude	Costly and energy-intensive,	Limited use	(131)
	treatment	adsorption	increased the	oil	not eco-friendly		
			wettability, leading to				
			hydrophobicity and				
			oleophobicity, but				
			lacks porosity				
LDPE pellet wax	Physical	Surface	Plasma-induced	<0.10g/g for crude	Costly and energy-intensive,	Limited use	131
	(melting and	adsorption	hydrophobicity and	oil	not eco-friendly		
	solidifying)		oleophobicity, but				
			lacks porosity,				
			leading to poor				
			adsorption				
Polyethylene wax	Physical and	adsorption	Chemical	3.4±0.2 g/g for	Low cost, not eco-friendly	Single use	(96)
waste	chemical		modification	crude oil			
			enhanced oil uptake				

8.12 Conclusion

This research bridges materials science and environmental engineering by investigating the fundamental material properties of polyethylene for oil sorption while applying these findings to develop an efficient and sustainable sorbent. A polyethylene-based sorbent has been developed from recycled wastewater sachets PE, demonstrating strong performance in remediating crude oil spills on water surfaces. The results indicate its effectiveness in adsorbing both crude and medium-weight oils, making it a versatile and practical solution. With an adsorption capacity of up to 8 g/g, and reusability of over 18 cycles, this approach proves highly promising for a simply-modified waste material, reducing its cost per use and increasing economic feasibility.

This study directly addresses the first objective of this research work by utilising an abundant, low-cost waste material and modifying it mechanically and through weathering (to mimic natural sunlight) to enhance its hydrophobic and oleophilic properties. It is a readily available waste material in the environment, demonstrating exceptional durability, reducing raw material costs, making it economically viable. Its performance under weathered conditions suggests that Waste water sachet polyethylene (WWSP) would remain effective even after environmental exposure, as the exposure does not compromise its effectiveness, thus expanding its practical applications. The findings also provide insight into the adsorption mechanisms and influencing factors by characterising the different forms of wastewater sachet PE and oil types, aligning with the objective of the study. The comparison of adsorption behaviour across various forms of modified PE (shredded, shredded-roughened and UVweathered) samples offers a deeper understanding of how surface structure and environmental exposure affect their performances. The observed stability of WWSP under natural conditions further expands its practical applications by ensuring its practical applications and its effectiveness even after lying in the environment for some time. Also, the correlation between natural and UV-weathered PE is relevant for accelerating the evaluation of weathering effects in laboratory settings, allowing for predictive modelling of long-term environmental behaviour and optimising the use of natural-weathered PE for oil sorption applications

This developed sorbent provides a solution to two environmental problems simultaneously (waste PE management and oil spill cleanup) with simple/minimal processing requirements means low energy input and reduced implementation costs.

While further research is needed to optimise its application and scalability, these sorbents show promise for deployment in calm, non-windy environments, either in their loose form or encased in suitable containment systems.

Overall, this study has highlighted the potential of the developed PE sorbent as a low-cost, sustainable, and environmentally friendly alternative to expensive commercial adsorbents and surfactants for oil spill remediation.

8.13 Limitations/observations/challenges

While the results of this study are promising, several limitations and observations must be acknowledged which might affect the results while carrying out the experiments.

8.13.1 Limitations

- 1. Actual shapes of PE particles vary. In other words, the particles can be amalgams or clumps that can deform and squeeze through mesh openings. These clumps, when spread on the surface of the oil does not reveal all its surface to make available the binding sites for the oil to attach.
- 2. The particle sizes are not a precise measurement of the mesh opening size: The particle sizes may not be reflective of the mesh size (which is fixed) because the PE particles fold and bend and these do so to different amounts. If these folds and bends are not reproducible, they could give variance.
- 3. The controlled conditions that are inherent in these experiments could undermine the accuracy of these results. In real life, the combinations of several environmental factors, such as wind, waves/currents, and other natural forces, have a considerable influence on the sorbent. Hence, the actual material performance observed in real conditions might not be comparable to those previously measured in laboratory settings.
- 4. For contact angle measurements/analysis, there are some limitations of the goniometer technique (considered to be the most convenient and applicable (88)), for instance, the measurement reproducibility greatly depends on the operation consistency. The telescope-

goniometer instruments still rely on the operator to determine the tangent line of the droplet; thus, there could be significant variation among different operators. Another limitation is that ultrasmall contact angles (usually less than 15°) could be difficult to measure depending on the camera's resolution and sample drop size (120; 121).

- 5. The experiments were conducted under controlled laboratory conditions, which may not fully replicate the complexities of real-world environments. This study did not consider factors such as varying oil compositions, environmental turbulence, and the presence of contaminants on PE and may affect adsorption performance.
- 6. The scalability of the column setup was evaluated on a limited scale. Larger-scale operations may require further optimisation of column dimensions, flow rates, and sorbent packing techniques to ensure consistent performance. The long-term durability and reusability of PE sorbents under continuous operation were not explored, leaving room for further investigation.

8.13.2 Challenges faced

- 1. Procurement of crude oil and transportation to the UK was a big challenge, and it took almost nine months to sort out the first batch.
- 2. Equipment limitations: Surface roughness of PE and the tensile strength of the PE could not be measured quantitatively, as there was no suitable equipment to handle the small particles of PE.
- 3. There was not enough naturally weathered PE to perform any adsorption experiments to be compared with the UV-weathered PE or the correlated time.
- 4. Limited sources of references: The limited availability of references posed a significant challenge during this research, as the topic is relatively novel, and prior studies were scarce. This lack of established references made it difficult to substantiate some of the discoveries and connect them to existing knowledge in the field. Consequently, the work relies heavily on primary experimentation and original observations, which highlights the need for further studies in this area to build a more comprehensive body of literature.

8.13.3. Recommendation for Further work

- 1. Future studies could explore the use of mixed polymer waste blends/ composite formation (polymer waste is often contaminated with other polymers and so may be present in the source of PE) to enhance the long-term stability and hydrophobic properties of the PE. Also comparison with other alternative sorbent materials to evaluate their relative performance, cost, and environmental impact.
- 2. Develop a comprehensive correlation between natural and UV-weathering of PE as this experiment was not controlled with specific conditions to match the two PE samples.
- 3. Future research could focus on balancing surface roughening (to enhance surface area, adhesion, and wettability) with the material's resilience to ensure sustained performance.
- 4. Development of large-scale PE-based sorbent booms for oil spill remediation in stable net structures without creating microplastic pollution.
- 5. Future work should investigate the effects of flow distribution and column packing on adsorption efficiency to bridge any performance gaps observed during scale-up.
- 6. To maintain high adsorption performance during scale-up, column parameters such as packing density, flow rate, and contact time should be optimised.
- 7. Modelling of the Column adsorption results to be used for designing an efficient fixed-bed adsorption system with the optimum required conditions
- 8. To understand their versatility across different spill scenarios, there should be broader tests on the adsorption performance of the developed PE sorbents with various types of crude oil and refined products.
- 9. Investigate the impact of real-world conditions, such as temperature fluctuations, salinity, and turbulence, on the adsorption efficiency of PE sorbents.
- 10. Explore other methods for regenerating and reusing PE sorbents to enhance their cost-effectiveness and sustainability.
- 11. Explore other types of surface modification techniques on the PE for enhanced oil sorption Carry out pyrolysis studies on spent sorbents and investigate other disposal or recycling options for the spent sorbents.

- 12. Study the economics of scaled-up operations to develop industrial-scale processing methods
- 13. Investigate use in land-based oil spill clean-up.

References

- [1]. Okorobia, A. M., & Olali, S. T. (2018). The Historical Trajectory of Crude Oil Exploration and Production in Nigeria, 1930–2015. In *The Political Ecology of Oil and Gas Activities in the Nigerian Aquatic Ecosystem* (pp. 17-31). Academic Press.
- [2]. NNPC, "Newsletter on Oil Production," 2021. (Online). Available: <a href="https://www.nnpcgroup.com/NNPC-Business/Upstream-Ventures/Pages/Oil-Production.aspx#:~:text=%E2%80%8BPRODUCTION&text=Nigeria%20produces%20only%20high%20value,Qua%2Dlboe%20Light%20and%20Ukpokiti.
- [3]. Ite, A. E., Ibok, U. J., Ite, M. U., & Petters, S. W. (2013). Petroleum exploration and production: Past and present environmental issues in the Nigeria's Niger Delta. *American Journal of Environmental Protection*, 1(4), 78-90.
- [4]. Ezeokpube, N. D., Obiora, C. J., & Phil-Eze, P. O. (2014). Environmental problems of sachet water waste disposal in Nsukka urban, Enugu State, Nigeria. *Methodology*, 6(1).
- [5]. Cao, S., Dong, T., Xu, G., & Wang, F. M. (2017). Oil spill cleanup by hydrophobic natural fibers. *Journal of Natural Fibers*, *14*(5), 727-735.
- [6]. Xu, M., Bian, J., Han, C., & Dong, L. (2016). Hydrophobic modification of polypropylene/starch blend foams through tailoring cell diameter for oil-spill cleanup. *RSC advances*, *6*(85), 82088-82095.
- [7]. Feng, J. (2017). Preparation and properties of poly (lactic acid) fiber melt blown non-woven disordered mats. *Materials Letters*, *189*, 180-183.
- [8]. Saleem, J., Ning, C., Barford, J., & McKay, G. (2015). Combating oil spill problem using plastic waste. *waste management*, *44*, 34-38.
- [9]. Ite, A. E., Ibok, U. J., Ite, M. U., & Petters, S. W. (2013). Petroleum exploration and production: Past and present environmental issues in the Nigeria's Niger Delta. *American Journal of Environmental Protection*, 1(4), 78-90.
- [10]. Jordan, R. E., & Payne, J. R. (1980). Fate and weathering of petroleum spills in the marine environment: a literature review and synopsis.
- [11]. Banerjee, S. S., Joshi, M. V., & Jayaram, R. V. (2006). Treatment of oil spills using organo-fly ash. *Desalination*, 195(1-3), 32-39.

- [12]. Aboul-Gheit, A. K., Khalil, F. H., & Abdel-Moghny, T. (2006). Adsorption of spilled oil from seawater by waste plastic. *Oil & gas science and technology*, *61*(2), 259-268.
- [13]. Edoga, M. O., Kovo, A. S., & Oledibe, M. C. (2014). Remediation of a simulated petroleum polluted water using pulverised used: Water sachet (Polyethylene). *J. Chemical Eng. and Materials Science*, *5*, 33-36.
- [14]. Atta, A. M., Brostow, W., Datashvili, T., El-Ghazawy, R. A., Lobland, H. E. H., Hasan, A.
 R. M., & Perez, J. M. (2013). Porous polyurethane foams based on recycled poly (ethylene terephthalate) for oil sorption. *Polymer international*, 62(1), 116-126.
- [15]. Demirbas, A. (2008). Heavy metal adsorption onto agro-based waste materials: a review. *Journal of hazardous materials*, *157*(2-3), 220-229.
- [16]. Ali, I. (2012). New generation adsorbents for water treatment. *Chemical reviews*, 112(10), 5073-5091.
- [17]. Bernard, H., & Jakobson, K. (1972, April). Effectiveness of Devices for the Control and Clean up of Oil Spills. In *Offshore technology conference* (pp. OTC-1525). OTC.
- [18]. Teas, C., Kalligeros, S., Zanikos, F., Stournas, S., Lois, E., & Anastopoulos, G. (2001). Investigation of the effectiveness of absorbent materials in oil spills clean up. *Desalination*, *140*(3), 259-264.
- [19]. Lehr, W. E. (1974). Containment and recovery devices for oil spill cleanup operations. *Journal of Petroleum Technology*, *26*(04), 375-380.
- [20]. Carmody, O., Frost, R., Xi, Y., & Kokot, S. (2007). Adsorption of hydrocarbons on organo-clays—implications for oil spill remediation. *Journal of Colloid and Interface Science*, 305(1), 17-24.
- [21]. Rajakovic, V., Aleksic, G., Radetic, M., & Rajakovic, L. (2007). Efficiency of oil removal from real wastewater with different sorbent materials. *Journal of hazardous materials*, *143*(1-2), 494-499.
- [22]. Arbatan, T., Fang, X., & Shen, W. (2011). Superhydrophobic and oleophilic calcium carbonate powder as a selective oil sorbent with potential use in oil spill clean-ups. *Chemical Engineering Journal*, *166*(2), 787-791.
- [23]. Wu, J., Wang, N., Wang, L., Dong, H., Zhao, Y., & Jiang, L. (2012). Electrospun porous structure fibrous film with high oil adsorption capacity. *ACS applied materials & interfaces*, *4*(6), 3207-3212..

- [24]. Holakoo, L. (2001). *On the capability of rhamnolipids for oil spill control of surface water* (Doctoral dissertation, Concordia University)..
- [25]. Ornitz, B., & Champ, M. (Eds.). (2002). *Oil spills first principles: prevention and best response*. Elsevier.
- [26]. Ladd, R. W., & Smith, D. D. (1970, October). System Study Of Oil Spills Cleanup Procedure. In *SPE Annual Technical Conference and Exhibition* (pp. SPE-3047). SPE.
- [27]. US Department of Agriculture. (2008). Design Guide for Oil Spill Prevention and Control at Substations. Washington, DC.
- [28]. Nomack, M., & Cleveland, C. (2010). Environmental impacts of oil spills. *Encyclopedia of Earth. Eds. Cutler J. Cleveland (Washington, DC: Environmental Information Coalition, National Council for Science and the Environment)*..
- [29]. Lin, C., Huang, C. L., & Shern, C. C. (2008). Recycling waste tire powder for the recovery of oil spills. *Resources, Conservation and Recycling*, *52*(10), 1162-1166.
- [30]. Johnson, R. F., Manjreker, T. G., & Halligan, J. E. (1973). Removal of oil from water surfaces by sorption on unstructured fibers. *Environmental science & technology*, 7(5), 439-443.
- [31]. Saleem, J., Dotto, G. L., & McKay, G. (2021). Current scenario and challenges in using plastic wastes as oil absorbents. *Journal of Environmental Chemical Engineering*, *9*(2), 104822.
- [32]. Graziano, A., Jaffer, S., & Sain, M. (2019). Review on modification strategies of polyethylene/polypropylene immiscible thermoplastic polymer blends for enhancing their mechanical behavior. *Journal of elastomers & plastics*, *51*(4), 291-336.
- [33]. Gulmine, J. V., Janissek, P. R., Heise, H. M., & Akcelrud, L. (2002). Polyethylene characterization by FTIR. *Polymer testing*, *21*(5), 557-563.
- [34]. Mba, I. C., Mba, E. I., Ogbuabor, J. E., & Arazu, W. O. (2019). Causes and terrain of oil spillage in Niger Delta region of Nigeria: The analysis of variance approach. *International Journal of Energy Economics and Policy*, *9*(2), 283-287.
- [35]. Castro, A., Iglesias, G., Carballo, R., & Fraguela, J. A. (2010). Floating boom performance under waves and currents. *Journal of hazardous Materials*, 174(1-3), 226-235.

- [36]. Agarwal, M. (2021). 10 Methods for Oil Spill Cleanup at Sea. Available: https://www.marineinsight.com/environment/10-methods-for-oil-spill-cleanup-at-sea/.
- [37]. National Response Team Science & Technology Committee (2007). Application of sorbents and solidifiers for oil spills. Available: https://www.epa.gov/sites/default/files/2013-09/documents/nrt_rrt_sorbsolidifierfactsheet2007finalv6.pdf
- [38]. ASTM. (2007). Standard Test methods for sorbent performance of Absorbents. Available: https://standards.iteh.ai/catalog/standards/astm/175b5689-a466-48ce-b6eb-4b02eaa006e4/astm-f716-07?srsltid=AfmBOopDYgg12gkaV225OEuJsxEApL-IPTFW_JsFtIqhHQiZhWWhYNny.
- [39]. Mitul, Z. (2004). *Absorbency characteristics of kenaf core particles* (Doctoral dissertation, PhD thesis, North Carolina State University, USA).
- [40]. Chaowalit, S. (2005). A comparative study of the efficiency of oil adsorption between pulp and polypropylene (Doctoral dissertation, PhD Thesis, Mahidol University, Thailand).
- [41]. Chatterjee, P. K., & Gupta, B. S. (Eds.). (2002). *Absorbent Technology. Textile Science and Technology, Volume 13*. Elsevier Science & Technology.
- [42]. Kehinde, O., Ramonu, O. J., Babaremu, K. O., & Justin, L. D. (2020). Plastic wastes: environmental hazard and instrument for wealth creation in Nigeria. *Heliyon*, *6*(10).
- [43]. Odetoye, T. E., Adeniyi, A. G., & Akande, O. (2020). Valorization of post-consumer polythene water sachet and Parinari polyandra shell residue for composites production. *SN Applied Sciences*, *2*, 1-10.
- [44]. Shah, J., Jan, M. R., Mabood, F., & Jabeen, F. (2010). Catalytic pyrolysis of LDPE leads to valuable resource recovery and reduction of waste problems. *Energy Conversion and Management*, *51*(12), 2791-2801.
- [45]. Ladd, R. W., & Smith, D. D. (1970, October). System Study Of Oil Spills Cleanup Procedure. In SPE Annual Technical Conference and Exhibition? (pp. SPE-3047). SPE.
- [46]. Enzler, S. M. (2006). Top 10 of anthropogenic and natural environmental disasters.

 Lenntech, Delft, the Netherlands. Available at:

 https://www.lenntech.com/environmental-disasters.htm

- [47]. Agius, P., Jagger, H., Fussel, D.R., & Johnes, G.L. (1976, May). Clean-Up Of Inland Oil Spills. In *9th World Petroleum Congress, Tokyo, Japan*.
- [48]. Lehr, W. E. (1974). Containment and recovery devices for oil spill cleanup operations. *Journal of Petroleum Technology*, *26*(04), 375-380.
- [49]. Baird, J. (2010). Oil's shame in Africa. Newsweek, 156(04), 27-27.
- [50]. Bhardwaj, N., & Bhaskarwar, A. N. (2018). A review on sorbent devices for oil-spill control. *Environmental pollution*, *243*, 1758-1771.
- [51]. Lessard, R. R., & DeMarco, G. (2000). The significance of oil spill dispersants. *Spill Science & Technology Bulletin*, *6*(1), 59-68.
- [52]. Dahunsi, B. I., Awogboro, O. S., Akinpelu, M., & Olafusi, O. S. (2013). Investigation of the properties of "pure water" sachet modified bitumen. *Civil and Environmental Research*, *3*(2), 47-61.
- [53]. Babatunde, M. A., & Biala, M. I. (2010). Externality effects of sachet water consumption and the choice of policy instruments in Nigeria: evidence from Kwara State. *Journal of Economics*, 1(2), 113-131.
- [54]. Choi, H. M., & Cloud, R. M. (1992). Natural sorbents in oil spill cleanup. *Environmental science* & technology, 26(4), 772-776.
- [55]. https://en.wikipedia.org/wiki/Niger_Delta#/media/File:NigerDeltaStates.png
- [56]. https://nosdra.oilspillmonitor.ng/
- [57]. Hoang, A. T., Nguyen, X. P., Duong, X. Q., & Huynh, T. T. (2021). Sorbent-based devices for the removal of spilled oil from water: a review. *Environmental Science and Pollution Research*, 28, 28876-28910.
- [58]. Oil Absorbent Pom Poms from China manufacturer China Deyuan Marine
- [59]. ITOPF Use of booms in oil pollution response
- [60]. Ge, J., Zhao, H. Y., Zhu, H. W., Huang, J., Shi, L. A., & Yu, S. H. (2016). Advanced sorbents for oil-spill cleanup: recent advances and future perspectives. *Advanced materials*, *28*(47), 10459-10490.
- [61]. Husseien, M., Amer, A. A., El-Maghraby, A., & Taha, N. A. (2009). Availability of barley straw application on oil spill clean up. *International Journal of Environmental Science & Technology*, *6*, 123-130.

- [62]. Asadpour, R., Sapari, N. B., Tuan, Z. Z., Jusoh, H., Riahi, A., & Uka, O. K. (2013). Application of Sorbent materials in Oil Spill management: A review. *Caspian Journal of Applied Sciences Research*, 2(2).
- [63]. Krishnan, M. R., Aldawsari, Y. F., & Alsharaeh, E. H. (2021). Three-dimensionally cross-linked styrene-methyl methacrylate-divinyl benzene terpolymer networks for organic solvents and crude oil absorption. *Journal of Applied Polymer Science*, 138(9), 49942.
- [64]. Wang Jintao, W. J., Zheng Yian, Z. Y., & Wang AiQin, W. A. (2012). Effect of kapok fiber treated with various solvents on oil absorbency. *Journal of Industrial Crops and Products*, 40 (178-184).
- [65]. Suni, S., Koskinen, K., Kauppi, S., Hannula, E., Ryynänen, T., Aalto, A., Jäänheimo, J., Ikävalko, J., & Romantschuk, M. (2007). Removal by sorption and in situ biodegradation of oil spills limits damage to marine biota: a laboratory simulation. *Ambio: A Journal of the human environment*, *36*(2), 173-179.
- [66]. Lee, J., Nam, C., & Lee, H. (2022). Polyolefin-based electrospun fibrous matrices embedded with magnetic nanoparticles for effective removal of viscous oils. *Chemosphere*, 303, 135161.
- [67]. Ghaly, A. E., & Pyke, J. B. (2001). In-vessel bioremediation of oil-contaminated peat. *Energy sources*, *23*(4), 305-325..
- [68]. Kök, M. V., Varfolomeev, M. A., & Nurgaliev, D. K. (2017). Crude oil characterization using tga-dta, tga-ftir and tga-ms techniques. *Journal of Petroleum Science and Engineering*, 154, 537-542.
- [69]. Mojumdar, S., Sain, M., Prasad, R., Sun, L., & Venart, J. (2007). Selected thermoanalytical methods and their applications from medicine to construction: part I. *Journal of Thermal Analysis and Calorimetry*, *90*(3), 653-662.
- [70]. Wang, Y., Ren, S., Zhang, L., Deng, J., Peng, X., & Cheng, H. (2018). New insights into the oxidation behaviors of crude oils and their exothermic characteristics: Experimental study via simultaneous TGA/DSC. *Fuel*, *219*, 141-150.
- [71]. Toledo, M. (2000). Interpreting DSC curves Part 1: Dynamic Measurements.
- [72]. Valentas, K. J., Rotstein, E., & Singh, R. P. (1997). *Handbook of food engineering practice*. CRC press.

- [73]. Q-Lab (2023). LU-8160 A Choice of Lamps for the QUV Accelerated Weathering Tester.

 Technical Bulletin. Available at https://www.q-lab.com/document-library/lu-8160-choice-lamps-quv-accelerated-weathering-tester.
- [74]. Huhtamäki, T., Tian, X., Korhonen, J. T., & Ras, R. H. (2018). Surface-wetting characterization using contact-angle measurements. *Nature protocols*, *13*(7), 1521-1538.
- [75]. Ranowsky, A. (2016). Contact Angle and Surface Tension A Fascinating Liaison. *CSC Scientific Blog.* Available at https://www.cscscientific.com/csc-scientific-blog/how-does-contact-angle-relate-to-surface-tension#:~:text=Low%20contact%20angle%20%3D%20high%20surface,better%20keep%20its%20droplet%20shape.
- [76]. Ghannam, M. T., Hasan, S. W., Abu-Jdayil, B., & Esmail, N. (2012). Rheological properties of heavy & light crude oil mixtures for improving flowability. *Journal of petroleum science and engineering*, 81, 122-128.
- [77]. Rønningsen, H. P. (2012). Rheology of petroleum fluids. *Annual transactions of the Nordic rheology society*, *20*, 11-18.
- [78]. Purdue University (No Date). Scanning Electron Microscope. Available at https://www.purdue.edu/ehps/rem/laboratory/equipment-safety/research-equipment/sem.html.
- [79]. Agilent (No Date). Gas Chromatography/ Mass Spectrometry Fundamentals. Available at https://www.agilent.com/en/product/gas-chromatography-mass-spectrometry-gc-ms/gcms-fundamentals#:~:text=It%20works%20by%20heating%20a,a%20chemical%20(station ary%20phase
- [80]. Majiya, H. M. (2023). Remediation of heavy metals from water using Modified Clay-Chitosan Composites. (Doctoral dissertation, PhD thesis, Sheffield Hallam University, United Kingdom).
- [81]. Q-Lab (2016). LU-8047-TM for QUV accelerated weathering tester. Technical Manual.
- [82]. Crini, G., & Badot, P. M. (2008). Application of chitosan, a natural aminopolysaccharide, for dye removal from aqueous solutions by adsorption processes using batch studies: A review of recent literature. *Progress in polymer science*, *33*(4), 399-447.

- [83]. Öztürk, N., & Kavak, D. (2005). Adsorption of boron from aqueous solutions using fly ash: batch and column studies. *Journal of hazardous materials*, *127*(1-3), 81-88.
- [84]. Mottaghi, H., Mohammadi, Z., Abbasi, M., Tahouni, N., & Panjeshahi, M. H. (2021). Experimental investigation of crude oil removal from water using polymer adsorbent. *Journal of Water Process Engineering*, 40, 101959.
- [85]. Ahmad, A. A., & Hameed, B. H. (2010). Fixed-bed adsorption of reactive azo dye onto granular activated carbon prepared from waste. *Journal of hazardous materials*, 175(1-3), 298-303.
- [86]. Janani, R. (2019). Synthesis and characterisation of sol-gel based ionogels as electrolyte for supercapacitors (Doctoral dissertation, PhD thesis, Sheffield Hallam University, United Kingdom).
- [87]. Ghandi, K. (2014). A review of ionic liquids, their limits and applications. *Green and sustainable chemistry*, 2014.
- [88]. Kwok, D. Y., & Neumann, A. W. (2003). Contact angle measurements and criteria for surface energetic interpretation. *Contact angle, wettability and adhesion, 3,* 117-159.
- [89]. Saleem, J., Riaz, M. A., & Gordon, M. (2018). Oil sorbents from plastic wastes and polymers: A review. *Journal of hazardous materials*, *341*, 424-437.
- [90]. Rabek, J. F., & Rabek, J. F. (1995). Physical aspects of the photodegradation of polymers. *Polymer Photodegradation: Mechanisms and experimental methods*, 1-23.
- [91]. Singh, V., Jinka, S., Hake, K., Parameswaran, S., Kendall, R. J., & Ramkumar, S. (2014).

 Novel natural sorbent for oil spill cleanup. *Industrial & Engineering Chemistry Research*, 53(30), 11954-11961.
- [92]. Ceylan, D., Dogu, S., Karacik, B., Yakan, S. D., Okay, O. S., & Okay, O. (2009). Evaluation of butyl rubber as sorbent material for the removal of oil and polycyclic aromatic hydrocarbons from seawater. *Environmental science & technology*, *43*(10), 3846-3852.
- [93]. Banerjee, S. S., Joshi, M. V., & Jayaram, R. V. (2006). Treatment of oil spill by sorption technique using fatty acid grafted sawdust. *Chemosphere*, *64*(6), 1026-1031.
- [94]. Gurav, R., Bhatia, S. K., Choi, T. R., Choi, Y. K., Kim, H. J., Song, H. S., Park, S.L., Lee, H.S., Lee, S.M., Choi, K.Y. & Yang, Y. H. (2021). Adsorptive removal of crude petroleum oil from water using floating pinewood biochar decorated with coconut oil-derived fatty acids. *Science of the Total Environment*, 781, 146636.

- [95]. Wei, Q. F., Mather, R. R., Fotheringham, A. F., & Yang, R. D. (2003). Evaluation of nonwoven polypropylene oil sorbents in marine oil-spill recovery. *Marine Pollution Bulletin*, *46*(6), 780-783.
- [96]. Hailan, S. M., Krupa, I., & McKay, G. (2024). Removal of oil spills from aqueous systems by polymer sorbents. *International Journal of Environmental Science and Technology*, 1-22.
- [97]. Nandiyanto, A. B. D., Ragadhita, R., & Fiandini, M. (2023). Interpretation of Fourier transform infrared spectra (FTIR): A practical approach in the polymer/plastic thermal decomposition. *Indonesian Journal of Science and Technology*, 8(1), 113-126.
- [98]. Unni, A. B., Chat, K., Duarte, D. M., Wojtyniak, M., Geppert-Rybczyńska, M., Kubacki, J., Wrzalik, R., Richert, R., & Adrjanowicz, K. (2020). Experimental evidence on the effect of substrate roughness on segmental dynamics of confined polymer films. *Polymer*, 199, 122501.
- [99]. Hoang, A. T., Nižetić, S., Duong, X. Q., Rowinski, L., & Nguyen, X. P. (2021). Advanced super-hydrophobic polymer-based porous absorbents for the treatment of oil-polluted water. *Chemosphere*, *277*, 130274.
- [100]. Yamaguchi, M., & Abe, S. (1999). LLDPE/LDPE blends. I. Rheological, thermal, and mechanical properties. *Journal of Applied Polymer Science*, *74*(13), 3153-3159.
- [101]. Cran, M. J., Bigger, S. W., & Scheirs, J. (2005). Characterizing blends of linear low-density and low-density polyethylene by DSC. *Journal of thermal analysis and calorimetry*, 81, 321-327.
- [102]. Cooper, D. A. (2012). Effects of chemical and mechanical weathering processes on the degradation of plastic debris on marine beaches. The University of Western Ontario (Canada).
- [103]. Kok, M. V. (2011). Characterization of medium and heavy crude oils using thermal analysis techniques. *Fuel processing technology*, *92*(5), 1026-1031.
- [104]. Singh, S., Srivastava, V. C., Goyal, A., & Mall, I. D. (2020). Breakthrough modeling of furfural sorption behavior in a bagasse fly ash packed bed. *Environmental Engineering Research*, 25(1), 104-113.
- [105]. Zang, T., Cheng, Z., Lu, L., Jin, Y., Xu, X., Ding, W., & Qu, J. (2017). Removal of Cr (VI) by modified and immobilized Auricularia auricula spent substrate in a fixed-bed column. *Ecological engineering*, *99*, 358-365.

- [106]. Zhang, Y., Wang, F., Cao, B., Yin, H., & Al-Tabbaa, A. (2022). Simultaneous removal of Pb and MTBE by mixed zeolites in fixed-bed column tests. *Journal of Environmental Sciences*, 122, 41-49.
- [107]. Gotore, O., Watanabe, M., Okano, K., Miyata, N., Katayama, T., Yasutaka, T., Semoto, Y., & Hamai, T. (2025). Effects of batch and continuous-flow operation on biotreatment of Mn (II)-containing mine drainage. *Journal of Environmental Sciences*, 152, 401-415.
- [108]. Thibodeaux, L. J., & Mackay, D. (Eds.). (2010). *Handbook of chemical mass transport in the environment*. CRC Press.
- [109]. Fingas, M. (2014). Oil and petroleum evaporation. *Handbook of oil spill science and technology*, 205-223.
- [110]. Fingas, M. (Ed.). (2010). Oil spill science and technology. Gulf professional publishing.
- [111]. Nunez-Delgado, A. (Ed.). (2021). Sorbents materials for controlling environmental pollution: current state and trends.
- [112]. Dave, D. A. E. G., & Ghaly, A. E. (2011). Remediation technologies for marine oil spills:

 A critical review and comparative analysis. *American Journal of Environmental Sciences*, 7(5), 423.
- [113]. Nwadiogbu, J. O., Ajiwe, V. I. E., & Okoye, P. A. C. (2016). Removal of crude oil from aqueous medium by sorption on hydrophobic corncobs: Equilibrium and kinetic studies. *Journal of Taibah University for Science*, *10*(1), 56-63.
- [114]. Choi, H. M., & Cloud, R. M. (1992). Natural sorbents in oil spill cleanup. *Environmental science* & technology, 26(4), 772-776.
- [115]. Quéré, D. (2008). Wetting and roughness. Annu. Rev. Mater. Res., 38(1), 71-99.
- [116]. Cassie, A. B. D., & Baxter, S. (1944). Wettability of porous surfaces. *Transactions of the Faraday society*, *40*, 546-551.
- [117]. Zhu, H., Qiu, S., Jiang, W., Wu, D., & Zhang, C. (2011). Evaluation of electrospun polyvinyl chloride/polystyrene fibers as sorbent materials for oil spill cleanup. *Environmental science & technology*, *45*(10), 4527-4531.
- [118]. Gurav, R., Bhatia, S. K., Choi, T. R., Choi, Y. K., Kim, H. J., Song, H. S., ... & Yang, Y. H. (2021). Adsorptive removal of crude petroleum oil from water using floating pinewood biochar decorated with coconut oil-derived fatty acids. *Science of the Total Environment*, 781, 146636.

- [119]. Torres, C. E., Quezada, T. S., López, I., de La Fuente, I. G., Rodríguez, F. E., Kharissova, O. V., & Kharisov, B. I. (2020). Development of Sorbent Materials based on Polymer Waste and their Compounds with Nanomaterials for Oil Spill Remediation. *Recent Patents on Nanotechnology*, 14(3), 225-238.
- [120]. Brandon, S., Haimovich, N., Yeger, E., & Marmur, A. (2003). Partial wetting of chemically patterned surfaces: The effect of drop size. *Journal of colloid and interface science*, *263*(1), 237-243.
- [121]. Letellier, P., Mayaffre, A., & Turmine, M. (2007). Drop size effect on contact angle explained by nonextensive thermodynamics. Young's equation revisited. *Journal of colloid and interface science*, *314*(2), 604-614.
- [122]. Wang, J., & Zhuang, S. (2017). Removal of various pollutants from water and wastewater by modified chitosan adsorbents. *Critical Reviews in Environmental Science and Technology*, 47(23), 2331-2386.
- [123]. Darmograi, G., Prelot, B., Geneste, A., De Menorval, L. C., & Zajac, J. (2016). Removal of three anionic orange-type dyes and Cr (VI) oxyanion from aqueous solutions onto strongly basic anion-exchange resin. The effect of single-component and competitive adsorption. *Colloids and Surfaces A: Physicochemical and Engineering Aspects*, 508, 240-250.
- [124]. Mansour, M., Bassyouni, M., Abdel-Kader, R. F., Elhenawy, Y., Said, L. A., & Abdel-Hamid, S. M. (2023, July). Artificial Intelligence for Predicting the Performance of Adsorption Processes in Wastewater Treatment: A Critical Review. In *International Work-Conference on Bioinformatics and Biomedical Engineering* (pp. 153-173). Cham: Springer Nature Switzerland.
- [125]. Liang, J., Wu, M., Hu, Z., Zhao, M., & Xue, Y. (2023). Enhancing lead adsorption capacity prediction in biochar: a comparative study of machine learning models and parameter optimization. *Environmental Science and Pollution Research*, *30*(57), 120832-120843.
- [126]. Miranda, M. N., Sampaio, M. J., Tavares, P. B., Silva, A. M., & Pereira, M. F. R. (2021). Aging assessment of microplastics (LDPE, PET and uPVC) under urban environment stressors. *Science of the Total Environment*, *796*, 148914.
- [127]. Fernando, B. M. D. (2011). *Polymer degradation and molecular relaxation during accelerated weathering of coatings*. North Dakota State University.

- [128]. Chakrabortty, S., Nayak, J., & Chakraborty, P. (2022). Chemical stabilization of oil by elastomizers. In *Advances in Oil-Water Separation* (pp. 233-248). Elsevier.
- [129]. Oliveira, L. M., Saleem, J., Bazargan, A., Duarte, J. L. D. S., McKay, G., & Meili, L. (2021). Sorption as a rapidly response for oil spill accidents: A material and mechanistic approach. *Journal of Hazardous Materials*, 407, 124842.
- [130]. Mothé, M. G., Carvalho, C. H., Sérvulo, E. F., & Mothé, C. G. (2013). Kinetic study of heavy crude oils by thermal analysis. *Journal of thermal analysis and calorimetry*, 111, 663-668.
- [131]. Wang, Q., Li, B., Liu, Q., Qi, Y., Zhao, M., Wang, H., ... & Uyama, H. (2022). Facile Preparation of Porous Low Density Polyethylene Monolith for Efficient Oil/Water Separation. *Bulletin of the Chemical Society of Japan*, *95*(6), 978-980.
- [132]. Hailan, S. M., Nogellova, Z., Popelka, A., Ilcikova, M., Mrlík, M., Minařík, A., ... & Krupa,
 I. (2025). Utilization of polyethylene waste for designing foamy oil sorbents. *Emergent Materials*, 1-13.
- [133]. ASTM, F. (2012, November). 726-12 Standard Test Method for Sorbent Performance of Adsorbents. Philadelphia: ASTM.
- [134]. Lee, G., Kim, K. J., Yu, W. R., & Youk, J. H. (2013). The effect of the surface roughness of carbon fibres on CNT growth by floating-catalyst chemical vapour deposition. *International journal of nanotechnology*, *10*(8/9), 800-810.
- [135]. Broje, V., & Keller, A. A. (2007). Effect of operational parameters on the recovery rate of an oleophilic drum skimmer. *Journal of hazardous materials*, *148*(1-2), 136-143.
- [136]. Atlas, R. M. (1995). Bioremediation of petroleum pollutants. *International Biodeterioration & Biodegradation*, *35*(1-3), 317-327.
- [137]. Atlas, R. M., & Bartha, R. (1973). Stimulated biodegradation of oil slicks using oleophilic fertilizers. *Environmental Science & Technology*, 7(6), 538-541.
- [138]. Law, R. J., & Moffat, C. F. (2011). The Braer oil spill, 1993. In *Oil Spill Science and Technology* (pp. 1119-1126). Gulf Professional Publishing.
- [139]. Al-Harbi, O. A., Khan, M. M., & Özgür, C. (2016). Designing of a low cost superhydrophilic membrane for wastewater treatment. *Materials & Design*, *96*, 296-303.
- [140]. Odetoye, T. E., & Adeoye, V. A. (2022). Biocomposite production from waste low-density polyethylene sachets and Prosopis africana pods biomass residue. *FUOYE J EngTechnol*, 7(2).

- [141]. https://www.aiche.org/resources/publications/cep/2015/september/making-plastics-monomer-polymer
- [142]. https://www.britannica.com/event/Deepwater-Horizon-oil-spill/Cleanup-efforts
- [143]. https://texasboom.com/containment-booms/installation-instructions?utm_source)
- [144]. Prince William Sound, AK (Mar. 28) Coast Guardsman checks oil recovery mesh as others steam blast rocks and shorelines soaked with crude oil from the spilled tanker Exxon Valdez.
 - [145]. https://en.wikipedia.org/wiki/Ixtoc I oil spil
 - [146]. https://commons.wikimedia.org/wiki/File:Oil Spill (Nueva Valencia, Guimar as).jpg
 - [147]. Ademiluyi, T., & Akpan, C. (2007). Preliminary evaluation of fuel oil produced from pyrolysis of low density polyethylene water-sachet wastes. Journal of Applied Sciences and Environmental Management, 11(3).
 - [148]. (https://www.agilent.com/en/product/gas-chromatography-mass-spectrometry-gc-ms/gcms-fundamentals#:~:text=It%20works%20by%20heating%20a,a%20chemical%20(stationary%20phase)
 - [149]. https://cdn.standards.iteh.ai/samples/94308/1904a99e34464afcb1db4c5969
 46e03f/ASTM-E473-16.pdf
 - [150]. Fouladi, M., Kavousi Heidari, M., & Tavakoli, O. (2023). Development of porous biodegradable sorbents for oil/water separation: a critical review. *Journal of Porous Materials*, *30*(3), 1037-1053.
 - [151]. Tijani, M. M., Aqsha, A., & Mahinpey, N. (2016). Development of oil-spill sorbent from straw biomass waste: Experiments and modeling studies. *Journal of environmental management*, 171, 166-176.
 - [152]. Al-Majed, A. A., Adebayo, A. R., & Hossain, M. E. (2012). A sustainable approach to controlling oil spills. *Journal of environmental management*, *113*, 213-227.
 - [153]. Lin, L., & Argon, A. S. (1994). Structure and plastic deformation of polyethylene. *Journal of materials science*, *29*, 294-323.
 - [154]. Anejionu, O.C., Ahiarammunnah, P. A. N., & Nri-ezedi, C. J. (2015). Hydrocarbon pollution in the Niger Delta: Geographies of impacts and appraisal of lapses in extant legal framework. *Resources Policy*, *45*, 65-77.

- [155]. Owolabi, R. U., & Amosa, M. K. (2010). Laboratory conversion of used water sachet (Polyethylene) to superwax/gloss like material. *International Journal of Chemical Engineering and Applications*, 1(1), 112.
- [156]. Gupta, S., & Tai, N. H. (2016). Carbon materials as oil sorbents: a review on the synthesis and performance. *Journal of Materials Chemistry A*, *4*(5), 1550-1565.
- [157]. Adelekan, I. O. (2022). Urban Water Supply and Waste Management in Nigeria: Challenges and Prospects. African Journal of Environmental Science.
- [158]. Chukwu, O. E., Musa, T., & Ojo, A. (2024). Plastic Pollution in Nigeria: Trends, Impacts, and Solutions. ScienceDirect. https://www.sciencedirect.com/science/article/pii/S2949750724000294
- [159]. Ezugwu, M., Okafor, C., & Olayemi, F. (2023). Sachet Water Waste Management in Small Nigerian Cities: A Case Study of Kafanchan. International Policy Brief. https://internationalpolicybrief.org/wp-content/uploads/2025/03/ARTICLE-4.pdf
- [160]. GreenHabitat. (2023). Sachet Water Waste: A Case of Uncontrolled Disposal. https://www.greenhabitat.ng/sachet-water-waste-a-case-of-uncontrolled-disposal
- [161]. Olalekan, M. I., Adeniyi, A. O., & Omotayo, A. M. (2020). The Proliferation of Sachet Water Factories in Lagos: Public Health and Waste Challenges. Journal of Urban Studies.
- [162]. UNEP. (2021). The Rarely Told Story of Widely Used Water Sachets. United Nations Environment Programme. https://www.unep.org/news-and-stories/story/rarely-told-story-widely-used-water-sachets
- [163]. Kausar, A. (2020). Surface Modification of Polymer Materials: Methods and Applications. Polymer-Plastics Technology and Materials, 59(7), 625–637. https://doi.org/10.1080/25740881.2020.1713872
- [164]. Uddin, F. (2018). Fundamentals of Materials Science. Springer.
- [165]. Song, S., Zhang, Y., & Li, Y. (2021). Soluble Abrasives for Polymer Surface Treatment: An Eco-Friendly Alternative. Journal of Applied Polymer Science, 138(18), e50481.
- [166]. Rahman, M. M., & Adnan, M. A. (2019). Comparative Study of Abrasive Materials in Polymer Surface Preparation. International Journal of Materials Science and Applications, 8(3), 45–51.

- [167]. Hussein, M., Amer, A. A., & Sawsan, I. I. (2011). Heavy oil spill cleanup using law grade raw cotton fibers: Trial for practical application. *Journal of Petroleum Technology and Alternative Fuels*, 2(8), 132-140.
- [168]. Majiya, H., Clegg, F., & Sammon, C. (2024). A chemometric approach using I-optimal design for optimising Pb (II) removal using bentonite-chitosan composites and beads. *Journal of Environmental Management*, *370*, 122557.
- [169]. Wang, Z., & Fingas, M. F. (2003). Development of oil hydrocarbon fingerprinting and identification techniques. *Marine pollution bulletin*, *47*(9-12), 423-452.
- [170]. Niessen, W. M. (Ed.). (2001). *Current practice of gas chromatography-mass spectrometry*. CRC Press.

APPENDICES

Appendix A1 – A7 (Chapter 4)

Appendix B1 – B30 (Chapter 6)

Appendix C1 – C2 (Chapter 7)

Appendix D – Ethics approval

Appendix A1-A4: GCMS account of the Oil compositions

Appendix A 1: GC-MS account of Natural Crude oil composition

			Crude	oil
Compound Group	Example Compound	m/z (El Mode)	Areas (counts/min) (Peaks with areas from 1500 counts/min)	Retention time (mins)
C1-C40	Alkanes	57	12035.85	4.225
		5/		
			34224.28	6.198
			19216.57	6.453
			34991.08	7.439
			6734.119	8.13
			14110.279	8.555
			34748.553	8.813
			5880.81	9.653
			25222.607	10.024
			54029.651	10.3
			119750.216	11.48
			7003.709	12.211
			9178.199	12.524
			30211.723	12.891
			25902.519	13.177
			4387.44	13.741
			18981.699	14.054
			24247.391	14.16

21562.581	14.442
168343.269	15.622
8224.086	16.421
29245.588	16.541
5041.407	17.01
6321.945	17.183
14752.91	17.928
7763.766	18.047
19339.16	18.183
13716.979	18.428
191443.168	19.567
6411.629	21.618
17070.98	21.969
12477.853	22.21
187482.622	23.281
51582.645	23.781
4943.379	25.142
16839.01	25.53
52047.187	25.842
183393.605	26.771
6534.943	27.373
7089.502	29.104
35433.93	29.305
155117.305	30.053
8254.8375	30.179
50802.383	32.005
6420.833	32.257
137534.112	33.158
5969.294	35.025
103925.114	36.09
28450.947	37.471
82467.294	38.875
79817.706	39.039
56218.929	41.521
17623.917	41.773
42138.177	44.038
29135.854	46.446
21210.165	48.745
14741.189	50.946
10482.564	53.055
7785.862	55.075
5896.642	57.024
2411911.964	

		/1	11000.000	4.208
			19087.404	7.439
			8277.695	8.558
			17410.538	10.024
			24451.528	11.483
			21206.436	12.895
			6261.27	14.061
			8466.375	14.17
			13674.239	14.435
			56519.702	15.622
			27500.915	16.541
			7974.65	18.051
			11410.862	18.183
			8782.3039	18.435
			77580.449	19.571
			4975.165	20.608
			5332.025	21.805
			8766.816	21.965
			5408.287	22.207
			86749.603	23.281
			18907.464	23.785
			8482.711	25.523
			34416.995	25.842
			88879.091	26.768
			6607.527	28.883
			25984.274	29.301
			77837.11	30.053
			33029.076	31.998
			69952.732	33.151
			54735.664	36.093
			11199.037	37.471
			42510.414	38.872
			49824.884	39.045
			30519.663	41.518
			10969.4	41.76
			22945.321	44.042
			15635.04	46.443
			11236.292	48.749
			8124.85	50.939
			6002.15	53.048
			1059304.846	
Naphthalene (C0)	Naphthalene	128	1532.5	11.48

71

11668.888

4.208

			20791.275 2794.9 25118.675	22.622
C1-C4 Naphthalenes	1-4 alkyl substitutions	142		
			22778.45	26.543
			12723.177	27.121
			35501.627	
		156	10072.2784	30.196
			8870.3722	30.669
			6866.4711	30.764
			2909.7875	31.274
			28718.9092	
		170	2712.7353	34.087
			1725.4393	34.57
			1780.0236	34.655
			1630.8331	35.059
			7849.0313	
			no integrated	
		184	peaks	
Fluorene (C0)	Fluorene	166	no integrated peaks	
C1–C4 Fluorenes	Methyl- to tetramethylfluorene	180, 194, 208, 222	no integrated peaks	
Phenanthrene (C0)	Phenanthrene	178	no integrated peaks	
C1–C4 Phenanthrenes	Methyl- to tetramethylphenanthre ne	192, 206, 220, 234	no integrated peaks	
Pyrene (C0)	Pyrene	202	no integrated peaks	
C1-C4 Pyrenes	Methyl- to tetramethylpyrene	216, 230, 244, 258	no integrated peaks	

Chrysene (C0)	Chrysene	228	no integrated peaks
C1-C4 Chrysenes	Methyl- to tetramethylchrysene	242, 256, 270, 284	no integrated peaks
Dibenzothiophene (C0)	Dibenzothiophene (DBT)	184	no integrated peaks
C1–C4 Dibenzothiophenes	Alkyl-DBTs	198, 212, 226, 240	no integrated peaks
Naphthobenzothiophene (C0)	Naphthobenzothiophen e (NBT)	184	no integrated peaks
C1–C4 Naphthobenzothiophene s	Alkyl-NBTs	198, 212, 226, 240	no integrated peaks

Appendix A2: GCMS account of Phillip Synthetic oil composition

			Phillip (oil
Compound Group	Example Compound	m/z (El Mode)	Areas (counts/min) (Peaks with areas from 1500 counts/min)	Retention time (mins)
C1-C40	Alkanes	57	4855.082	4.102
			5026.9272	4.126
			3510.659	4.643
			2829.419	4.667
			3365.122	4.932
			8438.328	4.98
			7329.374	5
			1519.512	5.878
			8135.705	6.055
			5990.282	6.065
			4526.38	6.32
			7652.84	6.333
			1576.962	9.877
			3056.081	10.16

6740.993	11.333
1689.003	11.353
1739.772	11.966
2274.774	12.044
1850.136	12.289
4681.733	12.36
15878.925	12.738
18907	13.023
3929.622	13.578
2968.509	13.636
13673.01	13.894
10145.59	14.006
11968.072	14.275
1660.531	15.343
36565.019	15.465
2071.095	16.033
1754.871	16.282
2755.708	16.367
7365.9475	16.38
2513.592	18.863
2396.151	17.026
1564.419	17.54
8238.163	17.765
2756.806	17.877
1978.392	17.897
7037.828	18.023
7076.218	18.278
28089.492	19.411
3563.824	20.043
1824.622	20.064
1681.645	20.441
3091.318	20.7
4628.161	21.468
1909.198	21.519
2842.746	21.645
6734.943	21.808
6794.38	22.053
16543.074	23.135
1639.572	23.523
9697.937	23.635
2885.126	23.784
4687.622	23.914
2795.779	24.145

			1979.022	24.329
			1630.658	24.342
			1666.378	24.611
			1710.318	24.842
			6497.271	24.985
			2853.368	25.053
			3353.963	25.216
			6884.455	25.373
			5579.74	25.601
			11409.709	26.624
			1460.437	26.76
			1952.206	28.294
			396381.5167	
		71	2725.887	4.089
			3169.809	4.13
			2269.702	6.089
			8186.296	12.738
			1859.336	13.897
			2755.139	14
			6254.518	14.272
			10398.726	15.459
			7723.385	16.384
			4172.859	17.88
			3483.386	18.02
			4046.953	18.271
			10285.799	19.414
			1741.052	21.812
			2427.641	22.053
			6726.118	23.128
			2927.02	23.638
			1578.893	24.992
			1758.924	25.063
			1869.072	25.216
			1810.579	25.386
			4410.668	26.621
			92581.762	
Naphthalene (C0)	Naphthalene	128	no integrated	
	наришионо	120	peaks	
C1-C4 Naphthalenes	1-4 alkyl substitutions	142	no integrated	
2. C. Hapminatonio	any i canonication		peaks	
		455	no integrated	
		156	peaks	

Fluorene (C0)	Fluorene	170 184 166	no integrated peaks no integrated peaks no integrated peaks no integrated peaks
C1–C4 Fluorenes	Methyl- to tetramethylfluorene	180, 194, 208, 222	no integrated peaks
Phenanthrene (C0)	Phenanthrene	178	no integrated peaks no integrated peaks
C1–C4 Phenanthrenes	Methyl- to tetramethylphenanthre ne	192, 206, 220, 234	no integrated peaks
Pyrene (C0)	Pyrene	202	no integrated peaks
C1–C4 Pyrenes	Methyl- to tetramethylpyrene	216, 230, 244, 258	no integrated peaks
Chrysene (C0)	Chrysene	228	no integrated peaks
C1–C4 Chrysenes	Methyl- to tetramethylchrysene	242, 256, 270, 284	no integrated peaks
Dibenzothiophene (C0)	Dibenzothiophene (DBT)	184	no integrated peaks
C1–C4 Dibenzothiophenes	Alkyl-DBTs	198, 212, 226, 240	no integrated peaks
Naphthobenzothiophen e (C0)	Naphthobenzothiophen e (NBT)	184	no integrated peaks
C1–C4 Naphthobenzothiophen es	Alkyl-NBTs	198, 212, 226, 240	no integrated peaks

Appendix A3: GCMS account of Camlab Synthetic oil composition

Compound Group	Example Compound	<i>m/z</i> (El Mode)	Camlab oil	
			Areas (counts/min) (Peaks with areas	Retention time
			from 1500	(mins)
			counts/min)	
C1-C40	Alkanes	57	1580.72	2.77
			3589.53	2.84
			2405.16	2.88
			14485.1	3.41
			21967.5	3.45
			5253.33	3.5
			18768.9	3.58
			19578	3.61
			16576.7	4.11
			17434.5	4.14
			2873.3	4.69
			2695.24	4.95
			2294.56	5
			2343.44	5.03
			11593.3	6.08
			4086.31	6.33
			2710.49	6.35
			5424.38	7.31
			1742.97	9.88
			4500.71	10.2
			21737.8	11.3
			2987.89	12.4
			1892.05	12.6
			10573.2	12.7
			9313.53	13
			2894.22	13.6
			10612.7	13.9
			8419.46	14
			9404.96	14.3
			57329.1	15.5
			1542.34	16.1
			3134.06	16.3
			7258.1	16.4
			2034.82	16.6
			2089.15	17

	4651.01	17.8
	2505.72	17.9
	4363.76	18
	4308.05	18.3
	26046.1	19.4
	1637.69	20.5
	3839.93	21.5
	2419.1	21.8
	2972.43	22.1
	1711.41	22.6
	32826.8	23.1
	13967.1	23.6
	1918.04	23.9
	1558.3	24.6
	2648.64	25
	1954.34	25.2
	3037.65	25.4
	4295.13	25.6
	12278.9	25.7
	33173.7	26.6
	3506.48	27.2
	1601.39	28.7
	2515.5	29.2
	6855.25	29.9
	489720	
71	2729.27	3.21
	2915.78	3.24
	6257.54	3.46
	15976.8	3.58
	14320.4	3.61
	2216.82	3.8
	1892.97	3.82
	13564.4	4.1
	14555.7	4.14
	1502.28	6.1
	1521.34	6.13
	2151.06	7.31
	4118.24	11.3
	4943.47	12.8
	1552.79	13.9
	2968.33	14
	5596.79	14.3
	17838.5	15.5

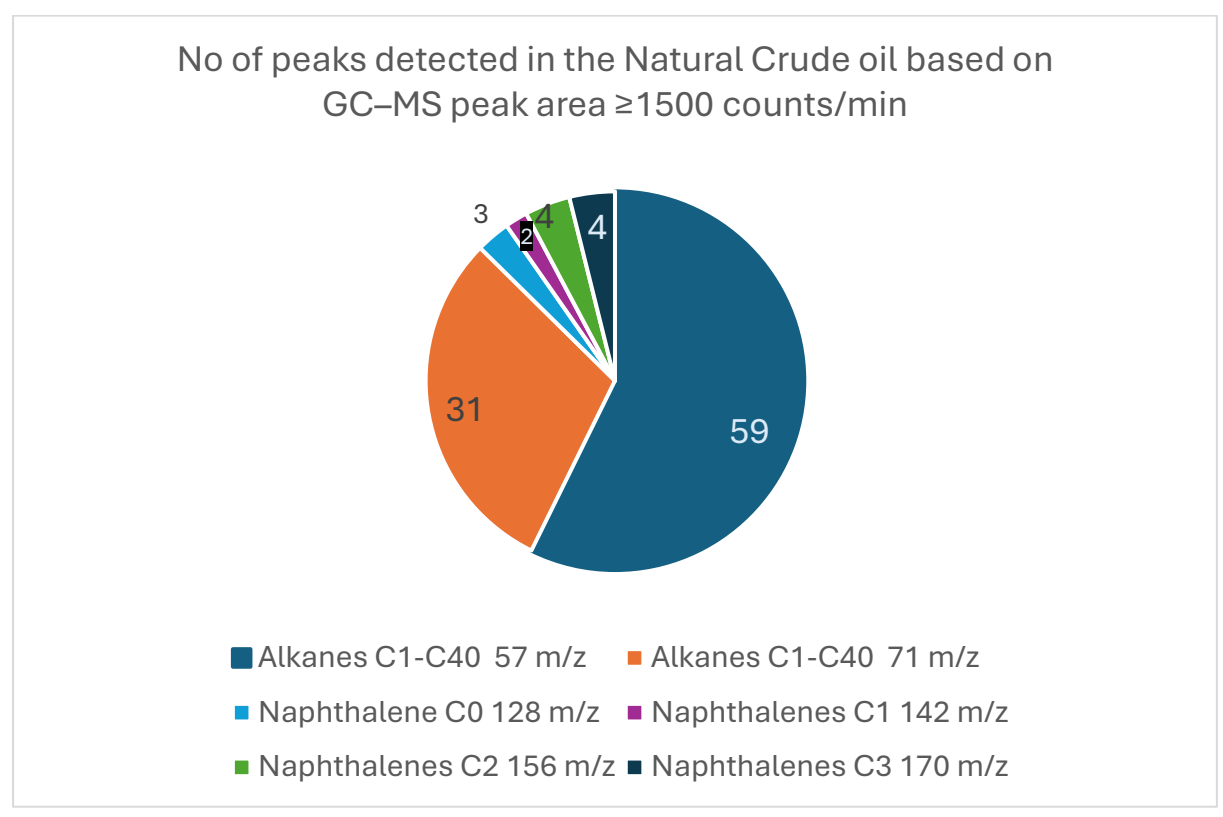
			0004.0
			1587.04
			2729.59
			2447.79
			2486.64
			9984.27
			14014.4
			2815.7
			2163.11
			2270.52
			7631.79
			14941
			1975.05
			2387.65
			190452
Nambahalana (OO)	Nambabalana	400	
Naphthalene (C0)	Naphthalene	128	no integrated peaks
C1–C4 Naphthalenes	1–4 alkyl substitutions	142	
			no integrated peaks
		156	no integrated peaks
		170	no integrated peaks
		184	no integrated peaks
Fluorene (C0)	Fluorene	166	no integrated peaks
C1–C4 Fluorenes	Methyl- to tetramethylfluorene	180, 194, 208, 222	
			no integrated peaks
Phenanthrene (C0)	Phenanthrene	178	no integrated peaks
C1–C4 Phenanthrenes	Methyl- to tetramethylphenanth	192, 206, 2 20, 234	
	rene	·	no integrated peaks
Pyrene (C0)	Pyrene	202	no integrated peaks
C1–C4 Pyrenes	Methyl- to tetramethylpyrene	216, 230, 2 44, 258	no integrated peaks
Chrysene (C0)	Chrysene	228	no integrated peaks

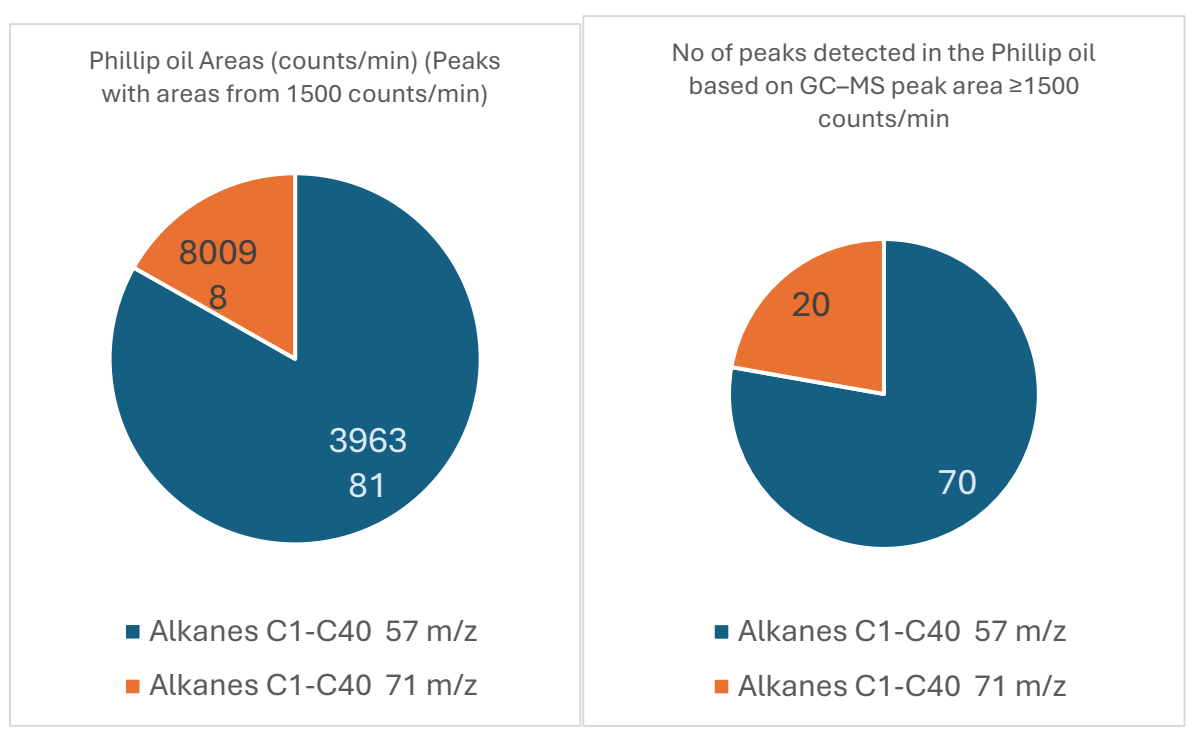
6394.6

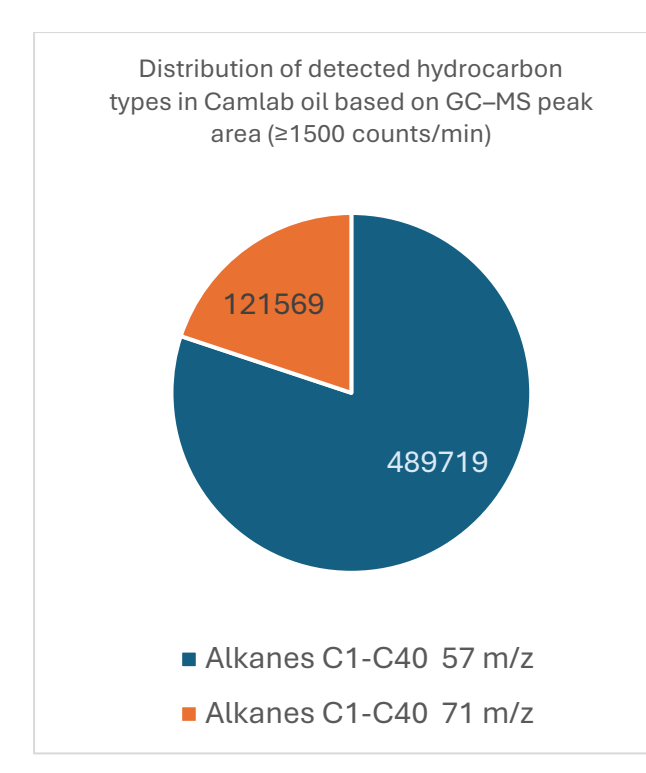
16.4 16.6 17.9 18 18.3 19.4 23.1 23.6 23.7 25.4 25.7 26.6 29.2 29.9

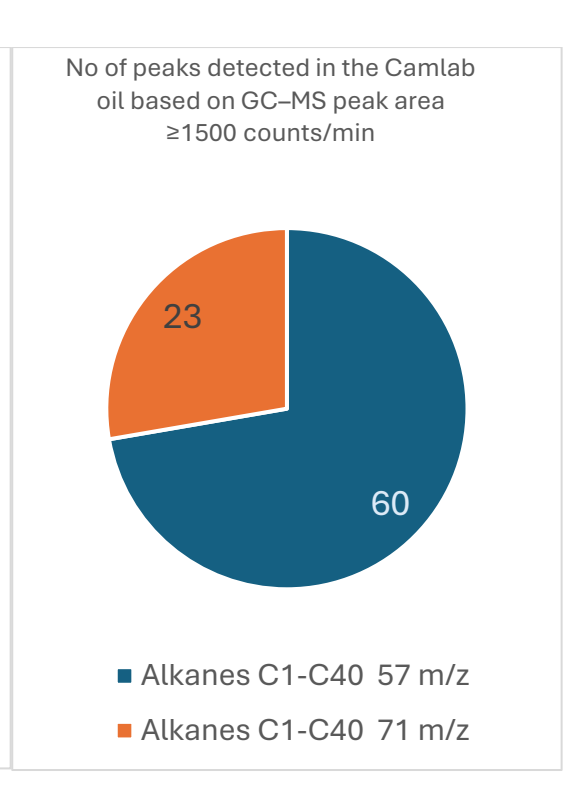
C1–C4 Chrysenes	Methyl- to tetramethylchrysene	242, 256, 2 70, 284	no integrated peaks
Dibenzothiophene (C0)	Dibenzothiophene (DBT)	184	no integrated peaks
C1–C4 Dibenzothiophenes	Alkyl-DBTs	198, 212, 2 26, 240	no integrated peaks
Naphthobenzothiophen e (C0)	Naphthobenzothioph ene (NBT)	184	no integrated peaks
C1–C4 Naphthobenzothiophen es	Alkyl-NBTs	198, 212, 2 26, 240	no integrated peaks

Appendix A 4: Pie chart showing the distribution of hydrocarbon types in crude oil, Phillip and Camlab Synthetic oils based on GC−MS peak area ≥1500 counts/min.









Appendix A 5: GC-MS chromatogram for fresh and weathered crude oil 3

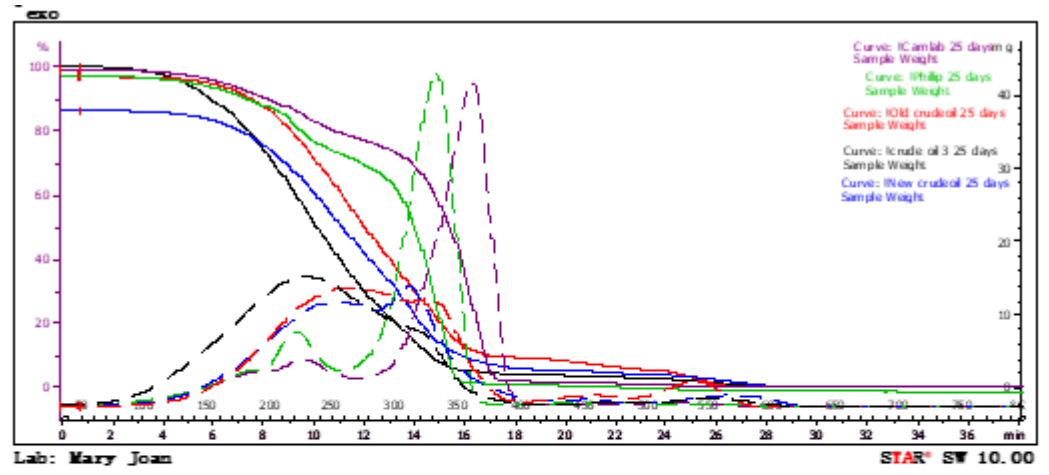


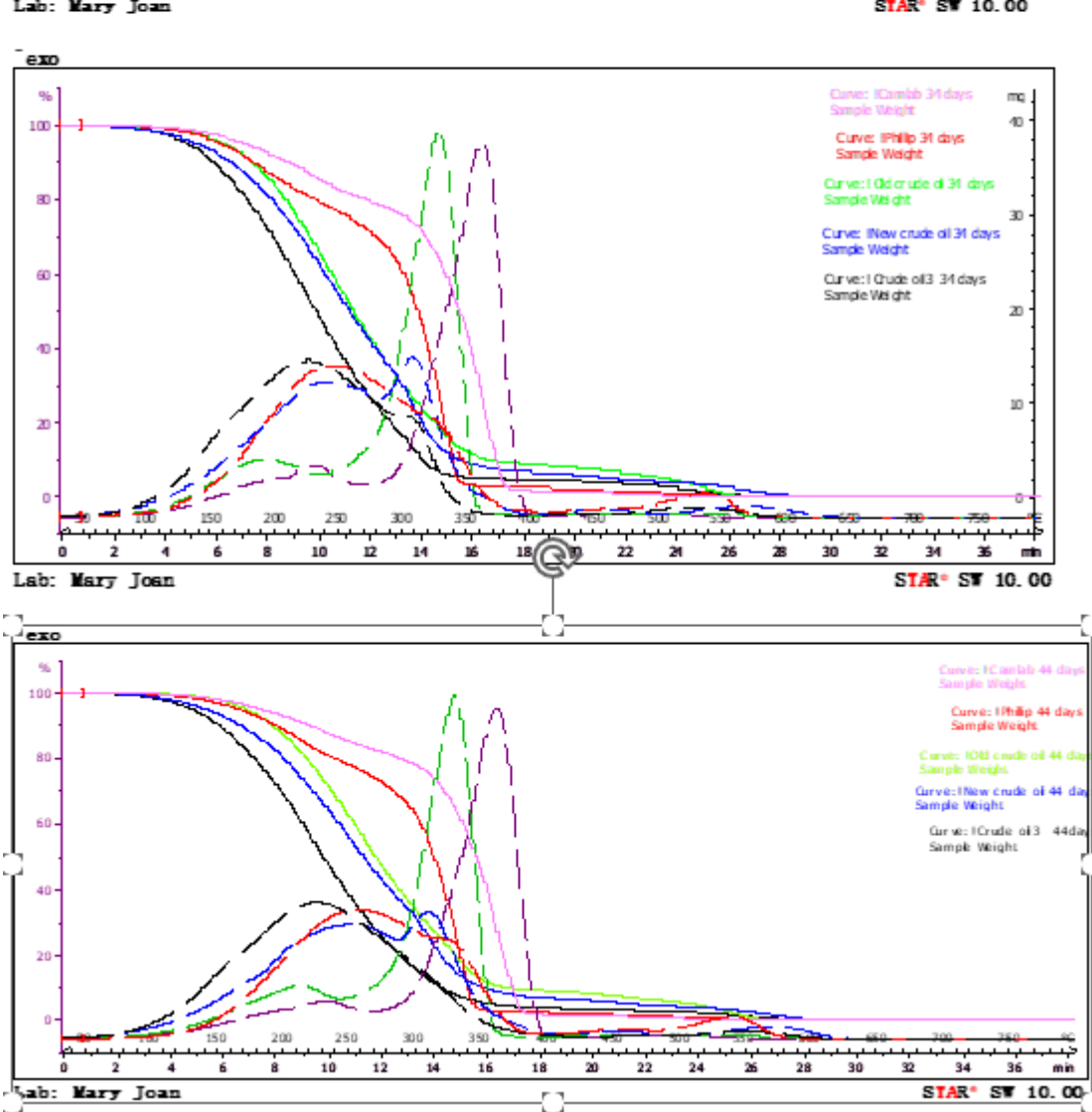
Appendix A 6: Physical weight loss experiment of 20g sample for the different oils in the fume cupboard for 65 days

Days	Camlab oil weight	Phillip oil weight	Natural Crude oil 3 weight
	(g)	(g)	(g)
0	20	20	20
1	18.45	17.74	19.62
2	18.02	17.51	19.44
3	17.88	17.36	19.37
4	17.75	17.27	19.23
7	17.59	16.99	19.19
8	17.54	16.87	19.02
9	17.42	16.72	18.98
10	17.38	16.87	18.86
11	17.35	16.72	18.67
14	17.25	16.50	18.61
15	17.08	16.25	18.49
16	17.00	16.13	18.37
17	16.93	16.03	18.28
18	16.82	15.80	18.16
21	16.68	15.62	18.08
22	16.61	15.53	17.98
23	16.56	15.45	17.92
24	16.53	15.41	17.89
25	16.50	15.38	17.73
28	16.42	15.17	17.61
29	16.39	15.12	17.57
30	16.37	15.11	17.50
31	16.34	15.09	17.45
32	16.32	15.06	17.33
35	16.26	14.98	17.25
41	16.14	14.83	17.22

44	16.10	14.79	17.19
45	16.09	14.74	17.07
46	16.08	14.71	17.03
47	16.06	14.70	16.98
50	16.05	14.69	16.96
51	16.03	14.68	16.93
52	16.01	14.67	16.85
53	15.99	14.65	16.82
54	15.97	14.63	16.81
57	15.96	14.62	16.79
58	15.95	14.61	16.78
59	15.94	14.59	16.72
60	15.93	14.58	16.62
61	15.92	14.57	16.59
64	15.91	14.56	16.58
65	15.90	14.55	16.57
Total	4.1	5.45	3.43
mass			
loss			
20			
19			Camlab oil
18			
(g) SS 17		-	Phillip oil
Па	300		1-0
= 16 Ö			→ Natural
15			Crude oil 3
14			
	0 20	40 60	0
	Day	s exposed	

Appendix A 7: TGA results of weathered Oils for various days





Appendix B

Appendix B 1: A 27-run Optimal Custom design for adsorption factors (generated with Design-Expert® 13 software) for optimal experimental design (I-optimal) of Phillip oil adsorption onto Shredded (W), and shredded-roughened PE (X) with their corresponding responses

							Response 1 (Ad (g/g))	sorption capacity	Response 2 (Adso %)	orption efficiency
	Facto	r 1	Facto	or 2						
	(Mass of PE)		(Mass of oil)		Factor 3	Factor 4				
Runs	Theoretical I	Measured	Theoretical	Measured	(Type of PE)	(Size of PE)	Experimental	Predicted	Experimental	Predicted
1	0.8925	0.89	7.45	7.45	W	2.8 mm	3.73	3.99	32.66	36.38
2	0.5	0.5	8.75	8.75	X	8.0 mm	5.45	5.57	25.42	27.49
3	1.0	1.0	5	5.0	X	8.0 mm	5.15	5.2	82.94	84.27
4	1.0	1.0	5	5.0	W	2.8 mm	3.93	3.73	58.56	64.78
5	0.6525	0.65	6.725	6.73	X	6.3 mm	5.38	5.45	42.53	43.62
6	0.74267	0.74	5.15	5.15	W	2.8 mm	4.39	4.5	48.96	48.80
7	0.96	0.96	6.3	6.30	W	6.3 mm	3.54	3.49	38.71	37.93
8	0.5	0.5	5.9	5.90	X	8.0 mm	5.85	5.78	41.14	43.60
9	0.725	0.73	5.7	5.70	W	8.0 mm	4.10	4.24	39.40	41.10

10	0.9925	0.99	5.687	5.69	W	8.0 mm	4.36	4.08	58.69	54.63
11	0.5	0.50	10	10.0	Χ	2.8 mm	7.00	7.01	30.00	32.60
12	0.59	0.59	9.575	9.58	W	6.3 mm	3.58	3.52	15.89	16.04
13	0.96	0.96	6.3	6.30	W	6.3 mm	3.35	3.49	35.74	37.93
14	0.775	0.78	9.275	9.28	Χ	8.0 mm	6.16	5.64	43.13	37.44
15	0.5166	0.52	7.1	7.10	W	2.8 mm	4.72	4.83	27.05	23.43
16	0.8125	0.81	10	10.0	W	2.8 mm	4.28	3.99	26.62	25.25
17	0.6875	0.69	5	5.0	Χ	2.8 mm	8.03	7.84	96.63	92.20
18	0.5	0.50	10	10.0	W	8.0 mm	4.65	4.52	18.25	20.73
19	0.725	0.73	5.7	5.70	W	8.0 mm	4.15	4.24	40.05	41.10
20	0.59	0.59	9.575	9.58	W	6.3 mm	3.39	3.52	14.70	16.04
21	1	1.0	10	10.0	Χ	6.3 mm	5.58	5.43	45.84	44.95
22	0.5	0.50	5	5.0	W	6.3 mm	3.82	3.64	28.25	27.69
23	0.99	0.99	7.85	7.85	Χ	2.8 mm	6.31	6.5	67.00	70.61
24	0.705	0.71	8	8.0	Χ	2.8 mm	7.16	7.14	54.28	53.00
25	0.6525	0.65	6.725	6.73	Χ	6.3 mm	5.37	5.45	42.36	43.62
26	0.775	0.76	9.275	9.28	Χ	8.0 mm	5.22	5.64	35.27	37.44
27	1	1.0	9	9.0	W	8.0 mm	4.66	4.84	40.70	40.46

Appendix B 2: A 27-run Optimal Custom design for adsorption factors (generated with Design-Expert® 13 software) for optimal experimental design (I-optimal) of Natural crude oil adsorption onto Shredded (W), and shredded-roughened (X) PE with their corresponding responses

							Response 1 (Adsorption (g/g))		Response 2 (Adsor (%))									
	Factor 1		Fact	or 2			(8/8//		(70))									
	(Mass of P												Factor 3	Factor 4				
Runs	Theoretical Mea	•	Theoretical	Measured	(Type of PE)	(Size of PE)	Experimental	Predicted	Experimental	Predicted								
1	0.8925	0.89	7.45	7.45	W	2.8 mm	4.45	4.47	41.31	40.51								
2	0.5	0.5	8.75	8.75	X	8.0 mm	5.22	5.58	24.11	25.25								
3	1.0	1.0	5	5.0	X	8.0 mm	4.88	5.31	77.60	76.15								
4	1.0	1.0	5	5.0	W	2.8 mm	4.27	4.4	65.32	64.91								
5	0.6525	0.65	6.725	6.73	Χ	6.3 mm	5.24	5.14	41.09	41.11								
6	0.74267	0.74	5.15	5.15	W	2.8 mm	4.51	4.52	50.63	49.56								
7	0.96	0.96	6.3	6.30	W	6.3 mm	4.06	3.97	46.67	47.3								
8	0.5	0.5	5.9	5.90	Х	8.0 mm	5.38	5.56	37.12	40.44								
9	0.725	0.73	5.7	5.70	W	8.0 mm	4.50	4.43	44.47	45.58								

Ī	10	0.9925	0.99	5.687	5.69	W	8.0 mm	4.20	4.3	55.87	59.66
	11	0.5	0.50	10	10.0	X	2.8 mm	6.16	5.69	25.80	26.78
	12	0.59	0.59	9.575	9.58	W	6.3 mm	3.56	4.18	15.77	16.57
	13	0.96	0.96	6.3	6.30	W	6.3 mm	4.05	3.97	46.51	47.3
	14	0.775	0.78	9.275	9.28	X	8.0 mm	5.19	5.45	34.99	35.53
	15	0.5166	0.52	7.1	7.10	W	2.8 mm	4.47	4.65	25.26	24.35
	16	0.8125	0.81	10	10.0	W	2.8 mm	4.22	4.53	26.18	29.35
	17	0.6875	0.69	5	5.0	X	2.8 mm	5.66	5.56	64.05	63.08
	18	0.5	0.50	10	10.0	W	8.0 mm	4.76	4.58	18.80	18.45
	19	0.725	0.73	5.7	5.70	W	8.0 mm	4.83	4.43	48.68	45.58
	20	0.59	0.59	9.575	9.58	W	6.3 mm	4.08	4.18	19.01	16.57
	21	1	1.0	10	10.0	Χ	6.3 mm	5.14	5	41.40	41.58
	22	0.5	0.50	5	5.0	W	6.3 mm	4.36	4.18	33.60	33.8
	23	0.99	0.99	7.85	7.85	Χ	2.8 mm	5.30	5.44	54.27	55.19
	24	0.705	0.71	8	8.0	Χ	2.8 mm	5.79	5.58	42.19	41.26
	25	0.6525	0.65	6.725	6.73	Χ	6.3 mm	5.26	5.14	41.30	41.11
	26	0.775	0.76	9.275	9.28	Χ	8.0 mm	5.68	5.45	39.08	35.53
	27	1	1.0	9	9.0	W	8.0 mm	4.78	4.33	42.00	40.56
- 1											

Appendix B 3: A 32-Run I-optimal design for evaluating adsorption factors and responses for Phillip oil adsorption on UV-weathered polyethylene using design-expert® 13 software

							Response 1 (Adso	orption capacity (g/g))	Response 2 (Adsorpt efficiency (%))	ion
	Fa	ctor 1	Factor	2						
	(Ma	ss of PE)	(Mass of	oil)	Factor 3	Factor 4				
Runs	Theoretical	Measured	Theoretical	Measured	(Size of PE)	(UV time)	Experimental	Predicted	Experimental	Predicted
1	0.6	0.60	8.812302927	8.81	2.8 mm	75 hrs	3.25	0.53	22.13	25.76
2	0.7675	0.77	9.525	9.53	6.3 mm	0 hr	2.90	0.59	23.33	24.34
3	0.8075	0.81	5	5.00	2.8 mm	0 hr	3.33	0.51	53.85	52.58
4	0.875	0.88	6.55	6.55	8.0 mm	0 hr	3.01	0.55	40.23	46.16
5	0.5	0.50	10	10.00	8.0 mm	0 hr	3.25	0.55	16.25	13.83
6	0.6272879	97 0.63	10	10.00	2.8 mm	150 hrs	1.39	0.76	8.73	9.97
7	1	1.00	10	10.00	6.3 mm	150 hrs	2.93	0.66	29.30	26.08
8	0.8	0.80	7.875	7.88	6.3 mm	150 hrs	2.20	0.66	22.32	24.99
9	0.8061852	25 0.81	5	5.00	6.3 mm	150 hrs	2.02	0.66	32.54	32.32
10	0.6475	0.65	6.5	6.50	2.8 mm	150 hrs	1.86	0.76	18.50	19.30

11	0.8825	0.88	9	9.00	8.0 mm	150 hrs	2.30	0.65	22.53	24.32
12	0.605	0.61	8.75	8.75	8.0 mm	150 hrs	3.17	0.65	21.89	16.11
13	0.875	0.88	6.55	6.55	8.0 mm	0 hr	3.72	0.55	49.68	46.16
14	0.5	0.50	5	5.00	2.8 mm	75 hrs	5.60	0.53	56.00	48.30
15	0.875	0.50	6.57854824	4 6.58	6.3 mm	75 hrs	3.67	0.52	48.87	47.69
16	0.5	0.50	5	5.00	6.3 mm	0 hr	2.62	0.59	26.20	27.70
17	1	1.00	5	5.00	8.0 mm	75 hrs	2.60	0.61	52.00	50.70
18	1	1.00	10	10.00	8.0 mm	75 hrs	2.51	0.61	25.12	18.16
19	0.58	0.58	7.25	7.25	8.0 mm	75 hrs	3.14	0.61	25.16	26.50
20	0.7675	0.77	9.525	9.53	6.3 mm	0 hr	3.25	0.59	26.17	24.34
21	0.875	0.88	6.57854824	4 6.58	6.3 mm	75 hrs	3.19	0.52	42.41	47.69
22	0.885	0.89	9.03647483	36 9.04	2.8 mm	75 hrs	2.73	0.53	26.73	30.79
23	1	1.00	10	10.00	2.8 mm	0 hr	4.05	0.51	40.50	43.56
24	0.5	0.50	5	5.00	8.0 mm	150 hrs	2.20	0.65	22.00	22.08
25	0.5	0.50	10	10.00	6.3 mm	75 hrs	4.20	0.52	21.00	16.89
26	0.58	0.58	7.25	7.27	8.0 mm	75 hrs	2.45	0.61	19.59	26.50
27	0.975	0.98	6.25	6.25	2.8 mm	150 hrs	2.08	0.76	32.40	30.35
28	0.5	0.50	8.125	8.13	2.8 mm	0 hr	3.86	0.51	23.75	24.94

29	0.5	0.50	8.15	8.15	6.3 mm	150 hrs	2.28	0.66	13.99	14.76
30	1	1.00	7.275	7.28	2.8 mm	0 hr	4.14	0.51	56.85	53.87
31	0.8825	0.88	9	9.00	8.0 mm	150 hrs	2.08	0.65	20.42	24.32
32	1	1.00	5.25	5.25	6.3 mm	0 hr	2.79	0.59	53.14	52.47

Appendix B 4: A 32-Run I-optimal design for evaluating adsorption factors and responses for Natural crude oil adsorption on UV-weathered polyethylene using design-expert® 13 software

					Response 1 (Adsor	ption capacity (g/g))	Response 2 (Adsorption efficiency (%))			
	Fac	tor 1	Fá	actor 2	Factor 3	Factor 4				
Runs	(Mass	s of PE)	(Ma	iss of oil)	(Size of PE)	(UV time)	Experimental	Predicted	Experimental	Predicted
	Theoretica	al Measured	<u>T</u> heoretica	l Measured						
1	6	6.0	8.81	8.81	2.8 mm	75 hrs	5.73	5.94	39.01	42.81
2	0.77	0.77	9.525	9.53	6.3 mm	0 hr	3.51	3.36	28.27	26.21
3	0.80	0.80	5	5.0	2.8 mm	0 hr	3.78	3.69	61.01	56.37
4	0.88	0.88	6.55	6.55	8.0 mm	0 hr	3.87	4.26	51.68	57.25
5	0.5	0.5	10	10.0	8.0 mm	0 hr	5.47	5.43	27.35	26.29

6	0.62	0.62	10	10.00	2.8 mm	150 hrs	3.48	3.36	21.83	17.86
7	1	1.0	10	10.00	6.3 mm	150 hrs	2.31	2.36	23.10	22.7
8	0.8	0.80	7.875	7.88	6.3 mm	150 hrs	2.84	2.94	28.83	32.63
9	0.81	0.81	5	5.00	6.3 mm	150 hrs	3.60	3.49	58.02	52.32
10	0.65	0.65	6.5	6.50	2.8 mm	150 hrs	2.64	2.6	26.35	25.95
11	0.88	0.88	9	9.00	8.0 mm	150 hrs	3.26	2.97	31.97	29.27
12	0.61	0.61	8.75	8.75	8.0 mm	150 hrs	2.75	3.07	19.03	21.4
13	0.88	0.88	6.55	6.55	8.0 mm	0 hr	4.62	4.26	61.76	57.25
14	0.5	0.50	5	5.00	2.8 mm	75 hrs	5.59	5.6	55.92	55.52
15	0.88	0.88	6.58	6.58	6.3 mm	75 hrs	5.57	5.08	74.03	68.35
16	0.5	0.50	5	5.00	6.3 mm	0 hr	3.20	3.29	32.00	32.76
17	1	1.00	5	5.00	0.77	75 hrs	3.66	3.72	73.20	72.65
18	1	1.00	10	10.00	8.0 mm	75 hrs	3.84	3.93	38.40	39.7
19	0.58	0.58	7.25	7.25	8.0 mm	75 hrs	4.78	4.6	38.21	37.07
20	0.77	0.77	9.53	9.53	6.3 mm	0 hr	3.30	3.36	26.59	26.21
21	0.88	0.88	6.58	6.58	6.3 mm	75 hrs	4.59	5.08	61.03	68.35
22	0.89	0.89	9.04	9.04	2.8 mm	75 hrs	5.03	4.81	49.29	45.89
23	1	1.00	10	10.00	2.8 mm	0 hr	4.67	4.8	46.73	47.16

24	0.5	0.50	5	5.00	8.0 mm	150 hrs	2.28	2.25	22.80	22.94
25	0.5	0.50	10	10.00	6.3 mm	75 hrs	5.19	5.19	25.96	24.33
26	0.58	0.58	7.25	7.25	8.0 mm	75 hrs	4.59	4.6	36.69	37.07
27	0.98	0.98	6.25	6.25	2.8 mm	150 hrs	1.88	2.05	29.36	33.73
28	0.5	0.50	8.13	8.13	2.8 mm	0 hr	5.20	5.21	32.00	34.96
29	0.5	0.50	8.15	8.15	6.3 mm	150 hrs	3.03	2.99	18.61	20.9
30	1	1.00	7.28	7.28	2.8 mm	0 hr	4.15	4.1	57.04	58.3
31	0.88	0.88	9	9.00	8.0 mm	150 hrs	2.97	2.97	29.08	29.27
32	1	1.00	5.25	5.25	6.3 mm	0 hr	3.65	3.65	69.52	71.2

Appendix B 5: Analysis of Variance (ANOVA) of reduced 2FI model for the response 1 (adsorption capacity for Natural crude oil on Shredded, and Shredded-roughened PE)

Source	Coefficient of estimate	Sum of Squares	df	Mean Square	F-value	p-value	Remarks
Model	4.87	9.37	7	1.34	22.49	<0.0001	significant
A-Mass of P.E	-0.1361	0.2573	1	0.2573	4.33	0.0513	
B-Mass of oil	0.0124	0.0021	1	0.0021	0.0353	0.8529	
C-Type of P.E	0.5204	6.58	1	6.58	110.67	<0.0001	
D-Size of P.E	0.1884 /-0.2579	0.9412	2	0.4706	7.91	0.0032	
CD	0.1298/0.0851	0.6573	2	0.3287	5.52	0.0129	
Residual		1.13	19	0.0595			
Lack of Fit		0.8171	14	0.0584	0.9314	0.5841	not significant
Pure Error		0.3133	5	0.0627			
Cor Total		10.50	26				

Standard deviation 0.2439; Mean 4.81; CV% 5.07; R 2 0.8923; Adjusted R 2 0.8526; Predicted R 2 0.7892; Adeq Precision 14.8424

Appendix B 6: Analysis of Variance (ANOVA) of reduced quadratic model for the response 2 (adsorption efficiency) for Natural crude oil on Shredded, and Shredded-roughened PE)

	Coefficient of			_			
Source	estimate	Sum of Squares	df	Mean Square	F-value	p-value	
Model	37.87	5715.45	10	571.54	115.78	< 0.0001	significant
A-Mass of PE	11.80	1930.48	1	1930.48	391.08	< 0.0001	
B-Mass of oil	-13.54	2359.47	1	2359.47	477.98	< 0.0001	
C-Type of PE	5.14	626.22	1	626.22	126.86	< 0.0001	
D-Size of PE	1.92 /-2.72	97.33	2	48.67	9.86	0.0016	
AB	-1.76	22.33	1	22.33	4.52	0.0494	
ВС	-1.28	22.04	1	22.04	4.46	0.0507	
CD	1.13 /0.4956	39.22	2	19.61	3.97	0.0397	
B ²	5.58	109.04	1	109.04	22.09	0.0002	
Residual		78.98	16	4.94			

Lack of Fit	 56.45	11	5.13	1.14	0.4735	not significant
Pure Error	 22.53	5	4.51			
Cor Total	 5794.43	26				

Standard deviation 2.22; Mean 40.85; CV% 5.44; R² 0.9864; Adjusted R² 0.9779; Predicted R² 0.9640; Adeq Precision 42.0072

Appendix B 7: Analysis of Variance (ANOVA) of 2FI model for the response 2 (adsorption capacity for Natural crude oil on UV-weathered PE)

Source	Coefficient of estimate	Sum of Squares	df	Mean Square	F-value	p-value	
Model	3.94	34.46	19	1.81	17.87	< 0.0001	significant
A-Mass of PE	-0.3115	1.61	1	1.61	15.83	0.0018	
B-Mass of oil	0.2176	0.6479	1	0.6479	6.38	0.0266	
C-Size of PE	0.1706 /-0.1021	0.8904	2	0.4452	4.39	0.0372	
D-UV time of PE	0.2209 /0.9135	21.36	2	10.68	105.25	< 0.0001	

AB	-0.1737	0.2591	1	0.2591	2.55	0.1361	
AC	-0.2870 /0.1386	0.5322	2	0.2661	2.62	0.1136	
AD	0.1929 /-0.3230	0.7324	2	0.3662	3.61	0.0593	
ВС	0.3054/-0.5737	2.45	2	1.22	12.05	0.0014	
BD	0.2919 /-0.2091	0.6482			3.19	0.0773	
CD	0.2267 /-0.6432 /0.1433 /0.3314	4.30			10.60	0.0007	
Residual		1.22					
Lack of Fit		0.3730	7	0.0777	0.3153	0.9178	not significant
Pure Error		0.8450	5	0.0963			
Cor Total		35.68	31				

Standard deviation 0.3186; Mean 3.91; CV% 8.15; R² 0.9659; Adjusted R² 0.9118; Predicted R² 0.7540; Adeq Precision 15.4732

Appendix B 8: Analysis of Variance (ANOVA) of 2FI model for the response 2 (adsorption efficiency for Natural crude oil on UV-weathered PE)

Source	Coefficient of estimate	Sum of Squares	df	Mean Square	F-value	p-value	
Model	40.88	8545.58	19	449.77	17.38	< 0.0001	significant
A-Mass of PE	10.68	1888.29	1	1888.29	72.97	< 0.0001	
B-Mass of oil	-11.78	2288.42	1	2288.42	88.43	< 0.0001	
C-Size of PE	0.3427 /0.7434	29.69	2	14.85	0.5737	0.5782	
D-UV time of PE	2.41 /9.16	2062.09	2	1031.05	39.84	< 0.0001	
АВ	-3.73	119.55	1	119.55	4.62	0.0527	
AC	-3.90 /1.67	98.82	2	49.41	1.91	0.1906	
AD	4.08 /-0.9333	125.97	2	62.99	2.43	0.1296	
ВС	2.81 /-5.97	264.24	2	132.12	5.11	0.0249	
BD	2.47 /-4.12	112.87	2	56.43	2.18	0.1557	

CD	2.88 /-6.38 /1.64 /3.11	453.37	4	113.34	4.38	0.0206	
Residual		310.54	12	25.88			
Lack of Fit		168.58	7	24.08	0.8482	0.5942	not significant
Pure Error		141.96	5	28.39			
Cor Total		8856.12	31				

Standard deviation 5.09; Mean 40.46; CV% 12.57; R² 0.9649; Adjusted R² 0.9094; Predicted R² 0.7085; Adeq Precision 13.6244

Appendix B 9: Final Equation in Terms of Actual Factors for adsorption capacity and efficiency of Natural crude oil on shredded, and shredded-roughened PE

(i) Adsorption Capacity (Y)

$$Y(W, 2.8mm) = 4.7809 - 5.444A + 0.00494B$$

$$Y(W, 6.3mm) = 4.3794 - 0.5444A + 0.00494B$$

$$Y(W, 8mm) = 5.0067 - 0.5444A + 0.00494B$$

$$Y(X, 2.8mm) = 6.0813 - 0.5444A + 0.00494B$$

$$Y(X, 6.3 \text{ mm}) = 5.5903 - 0.5444A + 0.00494B$$

$$Y(X, 8mm) = 5.6176 - 0.5444A + 0.00494B$$

(ii) Adsorption efficiency (Q)

 $Q(W, 2.8mm) = 69.2781 + 68.2814A - 16.1801B - 2.8126AB + 0.8925B^2$

$$Q(W, 6.3 \text{ mm}) = 65.2752 + 68.2814A - 16.1801B - 2.8126AB + 0.8925B^2$$

$$Q(W, 8 mm) = 70.9234 + 68.2814A - 16.1801B - 2.8126AB + 0.8925 B^{2}$$

$$Q(X, 2.8mm) = 89.5265 + 68.2814A - 17.2076B - 2.8126AB + 0.8925 B2$$

$$Q(X, 6.3 \text{ mm}) = 84.2509 + 68.2814A - 17.2076B - 2.8126AB + 0.8925B^2$$

$$Q(X, 8mm) = 85.6524 + 68.2814A - 17.2076B - 2.8126AB + 0.8925B^2$$

Appendix B 10:Final Equation in Terms of Actual Factors for adsorption capacity and efficiency of Phillip oil on UV-weathered PE

$$\frac{1}{\sqrt{Y_{(2.8mm,0hr)}}} = 0.497054 + 0.016461(A) + 0.000085(B)$$

$$\frac{1}{\sqrt{Y_{(2.8mm,75hrs)}}} = 0.516007 + 0.016461(A) + 0.000085(B)$$

$$\frac{1}{\sqrt{Y_{(2.8mm,150hrs)}}} = 0.745511 + 0.016461(A) + 0.000085(B)$$

$$\frac{1}{\sqrt{Y_{(6.3mm,0hrs)}}} = 0.576650 + 0.016461(A) + 0.000085(B)$$

$$\frac{1}{\sqrt{Y_{(6.3mm,75hrs)}}} = 0.510219 + 0.016461(A) + 0.000085(B)$$

$$\frac{1}{\sqrt{Y_{(6.3mm,150hrs)}}} = 0.642813 + 0.016461(A) + 0.000085(B)$$

$$\frac{1}{\sqrt{Y_{(8mm,0hrs)}}} = 0.536837 + 0.016461(A) + 0.000085(B)$$

$$\frac{1}{\sqrt{Y_{(8mm,75hrs)}}} = 0.599899 + 0.016461(A) + 0.000085(B)$$

$$\frac{1}{\sqrt{Y_{(8mm,150hrs)}}} = 0.634775 + 0.016461(A) + 0.000085(B)$$

(ii) Adsorption Efficiency (Q)

$$Q(2.8mm, 0hr) = 29.9659 + 51.4266A - 3.7829B$$

$$Q (6.3 \text{mm}, 0 \text{hr}) = 20.9010 + 51.4266 \text{A} - 3.7829 \text{B}$$

$$Q (8mm, 0hr) = 25.9447 + 51.4266A - 3.7829B$$

Appendix B 11: Final Equation in Terms of Actual Factors for adsorption capacity and efficiency of Natural crude oil on UV-weathered PE

(i) Adsorption Capacity (Y)

Y(2.8mm, 0hrs) = 1.7703 + 0.4617A + 0.5343B - 0.2779AB

Y (2.8mm, 75hrs) = 5.4302 - 1.6020A + 0.3340B - 0.2779AB

Y (2.8mm, 150hrs) = 1.1307 + 0.2104A + 0.3845B - 0.2779AB

Y (6.3mm, 0hr) = 1.9882 + 2.1643A + 0.1827B - 0.2779AB

Y (6.3mm, 75 hrs) = 6.7060 + 0.1006A - 0.0177B - 0.2779AB

Y (6.3mm, 150 hrs) = 2.9002 + 1.9130A + 0.0328B - 0.2779AB

Y (8mm, 0hr) = 0.5261 + 2.2032A + 0.5195B - 0.2779AB

Y (8mm, 75 hrs) = 3.3780 + 0.1396A + 0.3191B - 0.2779AB

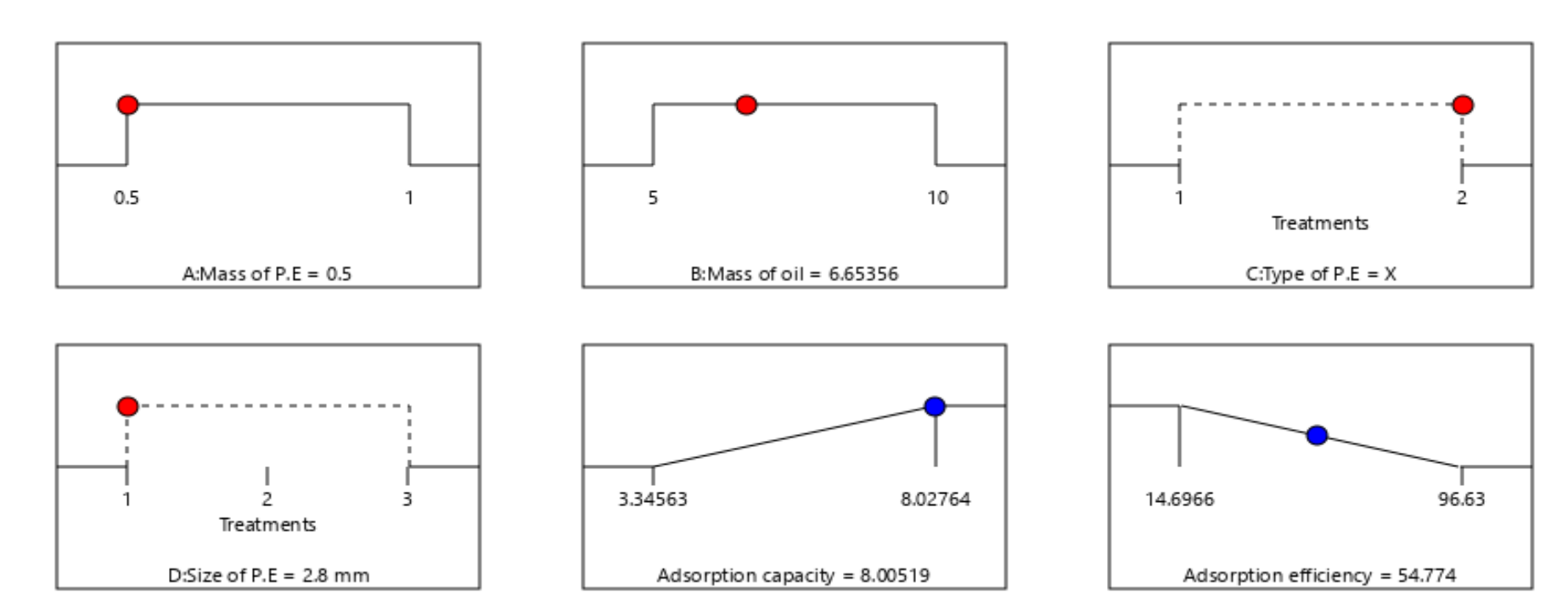
Y (8mm, 150 hrs) = 0.1250 + 1.9519A + 0.3697B - 0.2779AB

(ii) Adsorption Efficiency (Q)

Q (2.8mm, 0hr) = -0.1732 + 88.2396A + 1.8779B - 5.9690AB
Q (2.8mm, 75hrs) = 40.1436 + 68.1765A - 0.7580B - 5.9690AB
Q (2.8mm, 150hrs) = 2.5807 + 59.3132A + 1.5511B - 5.9690AB
Q (6.3mm, 0hr) = 0.5841 + 110.5286A - 1.6341B - 5.9690AB
Q (6.3mm, 75 hrs) = 51.6391 + 90.4655A - 4.2700B - 5.9690AB
Q (6.3mm, 150hrs) = 20.4001 + 81.6022A - 1.9609B - 5.9690AB
Q (8mm, 0hr) = -20.3930 + 112.7404A + 2.0157B - 5.9690AB
Q (8mm, 75hrs) = 12.9167 + 92.6773A - 0.6202B - 5.9690AB

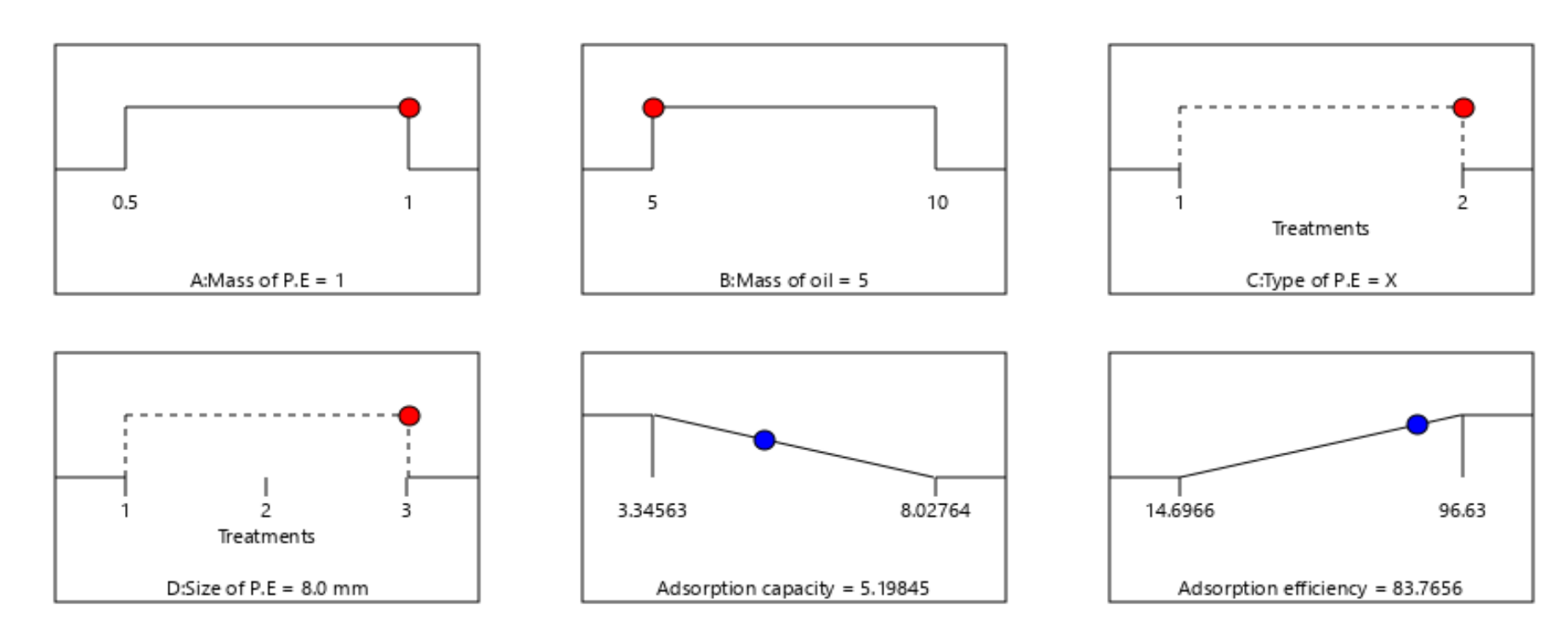
Q (8mm, 150hrs) = -12.4865 + 83.8140A + 1.6889B - 5.9690AB

Appendix B 12: Optimised conditions for adsorption capacity for Phillip oil by the non-weathered PE



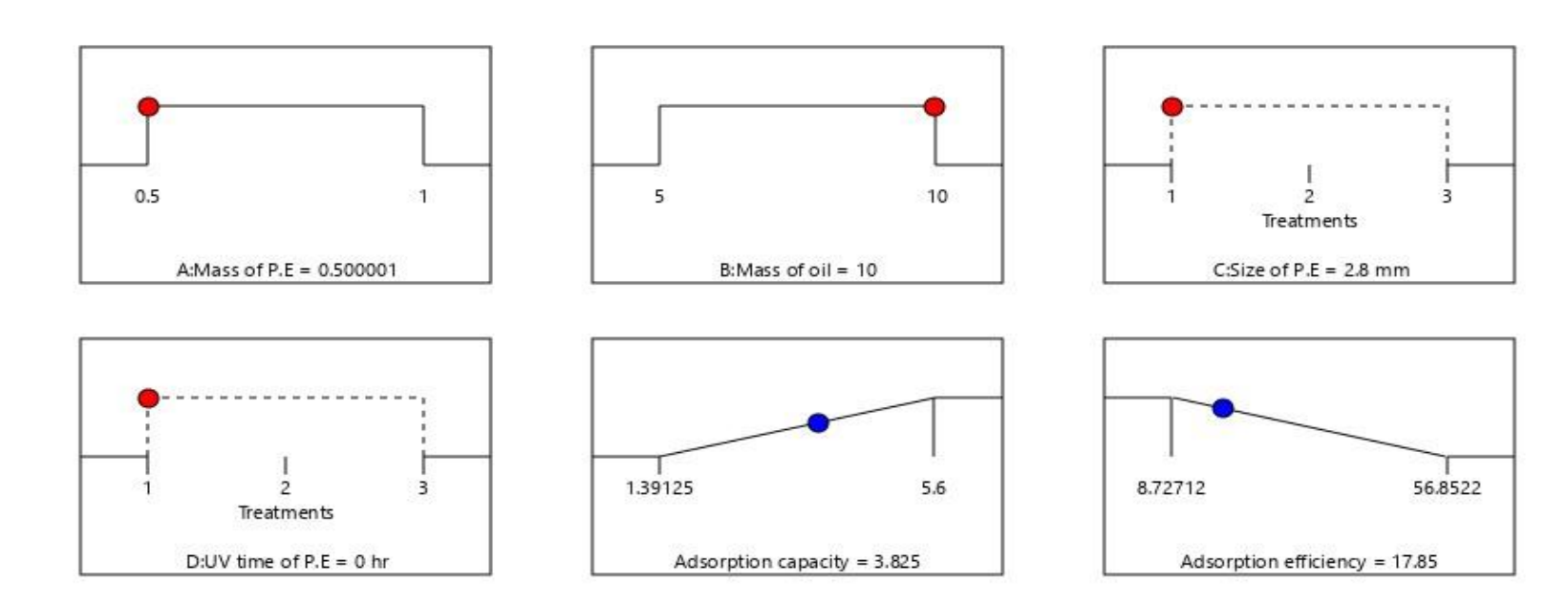
Desirability = 0.857 Solution 1 out of 40

Appendix B 13: Optimised conditions for adsorption efficiency for Phillip oil using the non-weathered PE



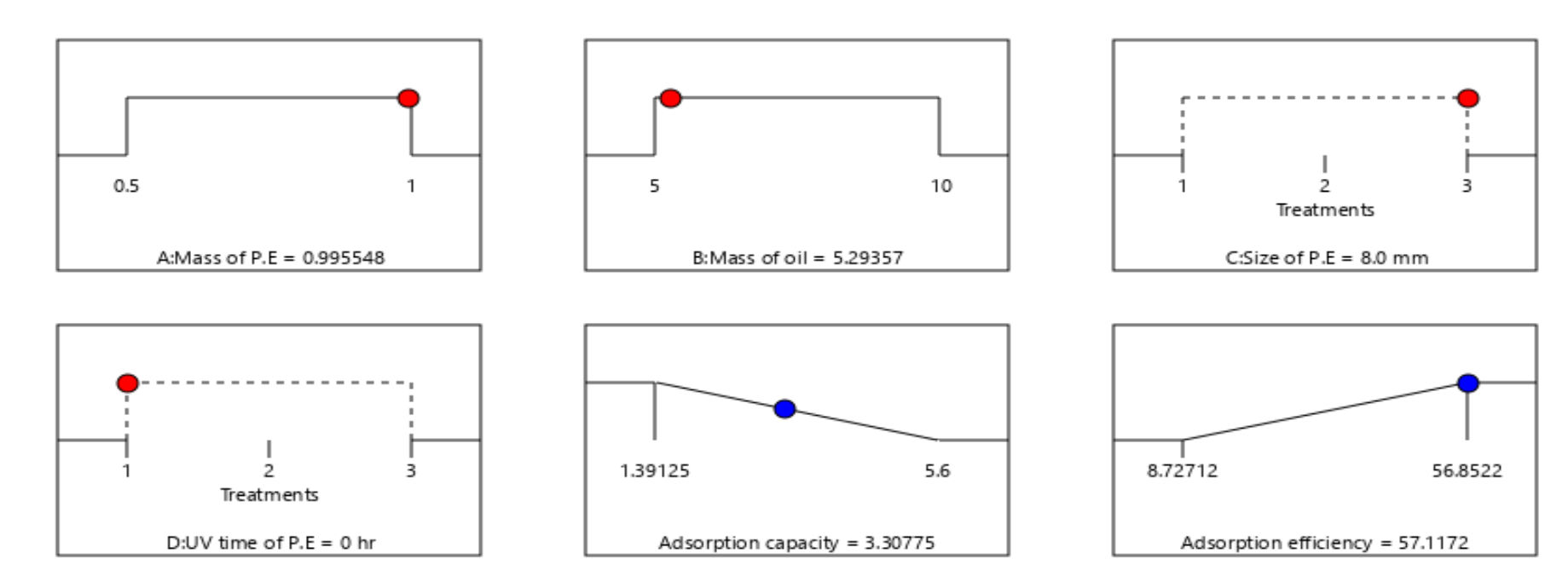
Desirability = 0.832 Solution 1 out of 41

Appendix B 14: : Optimised conditions for adsorption capacity for Phillip oil using the weathered PE



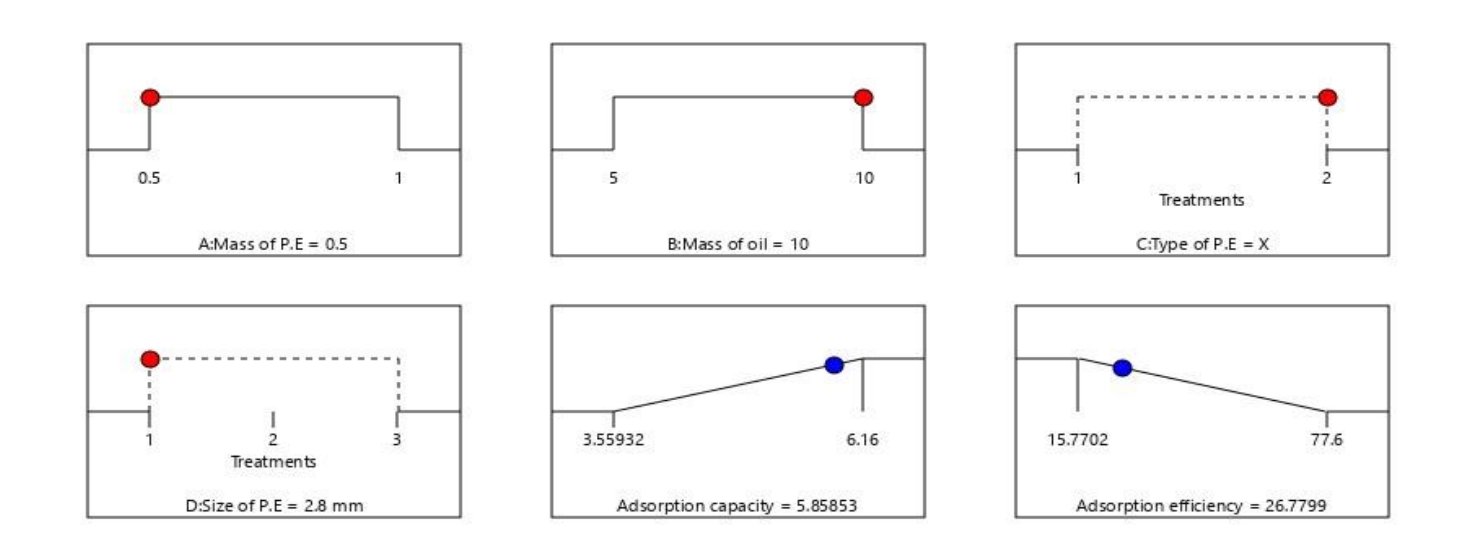
Desirability = 0.794 Solution 1 out of 100

Appendix B 15: Optimised conditions for adsorption efficiency for Phillip oil using the weathered PE



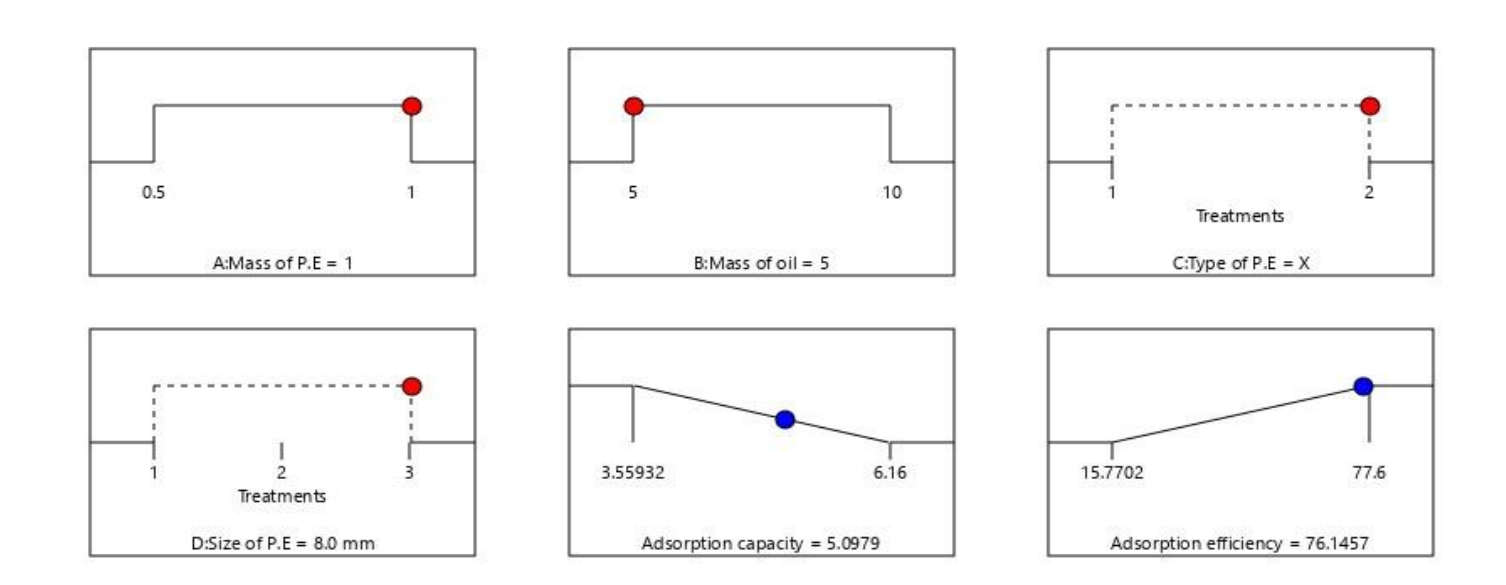
Desirability = 0.818 Solution 1 out of 100

Appendix B 16: Optimised conditions for adsorption capacity for Natural crude oil using the non-weathered PE



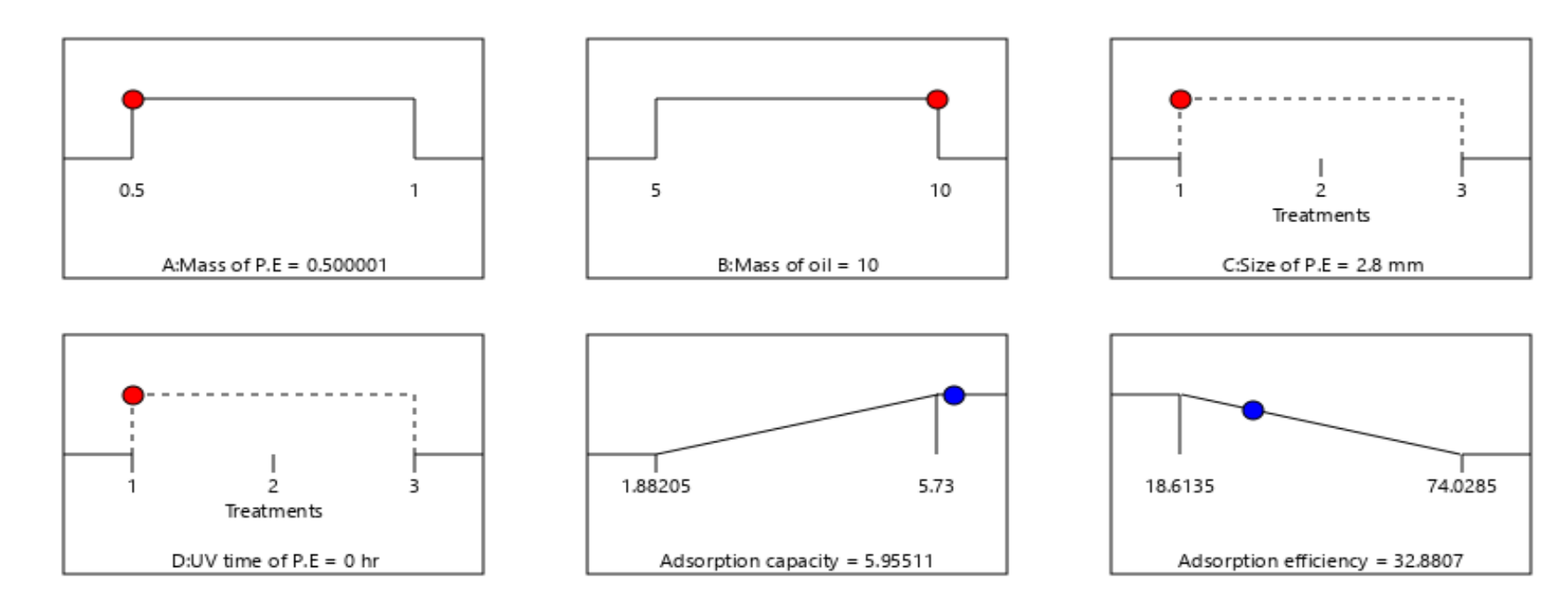
Desirability = 0.873 Solution 1 out of 48

Appendix B 17: Optimised conditions for adsorption efficiency for Natural crude oil using the non-weathered PE



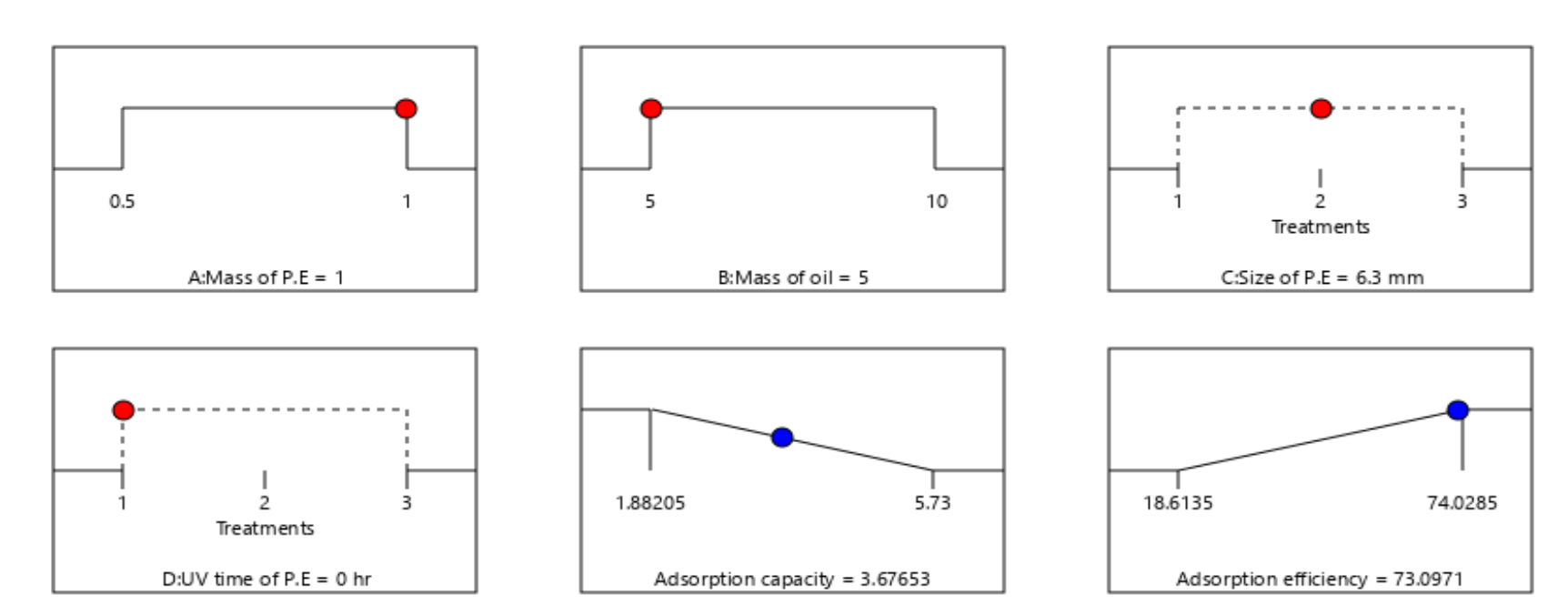
Desirability = 0.844 Solution 1 out of 37

Appendix B 18: Optimised conditions for adsorption capacity for Natural crude oil using the UV-weathered PE



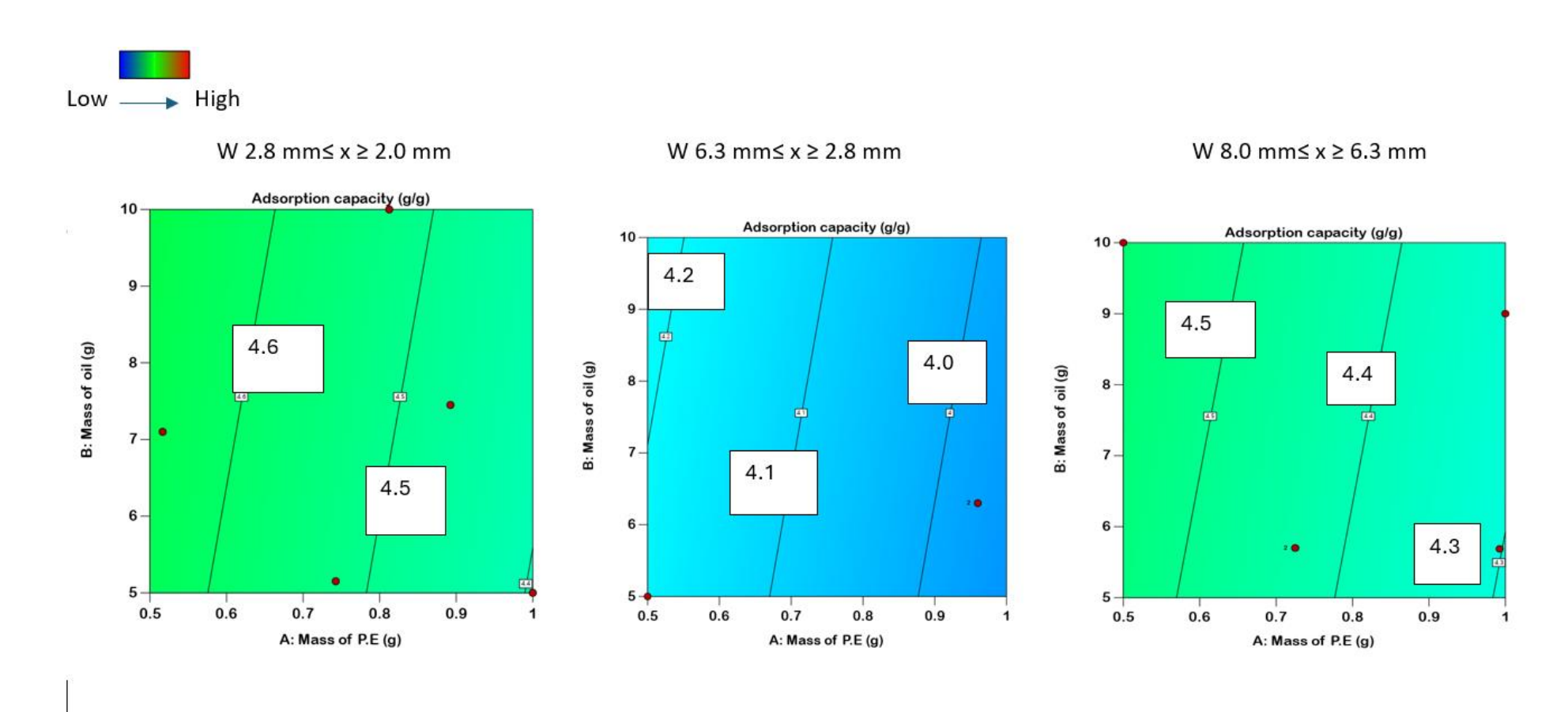
Desirability = 0.952 Solution 1 out of 72

Appendix B 19: Optimised conditions for adsorption efficiency for Natural crude oil using the UV-weathered PE

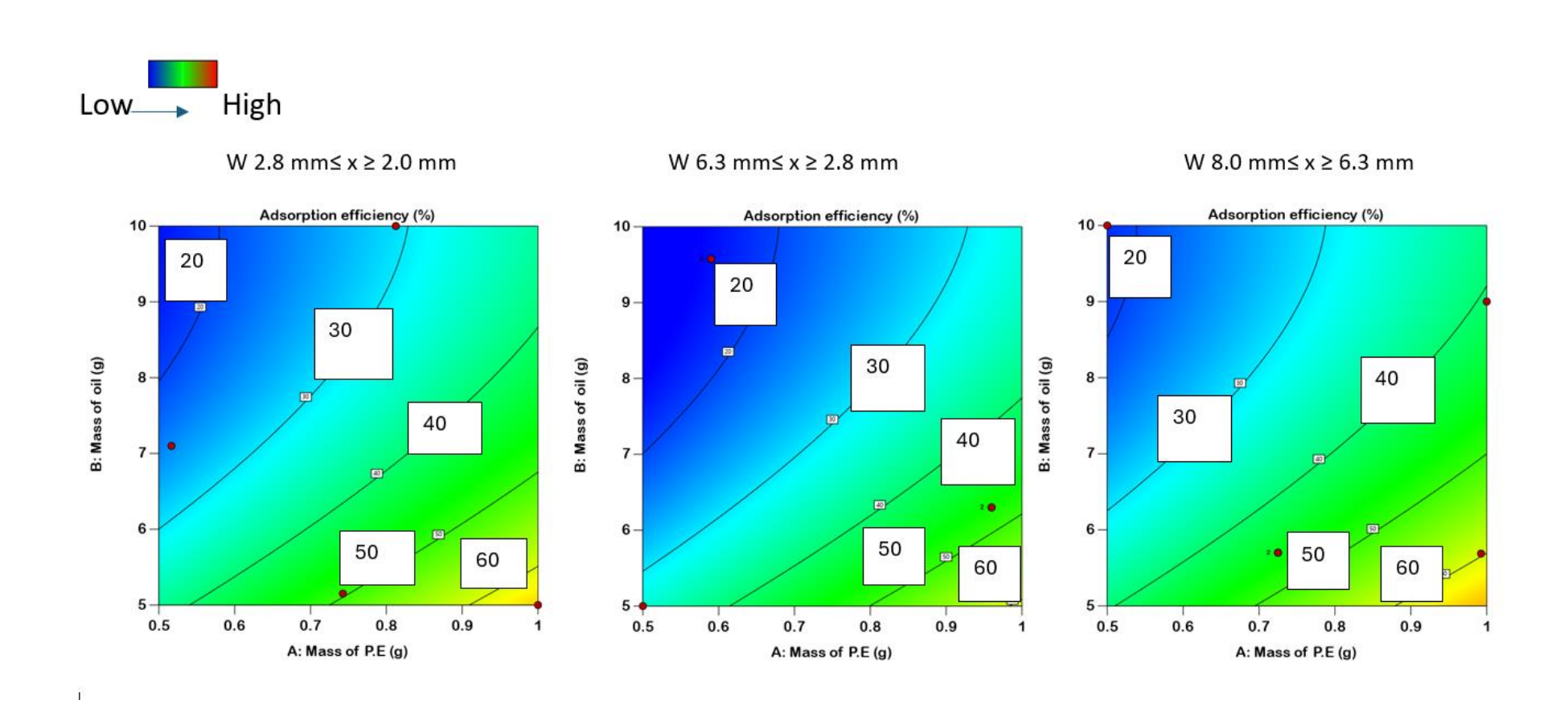


Desirability = 0.724 Solution 1 out of 46

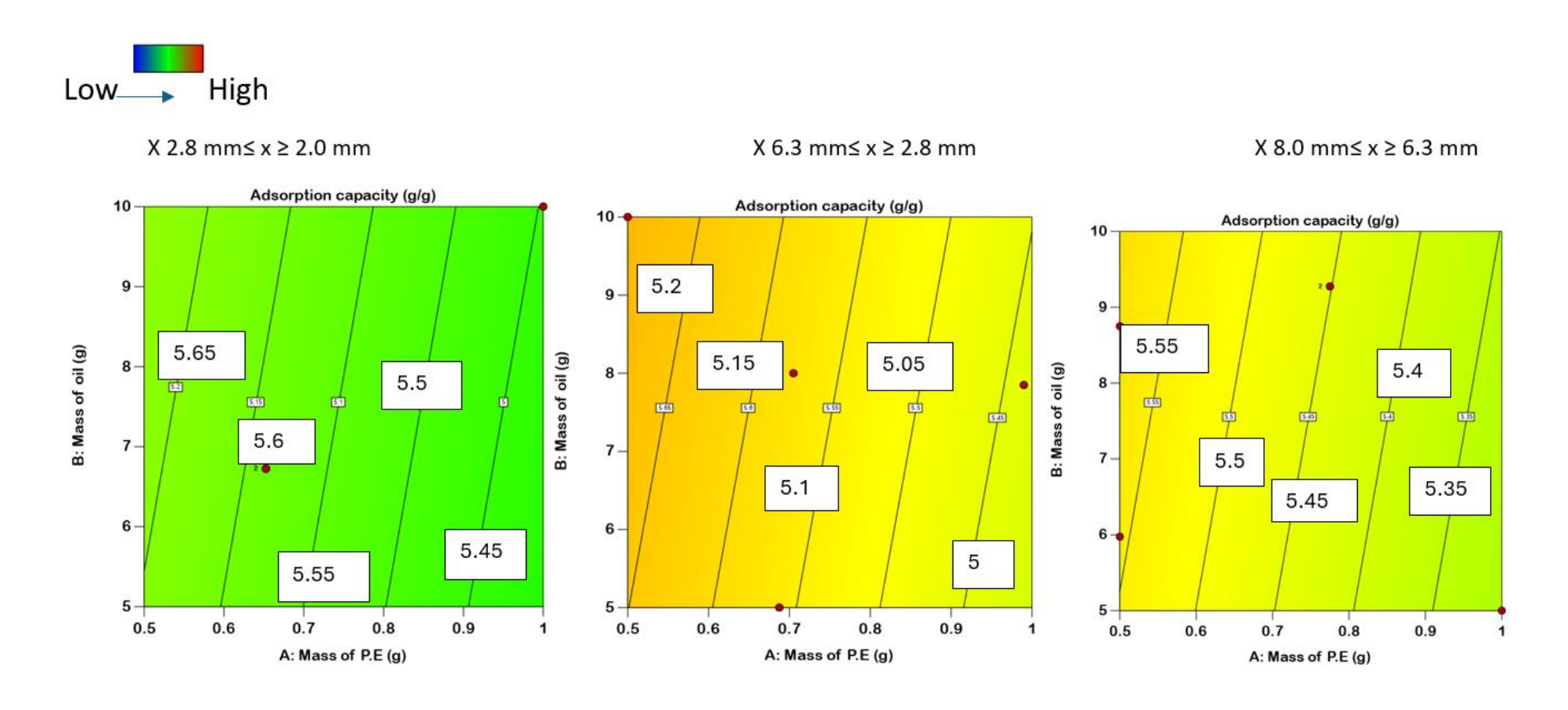
Appendix B 20: Adsorption capacity of natural crude oil with shredded PE (W) Particle size 2.8 mm \le x \ge 2.0 mm, shredded PE (W) Particle size 6.3 mm \le x \ge 2.8 mm and shredded PE (W) Particle size 8.0 mm \le x \ge 6.3 mm



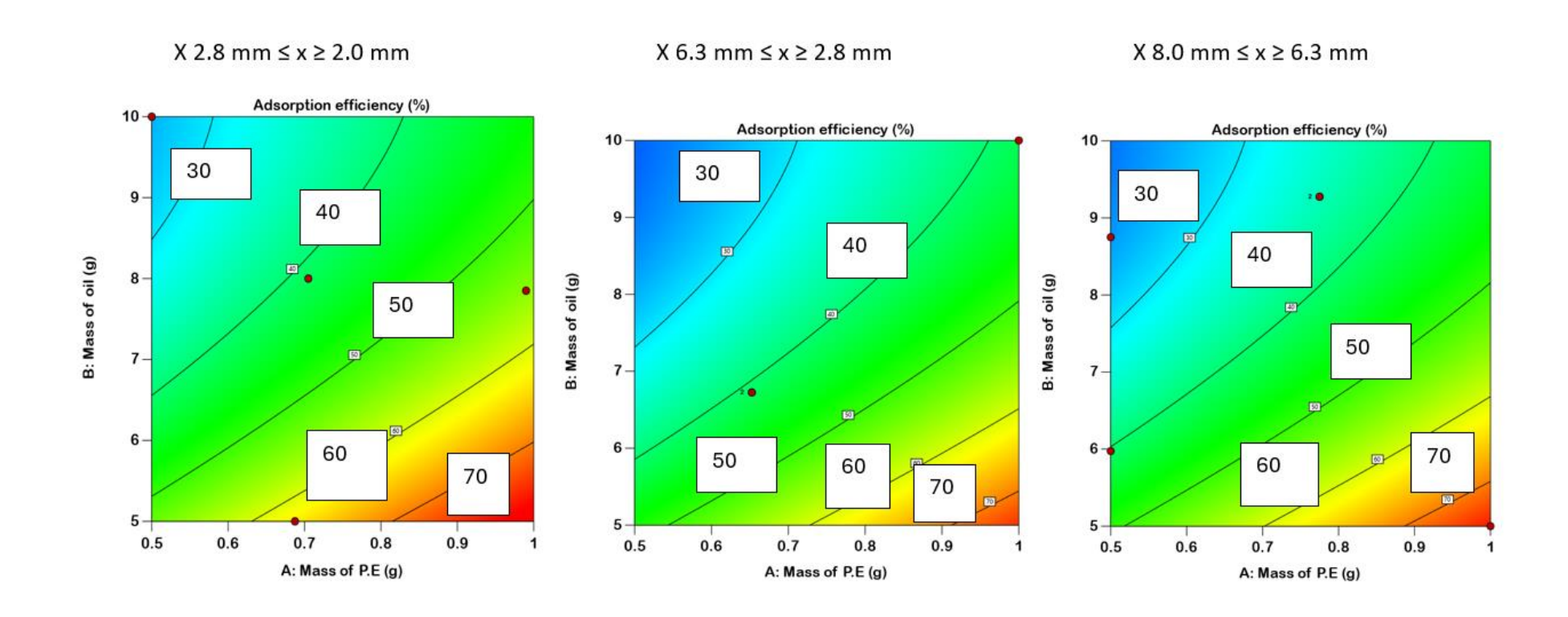
Appendix B 21: Adsorption efficiency of natural crude oil with shredded PE (W) Particle size 2.8 mm \le x \ge 2.0 mm, shredded PE (W) Particle size 6.3 mm \le x \ge 2.8 mm and shredded PE (W) Particle size 8.0 mm \le x \ge 6.3 mm



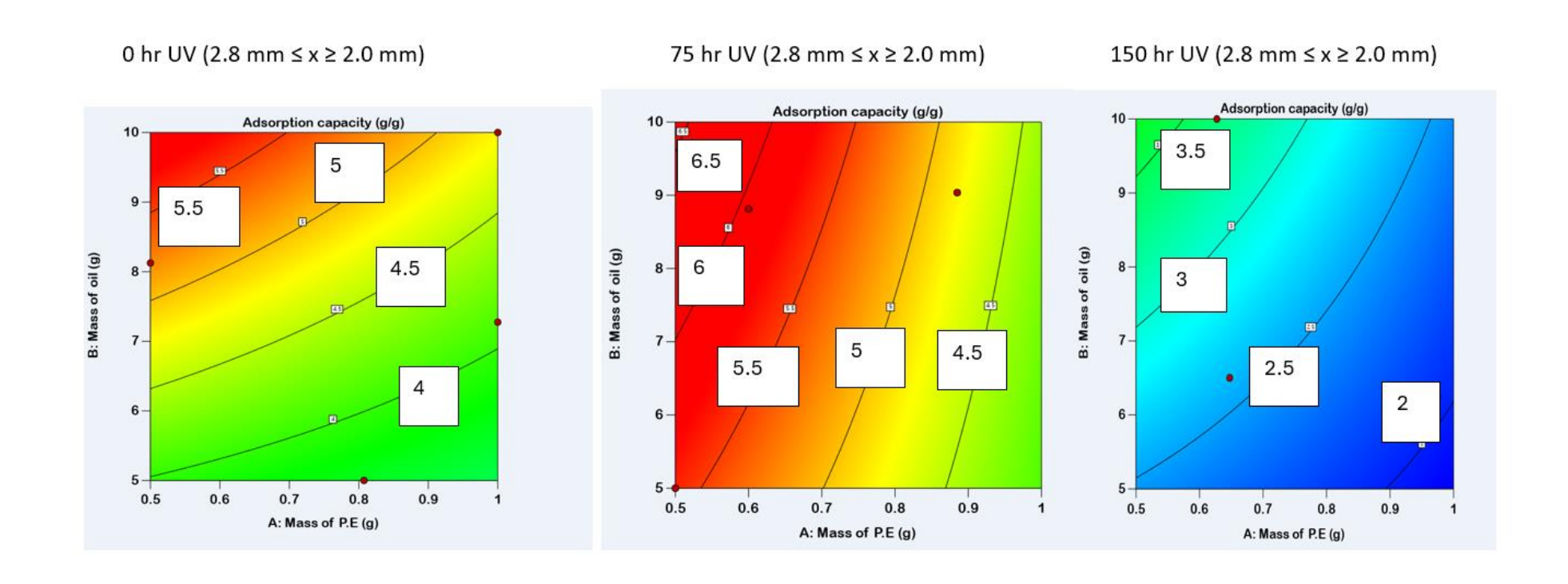
Appendix B 22: Adsorption capacity of natural crude oil with shredded-roughened PE (X) Particle size 2.8 mm \le x \ge 2.0 mm, shredded-roughened PE (X) Particle size 8.0 mm \le x \ge 6.3 mm and shredded-roughened PE (X) Particle size 8.0 mm \le x \ge 6.3 mm



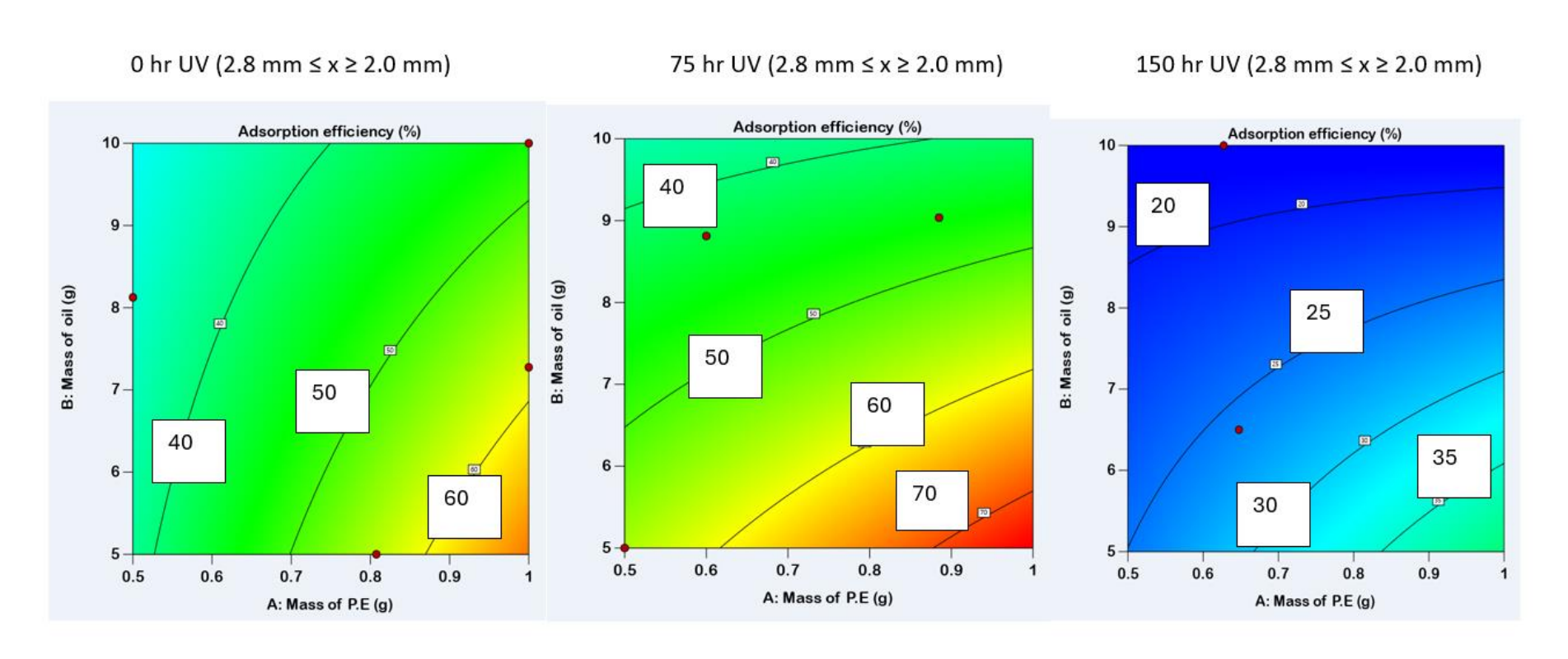
Appendix B 23:Adsorption efficiency of natural crude oil with shredded-roughened PE (X) Particle size 2.8 mm \le x \ge 2.0 mm, shredded-roughened PE (X) Particle size 8.0 mm \le x \ge 6.3 mm



Appendix B 24: Adsorption capacity of natural crude oil with 0 hr UV weathered PE Particle size 2.8 mm \le x \ge 2.0 mm, 75 hr UV weathered PE Particle size 2.8 mm \le x \ge 2.0 mm and 150 hr UV weathered PE Particle size 2.8 mm \le x \ge 2.0 mm

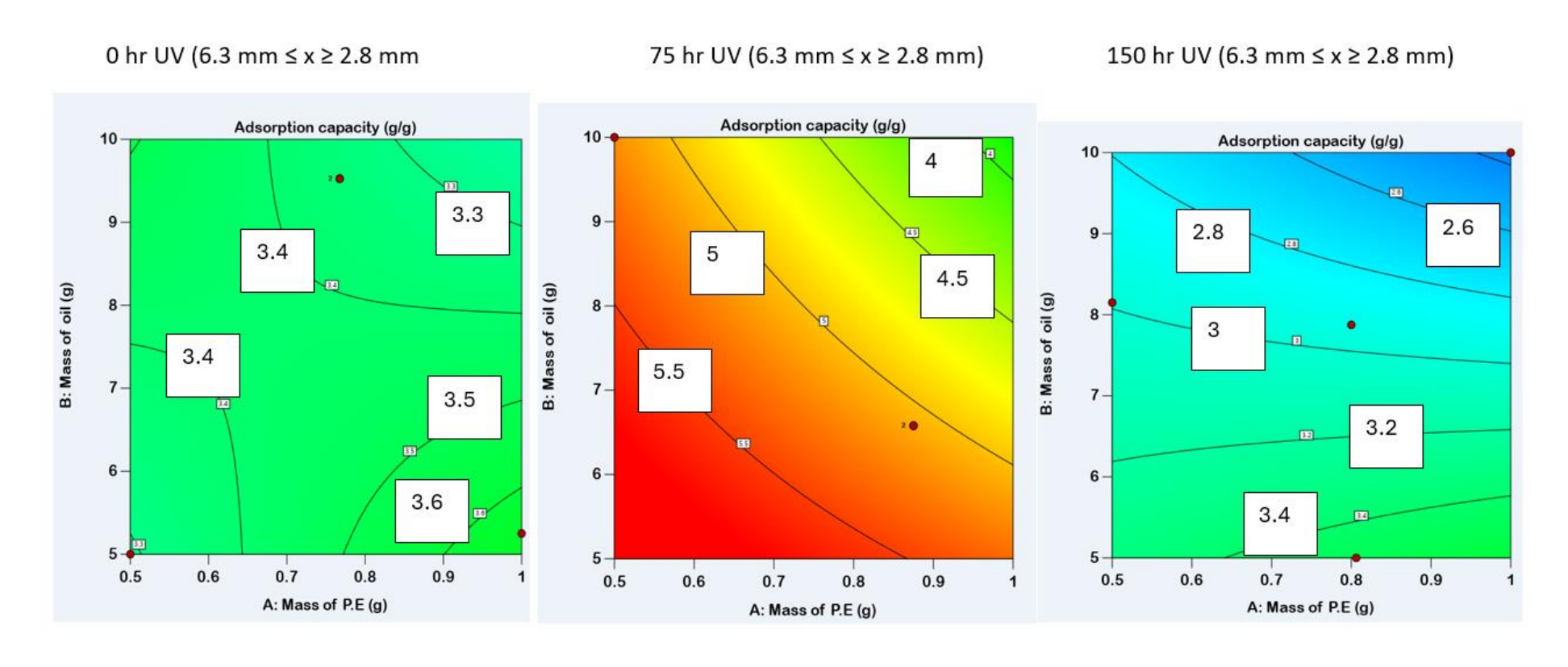


Appendix B 25: Adsorption efficiency of natural crude oil with 0 hr UV weathered PE Particle size 2.8 mm $\le x \ge 2.0$ mm, 75 hr UV weathered PE Particle size 2.8 mm $\le x \ge 2.0$ mm and 150 hr UV weathered PE Particle size 2.8 mm $\le x \ge 2.0$ mm

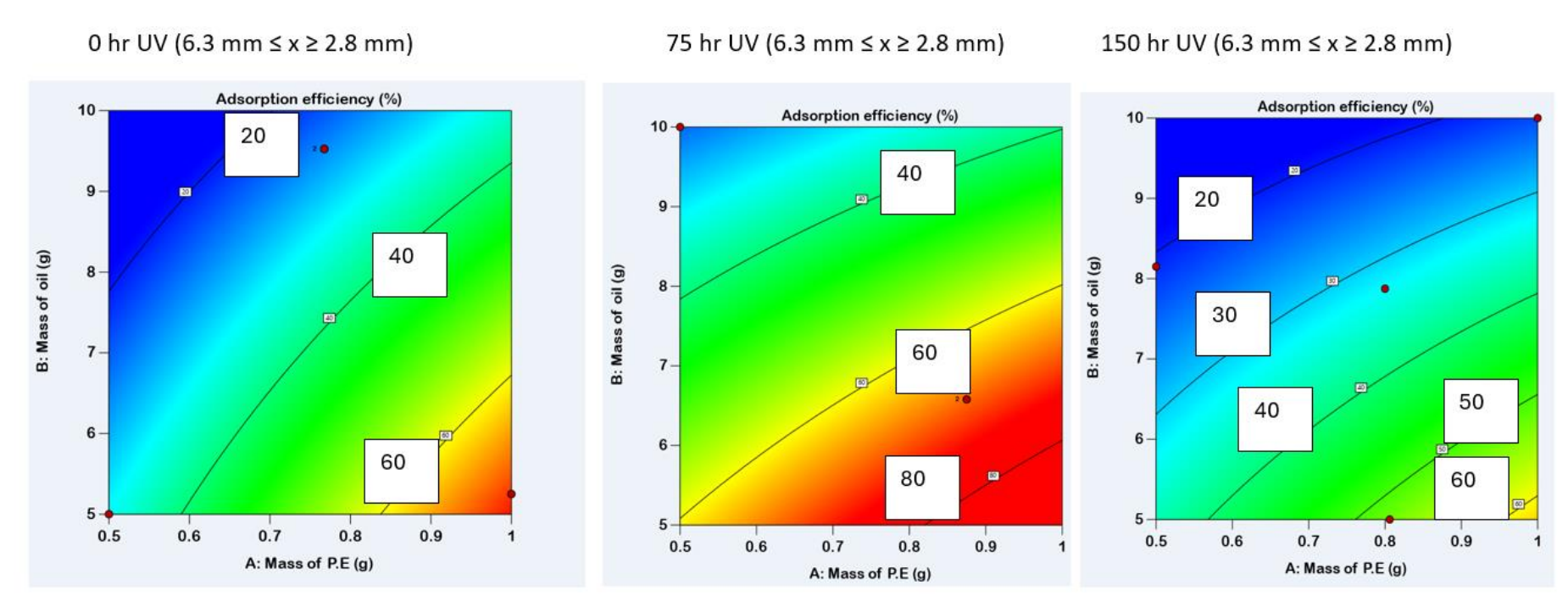


Appendix B26: Adsorption capacity of natural crude oil with 0 hr UV weathered PE Particle size 6.3 mm \le x \ge 2.8 mm, 75 hr UV weathered PE Particle size 6.3 mm \le x \ge 2.8 mm and 150 hr UV weathered PE Particle size 6.3 mm \le x \ge 2.8 mm

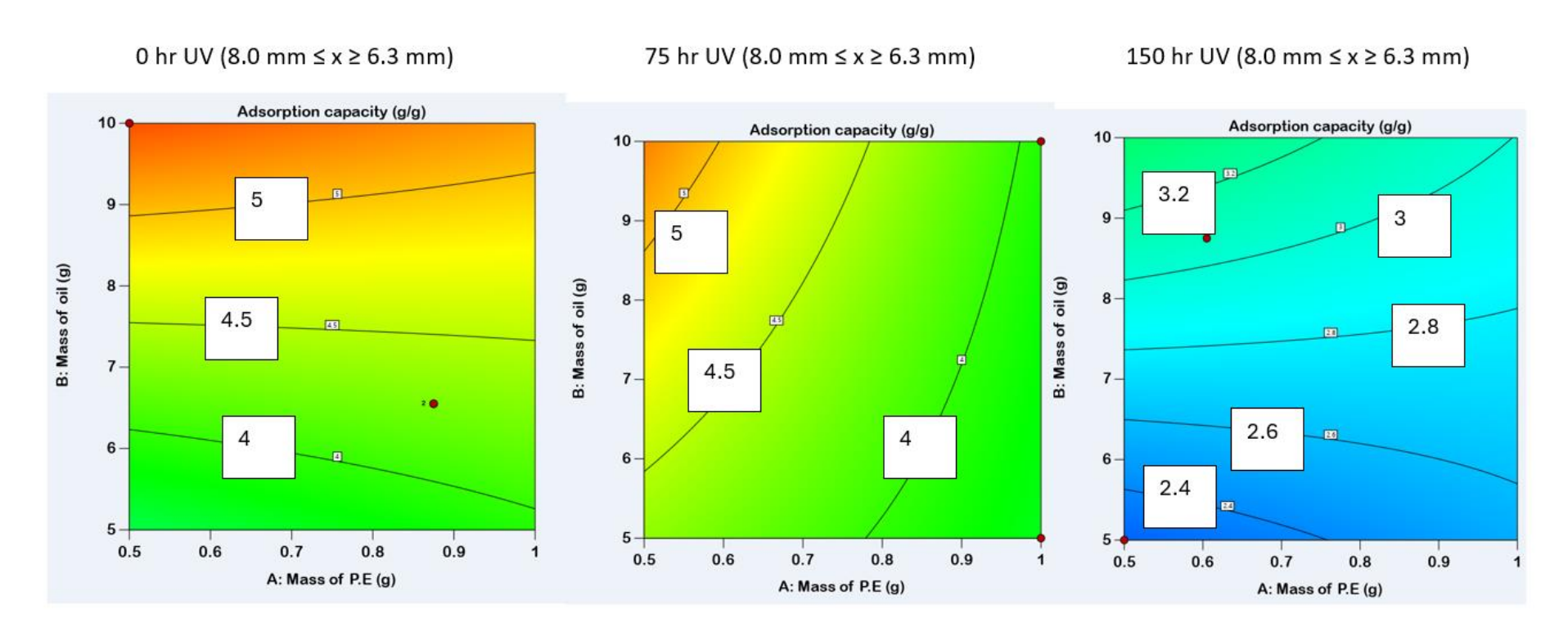
Appendix B 26: Adsorption capacity of natural crude oil with 0 hr UV weathered PE Particle size 6.3 mm \le x \ge 2.8 mm, 75 hr UV weathered PE Particle size 6.3 mm \le x \ge 2.8 mm and 150 hr UV weathered PE Particle size 6.3 mm \le x \ge 2.8 mm



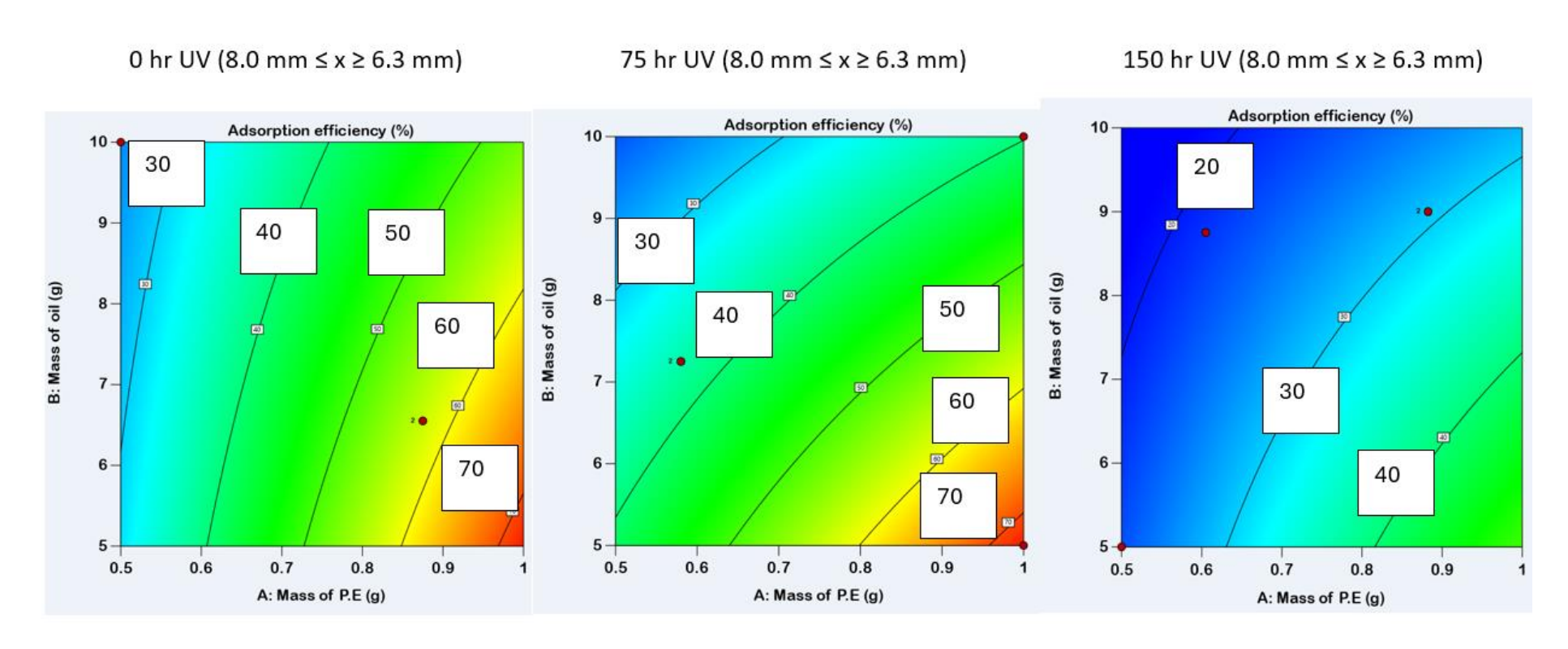
Appendix B 27: Adsorption efficiency of natural crude oil with 0 hr UV weathered PE Particle size 6.3 mm $\le x \ge 2.8$ mm, 75 hr UV weathered PE Particle size 6.3 mm $\le x \ge 2.8$ mm and 150 hr UV weathered PE Particle size 6.3 mm $\le x \ge 2.8$ mm



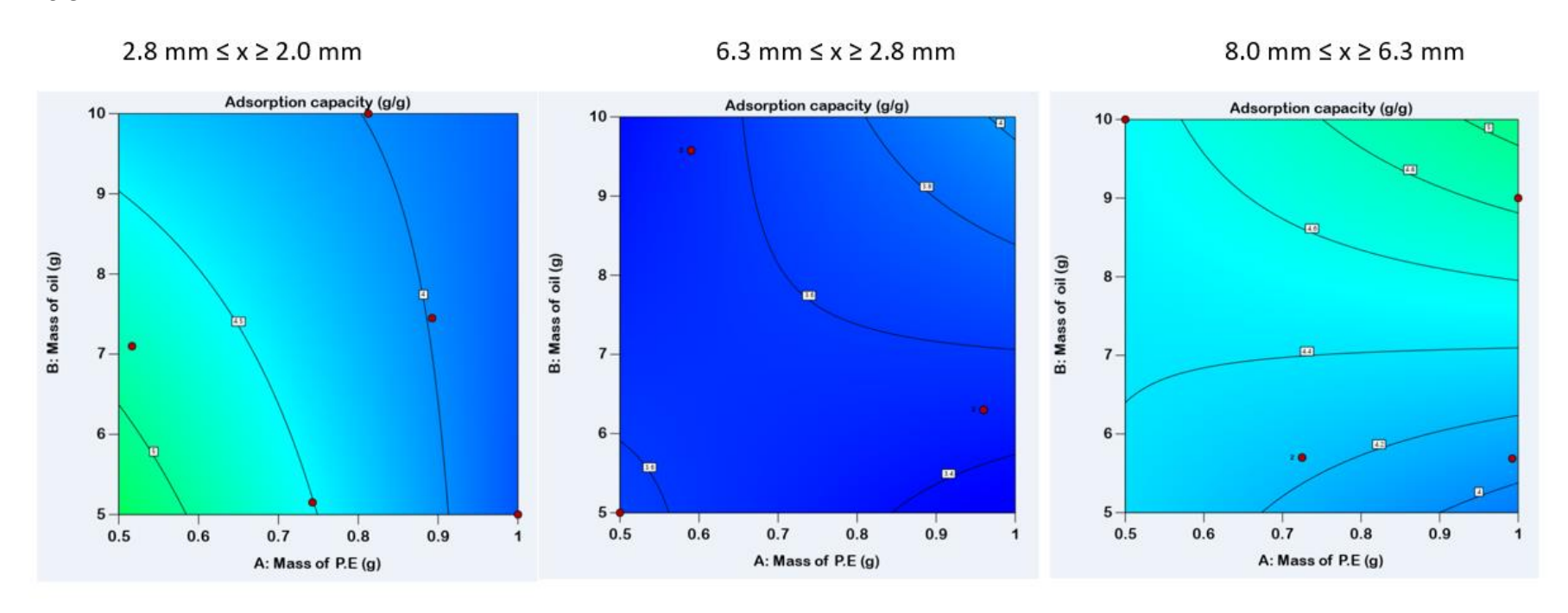
Appendix B 28: Adsorption capacity of natural crude oil with 0 hr UV weathered PE Particle size 8.0 mm \le x \ge 6.3 mm, 75 hr UV weathered PE Particle size 8.0 mm \le x \ge 6.3 mm and 150 hr UV weathered PE Particle size 8.0 mm \le x \ge 6.3 mm



Appendix B 29: Adsorption efficiency of natural crude oil with 0 hr UV weathered PE Particle size 8.0 mm \le x \ge 6.3 mm, 75 hr UV weathered PE Particle size 8.0 mm \le x \ge 6.3 mm and 150 hr UV weathered PE Particle size 8.0 mm \le x \ge 6.3 mm



Appendix B 30: : Adsorption capacity of Phillip oil with shredded PE (W) Particle size 2,8 mm \le x \ge 2.0 mm, 6.3 mm \le x \ge 2.8 mm and 8.0 mm \le x \ge 6.3 mm



Appendix C

Appendix C 1: Calculations for column Packing density

Internal diameter of column used for adsorption = 1.5cm

For the oil adsorption using the PE sorbent of mass 5g, the height of column occupied by PE (h) = 18cm

$$\rho p = \frac{m}{V}$$

 $V = A \times h$

Where A = Cross sectional area of the column (cm³) which can be calculated as:

$$A = \pi \times (\frac{d}{2})^2$$

Where d = column internal diameter 1.5cm

h = 18cm

 $\pi = 3.142$

thus A = 3.142 x $(\frac{1.5}{2})^2$

 $= 1.767 cm^2$

Thus packing density $\rho p = \frac{m}{A x h} = \frac{5}{1.767 \times 18}$

$$=\frac{5}{31.81}=0.157g/cm^3$$

For the oil adsorption using the PE sorbent of mass 2.5g, height of column occupied by PE (h) is approximately 10cm

Thus packing density $\rho p = \frac{m}{A x h} = \frac{2.5}{1.767 \times 10}$

$$=\frac{2.5}{17.67}=0.1415g/m^3$$

Appendix C 2: Results of the column adsorption experiment with the optimised conditions by the model (scaled up 5X) for shredded PE (W) and shredded-roughened PE (X) adsorption for Phillip and Natural crude oils

Type of oil	Type of PE	PE Particle size (cm)	Wt of PE (g)	Approx. height of column (cm)	Weight of oil (g)	Volume (ml)	Time of flow (mins)	Flow rate (ml/min)	Weight before oven drying (g)	Weight after oven drying (g)	Weight of oil sorbed (g)	Adsorption capacity (g/g)	Adsorption efficiency (%)
Phillip													
oil	Χ	2.8	2.5	10 cm	30	36.5	4.5	8.11	20.8	19.05	16.55	7.62	-
	Χ	8	5	18	25	30	4	7.5	22.2	20.06	15.06	-	60.24
	W	2.8	2.5	10	50	60	2.5	24	17.86	15.7	13.2	6.28	-
	W	8	5	18	25	30	5	6	21.09	19.62	14.62	-	58.48
Natural Crude oil	X	2.8	2.5	10cm	50	55	30	1.83	23.54	21.5	19	8.6	_
	Х	8	5	18	25	28	45	0.62	22.76	20.72	15.72	-	62.88
	W	2.8	2.5	10	50	55	3.5	15.71	21.74	17.8	15.3	7.12	-
	W	6.3	5	18	25	28	5	5.6	19.93	16.5	11.5	-	46

X = Shredded-roughened PE, W= Shredded PE/0 hour-UV-weathered PE. Height of 5g mass of PE = 18cm and height of 2.5g of PE = 10cm. The values of the adsorption capacity and efficiency were calculated for only the maximised responses. Packing density for adsorbents of mass of 5g = 0.157g/cm³, Packing density for adsorbents of mass of 2.5g = 0.1415 g/cm³

Appendix D: Converis ethics declaration

Thesis chapters	Research study	Ethics review	Approval date
		reference	
4-8	Remediation of		11 /11/2021
	Petroleum polluted		
	water using		
	Poly(ethylene)-based		
	waste and subsequent		
	waste recovery		